
From plants to plastics: continuous catalytic routes for the production of renewable monomers

Thesis submitted in accordance with the requirements of
Cardiff University for the degree of Doctor of Philosophy by

Laura Keiko Yakabi Diosdado

School of Chemistry

Cardiff University

2018



Supervisor

Dr. Ceri Hammond

Abstract

Moving towards a more sustainable chemical society requires the discovery and development of alternative catalytic routes to replace the current petrochemical industry. In this respect, the valorisation of biomass into commodity compounds, such as polymers, represents a great challenge. In order to tackle this challenge, various key points call for attention, including: i) the quest of identifying a suitable catalyst, ii) optimising operational conditions to obtain high levels of selectivity towards the desired product, and iii) studying potential process intensification.

This thesis provides a detailed investigation of two catalytic routes to produce renewable monomers: the Baeyer-Villiger oxidation (BVO) reaction of substituted cyclohexanones, and the selective hydrogenation of succinic acid to give rise to the corresponding lactones.

This work begins in Chapter 3, with the full elucidation of the kinetic, mechanistic and lifetime aspects of the BVO reaction of cyclohexanone to caprolactone, studied as a model reaction, using Sn- β as catalyst, and hydrogen peroxide as green oxidant. Taking the knowledge gained from the study of this model reaction, the substrate scope is broadened to various substituted cyclohexanones in Chapter 4, where various kinetic, steric, electronic, and thermodynamic elements of this transformation are investigated in greater detail than previously achieved. Additionally, the intensification of this process in continuous flow, and the production of polymer-grade lactone monomers, are also evaluated. Following this, Chapter 5 is focused on the coupling of *in situ* hydrogen peroxide production with the BVO system, in order to potentially upgrade the sustainability of this process. Subsequently, selective hydrogenation of succinic acid to γ -butyrolactone over various metal supported nanoparticles is discussed in Chapter 6, showing how the choice of metal, support and operational conditions determines the product distribution and catalytic activity obtained. In closing, Chapter 7 evaluates the consequences of the findings of this research, and the pertaining challenges that these findings open.

Table of contents

1. Introduction.....	1
1.1 Towards sustainable chemistry	1
1.2 Biomass exploitation	6
1.2.1 Lignocellulose valorisation.....	9
1.3 Bio-based polymers.....	14
1.3.1 Lactones as renewable monomers and bio-chemicals.....	15
1.3.1.1 BVO derived lactones.....	19
1.3.1.1.1 Classic BVO with peroxyacids.....	19
1.3.1.1.2 Enzymatic BVO.....	20
1.3.1.1.3 Catalytic BVO reaction using Sn- β and others.....	20
1.3.1.2 Selective hydrogenation derived lactone	22
1.3.1.2.1 SA from renewable sources	23
1.3.1.2.2 SA as platform molecule	24
1.3.1.2.3 Chemo-selective hydrogenation of SA to GBL.....	26
1.4. Objectives of the thesis	27
2. Experimental and methods.....	31
2.1. List of abbreviations	31
2.2 Formulas and expressions.....	33
2.3 Catalysts employed	34
2.3.1 Lewis acid silicalites	34
2.3.1.1 Sn- β preparation	34
2.3.1.2 Hierarchical Sn- β preparation.....	35
2.3.2 Metal supported nanoparticles.....	36
2.3.2.1 Sol immobilisation method (SI).....	36
2.3.2.2 Wet impregnation method (IMP).....	36
2.3.2.3 Co-precipitation method (COP)	37
2.3.2.4 Deposition precipitation method (DP)	37
2.3.3.5 Commercial catalysts employed.....	38
2.4 Kinetic evaluation	38

2.4.1 Batch Baeyer-Villiger Oxidation (BVO) reactions of cyclohexanone (CyO), substituted cyclohexanones (R-CyO) and substituted acetophenones (4-R-AcetoPhO)	38
2.4.2 Batch caprolactone (Capr) and substituted caprolactone (R-Capr) hydrolysis reactions	39
2.4.3 Poisoning experiments on BVO reaction	40
2.4.4 Continuous flow BVO reactions of CyO and 4- ^j Pr-CyO	40
2.4.5 Polymerisation studies	40
2.4.6 Batch <i>in situ</i> H ₂ O ₂ production	41
2.4.7 Batch coupling of <i>in situ</i> H ₂ O ₂ production and BVO reaction	41
2.4.8 Batch succinic acid (SA) hydrogenation reaction	42
2.4.9 Reusability studies for catalytic hydrogenation of SA	42
2.5 Analytical methods	43
2.5.1 Chromatography	43
2.5.1.1 Gas Chromatography (GC)	43
2.5.1.1.1 Quantification of BVO products	44
2.5.1.1.2 Quantification of SA hydrogenation liquid-products	47
2.5.1.1.3 Quantification of SA hydrogenation gas-products	47
2.5.1.2 High Performance Liquid Chromatography (HPLC)	48
2.5.1.2.1 Quantification of SA	49
2.5.1.3 Gel permeation chromatography (GPC)	49
2.5.1.3.1 Analysis of Capr oligomers and 4- ^j Pr-Capr polymer	51
2.5.1.4 Column chromatography	51
2.5.1.4.1 Lactone separation	51
2.5.2 Nuclear Magnetic Resonance (NMR) spectroscopy	51
2.5.2.1 Quantification of BVO products	54
2.5.3 Titration of hydrogen peroxide (H ₂ O ₂)	55
2.5.3.1 Quantification of H ₂ O ₂	55
2.5.4 Attenuated Total Reflectance (ATR) Infra-Red (IR)	55
2.5.4.1 Analysis of BVO products	56
2.5.5 Thermogravimetric analysis (TGA)	56
2.5.5.1 Experimental details for TGA	56
2.6 Catalyst characterisation techniques	57
2.6.1 Powder X-Ray Diffraction (XRD)	57
2.6.1.1 Experimental details	58
2.6.2 Surface area and porosimetry analysis	59

2.6.2.1 Experimental details	59
2.6.3 Electron Microscopy	60
2.6.3.1 Scanning electron microscopy (SEM)	60
2.6.3.1.1 Experimental details	60
2.6.3.2 Transmission electron microscopy (TEM)	61
2.6.3.2.1 Experimental details	61
2.6.4 Diffuse Reflectance Infrared Fourier Transformed (DRIFT) spectroscopy	61
2.6.4.1 Experimental measurement	62
2.6.5 Magic Angle Spinning NMR (MAS NMR) spectroscopy	63
2.6.5.1 Experimental details	64
2.6.6 X-Ray Photoelectron Spectroscopy (XPS)	64
2.6.6.1 Experimental details	65
2.7 Computational studies	66
2.7.1 Experimental details	66
3. Selectivity and lifetime effects in zeolite-catalysed Baeyer–Villiger Oxidation reaction	68
3.1. Introduction	68
3.2 The catalyst: Sn-β	70
3.3 Results and discussion	73
3.3.1 Impact of kinetic parameters	73
3.3.1.1 Standard BVO reaction	73
3.3.1.2 Impact of initial aluminium content of parental β zeolite	74
3.3.1.3 Impact of the Sn loading	76
3.3.1.4 Effect of H_2O_2 concentration	78
3.3.1.5 Effect of mass of catalyst	80
3.3.1.6 Effect of reaction temperature	81
3.3.2 Identification of by-products and closing the carbon balance	84
3.3.3 Caprolactone conversion studies	91
3.3.4 Intensification and catalyst stability in continuous flow	96
3.4 Conclusions	105

4. Continuous production of bio-renewable, polymer-grade lactone monomers through Sn-β catalysed Baeyer-Villiger Oxidation with H₂O₂.....	107
4.1. Introduction.....	107
4.2 The catalysts: Sn- β and Sn- β -H.....	110
4.3 Results and discussion	114
4.3.1 Extending the substrate scope.....	114
4.3.1.1 Effect of 2- and 4- substitution on catalytic activity of BVO of R-CyO	114
4.3.1.2 Evaluation of mass transfer limitation through Sn- β	118
4.3.1.3 Evaluation of the electronic and steric effects on R-CyO.....	120
4.3.2 Effect of 4- substitution on reaction selectivity for BVO of 4-R-CyO.....	125
4.3.3 Intensification of 4- <i>i</i> -Pr-CyO BVO in continuous flow	134
4.3.4 Probing lactone quality: Polymerisation studies	136
4.4 Conclusions	139
5. Upgrading the sustainability of BVO chemistry by coupling <i>in situ</i> H₂O₂ production.....	141
5.1. Introduction.....	141
5.1.1. Preliminary studies for H ₂ O removal from the BVO / Sn- β / H ₂ O ₂ system	142
5.2. Hydrogen peroxide (H ₂ O ₂) production	146
5.3 Results and discussion	150
5.3.1 Preliminary studies for coupling <i>in situ</i> H ₂ O ₂ production and BVO reaction.....	150
5.3.2 Catalysts for <i>in situ</i> H ₂ O ₂ production.....	152
5.3.3 Solvents for <i>in situ</i> H ₂ O ₂ production.....	156
5.3.4 Alternative solvents for BVO reaction.....	158
5.3.5 Coupling <i>in situ</i> H ₂ O ₂ production with BVO in one pot.....	162
5.3.5 Coupling <i>in situ</i> H ₂ O ₂ production with BVO in two pots	167
5.4 Conclusions	168
6. Chemo-selective lactonization of renewable succinic acid with heterogeneous catalysts.....	171
6.1. Introduction.....	171

6.2 Results and discussion	175
6.2.1 Preliminary studies for SA hydrogenation	175
6.2.1.1 <i>Optimisation of the initial H₂ pressure</i>	179
6.2.1.2 <i>Optimisation of the catalyst loading</i>	180
6.2.2 Preliminary identification of the reaction network	182
6.2.3 Catalyst design studies.....	184
6.2.3.1 <i>Investigating the choice of metal</i>	186
6.2.3.2 <i>Detailed investigation on 2Pd/Al₂O₃(COP)</i>	190
6.2.3.3 <i>Investigation of the preparation method</i>	196
6.2.3.4 <i>Effect of the Pd loading</i>	206
6.2.3.5 <i>Reusability of 2Pd/Al₂O₃(COP)</i>	211
6.3 Conclusions	212
7. Final conclusions and pertaining challenges.....	215
7.1. Final conclusions	215
7.2. Pertaining challenges.....	217
7.2.1. BVO of R-CyO using Sn-β and H ₂ O ₂	217
7.2.2 Selective hydrogenation of SA to GBL	220
Annex	223
Acknowledgements	226

1. Introduction

1.1 Towards sustainable chemistry

Over the last 150 years, human population growth, evolution of lifestyle and consumption patterns have been tightly related to the increment of energy usage and the chemical industry. As a matter of fact, world energy consumption has been gradually increasing over the last decades and it is predicted to keep increasing with time. As represented in Fig 1.1, according to the U.S. Energy Information Administration (EIA) latest “International Energy Outlook 2017”, world energy consumption is projected to grow by 28 % from 2015 to 2040. Most of this expected growth has been estimated based on the observed increasing energy demand in countries driven by continued population growth and economic development, especially in Asia.¹ Currently, fossil fuel feedstocks, which refer to natural fuels such as coal, gas and oils formed in the earth from plant or animal remains, represent about the 80 % of the world energy supply (approximately 37 % crude oil, 25 % coal and 23 % natural gas).

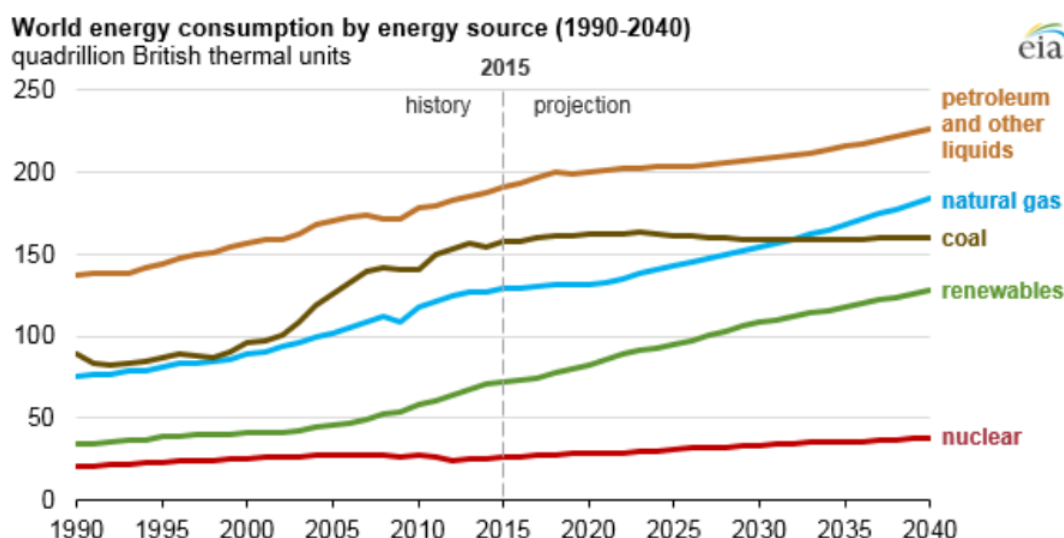


Figure 1.1. World energy consumption projection based on the latest International Energy Outlook 2017.¹

In addition to generating most of the world's energy, including heating, electricity supplies and fuels for transportation, crude oil is also the main source for the production of most of the chemicals essential to sustain human activity. Global crude oil consumption by sector can be divided in 56 % transportation, 28 % industry (approximately only 14 % in petrochemicals), 11 % other uses and 5 % power.² Crude oil consumption rate is increasing every year, by approximately 1.5 million of barrels per day every year, and its global consumption rate is predicted to reach 100 million of barrels per day in the forthcoming year (Fig 1.2).³ Hence, continuous exploitation of this raw material is required to cover the demand.

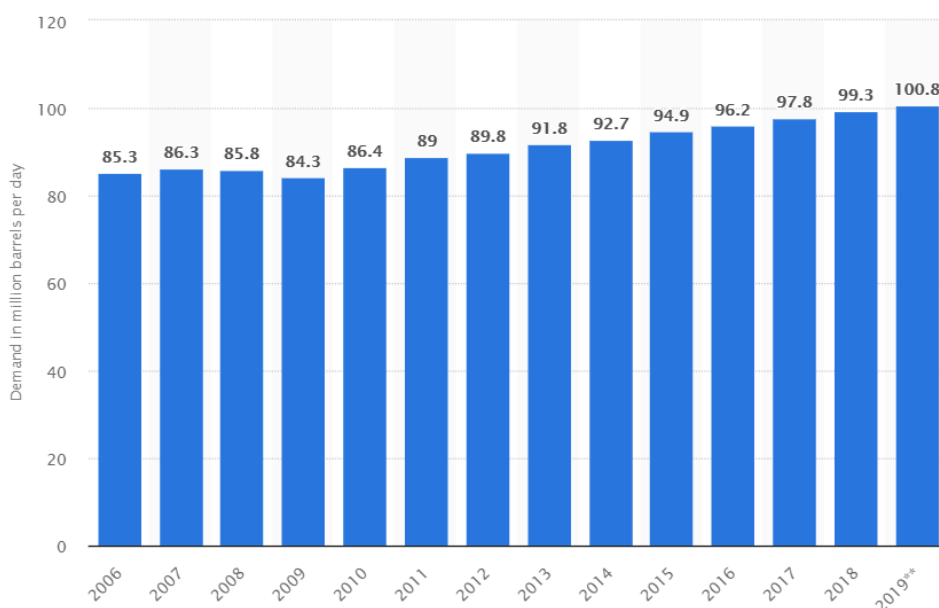


Figure 1.2. Daily global crude oil consumption rate.³

As well as crude oil, world coal consumption has also been increasing over the past 30 years, almost 3-fold since 1980 to 2013, from 3,600 to 8,700 million tonnes, respectively,⁴ China being the country that consumes the most, exploiting nearly half of the world's coal demand. However, this trend has stagnated over the past half-decade, and coal consumption has been predicted to shrink slightly from 27 to 26 % from 2016 to 2022, in favour of renewable sources.⁵ As can be appreciated from Fig 1.1, coal currently supplies a quarter of all world energy used, contributing up to 40 % of the global electricity generated, and is therefore the largest source for electricity production.⁶ Additionally, it plays a crucial role in industries, such as the iron and steel industries.

Along the same line, global natural gas consumption has also been forecasted to grow by 1.6 % per year for the next five years, from about 3,600 billion cubic meters (bcm) to almost 4,000 bcm by 2022.⁷ Natural gas is mainly used as fuel for generating electricity, accounting for approximately a quarter of the global electricity generated, as well as a fuel for heating processes in industry, and heating buildings and water in the residential sector. The demand from the industrial sector becomes the main engine of gas consumption growth, since natural gas also burns cleaner than coal or petroleum feedstocks.

However, these raw materials are finite, and if they will be used at the present consumption rates, these resources will run out in the forthcoming 120 years. Estimations based on the known reserves and annual production levels in 2015 predict that crude oil and gas reserves will become depleted by 2066 and 2068, respectively, leaving coal as the only remaining cost effective fossil fuel past this date, although this is also predicted to run out by 2129.⁸

Beside the limited repository, the use of fossil fuel resources leads to worldwide environmental problems, such as increasing CO_x and NO_x concentrations in the atmosphere, which contribute to the greenhouse effect responsible for global warming. For instance, coal, the largest source of energy for the generation of electricity across the globe, is also one of the largest CO₂ sources. In fact, CO₂ emissions increased by 3.4 % in 2013 due to the combustion of coal alone.⁹ Global awareness of these environmental issues have become increasingly visible in the last decades, initiating the development of greener policies with stricter control of emissions, and environmental regulations in order to prevent pollution and move towards a more sustainable chemical society.¹⁰

Moving towards sustainable chemistry thus requires solutions including: i) cleaner technologies involving the use of alternative feedstocks, to reduce the negative environmental impact; ii) process intensification, to reduce waste through a more efficient raw material utilisation; and iii) new/better catalysts, to obtain more efficient processes which diminish separation steps and energy cost, reducing the total economics of the process.

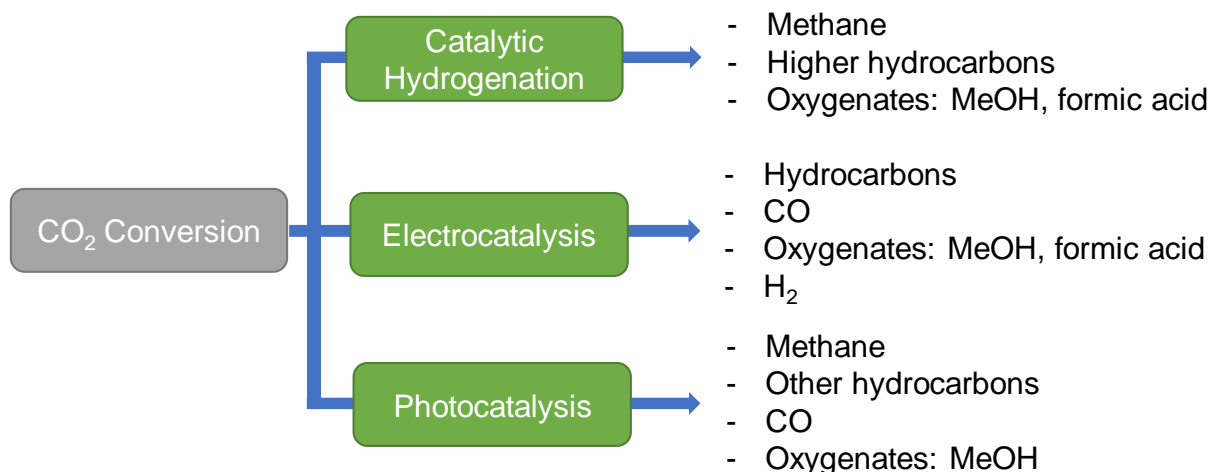
Therefore, increasing fossil fuel prices, depleting petroleum reserves, and promotion of environment-friendly processes have stimulated the industry to develop alternative sources to

the conventional feedstocks as raw materials for the continued production of energy and bulk commodity chemicals.¹¹

Amongst alternative feedstocks, renewables sources such as wind, geothermic, solar and hydro, or biomass present high potential for the production of energy supply. The electricity generated can be used for driving cars, heating homes, and fuelling industry, which are the major customers of fossil raw materials. In this regard, electrical vehicles which can include batteries, solar panels or electric generators to convert fuel to electricity have been extensively studied. For instance, fuel cells powered by H_2 can potentially operate as alternative energy supplier for vehicles. H_2 fuel cells can deliver CO_2 -free motoring and possess higher energy efficiency compared to internal combustion engine vehicles (2.5 times more). Nonetheless, one crucial point to have in mind is that H_2 does not naturally exist in its pure molecular form. Thus, H_2 must be derived from natural gas, oil or coal, with steam reforming of methane being the main source of H_2 nowadays. Alternatively, H_2 can also be sourced from renewable feedstock such as biomass or water, *via* water electrolysis, the latter being the most promising solution. However, low density of H_2 makes difficult the storage of enough supply to power the vehicle demand and thus, it is keeping it to be finally implemented as alternative to conventional combustion in a major scale.¹² Given the current disadvantages of this technology, hybrid vehicles, which combine internal combustion and electric engines, are expected to dominate the automotive market while a greener and more permanent alternative is developed. Accordingly, liquid fuels formed from biomass, which can potentially be used in the conventional combustion engines, are of high interest and their efficient development could highly contribute to reducing the environmental issues related to transportation.^{13,14}

However, the chemical industry is built upon carbon-containing materials, and therefore, it requires more sustainable C-based raw materials. Regarding alternative C-based raw materials for the petrochemical industry, the options are limited to either biomass or atmospheric carbon; the only two large scale sources of renewable carbon on the planet.

The use of atmospheric carbon (CO_2) may contribute to reducing climate impact while replacing the fossil fuel feedstock to generate valuable fuels and chemicals. The most promising technologies explored to convert CO_2 are based on catalytic hydrogenation and electro- and photo-catalytic processes (Scheme 1.1).



Scheme 1.1. Main catalytic routes for CO₂ conversion into valuable fuels and chemicals.

From the catalytic hydrogenation of CO₂, highly important industrial compounds can potentially be produced including methane, higher hydrocarbons and other oxygenated compounds such as alcohols (methanol) and carboxylic acids (formic and acetic acid). However, catalytic hydrogenation of CO₂ presents a key issue already mentioned, the generation of H₂. Typically sourced from steam reforming of methane, only its production from water splitting can truly reduce CO₂ emissions when employed for hydrogenation of CO₂, since it solely produces H₂ and O₂, while on the contrary, fossil fuels and biomass usually co-generate CO₂ and CO along with H₂. Although catalytic hydrogenation of CO₂ to methanol and methane are now at commercial scale, the efficient production of other compounds, that require the use of more active catalysts is still under investigation.¹⁵

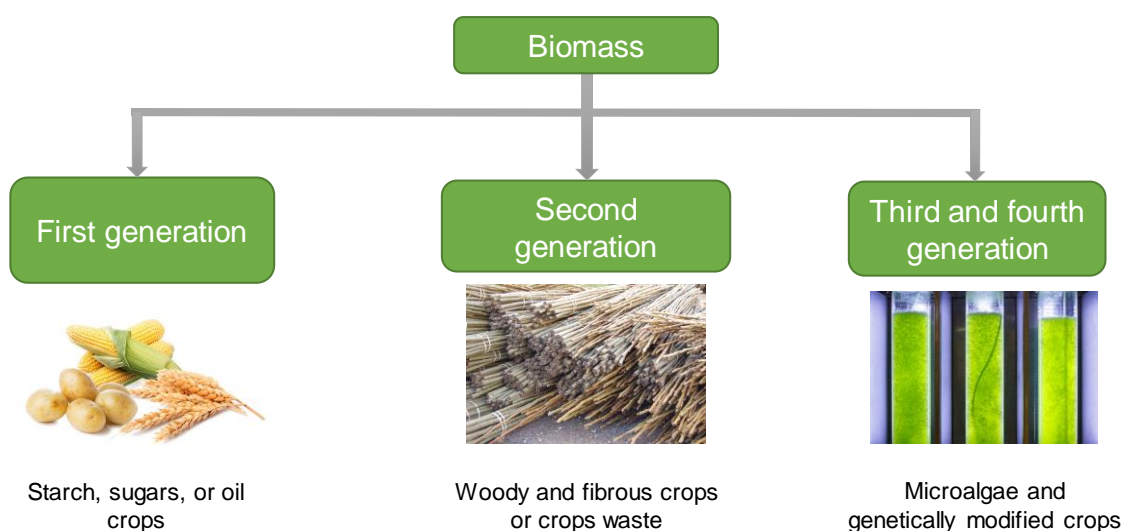
From electrocatalytic reduction of CO₂, especially over metal electrodes, also methane and higher hydrocarbons, small carboxylic acids, CO and H₂ can be generated. Nevertheless, despite many advances in this field, electrocatalytic CO₂ reduction generally suffers from high overpotentials and low current densities, requiring the development of quite complex systems and the maturity of this technology is still insufficient for practical implementation.¹⁶

Photocatalytic conversion of CO₂ can also give rise to methane and other higher hydrocarbons, formaldehyde and other oxygenated small products, and H₂. Photocatalytic transformation of CO₂ using solar energy is potentially more sustainable and favourable than other technologies because of zero addition of supplementary energy consumption and environmental deterioration. For such a phenomenon, the selective catalysts must have the desired band gap energy for visible light response. Some of the most studied groups of photocatalysts include semiconductor materials (TiO₂, ZnO, etc), graphene-based nanocatalysts and organometallic complexes, and their development is under continuous investigation in order to make this technology applicable to the industry.^{17,18}

Herein, although existing routes are currently being explored to convert atmospheric CO₂ to liquid products, they present low efficiency and productivity, and they are more complicated and expensive than those used for exploitation of plant-based resources, leaving biomass as the most realistic solution as alternative source to fossil fuels for the production of chemicals. Biomass valorisation into fuels and especially valuable chemicals is further discussed in the following section.

1.2 Biomass exploitation

Biomass refers to all organic matter generated through photosynthesis and many other biological processes.¹⁹ It can have a vegetal or animal origin, the vegetal source being the most exploited and also the most abundant.²⁰ Vegetal-based biomass includes waste (30 %), agriculture (27 %), forestry (23 %) and others (20 %). Agriculture englobes energy crops such as starch crops, sugar crops, grasses, woody crops or vegetal oils; forestry products include wood, trees and logging residues; waste materials include agricultural residues, wood wastes and urban wastes; and others include aquatic biomass such as algae and aquatic weed.^{21,22} Therefore, the composition of biomass is complicated due its heterogeneous nature. However, broadly, biomass can be classified as first, second, third, and fourth generation. First generation biomass refers to traditional plant biomass such as sugar, starch crops and vegetable oil. Second generation biomass refers to non-food parts of crops, and from other forms of lignocellulosic biomass, such as wood, grasses, agricultural and municipal solid wastes. Third and fourth generation biomass refer to algae-derived fuels such as biodiesel from microalgae oil, bioethanol from micro algae and seaweeds, and genetically modified crop.



Scheme 1.2. Biomass classification according to its origin.

As observed in the previous section (Fig 1.1), biomass contributes nowadays to approximately 10 % of the global energy demand and its use has been predicted to keep increasing with time. Comparatively with coal energy production, the production of energy from renewable sources is potentially CO₂ neutral as biomass absorbs CO₂ during growth and then emits it during combustion.¹⁰ Additionally, woody biomass virtually contains no sulphur, and thus co-firing with biomass results in reduced emissions of SO₂, NO₂, and fossil CO₂ per unit of energy produced as compared to using coal only.²³ This zero net greenhouse effect will allow to reduce greenhouse gas emissions. Furthermore, its utilisation could help avoid political problems between countries, since it is found in large quantities worldwide and each country has access to its own source from within its boundaries, in contrast to the current geopolitical and economic issues related to the unequal distribution of petroleum reserves, controlled mainly by United States, Saudi Arabia and Russia.^{24,25}

Consequently, in view of the globally demanded substitution of non-renewable fossil resources by a renewable source, biomass has been extensively studied in the last decades, since it represents a sustainable feedstock for the production of biofuels, commodity chemicals, and new bio-based materials such as bioplastics.²⁶

In light of this, biomass has emerged as a leading contender as an alternative resource (2.4 billion € market value in 2015), and it will be the only reliable source for organic carbon-based chemicals in the long term, making essential that cost-effective methods of bio-refinery are developed.^{27,28} Besides being a renewable source and/or a waste originated from human activity, and hence, an environmental-friendly feedstock, biomass feedstock is highly varied, allowing it to be processed for the production of fuel as well as for chemical and polymer manufacturing. However, currently, bio-based chemicals are under severe economic competition from those synthesised from petrochemical routes by processes that have been slowly optimised over the last 100 years.²⁹

Regarding its use as fuel source, initial utilisation of biomass for fuel production such as first generation of bio-ethanol from sugar cane or corn-based sugars opened an ethical debate due to the direct competition with food sources, although this issue was overcome by producing second generation biofuels from agricultural residues, wastes and grown energy crops, which do not compete directly with food sources.³⁰

The future potential for energy from biomass depends to a great extent on land availability. Currently, according to the Food and Agriculture Organisation (FAO), worldwide there are approximately 13 billion hectares (bha), of which 4.5 bha are suitable for crop production. 1.8 bha, out of this 4.5 bha, is used for non-agricultural purposes (urban or protected areas), leaving 2.7 bha of land available, from which 1.5 bha is dedicated to food crops. Hence, 1.2 bha of land may be potentially suitable, but unused to date, to grow energy crops for bio-energy in the future, nowadays, only 0.025 bha are used for this purpose.^{31,32} Nevertheless,

the ever growing population leads to increasing primary food demand, making it difficult to dedicate more land to grow energy crops, since they rely on the same land and water resources. Instead, bioenergy demand will have to rely on the current land available for energy crops, agricultural residues and waste to produce biofuels. Alternatively, advanced biofuels can be sourced from lignocellulosic crops. For instance, in 2012, 230 million L of cellulosic biofuel were available worldwide, although the cost of cellulosic ethanol is still considerably higher than first generation bio-ethanol.³²

Furthermore, the cost of producing fuels from biomass is currently higher than their oil-derived equivalents. The cost of biofuels depends on biomass feedstock price, which is correlated to its location and availability, but market fluctuation and processing costs are big factors that must be considered. Therefore, it is essential that biomass upgrading processes for biofuels are developed to match the existing infrastructure to minimise costs, because even with the benefits associated with them, they are still rather expensive, preventing their use to become more popular.

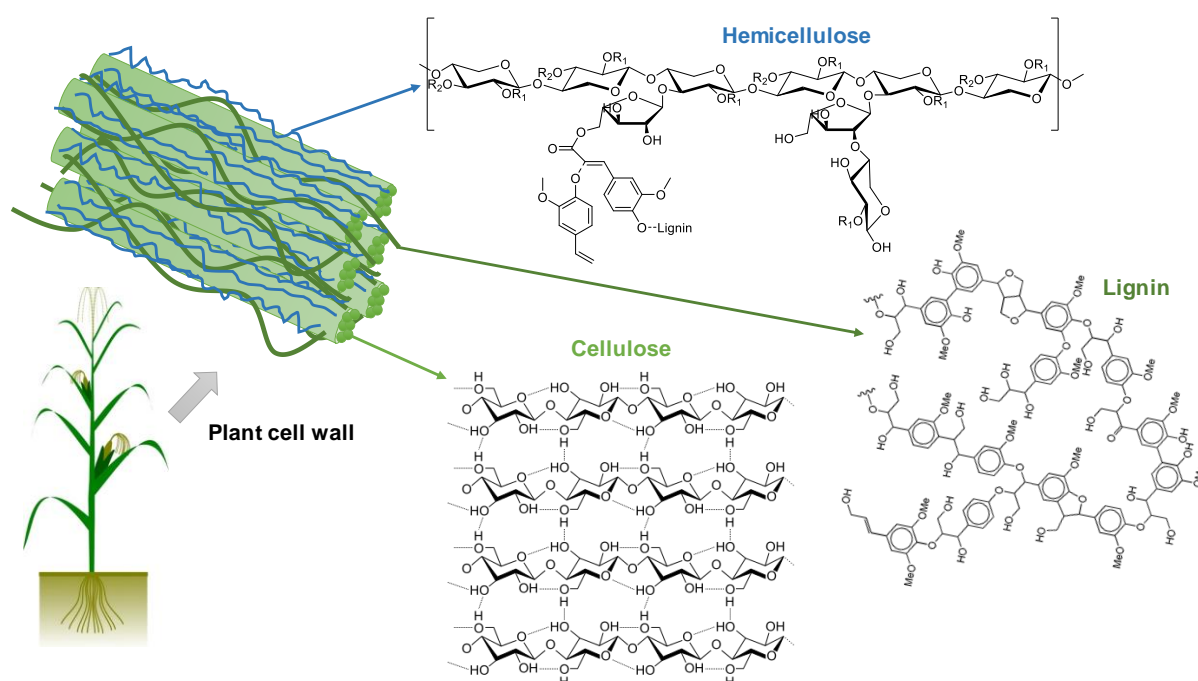
A more important key point, besides the cost, is that biofuels are mainly C-H based while the original structure of biomass is highly oxygenated and functionalised. Accordingly, the process to generate biofuels from biomass requires the removal of most of the oxygen, leading to a final product which has significantly reduced its mass, resulting in poor atom economy. Although the implementation of biofuels has already been gradually increasing in the transportation sector as short and middle term solution, the scale of biomass required to reach an equivalent amount of fossil resource for fuels is enormous, since biofuels contain half of carbon content of the classical feedstock. Herein, considering the complex relationship between food and biomass crops and the controversy arising from the employment of large quantities of forestry, the supply of enough biomass feedstock to fully replace conventional fuels is challenging, and thus, other technologies should be considered. Alternatively, the combination of biofuels with electrical engines in the hybrid cars, may result in a suitable approach to make biofuel production valuable as part of a more competent solution in the long term. Nonetheless, biofuels, such as bio-ethanol, have also started to be considered as platform chemicals for valuable biomass derived chemical production, thus, their continuous development is of high importance.

As a result of the disadvantages faced for the full replacement of conventional fuels for biofuels, the conversion of biomass into value-added chemicals, such as monomers and commodities, is a more ideal use of this resource. In this regard, the biomass feedstock available is sufficient to cover the global demand, since as already mentioned, only about 14 % of the petroleum consumed worldwide is used for the production of chemicals.

1.2.1 Lignocellulose valorisation

The potential use of biomass as chemical source is based on the fact that its diversity allows a wide range of different products to be obtained by chemical conversion. These products can potentially fit into already well established industrial processes and their high functionalisation allows also more versatile and completely new molecules to be synthesised. To be a viable contender in the replacement of fossil fuel feedstocks for chemical production, the matter must fulfil certain criteria such as: i) it must be producible in large enough quantities to make an impact on global energy demands, ii) it must do this without harming the food supply and iii) it must be inexpensive to produce and have less negative environmental impacts than the feedstock it is displacing.

Amongst all biomass sources, lignocellulose, the key structural element of plants, is the most abundant form of biomass, with an annual production of 170 billion tonnes.²² In view of this, lignocellulosic biomass is positioned as leading contender for fossil fuel replacement in the chemical production, as it is abundant, renewable and fulfils the criteria stated above.³³ However, lignocellulose matter composition is not homogeneous and depends on the type of lignocellulose source. Nevertheless, it always possesses this main three components: cellulose (30 - 50 %), hemicellulose (15 - 25 %), which are carbohydrate polymers, and lignin (15 - 30 %), which is composed of phenolic monomers.



Scheme 1.3. Representation of chemical structure of lignocellulosic biomass.

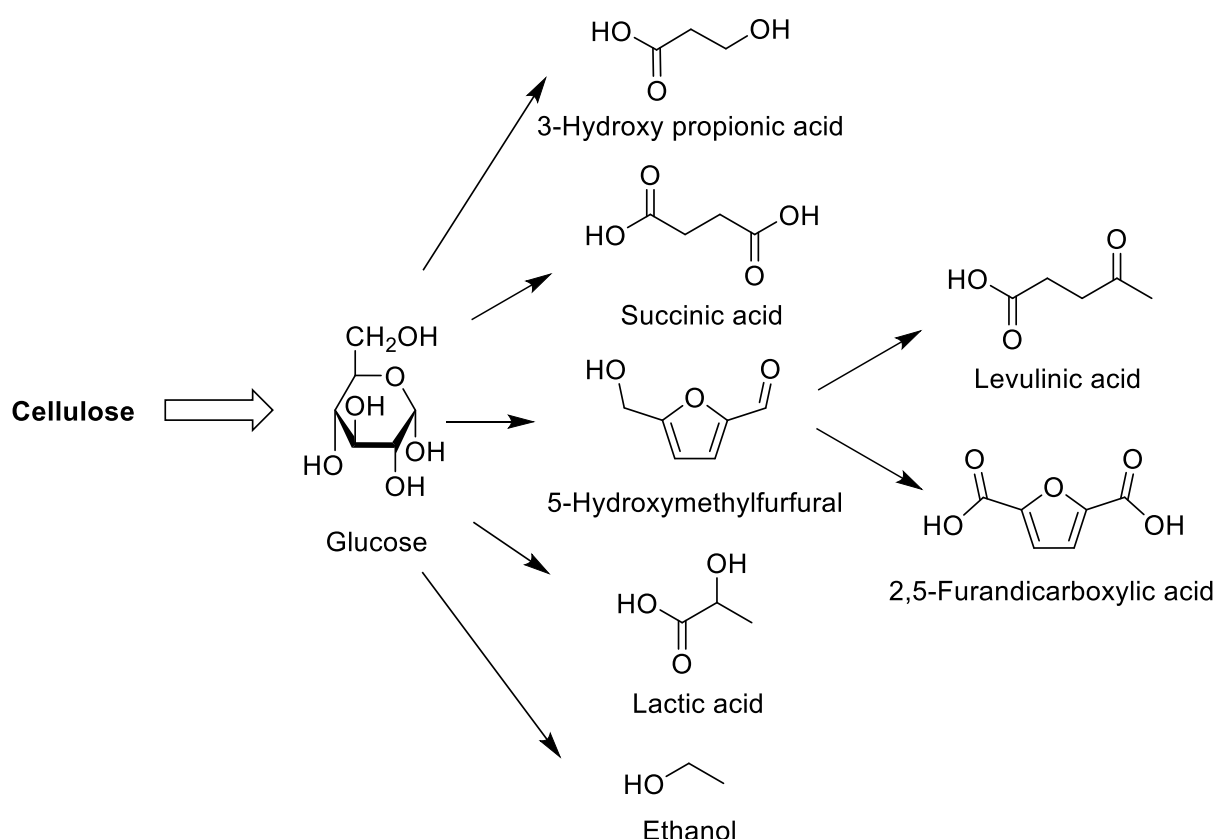
One of the major challenges of processing lignocellulose in general is that depolymerisation into smaller units is required, so that the constituent parts can be then further processed into final products such as bio-based chemicals and materials (such as bio-polymers).³⁴⁻³⁶ Various pre-treatments or fractionation methodologies exist to break down lignocellulose into its main components. Typical methodologies include biochemical transformation, mechanical fractionation and chemical pre-treatment, as well as combinations of those.³⁷ The kind of pre-treatment applied defines the chemical structure and polymeric nature of the resulting components, determining the whole future transformations derived from them. For instance, hydrolysis of cellulose and hemicellulose can be carried out enzymatically at mild operation conditions. However, lignin structure is generally unmodified by these processes, and the rates of hydrolysis are usually low.

Amongst the chemical pre-treatments available, pulping methodologies are employed to obtain high quality cellulose, regardless of the final state of the rest of the components. In these kind of methodologies, an acid is used at high temperatures to separate cellulose, and sometimes hemicellulose, while the resulting lignin suffers severe structural modifications.³⁸ The Organosolv process is often used as alternative of the acid hydrolysis and consists in the employment of organic solvents and water as co-solvent at high temperatures to extract lignin from the biomass matrix. During the process also hemicellulose is hydrolysed, leaving cellulose in the pulping fraction, which can be further enzymatically hydrolysed.³⁹

Interestingly, Reductive Catalytic Fractionation (RCF) has arisen as promising approach to separate lignocellulose into a solid carbohydrate pulp mix and a stable liquid lignin oil, which can be processed separately, simplifying the downstream separation steps. During RCF, native lignin is extracted from the biomass, followed by immediate depolymerisation and reductive stabilisation. Then, the remaining cellulosic carbohydrates in the solid fraction can easily be retrieved as a pulp upon filtration of the reaction mixture. Employing this methodology, hemicellulose can either be retained in the pulp or solubilised with the lignin, depending on the procedure followed.⁴⁰

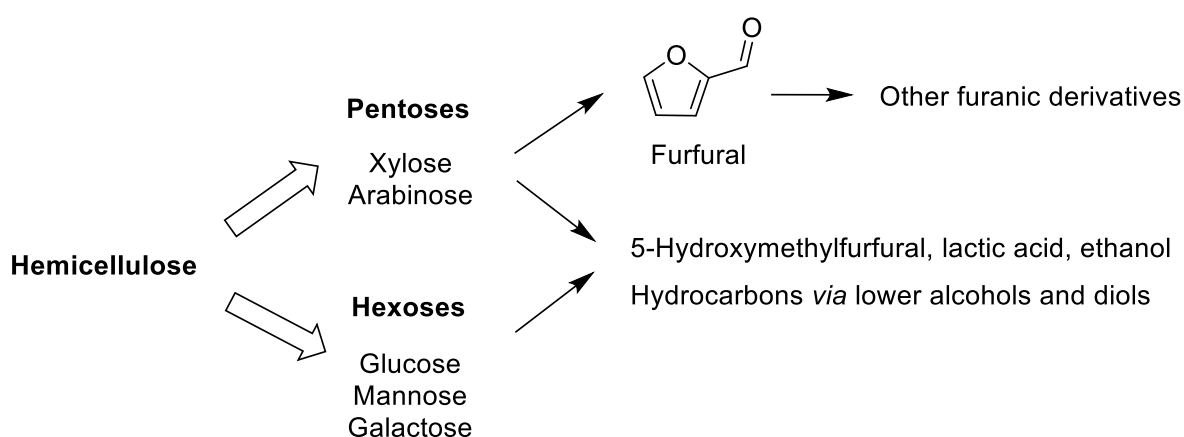
Although several advances have been made regarding effective fractionation of lignocellulose and improvement in the quality of the resulting fractions, the upstream process of lignocellulose to break it down to its main components is complex. Currently, most of the processes are still not cost-effective, and those that are cannot guarantee good quality of all the lignocellulosic components. However, continuous investigation of the upstream lignocellulosic biomass valorisation is moving forwards, allowing researchers to confidently focus attention also on the development and optimisation of the downstream processes derived from the lignocellulose components, in order to produce valuable chemicals. Herein, the downstream chemical productions emerged from cellulose, hemicellulose and lignin are discussed in more detail below.

Cellulose is composed of a crystalline carbohydrate polymer, formed by glucose units attached through β -linkages (1 \rightarrow 4). The structure generates linear chains that are highly stable and resistant to chemical attack because of the high degree of hydrogen bonding that typically occurs between chains. Chemical or enzymatic hydrolysis can break down cellulose to a cellobiose repeating unit, and finally to glucose monomers, the most common pathway being enzymatic hydrolysis, which gives rise to fermentable sugars. Then these sugars can be transformed into a variety of important building block chemicals and subsequently converted into high-value chemicals, often with lower functionality and reduced oxygen content. Some of the glucose derived valuable chemicals are succinic acid (SA), lactic acid, 3-hydroxy propionic acid (3-HPA), 5-hydroxymethylfurfural (HMF), ethanol and other liquid fuels, and most of these transformations can be produced on industrial scale by fermentation.^{41,42} Subsequently, the transformation of these platform molecules into a variety of commodity chemicals usually relies on catalytic conversion. For instance, HMF can be converted into 2,5-furandicarboxylic acid (FDCA) by oxidation over supported noble metal catalysts.⁴³



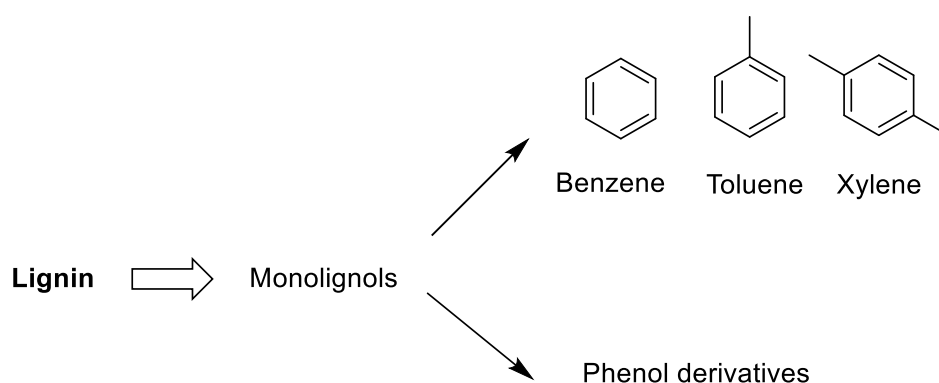
Scheme 1.4. General scheme for cellulose valorisation to glucose and its consequent pathways to some high-value chemicals.

Hemicellulose is an amorphous polymer which consists of short, highly branched chains of sugars. In contrast to cellulose, which is a polymer of only glucose, hemicellulose contains different sugars (such as xylose, arabinose, mannose, glucose and galactose). Analogously to cellulose, hemicellulose hydrolysis can be carried out by chemical or enzymatic transformations, the latter being the most employed. The branched nature of hemicellulose renders it amorphous, making it relatively easy to hydrolyse to its constituent sugars compared to cellulose. Subsequently, the generated pentoses and hexoses can be catalytically dehydrated to form products such as furfural (FF) and furfural derivatives.^{44,45} Additionally, pentoses and hexoses can also source hydrocarbons *via* formation of lower alcohols and diols by both chemo- and bio-catalytic strategies.³⁹



Scheme 1.5. General scheme for hemicellulose valorisation

Lignin is a non-carbohydrate amorphous polymer formed mainly of phenolic monomers.⁴⁶ It is a highly polymeric substance, with a complex, crosslinked, aromatic structure and high degrees of condensation and polymerisation, which makes it a challenging material to break down. Depolymerisation of lignin into smaller units *via* chemo- and/or bio-catalytic processes allows to obtain the aromatic ring molecules derivatives (such as benzene, xylene and phenol derivatives).⁴⁷ Lignin is not widely used commercially due to its low reactivity derived from its stable chemical structure and the difficulties faced to retrieve it intact from the lignocellulose fractionation. Alternatively, it is mainly used for energy and heating generation through its burning. However, it accounts for up to 30% of the energy in biomass and is the most abundant carbon source available in nature, so effective utilisation of this biomass component would greatly improve the economic viability of bio-refinery processes for second generation biofuels.



Scheme 1.6. General scheme for lignin valorisation.

Herein, the examples exposed above show the great potential of lignocellulose downstream conversion into valuable chemicals. Likewise, a large number of technologies based on biological, thermal, and chemical processes have been developed for biomass valorisation.⁴⁸ Although biological catalysis and fermentation generally dominate the breakdown of cellulose, hemicellulose and lignin into the initial platform molecules (C5 and C6 sugars and monolignols), chemical processing has gathered special attention to achieve further valorisation into commodity chemicals, since its resulting products can present very similar characteristics to fossil fuel-based products.

As occurs in the modern petrochemical industry, this is where catalysis plays an important role, enhancing the reaction rates and increasing the sustainability of the processes by avoiding stoichiometric reactions.⁴⁹ Although homogeneous catalysts can also be used for biomass valorisation, heterogeneous catalysts are more attractive for multiple reasons, including: i) variety of facile preparation methods, ii) low production costs, iii) high resistance to common reaction conditions, iv) durable lifetime and v) easy recovery from the reaction mixture, which may allow reusability, and generally lead to great industrial advantages.⁵⁰

The variety of heterogeneous catalysts that can be used for lignocellulosic biomass derivatives valorisation is enormous, in accordance with the huge variety of chemicals that can be sourced from them in order to mimic existing petrochemical processes as well as developing new routes to new bio-based chemicals. For example, many of the transformations involving lignocellulosic derivatives, such as glucose transformation to HMF *via* fructose, require acidic features, which can be provided by Brønsted and/or Lewis acidic solid catalysts such as heteropoly acids, zeolite-based catalysts, sulfonated solids and functionalised carbon materials amongst others.^{49,51,52} Additionally, most of the bio-derived platform molecules are often highly functionalised and oxygenated, requiring hydrogenation steps in order to yield several value-added chemicals, which can be carried out over noble metal supported materials. Hence, the choice of the kind of catalyst must be carefully thought, considering the targeted chemical transformation, compatibility of solvents and reaction conditions.

1.3 Bio-based polymers

In the chemical industry, polymers represent an enormous field; over 300 million tonnes of plastics are produced worldwide every year, and this quantity is continuously increasing.⁵³ Polymers are present in all daily commodity items such as plasticware for storage and packaging, synthetic fabrics, automotive and adhesives, as well as in tailored materials including biomedical devices, separation membranes, microelectronics and surface coatings, amongst others. In order to cover all this wide-range of applications, the polymer family is highly diverse and versatile with highly tuneable properties. For instance, a polymer can be stiff or soft, transparent or opaque, permeable or impermeable, conducting or insulating, amongst other physical and chemical properties, which will be entirely depending on their chemical structure.³⁴ In turn, their chemical structure depends on the nature of the constituent monomer (homopolymer) or monomers (heteropolymer or co-polymer), the chain structure adopted and the interactions between chains.

Unfortunately, at present, almost all polymeric materials are petroleum-based. Considering the globally increasing concerns on this fossil fuel feedstock environmental negative impact and its prompt depletion, as stated above in Section 1.1, investigation of sustainable monomers for the synthesis of polymeric materials with comparable or superior properties than their petroleum-based analogues has become a growing area of research interest.

The emerging bio-economy, and the development of improved routes to bio-derived chemicals from biomass, is offering the opportunity to source several bio-based monomers as replacements to the oil-derived ones. These monomers are potential candidates for polymer synthesis. In this regard, poly(lactic acid), obtained from renewable lactic acid *via* sugar fermentation, is currently being commercialised, representing a significant breakthrough.⁵⁴ In spite of this fact, nowadays only about 1 % of the polymers produced come from renewable sources,⁵³ hence, a lot of effort is being made to keep improving this percentage.

Having this in mind, tackling this great challenge requires: i) the improvement of bio-based catalytic routes towards already employed renewable monomers, in order to make them more economically profitable and competitive to the existing petroleum-based analogues, and/or ii) the development of new bio-based routes to investigate new monomer structures, given the highly oxidised original molecular structure of lignocellulosic biomass, which can supply additional functionalities to tailor physical properties of the final polymeric material and enrich the variety of the polymers catalogue.

In view of this, a broad assortment of biomass derived platform molecules is suitable to give rise to some of the primary monomers most commonly used in the polymer industry: diols, diacids and lactones. For example, as mentioned in Section 1.2.1, HMF and FF, obtained from catalytic lignocellulosic biomass valorisation, can be used as platform molecules for several

renewable monomers formation, e.g. FDCA, a diacid which constitutes a possible replacement for terephthalic acid and isophthalic acid for polyester formation.^{55,56} Additionally, catalytic reduction and hydrogenolysis of FF and HMF can lead to diverse cyclic and open chain diols such as 1,4-butanediol (BDO) or 1,6-hexanediol (1,6-HD).^{57,58} BDO can be used as monomer for poly(butylene terephthalate) and also poly(butylene succinate) formation, the latter by co-polymerisation with SA, obtainable from sugar fermentation.⁵⁹ Another example of renewable monomers from biomass derivatives can be itaconic acid, another diacid, which can be obtained from sugars fermentation and can potentially be used to substitute petrochemical-based acrylic or methacrylic acid mainly used as monomers or co-monomers in a variety of polymers with a broad spectrum of applications. Additionally, poly(itaconic) acid can be employed as superabsorbent.⁶⁰ The use of lactones as monomers is discussed in detail in the following section.

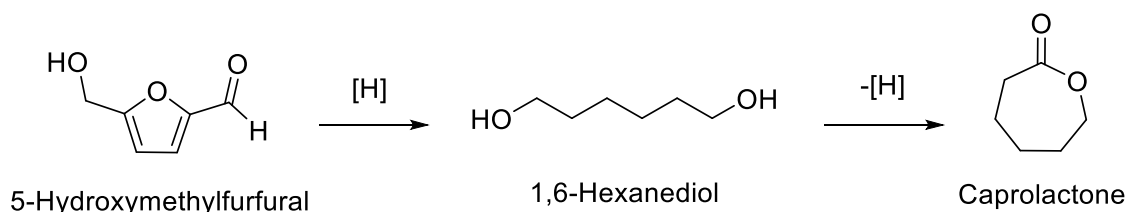
1.3.1 Lactones as renewable monomers and bio-chemicals

Amongst all the different kinds of monomers that can be obtained from lignocellulosic biomass, the family of the lactones comprises a variety of sizes and substituent groups in the ring which make them attractive chemical compounds to be used as monomers. Their versatility makes them suitable to be used as homopolymer sources as well as for co-polymer sources, opening a range of possibilities to tailor the polymer properties and prepare polymeric materials by design. For instance, many different combinations involving lactone monomers have been successfully reported to improve thermostability, bio-degradability, bio-compatibility, mechanical properties and other properties of the final polymer. Some of the multiple examples found in literature are co-polymerisation of D-gluconolactone with citric acid,⁶¹ ϵ -caprolactone (Capr) with lactic acid^{62,63} and γ -butyrolactone (GBL) with ω -pentadecalactone,⁶⁴ allowing to fine tune specific characteristics of the final material. Some of the most relevant lactone molecules that can be derived from lignocellulosic biomass are Capr and substituted caprolactones (R-Capr), GBL and γ -valerolactone (GVL), each of which constitutes a valuable building block in the polymer industry. Hence, a brief description of each of these lactones as monomers and how they can be obtained from lignocellulose derivatives is discussed next.

Capr is produced in about 50,000 tonnes per annum and used for the synthesis of caprolactam. Caprolactam is a precursor of Nylon-6, used as resistant fibres in textiles and carpets and molded parts used as insulator or pipes.⁶⁵ Furthermore, Capr also is used to produce poly(caprolactone), a biodegradable polymer with a low melting point, used in many pharmaceutical and medical applications.^{66,67}

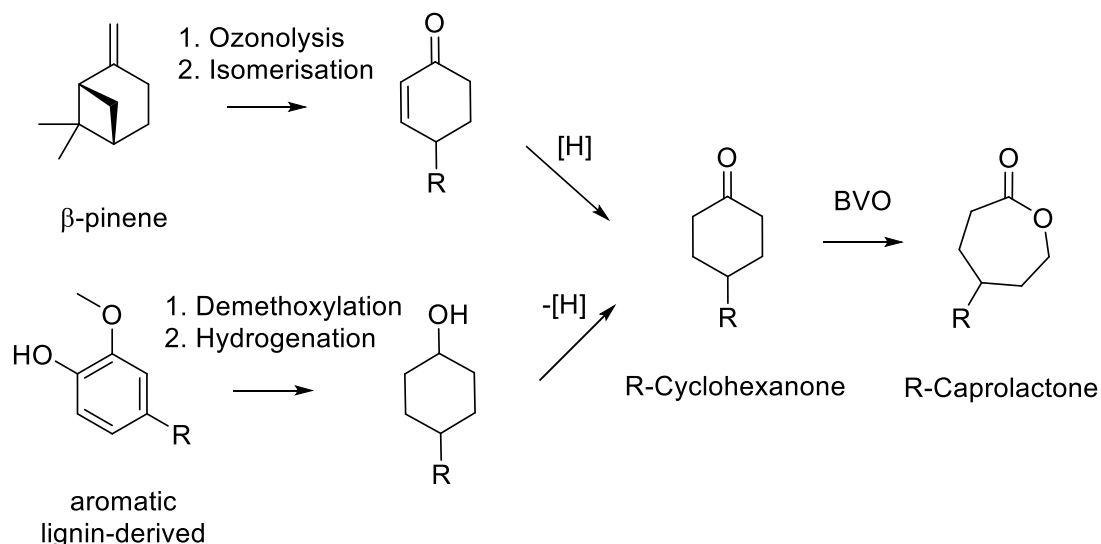
Typically, Capr is industrially produced from petroleum-based cyclohexanone (CyO) *via* Baeyer-Villiger Oxidation (BVO) reaction with peroxyacid-based oxidants. However, progress

has been made towards the finding of a sustainable route to Capr. For instance, the production of Capr was successfully reported by Buntara *et al.*⁶⁸ from HMF, obtainable from sugars, in a five-step synthesis *via* 1,6-HD as intermediate, reaching a maximal selectivity to the desired lactone of 95 % in the overall process. Most recently, a techno-economic analysis in two-steps has also been described by Thaore *et al.*⁶⁹ in regards of the same synthetical route.



Scheme 1.7. Sustainable catalytic route for Capr formation from bio-derived HMF.

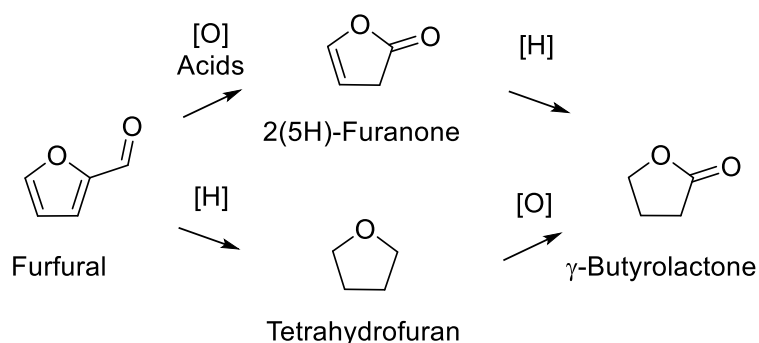
Another important approach to produce Capr and R-Capr from renewable sources is the use of renewable CyO and substituted cyclohexanones (R-CyO) and the subsequent BVO reaction to give rise to the corresponding lactone, whose sustainability can be further explored as it is discussed along this work. CyO and R-CyO can potentially be obtained from selective hydrogenation of lignin-derived phenols (e.g. anisole) over Pd or Ni catalysts;^{70,71} and also from terpenoids such as β -pinene.⁷² For instance, γ -methyl- ϵ -caprolactone (4-Me-Capr) can potentially be obtained from *p*-cresol (lignin-derived) or *p*-cymene (terpene-derived) and can also be used for the production of thermoplastic elastomers.⁷³



Scheme 1.8. Representative routes for the production of R-Capr *via* BVO of R-CyO.

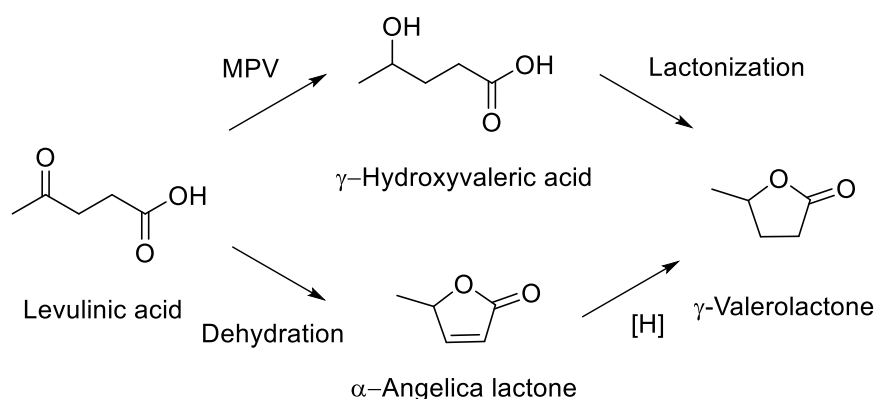
GBL is produced in about 50,000 tonnes per year in Europe, and has a wide range of uses, its use as solvent being the main example. Focusing in the polymer industry, GBL is a precursor of N-methyl-2-pyrrolidone (NMP) and N-vinyl-2-pyrrolidone (NVP) which can be used as monomers. Until now, GBL has been normally considered a “non-polymerizable” monomer due to its low strain energy of the five-membered ring. However, it has been recently successfully polymerised through ring opening mechanism and effectively employed to source poly(butyrolactone) and as co-monomer to modulate material properties of polyesters.^{74,75}

Currently, GBL is conventionally produced by the direct hydrogenation of maleic acid anhydride or *via* dehydrocyclisation of BDO.⁷⁶ However, the demand for the development of new, cheap bio-based platform chemical for its production has increased, pointing to SA to be the most promising alternative chemical feedstock for its production since it has already started to be commercialised from sugar fermentation.⁵⁵ The selective hydrogenation of SA to GBL is discussed deeper in Section 1.3.1.2.3. Interestingly, GBL can be also obtained from FF. One approach for this synthetical route was reported by Lange *et al.*⁷⁷ by first transforming FF to THF, followed by its oxidation to GBL. Alternatively, selective oxidation of FF to GBL in two steps was reported by Li *et al.*⁷⁸ *via* 2(5H)-furanone as intermediate.



Scheme 1.9. Alternative routes for the production of GBL from bio-derived FF.

GVL is a value-added renewable chemical with great potential as platform chemicals for the production of liquid transportation fuels. GVL can be successfully produced by the selective hydrogenation of levulinic acid, obtainable from bio-derived sugars. This transformation has been reported by two different reaction pathways: levulinic acid transfer hydrogenation *via* γ -hydroxyvaleric acid followed by lactonization, or levulinic acid dehydration *via* α -angelica lactone followed by hydrogenation, as shown in Scheme 1.10.⁷⁹⁻⁸¹



Scheme 1.10. Representation of the reaction pathways from levulinic acid to GVL.

Although at the present, GVL has not been reported as a monomer itself, various derivatives such as α -methylene- γ -valerolactone (MGVL) and methyl pentenoates have been of interest for polymerisation. For example, the structure of MGVL is similar to methyl methacrylate (MMA) making its investigation attractive for the polymer industry.⁸²

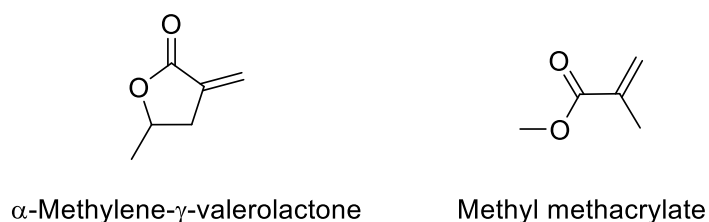


Figure 1.3. Representation of MGVL and MMA.

Lactone monomers can generally undergo ring opening polymerisation (ROP) mechanism in order to assemble the polymeric material. Typically, lactones possessing 4, 6 - 8 membered-ring are suitable for ROP, which can be anionic or cationic depending on the kind of catalyst employed. However, as mentioned above, the 5 membered-ring lactone GBL has recently been successfully polymerised by ROP. Additionally, ROP can usually be easily controlled to synthesise polymers with a targeted molar mass and low polydispersity index.⁸³

Importantly, many polyesters derived from lactone monomers are also bio-degradable, and if those are obtained from renewable feedstocks, the sustainability of the process is remarkably increased, e.g. the already mentioned poly(caprolactone).

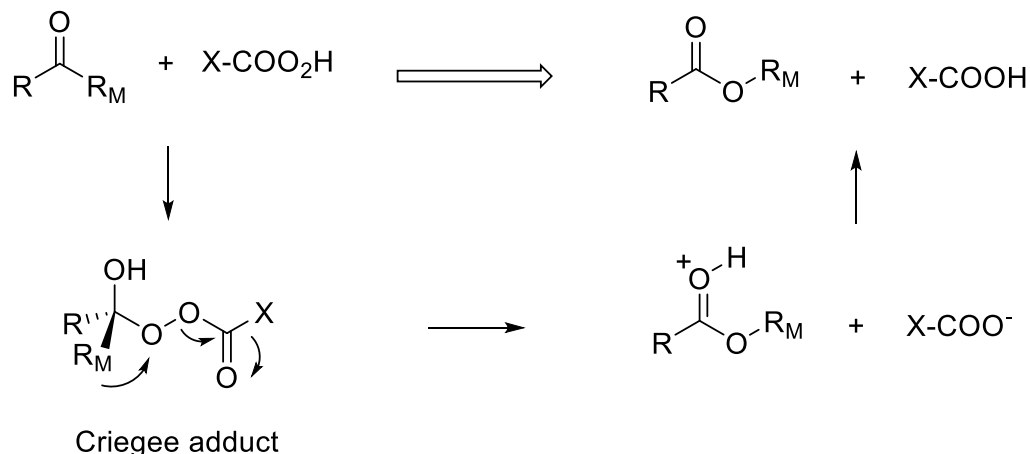
Herein, the obtainment of lactone monomers by various catalytic routes that can later suitably undergo ROP constitutes the central point of this work. Amongst several other catalytic routes available to produce lactones, this work is focused on two approaches: the BVO reaction, and the selective hydrogenation reaction of SA to produce the desired corresponding lactones.

1.3.1.1 BVO derived lactones

1.3.1.1.1 Classic BVO with peroxyacids

The first BVO reaction was reported by Adolf Baeyer and Victor Villiger in 1899 to convert a cyclic ketone into the corresponding lactone with a peroxyacid as oxidant.⁸⁴ This chemical transformation has been widely studied since its discovery and employed industrially to convert ketones into more valuable chemicals such as lactones and esters. An excellent example of that is the industrially used BVO of CyO to Capr using *meta*-chloroperoxybenzoic acid (*m*CPBA).

The key of the success of the BVO reaction relies on the compilation of several intrinsic advantages. Firstly, it is chemo-selective, and tolerates the presence of other functional groups in the molecule, *i.e.* the reaction can occur even in the presence of unsaturated ketones with a C-C double bond. Secondly, it is regio-selective; in order to form the corresponding lactone or ester, the BVO will always take place according to a migratory aptitude scale of the different adjacent groups, *i.e.* the insertion of the oxygen takes place between the carbonyl and the more substituted carbon atom neighbour (migratory preference: tertiary > secondary > primary > methyl). Finally, it is stereo-selective, and chiral carbon atoms will retain their absolute configuration in the product formed.⁸⁵



Scheme 1.10. Mechanism of BVO proposed by Criegee where R_M represents the migrating group.

The most accepted mechanism was proposed by Criegee about 50 years ago, described in Scheme 1.10.⁸⁶ In this mechanism, the BVO reaction proceeds through a two-step process which consists in an initial nucleophilic attack of the oxidant at the carbonyl group followed by the migration of one of the adjacent alkyl groups onto the peroxygen and the subsequent release of the carboxylic acid moiety, to form again the C=O on the lactone or ester product formed. Generally, the migration step is the rate determining step of the reaction.

The most popular peroxyacid-based oxidants employed for BVO reaction are *m*CPBA, trifluoro peroxyacetic acid (TFPAA), peroxybenzoic acid and peroxyacetic acid. However, the use of peroxyacid-based oxidants presents several drawbacks such as: i) their low active oxygen content, e.g. TFPAA active oxygen content is 9.2 %, ii) their potential explosiveness, iii) the co-production of by-products that require separation, *i.e.* carboxylic acid as leaving groups, iv) the requirement for undesirable chlorinated solvents and v) their lack of selectivity due to the ability of the peroxyacids to oxidise other functional groups present in the substrate.⁸⁵ Accordingly, significant effort has been made in order to replace the peroxyacid-based for a greener oxidant, such as hydrogen peroxide (H₂O₂), which is discussed in detail in Section 1.3.1.1.3.

1.3.1.1.2 Enzymatic BVO

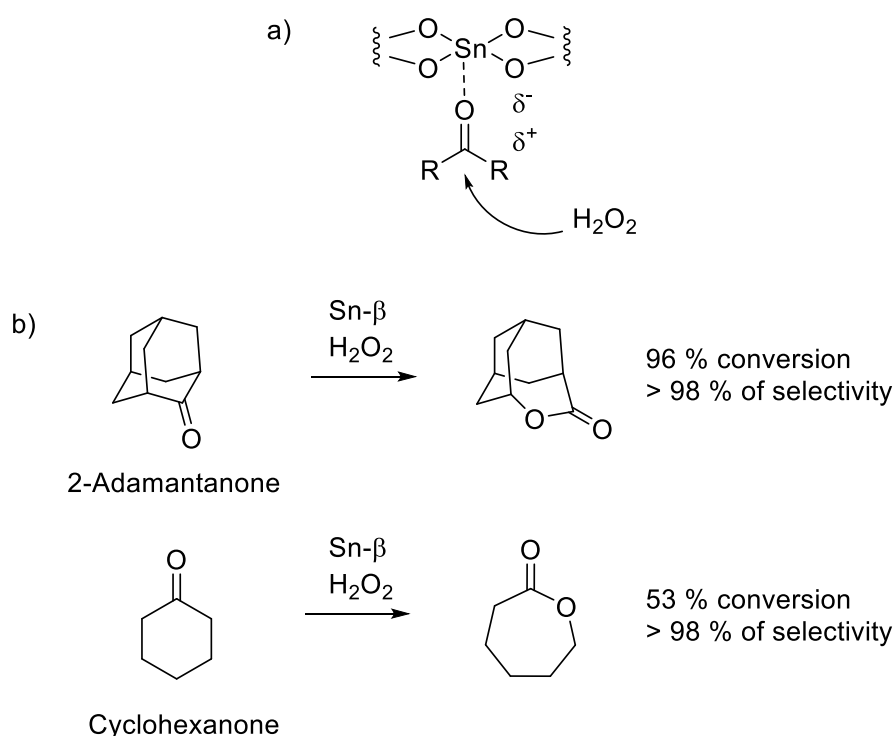
Another relevant approach for the synthesis of lactones *via* BVO transformation involves the use of enzymes. This kind of enzymes are a type of flavoenzymes known as Baeyer–Villiger monooxygenases (BVMOs), produced from numerous bacteria. Amongst this big family of BVMOs, cyclohexanone monooxygenase (CHMO) from *Acinetobacter calcoaceticus* is the best characterised and one of the most efficient, since it has proved to oxidise more than 80 different ketones, often with very high enantioselectivities.⁸⁷ It should be mentioned that the use of BVMOs allows to perform BVO transformation with outstanding degrees of selectivity, especially in asymmetric BVO transformations to access optically pure organic compounds. However, generally, they are very energy demanding, with rigid operational conditions that do not allow high productivities to be achieved, nor provide much operational flexibility. Moreover, they often present substrate and/or product inhibition, disfavours the development of cost-effective processes and limiting their utilisation for large-scale processes. For these reasons, finding alternatives to enzymatic biocatalysts is of crucial importance for developing a sustainable chemistry that uses biomass as starting materials. In this regard, heterogeneous catalysis offers a very good alternative for this kind of chemistry, as its role in the BVO reaction system is discussed in the following section.

1.3.1.1.3 Catalytic BVO reaction using Sn-β and others

As mentioned briefly at the end of Section 1.3.1.1.1, many efforts have been made in the last decades to replace the peroxyacid-based oxidants for greener and potentially cheaper, H₂O₂ being a very promising candidate. The use of H₂O₂ presents multiple benefits such as i) higher active oxygen content (47 %), and ii) it only produces H₂O as by-product, avoiding the issues of the separation of the carboxylic acid formed with the peroxyacid-based oxidants and resulting more environmentally friendly.

However, it has been reported that the reactivity of H_2O_2 is lower than most of the peroxyacid-based oxidants, requiring the use of a catalyst to activate the oxidant, by forming more nucleophilic M-OOH species, where M represents a transition metal.⁸⁵ In this regard, various homogeneous catalysts, especially Pt-based, as well as heterogeneous catalysts such as Ti containing zeolites, e.g. Ti-silicalite-1, have been reported to suitably activate H_2O_2 for the BVO reaction.^{88,89}

In an alternative approach, the carbonyl group can also be activated using a Lewis acid, instead of activating the oxidant, in order to promote the reaction. This approach was firstly reported by Corma *et al.*⁹⁰ by using zeolite beta (β) containing Sn incorporated in the framework ($\text{Sn-}\beta$) for the BVO of 2-adamantanone and CyO. In said report, 96 % of 2-adamantanone was converted at a lactone selectivity > 98 % after 6 h of reaction. Similarly, 53 % of CyO conversion with > 98 % of lactone were reached after 3 h. The success of this report opened up the usage of different kinds of solid Lewis acid catalysts, which have proven to be very efficient for reactions involving carbonyl groups.



Scheme 1.11. a) Representation of the activation of the carbonyl group by $\text{Sn-}\beta$ described by Corma *et al.* and b) scheme of BVO reaction of 2-adamantanone and cyclohexanone.⁹⁰

Amongst several metals potentially suitable to be incorporated in zeolites, mesoporous ordered catalysts or clays, notable examples being Fe, Ti, Zr or Sn, Sn-based catalysts are the most commonly employed for BVO reactions using H_2O_2 as an oxidant. In the last two

decades, several examples involving Sn-catalysts have been published, focusing mainly on the BVO reaction of either CyO or 2-adamantanone. Some of the most relevant results are stated below.

Sn-palygorskite was reported by Lei *et al.*⁹¹ as suitable catalyst for the BVO of 2-adamantanone, CyO and various other cyclic ketones, obtaining 100 % of 2-adamantanone conversion with 100 % of selectivity towards the lactone after 24 h, while only 16 % of CyO conversion with 90 % of lactone selectivity was reported after the same reaction period. The use of Sn-MFI was reported by Jinka *et al.*⁹² reaching 100 % of 2-adamantanone and norboranone with 100 % of lactone selectivity after 8 h of reaction. Recently, Sn-MFI nanosheets have also been successfully reported by Luo *et al.*,⁹³ obtaining 99 % of 2-adamantanone conversion and > 98 % of lactone selectivity after 16 h of reaction. Sn-MCM-41 has also been reported by Corma *et al.* for BVO of 2-adamantanone and CyO. While 94 % of 2-adamantanone conversion with > 99 % of lactone selectivity could be observed after 7 h of reaction, only conversion values < 40 % have been reported for CyO, although at high lactone selectivity (> 97 %).^{94,95} Similar materials such as Sn-SBA-15 have been also reported for BVO of CyO, showing > 60 % of conversion with 88 % of selectivity to the lactone after 4 h.⁹⁶

From this selection, it can be noticed that the obtainment of high selectivity towards Capr in the BVO of CyO is challenging, the result with Sn- β reported by Corma *et al.* being only the one that reached high conversion with high selectivity.⁹⁰ After this report, many researchers have intensively studied the synthesis of Sn- β and its catalytic application for the BVO reaction.⁹⁷⁻⁹⁹

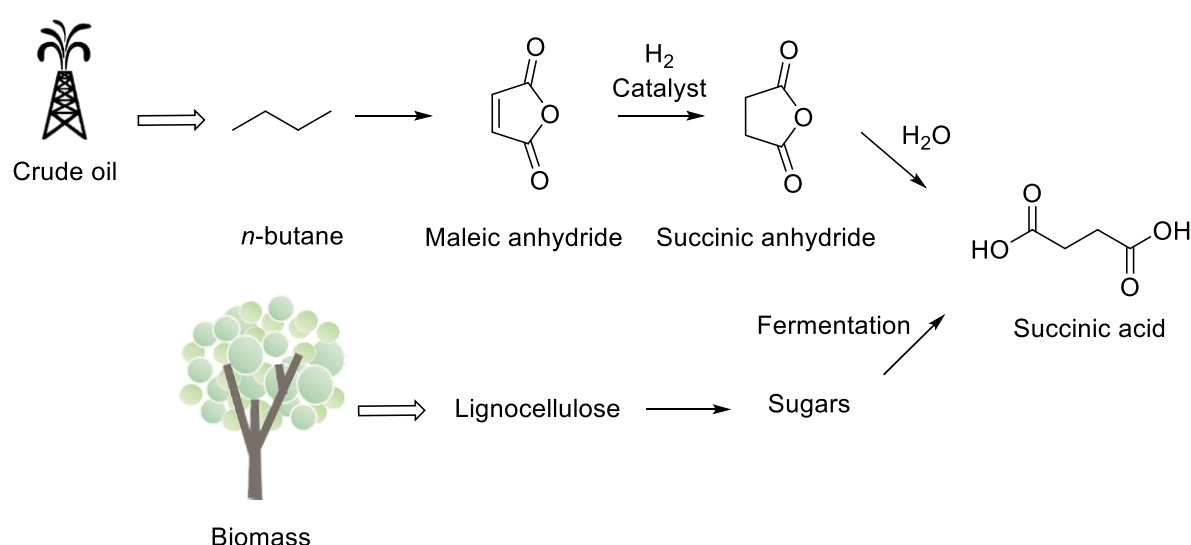
However, at the time of this work, many essential challenges remained on the BVO of CyO employing H₂O₂ as oxidant and Sn- β as catalyst, including: i) the drop of selectivity often observed at high levels of conversion, ii) the disclosure of the full reaction network, iii) the study of potential scalability of the system, particularly in the continuous regime, and iv) the broadening of the substrate scope beyond CyO using this system. Accordingly, these are some of the key points that this work will cover along with others.

1.3.1.2 Selective hydrogenation derived lactone

As already mentioned in Section 1.3.1, selective hydrogenation of platform molecules can also give rise to lactone products. Amongst some of the example displayed above, the selective hydrogenation of SA to GBL is one of the subjects of interest in this work, since GBL is not only valuable for the polymer industry, but also for bulk chemical production. The attractiveness of this transformation relies not only in the value of GBL itself, but also on the increasing production of SA from renewable sources and its promising use as C4 platform molecule.

1.3.1.2.1 SA from renewable sources

SA is commonly produced in bulk (approximately 25,000 tonnes per year) from maleic anhydride (MAN) which is petrochemically sourced from *n*-butane oxidation.²⁹ The most direct route is a two-step process *via* succinic anhydride as intermediate which is later hydrated to give rise to SA. This reaction is usually performed in the liquid-phase, at temperatures ranging 120 - 180 °C and H₂ pressure < 40 bar, under metal-based catalysts, typically Ni or Pd.¹⁰⁰ However, MAN price has been gradually increasing in the last decade due to less cracking of crude oil to source *n*-butane. Therefore, the amount of MAN produced has also diminished. This fact, besides the increasing global awareness to move towards more sustainable chemical processes, makes it essential to find alternative routes to source SA.



Scheme 1.12. Petrochemical and bio-derived routes for the production of SA.

With this aim, bio-derived SA (BioSA) production has been widely studied over the last decade, its production *via* the fermentation of sugars being the most predominantly employed. Fermentation is an energy-deriving reaction in eukaryotic and prokaryotic organisms, which converts a simple carbon source into various alcohols. This reaction is more specifically carried out by bacterial or fungal cells that possess specific genes encoding enzymes necessary for their pathways. Each pathway contains its own distinctive intermediates, co-factors, and enzymes.

Recent advances in fermentation and purification technologies have succeeded in making BioSA economically attractive. As of 2014, five different groups are active in commercial scale capacity development, Bioamber and Myriant Technologies being the two leading bioSA producers.¹⁰¹ For instance, BioAmber fermentation performance achieved in 2015 was significantly above the initial targets, and the yield and productivity levels already exceeded

the targets the plant was designed to hit longer term, hence, they opened its first commercial plant to increase production volumes progressively to reach full capacity in 2017, with \$12 million in BioSA sales. Although unfortunately BioAmber went bankrupt in 2018, the company is working on its rebuilt and seeking to continue with BioSA production.^{102,103}

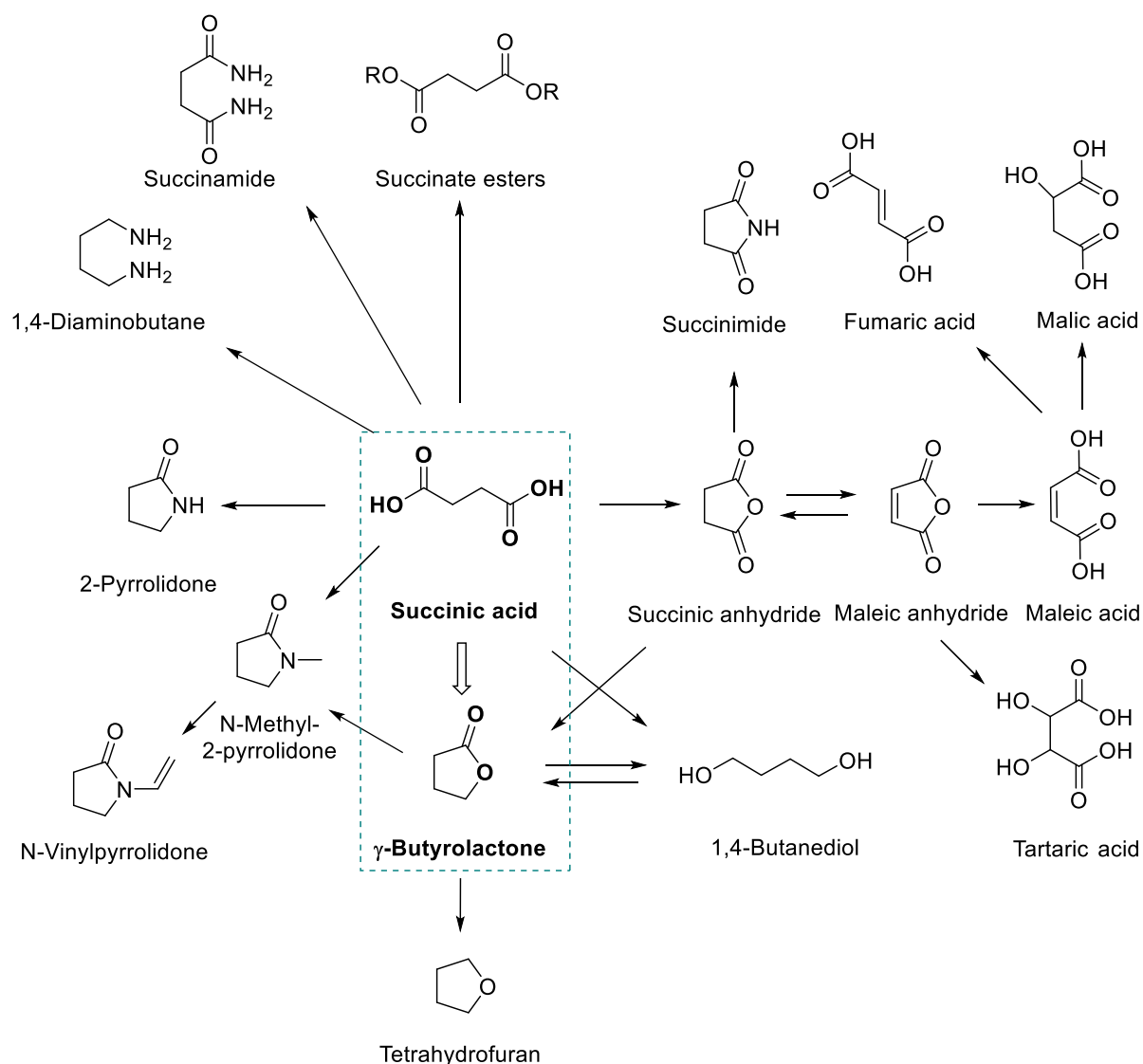
Several bacteria can produce succinate *via* glucose fermentation. Some of the examples are *Anaerobiospirillum succiniciproducens* and *Mannheimia succiniciproducens*, which are natural producers of SA.¹⁰⁴ Additionally, genetic manipulation of the microorganism to enhance the productivity, by the blockage of competitive pathways of BioSA, have also been developed such as Recombinant *E. Coli*.¹⁰⁵ These improvements allow high yields to be obtained.

In general, the correct operation of these microorganisms strongly depends on the pH and the availability of CO₂ in order to produce relatively large amounts of BioSA, requiring then a highly controlled environment. If the pH, temperature and concentration of substrate are not carefully controlled the activity will not be optimum and the enzymes will potentially denature. Nevertheless, the fact that CO₂ is needed by the microorganisms for SA production is another interesting feature that increases the sustainability of the overall process.

Generally, the largest part of the total cost of the fermentation process is actually from the purification and downstream processing of the SA after fermentation. Typically highly diluted concentrations are typically produced, leading to low product concentration in the fermentation broth and the presence of some impurities, which may affect later the reactivity of this BioSA. The cost of downstream processing can make up a large portion of the total production cost, mounting up to about 50 – 70 %.¹⁰⁶ Hence, improvements on SA fermentative production and downstream processing are under continuous study in order to increase its competitiveness and finally overpass the petrochemical process.

1.3.1.2.2 SA as platform molecule

In 2004, the U.S. Department of Energy (DOE) identified the “top value-added chemicals from biomass” that would economically and technically support the production of fuels and chemicals in an integrated biorefinery and identify the common challenges and barriers of associated production technologies. From an initial list of 30 candidates, which included C1, C3 to C6 compounds, it was reduced to 15, and one of those was SA.⁵⁵ SA was included in the “top list” based on the significant advances in its production from fermentation of sugars, mentioned in the section above, and its potential valorisation into high value chemicals. Accordingly, this platform molecule, containing two carboxylic groups, one in each extreme of the linear non-aliphatic chain, is considered a strategic bio-derived C4 building block that can be used to source a wide range of chemicals by its chemical conversion, as can be seen in Scheme 1.13.



Scheme 1.13. Most relevant reaction pathways from SA to high-value chemicals.

Most SA derivatives are produced by hydrogenation or reductive amination, and are employed in the chemical, pharmaceutical, food and agricultural industries. The widespread diversity of high-value chemicals that can be derived from SA makes it a very attractive platform molecule to be exploited. For example, focusing only in the hydrogenation-derived products, its direct hydrogenation leads to the production of a large variety of useful chemicals including GBL, THF and BDO. As already mentioned above, GBL main use is as solvent and as a starting material to NMP and others pyrrolidones, such as NVP, widely used as monomers. THF can also be used as a solvent or as monomer in production of poly(tetra-methylene) ether glycol (PTMEG), and a solvent in pharmaceuticals and coatings; while BDO is an intermediate for GBL and THF synthesis as well as a precursor to biodegradable plastics.¹⁰⁷

The hydrogenation/reduction chemistry for the conversion of SA to BDO, THF and GBL is well known and is similar to the conversion of MAN to the same family of compounds, hence,

similar catalytic routes can be investigated. The challenge is found on the selective obtainment of these products with high productivity, as explained in more detail in the following section.

1.3.1.2.3 Chemo-selective hydrogenation of SA to GBL

Amongst the useful chemicals that can potentially be derived from SA, GBL is especially attractive due to its valuable use in both bulk chemical and polymer industries. Considering the increasing popularity of SA as bio-derived platform molecule, several publications can be found on direct hydrogenation of SA to GBL, THF and/or BDO. However, generally, highly selective hydrogenation processes are difficult to obtain, ending up with mixture of products in the final reaction solution, since GBL and BDO may interconvert and GBL may also be further hydrogenated to THF. As such, control of the catalytic activity of SA towards these three main products, to obtain high selectivity towards one of them, is extremely challenging and strongly depends on both the type of catalyst and the reaction conditions applied.

The most employed kind of catalysts for SA hydrogenation reported in the open literature are metal supported nanoparticles. In this regard, many typical hydrogenating metals, such as Pd, Pt, Re or Ru, supported on various materials, can be found for the reductive valorisation of SA. For instance, Hong *et al.* reported that monometallic noble metal catalysts such as Pd or Ru can be used for liquid-phase hydrogenation of SA to GBL obtaining high selectivity (> 90 %),^{108,109} whereas the use of Re-based catalysts, monometallic or in combination with Pd, tend to favour mixture of products leading also to BDO and THF formation.^{110,111}

In addition to the choice of the metal, a high proportion of research conducted on this reaction has focused on discerning the best supporting material, whose nature (physical and chemical properties) may assist the metal centre to drive the reaction. Generally, there is a close relationship between catalysts with large active surface area, *i.e.* high dispersion of the active phase, and high activity. This is mainly due to the fact that small metal particles tend to sinter at relatively low temperatures, requiring to be supported onto a material which itself has a large surface area and a high thermostability.¹¹² For example, some of the most frequently used support materials are alumina, silica and carbon, due to their high decomposition temperatures and physical characteristics like surface area, pore size distribution, density and mechanical strength.

Some of the most relevant literature examples of metal particles supported on various materials include Pd on alumina xerogel, which converted 34 % of SA with 96 % of selectivity towards GBL;¹⁰⁸ Pd in amino-functionalised silica, which reached 100 % of SA with 94 % of GBL selectivity;¹¹³ and Re supported on mesoporous carbon, which led to 91 % of SA conversion with 60 % of GBL selectivity.¹¹⁴ However, in most of these reports, where high selectivity towards GBL is achieved, harsh reaction conditions are required, such as high reaction temperatures (< 240 °C) and high pressures (< 80 bar); and most reports present low

GBL productivities.¹¹⁴⁻¹¹⁶ On the other hand, those reports that reached higher GBL productivities typically exhibit a lack of high selectivity towards GBL, producing a mixture of products.^{110,117}

Accordingly, taking the previous literature into account, many factors play an important role on catalyst activity and GBL selectivity, such as the choice of metal, support and operational conditions. Herein, finding a suitable catalyst that can operate at milder conditions and achieve high selectivity towards GBL and high productivity remains a challenge.

1.4. Objectives of the thesis

The focal points of this thesis are the investigation of various catalytic routes to convert bio-derived chemicals into valuable lactones, of potential use to the polymer industry. The present work divides its attention into two systems of study: i) the BVO reaction of substituted cycloketones using Sn- β as catalyst and H₂O₂ as oxidant, and ii) the selective hydrogenation of SA to GBL using various metal supported nanoparticles.

To investigate the first catalytic system, Chapter 3 aims to initially focus the study on a model reaction, BVO of CyO into Capr, in order to fully optimise the reaction system, elucidate the whole reaction network and explore the viability of this system to operate under continuous operation, which is always highly beneficial to: i) increase the system productivity, ii) analyse the catalyst stability, and iii) evaluate the feasibility to scale up the system. Upon full understanding of the model reaction and working at its optimised conditions, the broadening of the substrate scope for the BVO / H₂O₂ / Sn- β system is investigated in Chapter 4. In said chapter, kinetic, steric and electronic effects of various substituent groups in the cyclohexanone ring are extensively analysed to better comprehend the relationship between the position and size of the substituent group and the catalytic activity observed. Furthermore, the upgrading of the sustainability of the BVO / Sn- β system is evaluated by several approaches in Chapter 5, in order to potentially increase the lactone selectivity, including the coupling of *in situ* H₂O₂ production with the BVO system.

To investigate the second catalytic system, research in Chapter 6 is focused on finding a suitable catalyst able to selectively convert SA into GBL at milder conditions and better performance (productivity, selectivity) than those previously reported. Firstly, the investigation of SA hydrogenation is carried out over various commercial catalysts and subsequently, GBL selectivity is maximised by optimising catalyst design. Through the investigation of the structure - activity relationship observed for the metal supported nanoparticles employed, the features of a suitable material required to obtain high productivity of GBL are exposed.

References

- (1) U.S. Energy Information Administration, “*International Energy Outlook 2017*”
- (2) S. Dale, T. D. Smith, “Back to the future: electric vehicles and oil demand”, BP
- (3) Statista, “*Daily demand for crude oil from 2006 to 2019 (in million barrels)*”
- (4) IndexMundi, “*World Coal Consumption by Year*”
- (5) International Energy Agency, “*Global coal consumption forecast to slow*”, The Guardian, 2017
- (6) International Energy Agency, “*Share of electricity production from fossil fuels*”, The World Bank, 2016
- (7) International Energy Agency, “*IEA sees global gas demand rising to 2022 as US drives market transformation*”, 2017
- (8) Our World in Data, “*Years of fossil fuel reserves left*”, based on BP Statistical Review of World Energy 2016
- (9) M. S. Roni, S. Chowdhury, S. Mamun, M. Marufuzzaman, W. Lein, S. Johnson, *Renew. Sustain. Energy Rev.*, 2017, **78**, 1089 – 1101
- (10) P. Gallezot, “*Catalysis for Renewables: From Feedstock to Energy Production*”, Wiley, Weinheim, 2007
- (11) S. Production, F. Biomass, A. C. S. S. Series and A. C. Society, “*Sustainable Production of Fuels, Chemicals, and Fibers from Forest Biomass*”, 2011, vol. 1067
- (12) M. Gurz, E. Baltacioglu, Y. Hames, K. Kaya, *Int. J Hydrogen Energy*, 2017, **42**, 23334 - 23346
- (13) F. Ma, M. A. Hanna, *Bioresour. Technol.*, 1999, **70**, 1 - 15
- (14) H. Zabed, J. N. Sahu, A. Suey, A. N. Boyce, G. Faruq, *Renew. Sust. Energ. Rev.*, 2017, **71**, 475 - 501
- (15) E. V. Kondratenko, G. Mul, J. Baltrusaitis, G. O. Larrazábal, J. Pérez-Ramírez, *Energy Environ. Sci.*, 2013, **6**, 3112 - 3135
- (16) G. Centi, S. Perathoner, *Catal. Today*, 2009, **148**, 191 - 205
- (17) S. C. Roy, O. K. Varghese, M. Paulose, C. A. Grimes, *ACS Nano*, 2010, **4**, 1259 - 1278
- (18) S. Das, W. M. A. Wan Daud, *RSC Adv.*, 2014, **4**, 20856 - 20893
- (19) C. O. Tuck, E. Pérez, I. T. Horváth, R. A. Sheldon, M. Poliakoff, *Science*, 2012, **337**, 695 - 699
- (20) R. A. Sheldon, *Green Chem.* 2014, **16**, 950 - 963
- (21) D. A. Bulushev, J. R. H. Ross, *Catal. Today*, 2011, **171**, 1 – 13
- (22) C. Li, X. Zhao, A. Wang, G. W. Huber, T. Zhang, *Chem. Rev.*, 2015, **115**, 11559 – 11624
- (23) L. Baxter, *Fuel*, 2005, **84**, 1295 - 1302
- (24) J. Hill, E. Nelson, D. Tilman, S. Polasky, D. Tiffany, *Proc. Natl. Acad. Sci. U. S. A.*, 2006, **103**, 11206 - 11210
- (25) S. Shylesh, A. A. Gokhale, C. R. Ho, A. T. Bell, *Acc. Chem. Res.*, 2017, **50**, 2589 – 2597
- (26) W. N. R. Wan Ishak, M. W. M. Hisham, M. A. Yarmo, T. Y. Y. Hin, *Renew. Sust. Energ. Rev.*, 2012, **16**, 5910 - 5923
- (27) A. Mazière, P. Prinsen, A. García, R. Luque, C. Len, *Biofuels, Bioprod. Biorefining*, 2017, **11**, 908 – 931
- (28) J. Van Haveren, E. L. Scott, J. Sanders, *Biofuels, Bioprod. Bioref.*, 2008, **2**, 41 – 57
- (29) P. Gallezot, *Chem. Soc. Rev.*, 2012, **41**, 1538 – 1558
- (30) G. W. Huber, S. Iborra, A. Corma, *Chem. Rev.*, 2006, **106**, 4044 – 4098
- (31) S. Ladanai, J. Vinterback, “*Global Potential of Sustainable Biomass for Energy*”, Report 013, ISSN 1654 - 9406, Uppsala 2009
- (32) International Renewable Energy Agency, “*Global Bioenergy, supply and demand projections*”, 2014
- (33) F. D. Pileidis, M. M. Titirici, *ChemSusChem*, 2016, **9**, 562 – 582
- (34) C. H. Zhou, X. Xia, C. X. Lin, D. S. Tong, J. Beltramini, *Chem. Soc. Rev.*, 2011, **40**, 5588 – 5617
- (35) F. H. Isikgor, C. R. Becer, *Polym. Chem.*, 2015, **6**, 4497 - 4559
- (36) A. Shrotri, H. Kobayashi, A. Fukuoka, *Acc. Chem. Res.*, 2018, **51**, 761 - 768
- (37) P. Harmsen, W. Huijgen, L. Bermudez, R. Bakker, “*Literature review of physical and chemical processes for lignocellulosic biomass*”, Biosynergy, 2010
- (38) Z. Sun, K. Barta, *Chem. Commun.*, 2018, **54**, 7725
- (39) R. A. Sheldon, *ACS Sustainable Chem. Eng.*, 2018, **6**, 4464 - 4480
- (40) T. Renders, E. Cooreman, S. Van den Bosch, W. Schutsy, S. F. Koelewijn, T. Vangeel, A. Deneyer, G. Van Bossche, C. M. Cortin, B. F. Sels, *Green Chem.*, 2018, **20**, 4607 - 4619

- (41) A. A. Rosatella, S. P. Simeonov, R. F. M. Frade, C. A. M. Afonso, *Green Chem.*, 2011, **13**, 754 - 793
- (42) D. M. Alonso, S. G. Wettstein, J. A. Dumesic, *Green Chem.*, 2013, **15**, 584 - 595
- (43) C. Vilela, A. F. Sousa, A. C. Fonseca, A. C. Serra, J. F. J. Coelho, C. S. R. Freire, A. J. D. Silvestre, *Polym. Chem.*, 2014, **5**, 3119 - 3141
- (44) E. I. Gurbuz, J. M. R. Gallo, D. M. Alonso, S. G. Wettstein, W. Y. Lim, J. A. Dumesic, *Angew. Chem. Int. Ed.*, 2013, **52**, 1270 - 1274
- (45) M. S. Singhvi, S. Chaudhari, D. V. Gokhale, *RSC Adv.*, 2014, **4**, 8271 - 8277
- (46) S. Laurichesse, L. Averous, *Prog. Polym. Sci.*, 2014, **39**, 1266 - 1290
- (47) S. Guadix-Montero, M. Sankar, *Top Catal.*, 2018, **61**, 183 - 198
- (48) X. Zhang, H. Lei, S. Chen, J. Wu, *Green Chem.*, 2016, **18**, 4145 - 4169
- (49) P. Sudarsanam, R. Zhong, S. Van den Bosch, S. M. Coman, V. I. Parvulescu, B. F. Sels, *Chem. Soc. Rev.*, 2018, **47** (22), 8349 - 8402
- (50) G. Ertl, "Handbook of Heterogeneous Catalysis", Wiley-VCH, Weinheim-New York, 2nd edition, 2008
- (51) T. Ennaert, J. Van Aelst, J. Dijkmans, R. De Clercq, W. Schutyser, M. Dusselier, D. Verboekend, B. F. Sels, *Chem. Soc. Rev.*, 2016, **45**, 584 - 611
- (52) S. S. Chen, T. Maneerung, D. C. W. Tsang, Y. Sik Ok, C. Wang, *Chem. Eng. J.*, 2017, **328**, 246 - 273
- (53) Plastics Europe, "Plastic - The Facts 2016", www.plasticseurope.org
- (54) C. K. Williams, M. A. Hillmyer, *Polym. Rev.*, 2008, **48** (1), 1 - 10
- (55) T. Werpy, G. Petersen, "Top Value-Added Chemicals from Biomass Volume I — Results of Screening for Potential Candidates from Sugars and Synthesis Gas", U.S. Department of Energy: Oak Ridge
- (56) A. J. J. E Eerhart, A. P. C. Faaij, M. K. Patel, *Energy Environ. Sci.*, 2012, **5**, 6407 - 6422
- (57) M. Kunioka, T. Masuda, Y. Tachibana, M. Funabashi, *Polym. Degrad. Stab.*, 2014, **109**, 393 - 397
- (58) J. Tuteja, H. Choudhary, S. Nishimura, K. Ebitani, *ChemSusChem.*, 2014, **7** (1), 96 - 100
- (59) Y. Tachibana, T. Masuda, M. Funabashi, M. Kunioka, *Biomacromolecules*, 2010, **11**, 2780 - 2785
- (60) Nexant ChemSystems, "Biochemical Opportunities in the United Kingdom NNFFC project 08-008, A study funded by Defra, project managed by The National Non-Food Crops Centre (NNFFC)", 2008
- (61) P. A. J. M. de Jongh, P. K. C. Paul, E. Khoshdel, P. Wilson, K. Kempe, D. M. Haddleton, *Polym. Int.*, 2017, **66**, 59 - 63
- (62) T. Rosen, I. Goldberg, W. Navarra, V. Venditto, M. Kol, *Angew. Chem. Int. Ed.*, 2018, **57**, 7191 - 7195
- (63) J. H. Park, B. K. Lee, S. H. Park, M. G. Kim, J. W. Lee, H. Y. Lee, H. B. Lee, J. H. Kim, M. S. Kim, *Int. J. Mol. Sci.*, 2017, **18**, 671 - 686
- (64) P. Walther, S. Naumann, *Macromolecules*, 2017, **50**, 8406 - 8416
- (65) G. Dahlhoff, J. P. M. Nierderer, W. F. Hoelderich, *Cat. Rev.-Sci. Eng.*, 2001, **43**, 4, 381 - 441
- (66) M. Labet, W. Thielemans, *Chem. Soc. Rev.*, 2009, **38**, 3484 - 3504
- (67) C.H. Huang, F.C. Wang, B.T. Ko, T.L. Yu, C.C. Lin, *Macromolecules*, 2001, **34**, 356 - 361
- (68) T. Buntara, S. Noel, P. H. Phua, I. Melian-Cabrera, J. G. de Vries, H. J. Heeres, *Angew. Chem. Int. Ed.*, 2011, **50**, 7083 - 7087
- (69) V. Thaore, D. Chadwick, N. Shah, *Chem. Eng. Res. Des.*, 2018, **135**, 140 - 152.
- (70) G. Xu, J. Guo, Y. Zhang, Y. Fu, J. Chen, L. Ma, Q. Guo, *ChemCatChem.*, 2015, **7**, 2485 - 2492
- 71 Q. Meng, M. Hou, H. Liu, J. Song, B. Han, *Nature Comm*, DOI: 10.1038/ncomms14190
- 72 H. C. Quilter, M. Hutchby, M. G. Davidson, M. D. Jones, *Polym. Chem.*, 2017, **8**, 833 - 837
- 73 G. X. de Hoe, M. T. Zumstein, B. J. Tiegs, J. P. Brutman, K. McNeill, M. Sander, G. W. Coates, M. A. Hillmyer, *J. Am. Chem. Soc.*, 2018, **140**, 963 - 973
- (74) M. Hong, Y. E. Y. X. Chen, *Nature Chemistry*, 2016, **8**, 42 - 49
- (75) M. Hong, X. Tang, B. S. Newell, E. Y. X. Chen, *Macromolecules*, 2017, **50**, 8469 - 8479
- (76) T. J. Hu, H. B. Yin, R. C. Zhang, H. X. Wu, T. S. Jiang, Y. J. Wada, *Catal. Commun.*, 2007, **8**, 193 - 199
- (77) J. P. Lange, E. van der Heide, J. van Buijtenen, R. Price, *ChemSusChem*, 2012, **5**, 150 - 166
- (78) X. Li, X. Lan, T. Wang, *Green Chem.*, 2016, **18**, 638 - 642
- (79) J. Wang, S. Jaenicke, G. Chuah, *RSC Adv*, 2014, **4**, 13481 - 13489
- (80) M. Al-Naji, A. Yopez, A. M. Balu, A. A. Romero, Z. Chen, N. Wilde, H. Li, K. Shih, R. Glaser, R. Luqueb, *J Mol Catalysis A*, 2016, **417**, 145 - 152
- (81) S. Xu, D. Yu, T. Ye, P. Tian, *RSC Adv.*, 2017, **7**, 1026 - 1031
- (82) Z. Zhang, *ChemSusChem.*, 2016, **9**, 156 - 171
- (83) O. Nuyken, S. D. Pask, *Polymers*, 2013, **5**, 361 - 403

- (84) A. Baeyer, V. Villiger, Ber. Dtsch. Chem. Ges., 1899, **32**, 3625 – 3633
- (85) G. Strukul, Angew. Chem. Int. Ed. 1998, **37**, 1198 – 1209
- (86) R. Criegee, Justus Liebigs Ann. Chem., 1948, **560**, 127 - 135
- (87) J. D. Stewart, Curr. Org. Chem., 1998, **2**, 211 - 232
- (88) A. Carvarzan, G. Bianchini, P. Sgarbossa, L. Lefort, S. Gladiali, A. Scarso, G. Strukul, Chem. Eur. J., 2009, **15**, 7930 – 7939
- (89) C. Xia, L. Ju, Y. Zhao, H. Xu, B. Zhu, F. Gao, M. Lin, Z. Dai, X. Zou, X. Shu, Chin. J. Catal., 2015, **36**, 845 - 854
- (90) A. Corma, L. T. Nemeth, M. Renz, S. Valencia, Nature, 2001, **412**, 423 – 425
- (91) Z. Lei, Q. Zhang, J. Luo, X. He, Tetrahedron Lett., 2005, **46**, 3505 - 3508
- (92) K. M. Jinka, S. Lee, S. Park, R. V. Jasra, "Zeolites and Related Materials: Trends, Targets and Challenges, Proceedings of 4th International FEZA Conference", 2008
- (93) H. Y. Luo, W. R. Gunther, E. Min, Y. Román-Leshkov, ACS Catal., 2012, **2**, 2695 – 2699
- (94) A. Corma, M. T. Navarro, L. Nemeth, M. Renz, Chem. Commun., 2001, 2190 - 2191
- (95) A. Corma, M. T. Navarro, M. Renz, J Catal., 2003, **219**, 242 - 246
- (96) T. Chen, B. Wang, Y. Li, L. Li, S. Qiu, J Porous Mater., 2015, **22**, 949 - 957
- (97) P. Li, G. Liu, H. Wu, Y. Liu, J. Jiang, P. Wu, J. Phys. Chem. C, 2011, **115**, 3663 – 3670
- (98) C. Hammond, S. Conrad, I. Hermans, Angew. Chem. Int. Ed., 2012, **51**, 11736 – 11739
- (99) Z. Kang, H. Liu, X. Zhang, Chin. J. Catal., 2012, **33**, 898 – 904
- (100) J. M. Pinazo, M. E. Domine, V. Parvulescu, F. Petru, Catal. Today, 2015, **239**, 17 - 24
- (101) S. Vaswani, "PEP Review 2010-14 Bio-based Succinic Acid"
- (102) Construction Boxscore database, "BioAmber Sarnia starts production of bio-succinic acid at commercial scale", Hydrocarbon processing, 2018
- (103) M. McCoy, "Succinic acid maker BioAmber is bankrupt", C&en, Biobased chemicals, 2018, 96 (20)
- (104) I. Meynial-Salles, S. Dorotyn, P. Soucaille, Biotechnol. Bioeng., 2007, **99**, 129 – 135
- (105) A. M. Sánchez, G. N. Bennett, K. Y. San, Biotechnol. Prog., 2005, **21**, 358 – 365
- (106) I. Bechthold, K. Bretz, S. Kabasci, R. Kopitzky, A. Springer, Chem. Eng. Technol., 2008, **31** (5), 647 - 654
- (107) C. Delhomme, D. Weuster-Botz, F. E. Kühn, Green Chem., 2009, **11**, 13 - 26
- (108) U. G. Hong, S. Hwang, J. G. Seo, J. Yi, I. K. Song, Catal Lett., 2010, **138**, 28 - 33
- (109) U. G. Hong, H. W. Park, J. Lee, S. Hwang, I. K. Song, J. Ind. Eng. Chem., 2012, **18**, 462 – 468
- (110) Z. Shao, C. Li, X. Di, Z. Xiao, C. Liang, Ind. Eng. Chem. Res., 2014, **53**, 9638 – 9645
- (111) B. K. Ly, B. Tapin, M. Aouine, P. Delichere, F. Epron, C. Pinel, C. Especel, M. Besson, ChemCatChem, 2015, **7**, 2161 – 2178
- (112) M. L. Toebes, J. A. Van Dillen, K. P. De Jong, J. Mol. Catal. A Chem., 2001, **173**, 75–98.
- (113) C. You, C. Zhang, L. Chen, Z. Qi, Appl. Organometal. Chem., 2015, **29**, 653 – 660
- (114) X. Di, Z. Shao, C. Li, W. Li, C. Liang, Catal. Sci. Technol., 2015, **5**, 2441 - 2448.
- (115) K. H. Kang, U. G. Hong, Y. Bang, J. H. Choi, J. K. Kim, J. K. Lee, S. J. Han, I. K. Song, Appl. Catal., A, 2015, **490**, 153 – 162
- (116) C. Zhang, L. Chen, H. Cheng, X. Zhu, Z. Qi, Catal. Today, 2016, **276**, 55 – 61
- (117) U. G. Hong, S. Hwang, J. G. Seo, J. Lee, I. K. Song, J. Ind. Eng. Chem., 2011, **17**, 316 – 320

2. Experimental and methods

2.1. List of abbreviations

Baeyer-Villiger oxidation	BVO
Cyclohexanone	CyO
ϵ -Caprolactone (or caprolactone)	Capr
<i>meta</i> -chloroperbenzoic acid	<i>m</i> CPBA
Hydrogen peroxide	H ₂ O ₂
Tin beta zeolite	Sn- β
Zeolite beta (BEA)	β
Dealumination	deAl
Solid-State Incorporation	SSI
Powder X-Ray Diffraction	XRD
Transmission Electron Microscopy	TEM
Scanning Electron Microscopy	SEM
Diffuse Reflectance Infrared Fourier Transformed spectroscopy	DRIFTS

Magic Angle Spinning Nuclear Magnetic Resonance	MAS NMR
Gas Chromatography	GC
Flame Ionization Detector	FID
Silanol groups	Si-OH
Apparent kinetic constant	k_{app}
Activation energy	E_{act}
High Performance Liquid Chromatography	HPLC
Attenuated Total Reflectance Infra-Red	ATR-IR
6-Hydroxyhexanoic Acid	6-HHA
Adipic Acid	AA
Proton Nuclear Magnetic Resonance	^1H NMR
Carbon Nuclear Magnetic Resonance	^{13}C NMR
Tetramethylsilane in deuterated chloroform	TMS/ CDCl_3
Biphenyl	Bp
Thermogravimetric Analysis	TGA
Gel Permeation Chromatography	GPC
Average molecular weight	M_n
Poly-Dispersity index	PDI
Plug Flow Reactor	PFR
Back Pressure Regulator	BPR
Substituted ϵ -Caprolactone	R-Capr
Substituted Cyclohexanone	R-CyO
Hierarchical Sn- β	Sn- β -H
Energy-Dispersive X-ray spectroscopy	EDX
Desilication	deSi
Brunauer–Emmett–Teller surface area	S_{BET}
Barret-Joyner-Halenda method	BJH
Brunauer-Deming-Deming-Teller classification	BDDT
Density Functional Theory	DFT
<i>para</i> -substituted Acetophenone	4-R-AcetoPhO
Hammett constant	σ
Triazabicyclodecene	TBD
Gel Permeation Chromatography	GPC
Size Exclusion Chromatography	SEC
Sol Immobilisation	SI
Polyvinyl alcohol	PVA
Wet Impregnation	IMP

Succinic Acid	SA
1,4-Butanediol	BDO
γ -Butyrolactone	GBL
Tetrahydrofuran	THF
Propionic Acid	PA
Butyric Acid	BA
Citric Acid	CA
Co-precipitation	COP
Deposition-precipitation	DP
X-ray Photoelectron Spectroscopy	XPS
Space Time Yield	STY

2.2 Formulas and expressions

Conversion:

$$X_{(Substrate)} = \frac{([Substrate]_0 - [Substrate]_t)}{[Substrate]_0} \times 100 \quad [Equation 2.1]$$

Yield:

$$Y_{(Product)} = \frac{[Product]_t}{[Substrate]_0} \times 100 \quad [Equation 2.2]$$

Selectivity:

$$S_{(Product)} = \frac{[Product]_t}{([Substrate]_0 - [Substrate]_t)} \times 100 \quad [Equation 2.3]$$

Carbon Balance:

$$C\ Bal = \frac{\sum Carbon_t}{\sum Carbon_0} \times 100 \quad [Equation 2.4]$$

Turnover Frequency:

$$TOF = \frac{\text{moles of substrate converted}}{\text{moles of metal} \times \text{time}} \quad [Equation 2.5]$$

2.3 Catalysts employed

In this study two main kinds of heterogeneous catalysts were employed: Lewis acid silicalites and metal supported nanoparticles.

Details for material preparations for all the catalysts presented in this work are described below.

2.3.1 Lewis acid silicalites

2.3.1.1 Sn- β preparation

Commercial zeolite Al- β (CP814E, Zeolyst, NH_4 -form, $\text{SiO}_2/\text{Al}_2\text{O}_3 = 38$) was dealuminated by treatment in a solution of HNO_3 (13 M HNO_3 , 100 °C, 20 h, 20 mL g^{-1} of zeolite). The dealuminated powder (deAl- β) was filtered, washed with water and dried overnight at 110 °C. Subsequently, Solid-State Incorporation (SSI) of Sn was performed by grinding the appropriate amount of Sn (II) acetate with the necessary amount of deAl- β for 10 min in a pestle and mortar, prior to heat treatment in a combustion furnace (Carbolite MTF12/38/400). During heat treatment, the sample was placed in an alumina boat within a sealed horizontal quartz tube. A two-stage heat treatment was employed: 550 °C (10 °C min^{-1} ramp rate, 60 mL min^{-1}) first in a flow of N_2 (3 h) and subsequently in air (3 h).

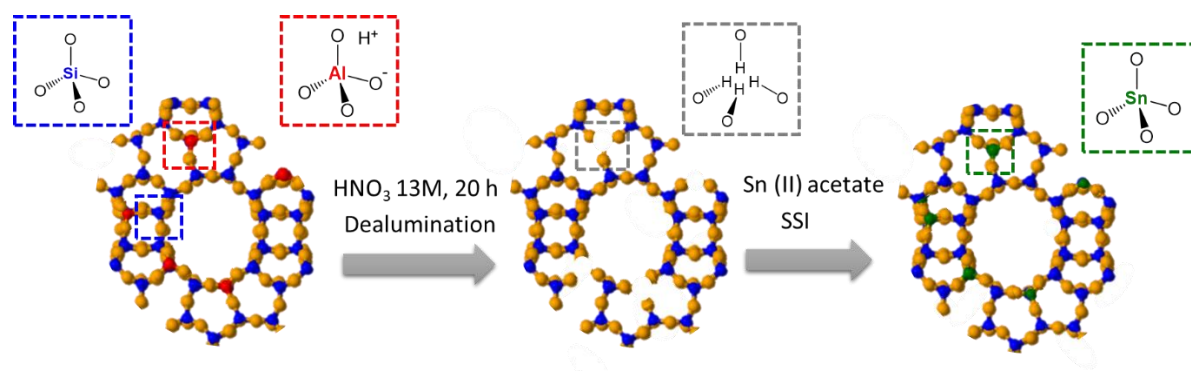


Figure 2.1. Representation of the synthesis of Sn- β , where the coloured atoms are: yellow = O, blue = Si, red = Al and green = Sn.

Typically, the prepared samples possessed a 2 wt. % Sn loading, henceforth denoted 2Sn- β . Where required, samples with different wt. % Sn loadings were prepared by adjusting the amount of the Sn precursor used. These samples are denoted XSn- β , where X represents the wt. % of Sn. Additionally, samples with different initial Al contents were also prepared from zeolite Al- β (Zeolyst, NH_4 -form) with $\text{SiO}_2/\text{Al}_2\text{O}_3 = 25$ and 300, denoted 2Sn- β (25) and 2Sn- β (300), respectively.

2.3.1.2 Hierarchical Sn- β preparation

Commercial zeolite Al- β (CP814E, Zeolyst, NH_4 -form, $\text{SiO}_2/\text{Al}_2\text{O}_3 = 38$) was first converted into the protonic form by calcination in static air at $550\text{ }^\circ\text{C}$ ($5\text{ }^\circ\text{C min}^{-1}$) for 5 h. The H-form zeolite β (H- β) was subsequently suspended in a solution of NaOH (0.2 M, $45\text{ }^\circ\text{C}$, 0.5 h, 30 mL g^{-1} of zeolite) to obtain a desilicated zeolite β (deSi- β). The desilication procedure was then stopped immediately by cooling the container in an ice bath. The remaining solid product was centrifuged, thoroughly washed with deionized water until neutral pH was attained, and finally dried at $110\text{ }^\circ\text{C}$ overnight. The deSi- β powder was then dealuminated following the same procedure described above in Section 2.3.1.1. After filtering and drying the sample, the sample was reconverted into NH_4 -form by ion exchange in an aqueous solution of NH_4NO_3 (1 M, 2 h, $85\text{ }^\circ\text{C}$, $30\text{ mL solution g}^{-1}$ of zeolite). SSI of Sn by the exact protocol described above was then performed. Typically, the hierarchical samples prepared possessed 2 wt. % Sn loading, denoted 2Sn- β -H.

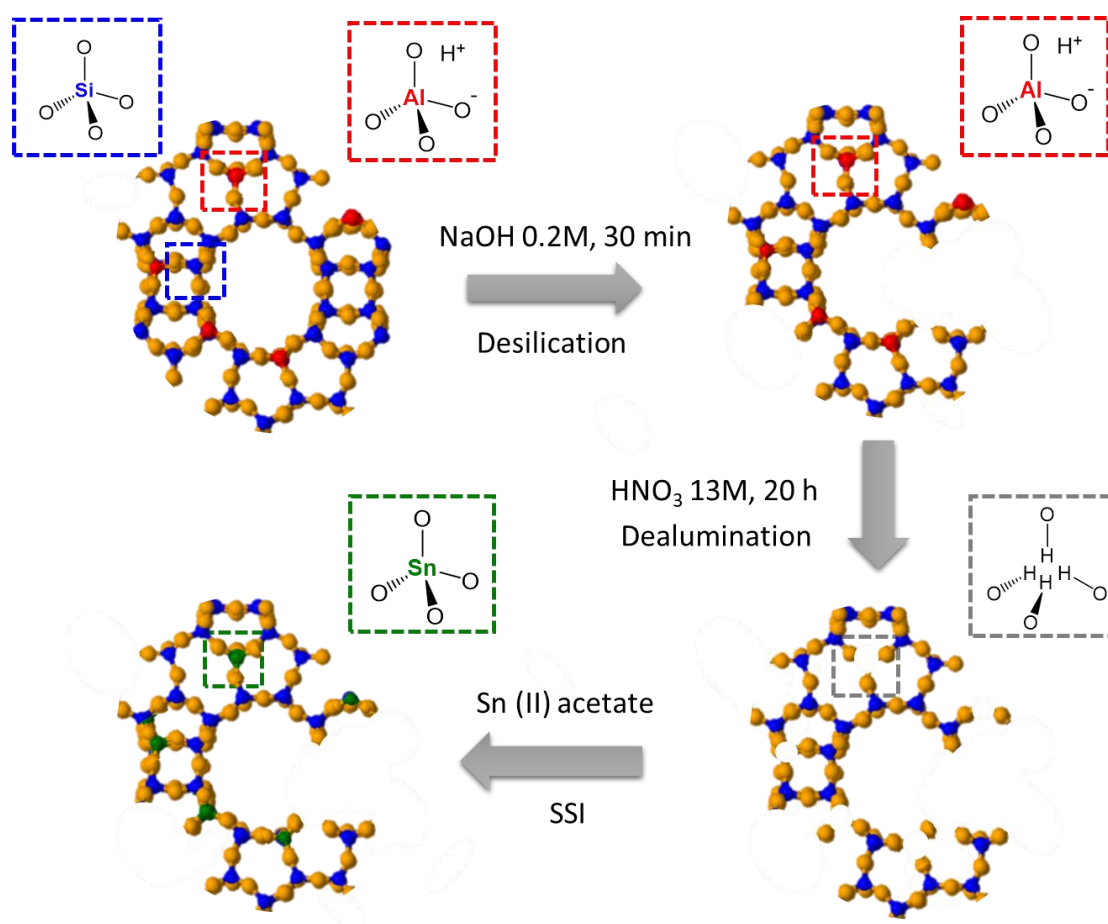


Figure 2.2. Representation of the synthesis of Sn- β -H, where the coloured atoms are: yellow = O, blue = Si, red = Al and green = Sn.

2.3.2 Metal supported nanoparticles

A series of metal nanoparticles (Pd, Au, Ru, Ni, Ir, Cu) were supported on various materials (TiO_2 , Al_2O_3 , MgO, hydrotalcite, H- β , MCM-41) using different preparation techniques.

The following compounds were used as metal precursors: potassium tetrachloropalladate (II) (Sigma Aldrich), gold (III) chloride trihydrate (Sigma Aldrich), ruthenium (III) chloride hydrate (Sigma Aldrich), nickel (II) chloride hexahydrate (Alfa Aesar), copper (II) chloride dihydrate (Alfa Aesar) and iridium (IV) chloride (Alfa Aesar). Each metallic solution was analysed by Microwave Plasma-Atomic Emission Spectrometer to obtain the exact concentration.

The following materials were employed as supports: titanium oxide (TiO_2 , P25, Degussa), γ -alumina (Sigma Aldrich), magnesium oxide (MgO light, BDH), mesoporous silica (MCM-41, Sigma Aldrich), hydrotalcite (Sigma Aldrich) and β zeolite (Zeolyst, NH_4 -form, $\text{SiO}_2/\text{Al}_2\text{O}_3 = 38$) converted into the protonic form (H- β) by calcination at 550 °C in static air for 5 h.

Surfactant and precipitating agents used in this study were polyvinyl alcohol (PVA, MW = 89,000 - 98,000, hydrolysed, Sigma Aldrich), NaBH_4 (98 %, Sigma Aldrich), Na_2CO_3 (99 %, Sigma Aldrich), NaOH (98 %, Fisher Scientific).

2.3.2.1 Sol immobilisation method (SI)

Monometallic Pd and Au and bimetallic Pd-Au nanoparticles were supported on TiO_2 by sol immobilisation method (SI).

Firstly, aqueous solutions of 1 wt. % PVA and 0.1 M NaBH_4 were prepared. For a typical preparation, the required amount of metal precursor(s) was added to 800 mL of deionized water, prior to addition of the required amount of PVA (PVA / Metal = 0.65 (or 1.2 for bimetallic) weight ratio). Subsequently, NaBH_4 solution was added (NaBH_4 / Metal = 5 molar ratio) and stirred for 30 min, to allow formation of colloids. Following this, the desired amount of support was added, alongside 5 - 10 drops of sulphuric acid to lower the pH to 1 - 2 and enhance colloidal immobilisation. The mixture was then stirred for 1 h, while adsorption of the colloids onto the support occurred and the solution became colourless. The final powder obtained was filtered, washed with water until a neutral pH was reached, and dried overnight at 110 °C. When required, catalysts were heat treated in a tubular combustion furnace (Carbolite MTF12/38/400) at 400 °C for 3h in air (10 °C min^{-1} ramp rate, flow rate of 100 mL min^{-1}).

Catalysts prepared by this methodology were: 1 wt. % Pd on TiO_2 , 1 wt. % Au on TiO_2 and 1 wt. % Pd 1 wt. % Au on TiO_2 , denoted 1Pd/ TiO_2 , 1Au/ TiO_2 and 1Pd-1Au/ TiO_2 , respectively.

2.3.2.2 Wet impregnation method (IMP)

Monometallic Pd, Au and bimetallic Pd-Au samples supported on different materials were prepared by wet impregnation method (IMP).

The required amount of metal chloride precursor solution to prepare 1 g of catalyst was added into a 50 mL round bottom flask with a magnetic stirrer (700 rpm) at 25 °C. Deionized water was added to adjust the total volume to 16 mL, before the flask was immersed in an oil bath and the temperature was increased to 60 °C. Once the temperature was reached, the support was gradually added, and the resultant slurry was stirred for 15 minutes. The oil bath temperature was then increased to 95 °C and stirred until full evaporation of the water, leaving a dry solid. When required, catalysts were heat treated in a tubular combustion furnace (Carbolite MTF12/38/400) at 400 °C for 3h in air (10 °C min⁻¹ ramp rate, flow rate of 100 mL min⁻¹) or 200 °C for 3h in 5% H₂/Ar (10 °C min⁻¹ ramp rate, flow rate of 100 mL min⁻¹).

Catalysts prepared by this methodology were: 2.5 wt. % Pd on 2Sn-β, 2.5 wt. % Au on 2Sn-β and 0.5 wt. % Pd 0.5 wt. % Au on 2Sn-β, denoted 2.5Au/2Sn-β, 2.5Pd/2Sn-β and 0.5Au-0.5Pd/2Sn-β. Likewise, 2 wt. % Pd supported on commercial γ-alumina and alumina prepared by co-precipitation, denoted 2Pd/Al₂O₃(IMP) and 2Pd/Al₂O₃(IMP@COP), were also synthesised. Finally, 2 wt. % Pd supported on MgO, MCM-41, hydrotalcite and H-β, denoted simply 2Pd/support were also prepared.

2.3.2.3 Co-precipitation method (COP)

Various metals (Pd, Ru, Ir, Ni, Cu) supported on alumina were prepared by the co-precipitation method (COP).

The required amount of metal chloride precursor solution to prepare 1 g of a 2 wt. % loading catalyst, was added into a beaker with 50 mL of deionized water under stirring (700 rpm) at 25 °C. The support precursor (aluminium nitrate nonahydrate, 99.9 %, Sigma-Aldrich) was then added, and the pH adjusted to 9 through gradual addition of solid sodium carbonate. The suspension was then equilibrated under stirring for 1 h and the resultant slurry filtered and washed extensively with deionized water (3 L per g of catalyst). The solid was then oven dried overnight at 110 °C and reduced in a combustion furnace (Carbolite MTF12/38/400) at 200 °C for 3 h under 5% H₂/Ar flow (10 °C min⁻¹ ramp rate, 100 mL min⁻¹). When a catalyst with different metal loading was prepared, the required amounts of metal and support precursor were adjusted appropriately.

Catalysts prepared by this methodology were 2 wt. % metal loading, denoted 2M/Al₂O₃(COP), where M represents the metal employed and 5 wt. % Pd on alumina, denoted 5Pd/Al₂O₃(COP).

2.3.2.4 Deposition precipitation method (DP)

2 wt. % Pd on γ-alumina and 2 wt. % Pd on alumina prepared by COP, denoted 2Pd/Al₂O₃(DP) and 2Pd/Al₂O₃(DP@COP) were prepared by deposition-precipitation method (DP).

In a beaker containing 160 mL of deionized water, the required amount of metal precursor was added. Subsequently, the pH was adjusted to 10 by dropwise addition of 0.2 M NaOH

solution under continuous stirring. Then, this solution was poured into a second beaker containing 40 mL of deionized water and the required amount of support, and the pH was adjusted again to 10 and stirred for 1 h. The resulting powder was filtered, washed extensively with water and oven dried at 110 °C for 16 h before being reduced at 200 °C for 3 h under 5% H₂/Ar flow (Carbolite MTF12/38/400, 10 °C min⁻¹ ramp rate, flow rate of 100 mL min⁻¹).

2.3.2.5 Commercial catalysts employed

In addition to the synthesised materials described above, some commercial catalysts were employed for the SA hydrogenation where stated. These materials were: 5 wt. % Ru and 5 wt. % Pd on γ -alumina and carbon (Sigma Aldrich), denoted: 5Ru/Al₂O₃(COM), 5Ru/C_(COM), 5Pd/Al₂O₃(COM) and 5Pd/C_(COM), respectively.

2.4 Kinetic evaluation

2.4.1 Batch Baeyer-Villiger Oxidation (BVO) reactions of cyclohexanone (CyO), substituted cyclohexanones (R-CyO) and substituted acetophenones (4-R-AcetoPhO)

Batch BVO reactions were performed in a 100 mL round-bottom flask equipped with a water-free reflux condenser. The reaction temperature was controlled by immersion in a silicon oil bath. The vessel was charged with a solution of CyO (or similar substrate tested) in 1,4-dioxane (10 mL, 0.33 M), which also contained an internal standard (biphenyl, 0.01 M), and the appropriate amount of catalyst, typically 1 mol. % Sn with respect to the substrate. The vessel was subsequently heated to the desired temperature (typically, 100 °C internal temperature). The reaction was initiated by addition of an appropriate amount of H₂O₂ (50 wt. % in aqueous solution), typically corresponding to a H₂O₂:ketone ratio of 1.5. The solution was stirred at 750 rpm with an oval magnetic stirrer. Aliquots of the reaction solution were taken periodically for analysis and were centrifuged prior to injection into a gas chromatograph (GC). The GC employed was an Agilent 7820 equipped with a 25 m CP-Wax 52 CB capillary column and a Flame Ionisation Detector (FID), with He as carrier gas (5 mL min⁻¹). Reactants were quantified against biphenyl (Bp) as internal standard. More details on this analytical technique can be found in Section 2.5.1.1.

Additionally, when analysis and quantification of 6-hydroxyhexanoic acid (6-HHA), and analogues, were required, aliquots from BVO reaction were analysed by proton Nuclear Magnetic Resonance (¹H NMR) spectroscopy and quantified against a tetramethylsilane insert previously calibrated, following the experimental procedure described in Section 2.5.2.1.

Kinetic parameters studied such as conversion, yield, selectivity, carbon balance and turnover frequency were calculated according to Equations 2.1 to 2.5.

An identical procedure was also followed during investigation of BVO reactions for the coupling with *in situ* H₂O₂ production.

Kinetic evolution of H₂O₂ during BVO reactions was determined by titration of the remaining oxidant against a Ce⁴⁺ solution using ferroin as indicator, following the experimental procedure detailed in Section 2.5.3.1.

List of chemicals used for these experiments: cyclohexanone (99 %, Sigma Aldrich), 2-methyl-cyclohexanone (98 %, Sigma Aldrich), 2-ethyl-cyclohexanone (98 %, Alfa Aesar), menthone (97 %, Sigma Aldrich), 2-*tert*-butyl-cyclohexanone (98 % Sigma Aldrich), 4-methyl-cyclohexanone (97 %, Sigma Aldrich), 4-ethyl-cyclohexanone (98 %, Alfa Aesar), 4-*iso*-propyl-cyclohexanone (96 %, Alfa Aesar), 4-*tert*-butyl-cyclohexanone (99 %, Sigma Aldrich), 4-amino-acetophenone (99 %, Alfa Aesar), 4-methoxy-acetophenone (99 %, Alfa Aesar), 4-ethoxy-acetophenone (98 %, Alfa Aesar), 4-*tert*-butyl-acetophenone (98 %, Alfa Aesar), 4-methyl-acetophenone (99 %, Alfa Aesar), acetophenone (99 %, Alfa Aesar), 4-chloride-acetophenone (99 %, Sigma Aldrich), 4-nitro-acetophenone (99 %, Alfa Aesar), hydrogen peroxide aqueous solution (50 wt. %, Sigma Aldrich), caprolactone (97 %, Sigma Aldrich), 6-hydroxyhexanoic acid (95 %, Sigma Aldrich), 1,4-dioxane (Alfa Aesar), methanol, ethanol, isopropanol, acetone (all of them laboratory reagent grade, Fisher Scientific).

2.4.2 Batch caprolactone (Capr) and substituted caprolactone (R-Capr) hydrolysis reactions

Batch Capr and 4-*i*Pr-Capr hydrolysis reactions were performed following the same experimental procedure of the standard BVO reaction, although the ketones were replaced by the lactones and the oxidant was replaced by the equivalent amount of water added for BVO (typically, 0.3 mL of aqueous 50 wt. % H₂O₂), hence, 0.15 mL of H₂O, otherwise stated along Chapter 3.

Aliquots of the reaction solution were periodically taken for analysis and centrifuged prior to injection into a GC, and/or analysis by ¹H NMR (when required), following the experimental procedures described in Section 2.4.1.

4-isopropyl-caprolactone (4-*i*Pr-Capr), which could not be purchased from any chemical supplier, was isolated, from the final reactant solution of BVO of 4-*i*Pr-CyO after 6 h of reaction by column chromatography, as described in detail in Section 2.5.1.4.1. The isolated product was then used as substrate for hydrolysis studies.

Kinetic parameters studied such as conversion, yield, selectivity and carbon balance were calculated according to Equations 2.1 to 2.4.

2.4.3 Poisoning experiments on BVO reaction

Poisoning experiments for the BVO reaction were generally performed following the same exact experimental procedure of a typical BVO reaction, as described in Section 2.4.1. However, small amounts of the reaction (by-)products (Capr, H₂O and 6-HHA) were also added to the initial reaction solution in the vessel, *i.e.* 10, 25 and 50 mol. % of each product was co-added to the initial reaction solution.

The reactions were monitored by GC-FID as described in Section 2.5.1.1.

2.4.4 Continuous flow BVO reactions of CyO and 4-*i*-Pr-CyO

Continuous BVO reactions were performed in a home-made plug flow, stainless steel, tubular reactor (PFR). Reactant feed delivery (0.33 M CyO or 4-*i*-Pr-CyO in 1,4-dioxane, H₂O₂:ketone 1.5 (or 0.75 where stated)) was performed by an HPLC pump. The catalyst (0.2 g) was mixed with a diluent material (0.8 g of SiC (Fisher Scientific, grinded and meshed to a particle size of 63 – 75 µm)) to avoid back mixing and to minimise the pressure drop, and the bed was placed in between two plugs of quartz wool. The diluted catalyst was densely packed into a 1/4-inch stainless steel tube (4.1 mm ID), and a frit (0.5 mm) was placed at the end of the bed to avoid any loss of material. A contact time of 5.5 min was typically employed. The reactor temperature was controlled by immersion in a thermostatic oil bath, and the pressure was controlled by means of a Back Pressure Regulator (BPR).

The reaction feed was identical to that used for batch reactions and aliquots of the BVO reaction solutions were periodically taken from a sampling valve placed after the reactor and were analysed in the same manner as the batch reactions.

Analogously to the BVO batch reactions, kinetic parameters such as conversion, yield, selectivity and carbon balance were calculated according to Equations 2.1 to 2.4.

Regeneration of the catalyst bed used for BVO continuous reactions was performed heating the whole reactor in a combustion furnace (Carbolite MTF12/38/400) to 550 °C (10 °C min⁻¹) in air (3 h). After the heat treatment, the reactor was put back again in the reaction system and the reaction was re-started at the same initial conditions.

2.4.5 Polymerisation studies

Preliminary polymerisation studies of the lactone produced by BVO / H₂O₂/ Sn-β system were performed at Bath University as a result of a collaboration with Dr Antoine Buchard and Dr Eva María López Vidal.

In a glovebox, 4-*i*-Pr-Capr (0.35 g, 2.2 mmol), triazabicyclodecene (TBD, 22 mL of 1 M solution in anhydrous dichloromethane), 4-methylbenzylalcohol (22 mL of 1 M solution in anhydrous dichloromethane) were mixed and sealed in a flask under argon, before transferring the

solution onto an oil bath preheated at 110 °C. After the required time, the flask was opened to air, quenched with a few drops of MeOH, and the solvent removed under reduced pressure. A crude ^1H NMR spectrum was recorded to determine the conversion of monomers from the relative integrals of monomer and polymer resonances.

The polymer was then washed with MeOH to remove the unreacted monomer before drying under vacuum and analysis by Gel Permeation Chromatography (GPC). GPC analysis was carried out on an Agilent Technologies 1260 Infinity instrument with a flow rate of 1 mL min⁻¹ at 358° C with THF as eluent and referenced against polystyrene standards (RI). More details are reported in Section 2.5.1.3.1.

2.4.6 Batch *in situ* H₂O₂ production

Batch *in situ* H₂O₂ production was performed in a 50 mL Parr autoclave (4590 Micro Bench Top Reactor) equipped with a glass liner and a mechanical stirrer, controlled by a Parr 4848 reactor controller. In a typical reaction, the reactor vessel was charged with the appropriate amount of catalyst and 10 mL of the selected solvent and sealed. The reactor was purged three times prior charging it with 40 bar of 2.5 % H₂ / 5 % O₂ in CO₂ and subsequently cooled down to the desired temperature using an ice bath (typically, 10 °C internal temperature). The reaction was carried out for 30 min at 1000 rpm.

Final H₂O₂ production was analysed following the procedure described in Section 2.5.3.1.

Solvents employed for *in situ* H₂O₂ production include methanol, ethanol, isopropanol and acetone (all of them laboratory reagent grade, Fisher Scientific), acetonitrile (99 %, Sigma Aldrich) and 1,4-dioxane (99 %, Alfa Aesar).

2.4.7 Batch coupling of *in situ* H₂O₂ production and BVO reaction

Coupling of *in situ* H₂O₂ production and BVO reaction was performed in a 50 mL Parr autoclave (4590 Micro Bench Top Reactor) equipped with a glass liner and a mechanical stirrer, controlled by a Parr 4848 reactor controller following similar experimental procedure generally employed for batch *in situ* H₂O₂ production (Section 2.4.6). Reactant solution was composed of 10 mL of 0.33 M CyO dissolved in the chosen solvent mixture (MeOH/1,4-dioxane in a ratio 1:9) and a physical mixture of 1Pd-1Au/TiO₂₍₄₀₀₎ (10 mg) and 2Sn-β (1 mol. % Sn respect to CyO). The reactor was purged and charged with 40 bar of a gas mixture composed of 2.5 % H₂ / 5 % O₂ in CO₂, and subsequently cooled down to 10 °C. Reaction ran for 6 h and an aliquot of the reaction solution was taken and analysed by Ce⁺⁴ titration and GC-FID, as described in Section 2.4.1.

Kinetic parameters such as conversion, yield, selectivity and carbon balance were calculated according to Equations 2.1 to 2.4.

2.4.8 Batch succinic acid (SA) hydrogenation reaction

Catalytic evaluation of SA hydrogenation reaction was carried out using a 100 mL Parr autoclave (Compact Mini Bench Top Reactor 5500) connected to a Parr 4848 Reactor controller. In a typical reaction, 15 mL of 0.2 M SA solution in 1,4-dioxane (SA, 99.9 %, Sigma Aldrich and 1,4-dioxane, 99%, Alfa Aesar) and reduced catalyst (amount required depending on metal loading and mol. % substrate ratio used, usually 2 wt. % of Pd and 2 mol. % Pd with respect SA) were charged into the reactor vessel. The reactor was purged three times and then it was pressurised up to 30 bar with H₂. The reactant solution was heated to the reaction temperature (usually 170 °C) and the reaction initiated by stirring the vessel at 1000 rpm. The reaction was typically run under continuous stirring for a 4 h period, unless otherwise stated. When required, control reactions were performed by replacing the SA substrate for some of the products of the reaction. Otherwise, reactions were performed following the same experimental procedure.

Chemicals employed for this set of experiments were γ -butyrolactone (97 %, Alfa Aesar), propionic acid (97 %, Alfa Aesar), butyric acid (98 %, Sigma Aldrich) and 1,4-butanediol (98 %, Sigma Aldrich).

This reaction system required the analysis of the reaction products by two analytical techniques of GC-FID and High-Performance Liquid Chromatography (HPLC).

SA quantification was carried out by an Agilent 1220 HPLC equipped with a variable wavelength detector (VWD) and a Metacarb 87H Column 250 x 4.6 mm at 60 °C, with 0.4 mL min⁻¹ of 0.1 wt. % H₃PO₄ aqueous solution as eluent, against citric acid (CA) 0.01 M as external standard. More details on this analytical technique can be found in Section 2.5.1.2.1.

γ -Butyrolactone (GBL), 1,4-butanediol (BDO), butyric acid (BA) and propionic acid (PA) were quantified by an Agilent 7890B GC equipped with a FID detector and a 25m CP-Wax 52 CB column, against 0.01 M of Bp as external standard, following the same methodology described in Section 2.5.1.1.2.

Additionally, gas products were analysed using a Varian 450-GC gas chromatograph equipped with FID and a methanizer. More details are described in Section 2.5.1.1.3.

Kinetic parameters such as conversion, yield, selectivity and carbon balance were calculated according to Equations 2.1 to 2.4.

2.4.9 Reusability studies for catalytic hydrogenation of SA

Catalyst reusability studies were carried out after simple filtration of the catalyst. Between measurements, the catalyst was dried overnight at room temperature. The typical conditions and the methods employed for the standard reaction conditions were performed, as described above.

2.5 Analytical methods

Analytical details of the qualitative and quantitative analysis of the reactions reported in the whole project, are provided in this section.

2.5.1 Chromatography

Chromatography is an analytical technique commonly used to separate a mixture of chemical substances into its individual components, so that they can be analysed. The mixture is dissolved in a fluid called the mobile phase, which carries it through a structure holding a material called the stationary phase. The separation of the components is based on differential partitioning between the mobile phase and the stationary phase, depending from the affinity of the single component to bind to the stationary phase.

2.5.1.1 Gas Chromatography (GC)

Gas Chromatography (GC) is a common type of chromatography used for the separation and analysis of compounds that can be vaporised without decomposition. In this technique, the mixture to be separated is passed through the system by use of an inert carrier gas (typically He), which acts as the mobile phase. The fluid phase is continuously carried through the chromatographic column (usually a capillary column coated or supported with a thin polymeric film), which acts as the stationary phase. The molecules transported in the mobile phase interact differently with the stationary phase, leading to them being eluted from the column at different time (retention time, RT). Hence, a molecule that interacts strongly with the column will elute later (longer RT). At fixed conditions, RT is characteristic of each compound being eluted from the system (Fig 2.3).

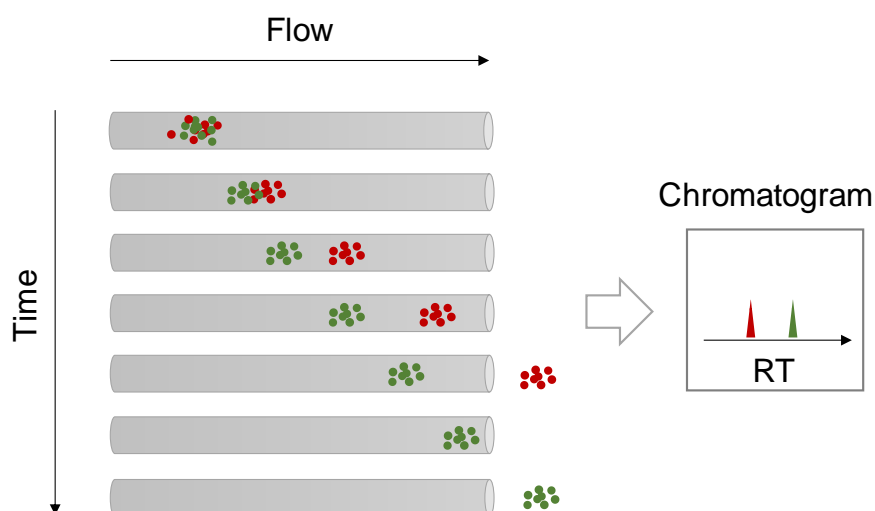


Figure 2.3. Representation of a chromatographic separation process.

Generally, a GC instrument is composed of a series of common elements. An injector, usually held at temperatures of 150 - 300 °C, vaporises the sample and introduces the mixture into the eluent gas, which carries the analytes into a column that is held in an oven. The oven controls the temperature at which the column is working, and its temperature range and ramp rates depend on the GC method chosen for the particular analysis. The separation of the analytes is strongly dependent of the temperature, in addition to the type of stationary phase, so the control of temperature represents one of the most important parameters in GC. Finally, the eluted analytes arrive to the detector, which generates a response that is proportional to the amount of the analyte detected. The type of detector chosen depends on the nature of the analytes and their sensitivity to generate a signal by the detection method. Generally, for the detection of hydrocarbon or organic molecules containing low quantities of oxygen, such as alcohols, ketones and ethers, a Flame Ionisation Detector (FID) is often employed. In this case, a H₂ flame burns the organic molecules producing a flow of ions that are collected, thereby generating a current that is transformed into a chromatographic signal. The analyte signal results in a gaussian peak whose area can be integrated and used for its quantification.

2.5.1.1.1 Quantification of BVO products

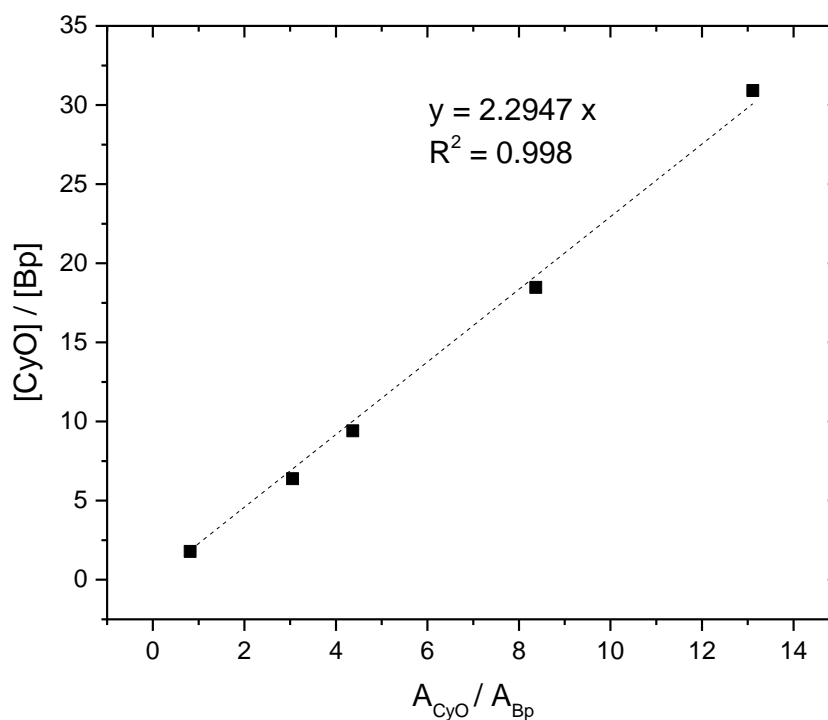
The evolution of BVO reaction was monitored by a GC (Agilent 7820, 25 m CP-Wax 52 CB column) equipped with an FID (at 250 °C) and He (5 mL min⁻¹) as carrier gas. The quantification of the reactant components was carried out against Bp as internal standard prior calibration of all the analytes of interests. Calibrations were performed by preparation of accurate solutions of the analytes at different concentrations (covering the full reaction range from 0 - 100 % conversion or yield) in a 1,4-dioxane with a fixed concentration of Bp (0.01 M). The area of the analytes and standard were obtained by integration of the corresponding signals in the chromatograph. The GC method employed was previously optimised to ensure the proper separation of all components. In this case, the temperature profile of the GC method consisted of an initial isothermal period at 35 °C for 7.5 min, a heating period with a ramp rate of 15 °C min⁻¹ until 200 °C and a final isothermal period at 200 °C for 8 min. Table 2.1 shows a representative example for the GC calibration of CyO.

Table 2.1. Concentrations and GC areas obtained for the calibration of CyO.

	CyO		Bp	
n°	Concentration / M	Area	Concentration / M	Area
1	0.334	481.0	0.011	588.8
2	0.196	1779.0	0.010	582.5
3	0.0982	2615.8	0.0106	598.8
4	0.069	4757.5	0.0108	568.5
5	0.0192	7460.3	0.0108	569

As reported in Fig 2.4, the calibration curve was generated by plotting the ratio of the concentration of the analyte and Bp against the ratio of the corresponding areas obtained by the chromatogram, according to Equation 2.6:

$$\frac{[CyO]}{[Bp]} = CF \frac{Area\ CyO}{Area\ Bp} \quad [Equation\ 2.6]$$

**Figure 2.4.** Calibration curve obtained by GC for CyO against Bp as internal standard.

The calibration factor (CF) was obtained by calculating the slope of the fitting curve of the calibration points, and it was used to obtain the unknown concentrations of each analyte during the reaction. For example, the CF obtained for CyO was 2.29. CF for Capr and R-CyO were calculated following the procedure described above and their CF as well as RT are compiled in Table 2.2. The corresponding lactone products of the BVO reaction of R-CyO, R-Capr, could not be purchased from any supplier and calibrated. Hence, considering that CF obtained for CyO and Capr were almost identical, the same CF of their original ketone was employed.

Table 2.2. CF and RT for BVO ketones and lactones obtained by GC.

Analyte	CF	RT / min
CyO	2.29	14.7
Capr	2.41	20.7
2-Me-CyO	1.77	14.2
2-Eth-CyO	1.66	15.4
Menthone (2- <i>i</i> Pr-CyO)	1.35	16.7
2- <i>t</i> Bu-CyO	1.32	17.0
4-Me-CyO	1.73	14.7
4-Eth-CyO	1.39	16.8
4- <i>i</i> Pr-CyO	1.47	18.3
4- <i>t</i> Bu-CyO	1.21	18.9

For quantification of *para*-substituted acetophenone (4-R-AcetoPhO) BVO products, a different GC method was required, whose temperature profile consisted in an initial isothermal period of 6 min at 55 °C, a heating step up to 158 °C at a ramp rate of 35 °C min⁻¹ followed by an isothermal period for 6 min and a final heating step up to 205 °C at a ramp rate of 35 °C min⁻¹, followed by an isothermal period of 14 min. Calibration curves of the analytes were obtained following the same experimental procedure against Bp as internal standard. All the CF obtained for 4-R-AcetoPhO were calculated following the exact procedure described above and their CF as well as RT are compiled in Table 2.3. As occurred with the substituted lactones, the corresponding esters produced from BVO of 4-R-AcetoPhO could not be purchased from any supplier and calibrated. Therefore, the same CF obtained for the original substrate was employed for the quantification of each ester.

Table 2.3. CF and RT for BVO 4-R-AcetoPhO obtained by GC.

Analyte	CF	RT / min
4-AcetoPhO	1.58	18.9
4-Me-AcetoPhO	1.40	12.7
4-MeO-AcetoPhO	1.47	14.7
4-EthO-AcetoPhO	1.45	17.9
4-^tBu-AcetoPhO	1.35	16.0
4-NH₂-AcetoPhO	1.72	20.4
4-NO₂-AcetoPhO	2.1	16.3
4-Cl-AcetoPhO	1.57	14.3

2.5.1.1.2 Quantification of SA hydrogenation liquid-products

The evolution of the products from the catalytic hydrogenation of SA hydrogenation was monitored by the same GC instrument, following the same experimental and GC method described in Section 2.5.1.1.1., with the only difference of using Bp as external standard, adding a fixed amount of solution of known concentration into the GC vial. CF and RT of the hydrogenation products are compiled in Table 2.4.

Table 2.4. CF and RT for SA hydrogenation products in the liquid phase obtained by GC.

Analyte	CF	RT / min
GBL	4.21	18.9
PA	6.70	18.0
BA	3.88	18.7
BDO	3.99	20.6

2.5.1.1.3 Quantification of SA hydrogenation gas-products

Quantification of gas products from the hydrogenation of SA was achieved using a Varian 450-GC gas chromatograph equipped with FID and a methanizer. The FID has little or no response to CO and CO₂ since they are unable to burn, and thus cannot generate a FID signal. However, when preceded by a methanizer, which consists of a hydrogenating reactor, CO and CO₂ can

be converted into methane, producing a feasible signal for the detector and allowing their quantification. By using an isothermal GC method at 35 °C with He (5 mL min⁻¹) as carrier gas, the gas products from the hydrogenation of SA were calibrated by injecting known concentrations of each analyte and plotting their resultant signal against these concentrations. The CF and RT obtained for each gas analyte are summarised in Table 2.5.

Table 2.5. CF and RT for SA hydrogenation products in the gas phase obtained by GC.

Analyte	CF	RT / min
CO	3130	5.05
CH ₄	3130	5.16
CO ₂	3130	5.40
Ethane	6650	5.52
Propane	9271	7.12

2.5.1.2 High Performance Liquid Chromatography (HPLC)

High Performance Liquid Chromatography (HPLC) is an alternative analytical methodology to GC, sharing similar principles for the separation of the components present in a mixture, which is achieved by interaction of the analyte in the mobile phase with the stationary phase. However, in this case the mobile phase is a liquid solution and the stationary phase a packed column, usually a polymeric resin. As occurs with GC, identification and quantification of analytes is generally obtained by comparison with the calibration curves of authentic standard of the analytes.

HPLC is preferred to GC when is not possible to vaporise the analytes without decomposing them, *i.e.* where the analytes are either poorly thermally stable, and/or possess low vapour pressure. To achieve an efficient interaction between mobile and stationary phase and a good separation, the instrument needs to be run at high pressures, normally between 40 - 100 bar. Hence, a pump is required to provide an accurate and constant flow of eluent through the whole system and provide the ability to operate at high pressure arises from the pressure drops caused by the densely packed chromatographic column. The choice of the stationary phase ultimately depends from the nature of the analytes being investigated. For instance, acidic resins are commonly used for organic acid separation. The detection of analytes in HPLC can be carried out with different detectors, hence, the HPLC technique can be assembled with more than one detector and their use will depend on the nature of the analytes. The most common liquid chromatography detectors are the UV-Vis and the Refractive Index

Detector (RID). The UV-Vis detector, for instance, is based on the detection of the differences in absorbance between the solution containing the analyte, and the eluent itself. Therefore, in this case, the analytes require a functional group that is UV-sensitive. Generally, HPLC methods are simple, with the column temperature, the eluent composition and the flow rates all kept constant. A gradient of eluent composition can also be used to improve separation of certain compounds.

2.5.1.2.1 Quantification of SA

SA quantification was carried out by an Agilent 1220 HPLC equipped with a variable wavelength detector (VWD) set up to 210 nm and a Metacarb 87H Column 250 x 4.6 mm at 60 °C, with 0.4 mL min⁻¹ of 0.1 wt. % H₃PO₄ solution as eluent, against 0.01 M citric acid (CA) as external standard.

Calibration of SA was performed by preparation of accurate solutions at different concentrations, covering the full reaction range from 0 - 100 % conversion, in 1,4-dioxane. Prior to injection, samples were diluted in water to operate within an optimal UV signal range. At the same time, a known amount of external standard was co-added to each solution. Typically, each HPLC sample contained: 9.8 mL of water, 0.1 mL of sample and 0.1 mL of CA solution. The area of the analyte and standard were obtained by integration of the corresponding signals in the chromatograph. Analogous to the calibration by GC, a calibration curve could be obtained by plotting the ratio of the concentration of SA and CA against the ratio of the corresponding area obtained by the chromatogram. A CF of 3.48 was obtained by calculating the slope of the fitting curve equation of the calibration points, and it was used to obtain the unknown concentrations of SA during the reactions.

2.5.1.3 Gel permeation chromatography (GPC)

Gel Permeation Chromatography (GPC) or Size Exclusion Chromatography (SEC) is a versatile type of liquid chromatography (LC), in which, a solid stationary phase and a liquid mobile phase are used.¹ Its separation mechanism relies on the size of the analytes, usually polymers, rather than any chemical interaction between them and the stationary phase. GPC is able to determine several important parameters for polymers such as number average molecular weight (M_n), weight average molecular weight (M_w), and the most fundamental characteristic of a polymer, its molecular weight distribution curve and polydispersity index (PDI).

A GPC/SEC instrument consists of a pump to push the solvent through the instrument, an injection port to introduce the test sample onto the column, a column to hold the stationary phase, one or more detectors to detect the components eluted by the column, and a software to control the different parts of the instrument and calculate and display the results.

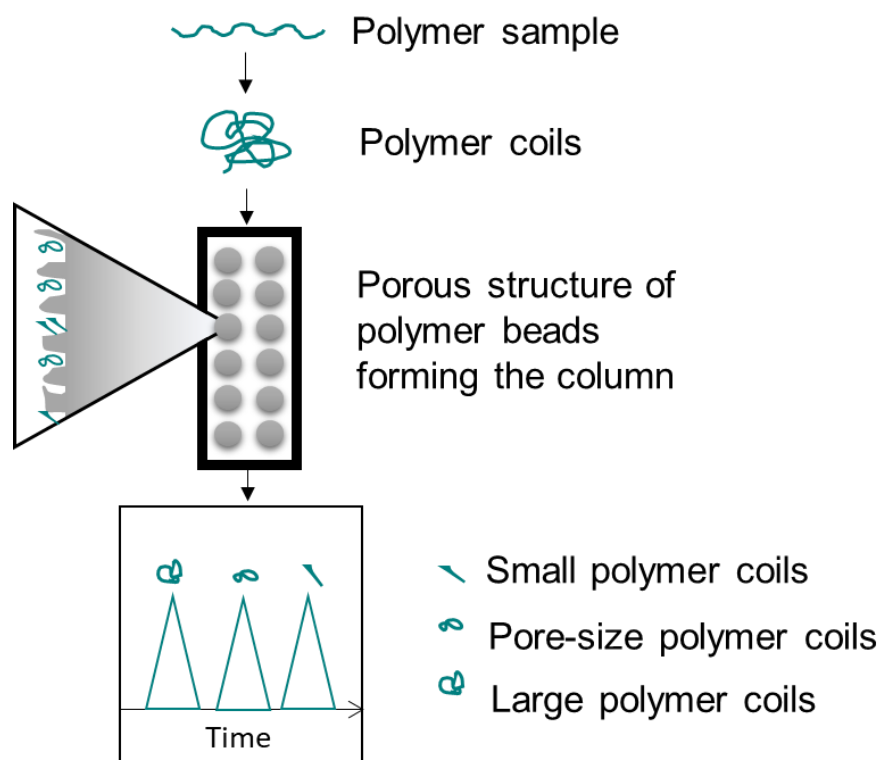


Figure 2.5. Representation of the separation mechanism of polymers by GPC/SEC, based on different sizes.

Firstly, the polymer is dissolved in a solvent to adopt a coiled formation of long molecules. Subsequently, these coiled up polymer molecules are introduced into the mobile phase and flowed into the GPC/SEC column, where they pass the column made of a porous structure of polymer beads as the mobile phase carries them through. Depending on the size of the polymer coils, they can be accommodated in the pores of the beads, along the column. The larger coiled polymers, which do not enter into the pores, flow straight out of the column; the coiled polymer with a similar size than the pore beads can be accommodated along the column, occupying some of the stationary phase; while the smallest polymer coils can enter any of the pores in the beads. This partitioning occurs repeatedly, with diffusion acting to bring the molecules into and back out of any pores they pass as they travel down the column. As a result, small polymer coils that can enter into many pores in the beads take a long time to pass through the column and therefore exit the column slowly, whilst the largest polymer coils are eluted faster. As the different sizes of polymer exited the column, they are detected by various ways, typically RID, and their signals are displayed in a chromatogram.

The data is compared to the calibration of a polymer with a series of known molecular weights which elute the column at certain retention times, allowing the calculation of the molecular weight distribution of the sample and the rest of the parameters relevant for polymer analysis.

2.5.1.3.1 Analysis of Capr oligomers and 4-ⁱPr-Capr polymer

Analysis of Capr oligomers, and the poly(4-ⁱPr-Capr) polymer product formed were conducted on an Agilent Technologies 1260 Infinity instrument equipped with a PLgel 5 μ m MIXED-D 300 x7.5mm column at 35 °C. A flow rate of 1 mL min⁻¹ of THF was used as eluent and polymeric samples were dissolved at a concentration of 2 mg mL⁻¹ and referenced against polystyrene standards.

2.5.1.4 Column chromatography

Column chromatography is frequently used in organic chemistry to purify liquids or solids. Typically, a sample is loaded onto the stationary phase, composed of a column of adsorbant material, such as silica gel or alumina. An organic solvent, or mixture of solvents, are then passed through the stationary phase, acting as a mobile phase. The individual components of the mixture can be separated from each other by partitioning between the stationary packing material and the mobile eluent. Therefore, they move through the column at different rates. The eluent is collected in fractions that are commonly analysed by thin-layer chromatography (TLC), to monitor the elution, and hence, separation, of the individual components of the analysed mixture. TLC is based on the separation of compounds by their polarity and interaction with the silica plate.

2.5.1.4.1 Lactone separation

Separation and purification of lactones produced from BVO of CyO and R-CyO were carried out by column chromatography. The crude sample was charged onto a packed silica column and components were separated using hexane as eluent to separate the biphenyl, and subsequently, a mixture hexane/ethyl acetate (3:1) was used to separate the ketone and the lactone. Fractions containing the lactone were identified by TLC and were isolated by evaporating the column chromatographic solvent by a rotavapor. The presence and purity of the corresponding lactone was confirmed by ¹H NMR analysis. After its isolation, the desired lactone was used either to investigate the hydrolysis reaction step or to perform polymerisation studies.

2.5.2 Nuclear Magnetic Resonance (NMR) spectroscopy

Nuclear Magnetic Resonance (NMR) spectroscopy is a powerful analytical technique that allows the identification and quantification of organic molecules in solution. The fundamentals of this technique are based on the application of a local magnetic field around a nucleus of a specific element in a particular sample, giving information on how the atoms in the molecule are spatially arranged.²

The principle behind NMR is that many nuclei have spin and all nuclei are electrically charged. In some atoms (^{12}C , ^{16}O , ^{32}S) these spins are paired and cancel each other out so that the nucleus of the atom has no overall spin. However, in many atoms (^1H , ^{13}C , ^{31}P , ^{15}N , ^{19}F) the nucleus does possess an overall spin.

If an external magnetic field is applied (B_0), the magnetic moment of these spin active nuclei aligns, either with or against the direction of the external magnetic field. In doing so the degenerated nuclear energy level splits, forming different energy levels, which are given by a magnetic number, m . Each single energy level can therefore be defined as:

$$E = \pm m\hbar\gamma B_0 \quad [\text{Equation 2.7}]$$

Where m is the magnetic number, \hbar is Planck constant divided by 2π , and γ is the magnetogyric ratio.

When m is $\pm\frac{1}{2}$, two nuclear energy levels are formed and the difference between these levels is expressed as:

$$\Delta E = \hbar\gamma B_0 \quad [\text{Equation 2.8}]$$

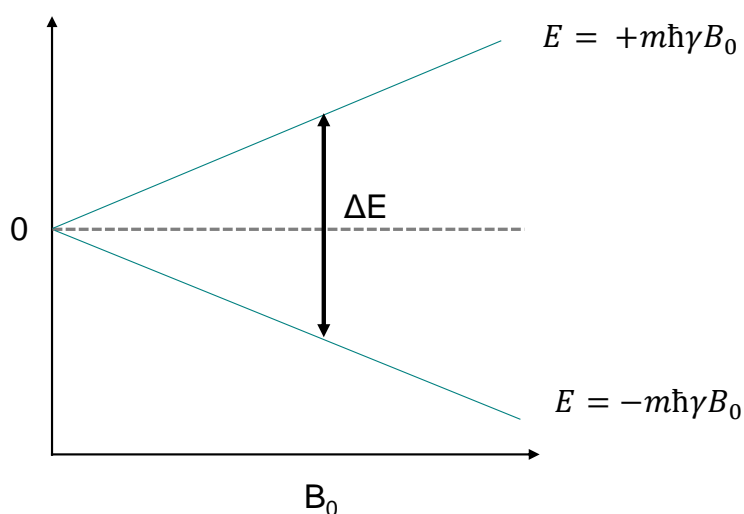


Figure 2.6. Representation of the spin energy level splitting of nuclei (with $m = \pm\frac{1}{2}$) as a function of the external magnetic field B_0 .

An energy transfer is possible between the lower energy to a higher energy level (generally a single energy gap). The energy transfer takes place at a wavelength that corresponds to radio frequencies (of order of hundreds of MHz or GHz). The exact frequency (Larmor frequency) depends on the type *i.e.* the identity, of the nucleus under study, and on the magnitude of the external magnetic field, as determined by:

$$\nu = \frac{\gamma B_0}{2\pi} \quad [\text{Equation 2.9}]$$

However, in molecules, all the nuclei are surrounded by electrons, which create a local magnetic field, B_e , which interact and oppose to the external magnetic field, B_0 . As a result, the effective resonance (ν_{eff}), which strongly depends on the interactions caused by the electrons, originates a characteristic and unique signal for each species in a sample, even if all species correspond to the same chemical element. Equation 2.9 is then re-defined as:

$$\nu_{\text{eff}} = \frac{\gamma(B_0 - B_e)}{2\pi} \quad [\text{Equation 2.10}]$$

Subsequently, the spin returns to its base level through a process called relaxation. Relaxation processes are complex and can be of different nature, however, the two more common relaxation modes are the spin-lattice (T_1) and spin-spin (T_2) relaxation. The relaxation modes can have different timescale and they are strictly dependent from the nature of the nuclei and their chemical surrounding. As such, two different nuclei of the same element can have a very different relaxation times and mechanisms, depending on the position they occupy in the molecules. In general, the more efficient the relaxation, the faster is the time of T_1 , and hence, the faster is the time of analysis. Consequently, the quality of the signal improves, since more spectra can be acquired per unit time, increasing the signal to noise (S/N) ratio, resulting in better signal quality and resolution.

The resonance frequency of a particular NMR signal is expressed in terms of chemical shift (δ), which has a ppm as unit. Chemical shift is the resonance frequency of a specific nuclei compared to the frequency of the same element nucleus when it is in an arbitrary standard molecule (ν_{ref}). The chemical shifts are normalised to the working frequency of the spectrometer and the same chemical shift is observed for the same nuclei in different machines.

$$\delta \text{ (ppm)} = \frac{(\nu_{\text{eff}} - \nu_{\text{ref}}) \text{ Hz}}{\nu_{\text{ref}} \times 10^6 \text{ Hz}} \quad [\text{Equation 2.11}]$$

For ^1H NMR, the reference is usually tetramethylsilane (TMS), $\text{Si}(\text{CH}_3)_4$. This compound has four $-\text{CH}_3$ groups single bonded to a silicon atom, hence all the protons are in the same electronic environment. Therefore, only one NMR signal is generated at 0 ppm.

2.5.2.1 Quantification of BVO products

Quantification of BVO reaction analytes was carried out with ^1H NMR, by using a capillary filled with TMS in deuterated chloroform (1% TMS/ CDCl_3) previously calibrated, against standards.

The ^1H NMR and ^{13}C NMR analysis were conducted on a 400MHz Bruker DPX instrument. For the calibration of the TMS insert by ^1H NMR, the insert was introduced into different NMR sample tubes containing 6-HHA solutions of various known concentrations. For each analysis, 0.3 mL of primary standard solution was placed into a round-bottom flask and solvent-evaporated by rotavapor. Subsequently, 0.7 mL of CDCl_3 was added to recover all the remaining analyte in the flask, and the solution carefully transferred into an NMR tube containing the TMS insert. As described above, TMS presents a characteristic singlet signal at 0 ppm that could be integrated and calibrated to 1. Once this signal is calibrated, the rest of the signals to be analysed can also be integrated. By plotting the integration values of the signal at 1.4 ppm, originated from 6-HHA, against the theoretical concentration of 6-HHA used for each calibration point, a calibration curve was obtained as illustrated in Fig 2.7.

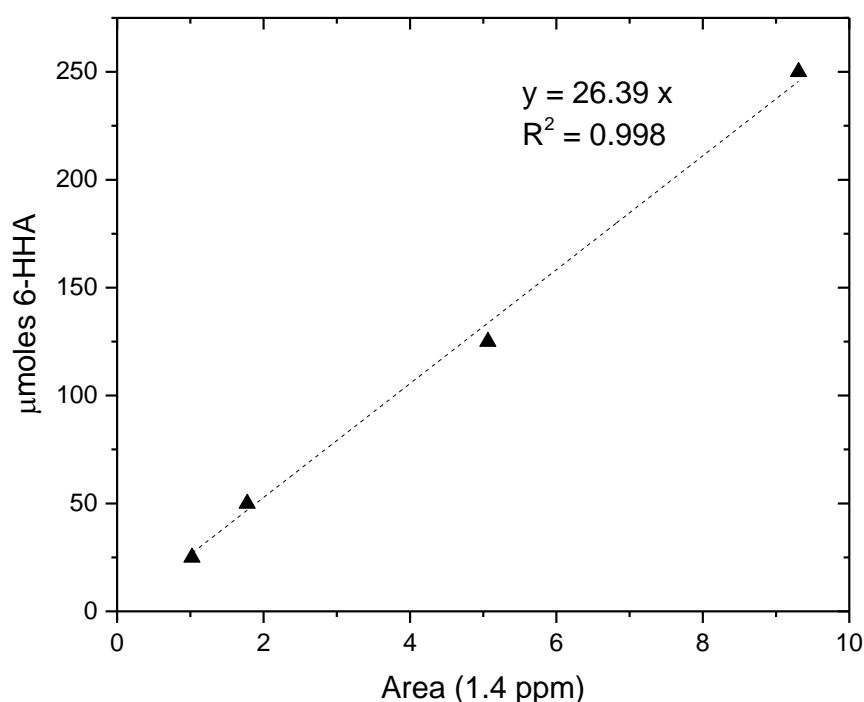


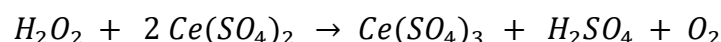
Figure 2.7. Calibration of TMS capillary against solutions of various 6-HHA concentrations.

The slope obtained from the fitting curve equation corresponds to the CF of the TMS insert. The CF value obtained was 26.39 and used to quantify all unknown analytes of the sample.

Typically, ^1H NMR analysis was performed following the same analytical procedure, and the analytes present were quantified against the previously calibrated TMS insert, placed inside the NMR tube. As long as the signal of the analyte arises from the same number of protons, the same CF of the insert calibrated with 6-HHA can be used. Therefore, the Capr signal chosen (4.2 ppm), which arises also from two protons, did not require a new CF and the same than for 6-HHA could be used for its quantification by ^1H NMR. The same principle can be restored for 4-R-6-HHA, where the same CF obtained for the resonance originated by 6-HHA at 1.4 ppm can be employed for their quantification. However, in the presence of 4-R, the analogous resonance of 1.4 ppm corresponds to only one proton, hence, this cannot be used, instead the resonance at 3.8 ppm (analogous to the 3.6 ppm signal of 6-HHA), still arising from two protons, allowed proper quantification of 4-R-6-HHA formed.

2.5.3 Titration of hydrogen peroxide (H_2O_2)

Hydrogen peroxide (H_2O_2) concentration was determined by titration with cerium (IV) sulfate ($\text{Ce}(\text{SO}_4)_2$) using ferroin as indicator. This titration is based on the redox reaction occurring between the two compounds, which end point is detected by a colorimetric change from red to pale blue:



2.5.3.1 Quantification of H_2O_2

Typically, 0.1 mL of sample was placed into a glass vial with 0.5 mL of 2 wt. % H_2SO_4 solution and some drops of ferroin. Samples were titrated with $\text{Ce}(\text{SO}_4)_2$ solution, previously standardised using ammonium iron sulphate and ferroin, until the initially red solution became pale blue. The volume of titration solution was used to calculate the oxidant concentration.

2.5.4 Attenuated Total Reflectance (ATR) Infra-Red (IR)

Attenuated Total Reflectance (ATR) is an Infra-Red (IR) technique that allows a wide variety of solid and liquid samples to be measured without any complex sample preparation.³

The IR technique is based on the fact that all molecules are capable of absorbing IR radiation when the energy of the incident beam matches the energy necessary to excite a particular mode of vibration of the chemical bonds present in the molecule. Therefore, IR spectroscopy is used to determine the type and strength of the bonds present in the molecules. This is very useful to identify components of a mixture by their particular IR signals.

The ATR crystal consists of an IR transparent material with a high refractive index and has polished surfaces. The IR beam enters the crystal at 45° and is totally reflected at the crystal

to the sample interface. Different kinds of materials can be used as ATR crystals, with diamond being particularly good, as it is very robust and chemically inert; thus, diamond is an ideal crystalline material for routine measurements with a wide range of possible samples. After one or several internal reflections, the IR beam exits the ATR crystal and is directed to the IR-detector. ATR-IR measurement is transformed by the detector into the corresponding IR spectrum, usually in the range of $4000 - 400 \text{ cm}^{-1}$.

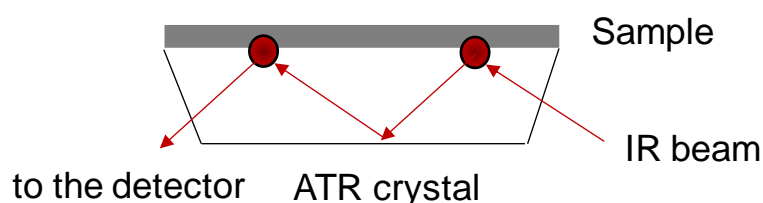


Figure 2.8. ATR principle of IR beam reflection through the crystal and sample interface.

2.5.4.1 Analysis of BVO products

ATR-IR spectroscopy was used to analyse the spectra of the potential species involved in the BVO reaction (CyO, Capr, 6-HHA and adipic acid (AA)). The standards were placed directly on to a Platinum ATR cell, equipped with a diamond crystal, mounted on a Bruker Vertex 70v, and were measured without any further sample preparation.

2.5.5 Thermogravimetric analysis (TGA)

Thermogravimetric analysis (TGA) is a technique in which the mass of the sample is measured while its temperature is changed over time. The information provided by this technique relate to the thermal stability of the sample, or the species adsorbed on the material.

The main component of this instrumentation is a combustion chamber in which a balance constantly measuring the mass of the sample placed on an alumina crucible. The temperature can be accurately programmed and the atmosphere of the combustion chamber, gas flow and gas composition (*i.e.* N_2 or air), can be controlled as well. A plot of the mass of the catalyst vs. time and/or temperature is obtained from this analysis. Commonly, the first derivative of the mass loss against time or temperature is plotted to obtain a more clear and visual identification of at what temperature, a specific mass loss occurs.

2.5.5.1 Experimental details for TGA

TGA was performed using a Perkin Elmer TGA 4000. All samples were subjected to the same temperature programmed step in an air atmosphere, which consisted of an initial isothermal step at 30°C for 30 min, followed by a heating step with a temperature ramp of $10^\circ\text{C min}^{-1}$ up

to 550 °C and a final isothermal step at 550 °C for 30 min, prior cooling down to room temperature.

Prior to the analysis, the catalyst was treated with standard solutions (solvents, CyO, Capr, 6-HHA, AA and SA) for 4 h, filtered and dried overnight. First derivatives of each TGA were used to determine the desorption time of each analyte, to allow the identification of the adsorbed species in the used catalyst.

Samples analysed after reaction (BVO or SA hydrogenation) were subjected to the same procedure of filtering and drying prior being analysed by TGA. Knowing the specific desorption time of each analyte and the percentage of weight loss corresponding to each one from the TGA, the quantity of each analyte desorbed from the material can be estimated.

2.6 Catalyst characterisation techniques

To better understand catalytic performance, and to correlate the structure of the synthesised catalysts to their activity, multiple characterisation techniques were adopted in this study. Structural and textural analyses were performed with powder X-ray Diffraction and porosimetry, respectively, and the morphology of each material studied with Scanning Electron Microscopy and Transmission Electron Microscopy. Characterisation of the active sites in the zeolite catalysts was conducted through Magic Angle Spinning NMR spectroscopy, while the nature of the active species in metal supported nanoparticles was investigated by X-Ray Photoelectron Spectroscopy. Differences in acidity between alumina supports were analysed by Diffuse Reflectance Infrared Fourier Transformed spectroscopy. The combination of these techniques provides a deeper comprehension of the structure - activity relationships observed in the catalytic systems studied in this thesis. The theoretical background of each characterisation technique and experimental details employed with each method, are presented in the following sections.

2.6.1 Powder X-Ray Diffraction (XRD)

X-Ray Diffraction (XRD) is an essential technique used to analyse the crystalline structure of materials and to confirm phase purity by examination of their diffraction patterns.⁴ Crystalline solid materials are spatially arranged in a highly ordered manner that is repeated in the three dimensions of space. Hence, diffraction occurs when the incident X-ray beam interacts with their structure at certain angles that satisfy Bragg's Law,⁵ which provides information on the crystalline lattice:

$$n\lambda = 2d\sin\theta \quad [Equation 2.12]$$

Where n is an integer number, λ is the wavelength of the X-ray radiation, d is the spacing between the planes and θ is the angle between the diffracted beam and the sample. A schematic of the X-ray diffraction process is shown in Fig 2.9.

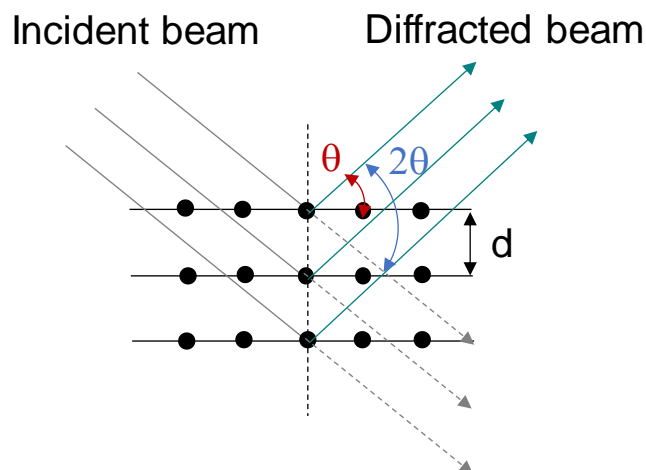


Figure 2.9. Scheme of diffraction phenomenon generated by the incidence of a monochromatic radiation into a crystalline structure according to the Bragg's law.

An XRD instrument is commonly composed of an X-Ray generator, a sample holder and a detector. The X-Ray beam is generated by irradiating a copper foil with a high-energy electron beam and is filtered by a monochromator that selects the typical CuK_α radiation (1.54 \AA) to converge upon the sample. The detector moves around the sample through an arc, collecting the diffracted radiation at a determined range of angles, usually from 5 to $80^\circ 2\theta$. The resulting diffractogram shows the intensity of the diffracted beam against the diffraction angle 2θ . By comparison of the obtained XRD patterns with references patterns on a data base, the phase or phases present in each sample can be identified, alongside the crystal planes corresponding to each main diffraction peak. Furthermore, it allows comparison of crystallinity between samples by measuring parameters such as the full width half maximum intensity.

2.6.1.1 Experimental details

In this work, a Panalytical X'PertPRO X-ray diffractometer was employed for powder XRD analysis. A CuK_α radiation source (40 kV and 30 mA) was employed and diffraction patterns were recorded between $5 - 80^\circ 2\theta$ (step size 0.0167° , time/step = 150 s). In case of the zeolite materials, patterns were compared with references on the data base, *i.e.* "Collection of simulated XRD powder patterns for zeolites".

2.6.2 Surface area and porosimetry analysis

Porosimetry is an analytical technique used to determine the porous properties of solid materials including pore diameter, total pore volume and surface area. It consists in the gradual physical adsorption of an inert gas (N_2 , Ar or Kr) at low temperature on the material surface, first forming a mono-layer and then subsequent multi-layers, generating an isotherm that is a function of the volume of gas adsorbed (v) and the relative pressure (P/P_0).⁶

One of the most relevant parameters studied by this technique is the surface area, commonly calculated by the Brunauer-Emmett-Teller (BET) method:⁷

$$\frac{1}{v[(P/P_0) - 1]} = \frac{c - 1}{v_m c} \left(\frac{P}{P_0} \right) + \frac{1}{v_m c} \quad [\text{Equation 2.13}]$$

Where v is the volume of adsorbed gas at a pressure P , P_0 is the saturation pressure, v_m is the molar volume of gas needed to make monolayer of adsorbed gas and C is the BET constant. According to the BET theory, it should be possible to obtain a straight line if the equation is applied in the relative pressure range of 0.05 – 0.35 P/P_0 . The slope calculated by this line contains the value of v_m and the specific surface area can be calculated as:

$$S_{BET} = \frac{v_m N s}{V a} \quad [\text{Equation 2.14}]$$

Where N is the Avogadro number, s is the adsorption cross-section of the adsorbing gas (for N_2 , $s = 0.162 \text{ nm}^2$), V is the molar volume of the adsorbing gas and a is the mass of the solid. The total pore volume can be directly extrapolated from the isotherm at partial pressure $P/P_0 = 0.99$, assuming all pores are filled with adsorbate. The pore size distribution is usually determined by the Barrett-Joyner-Halenda (BJH) model,⁸ a procedure for calculating pore size distributions from experimental isotherms using the Kelvin model of pore filling. BJH can only be correctly applied to mesopores and small macropores. The microporous volume and external surface area can be calculated by the t-plot,⁹ based on standard isotherms and thickness curves, which describes the statistical thickness of the film of adsorptive on a non-porous reference surface. The difference between the total pore volume and the micropore volume (obtained by t-plot) gives the mesopore volume.

2.6.2.1 Experimental details

Porosimetry analysis of all materials used in this work were carried out on a Quantachrome Quadrasorb, with N_2 as adsorbate, and the isotherms were collected at 77 K. Samples were degassed accordingly prior the N_2 adsorption measurements, depending on the kind of sample

analysed. Sn-catalysts were degassed at 277 °C for 16 h using a FLOVAC Degasser, while the metal supported nanoparticles were degassed at 120 °C for 6 h.

2.6.3 Electron Microscopy

Electron microscopy is a technique that uses a beam of accelerated electrons as a source of illumination to irradiate the sample and obtain detailed images at a very small scale. In catalysis, this technique is typically employed to obtain information on the morphology of solid samples.¹⁰

2.6.3.1 Scanning electron microscopy (SEM)

Scanning Electron Microscopy (SEM) provides images of the sample surface by scanning it with a focused beam of electrons. When the incident electrons are deflected by the specimen atom nucleus or by similarly energetic external shell electrons, the interaction are defined as elastic. In these interactions, negligible energy is lost in the collision and produces wide angle of electronic scattering. The Back-Scattered Electrons (BSE) reflected from the sample through elastic scattering at angles $> 90^\circ$ provides a good signal for imaging. On the contrary, inelastic scattering occurs when the interactions between the fallen electrons and the atoms and electrons of the specimen, lead to the transfer of essential energy to the atoms. As a result, Secondary Electrons (SE) would be generated from the excitation of the sample electrons during the ionisation of the atoms. These electrons are typically known to possess energies lower than 50 eV and can be applied as a useful tool to analyse or generate images of the specimen. Both BSE and SE can generate images at very high magnifications.

Additionally, another type of signal widely used in SEM analysis is the X-ray, which is generated by the energy difference of the transition of a higher energy shell electron filling up a hole that has been formed when an electron of a lower energy shell has been exited by the electron beam. This X-ray has an energy that is characteristic of the energy difference between these two shells. It depends on the atomic number, which is a unique property of every element. In this way, this X-rays can be used to identify and quantify the elements present in each sample. This process is known as Energy-Dispersive X-ray (EDX) analysis. Hence, SEM images are a useful way of providing information on the elemental distribution and to compare crystal morphology between samples, in order to relate any changes in activity to changes in the structure.

2.6.3.1.1 Experimental details

For their analysis, samples were dispersed in a carbon film and placed into the SEM chamber under vacuum. A Hitachi TM3030Plus SEM instrument was used to acquire images at an energy of 15 kV, and EDX was utilised to analyse the elemental composition and distribution.

2.6.3.2 Transmission electron microscopy (TEM)

Transmission Electron Microscopy (TEM) is a powerful microscopy technique. A high energy beam of electrons is passed through a very thin sample, allowing features such as crystal structure, grain boundaries and dislocations to be observed due to the interactions between the electrons and the atoms.

In a TEM instrument, the electron gun generates the electron beam, which hits the sample, and transmitted electrons are magnified by electromagnetic lenses. The optics bring the scattered electron from the same point in the sample to the same point in the image. The image recorder transforms the electron signals into a form perceivable by the human eye. While SEM works on the topological and compositional structure of a surface, TEM obtains information from the electron beam as it interferes with the mass in a two-dimensional image. This technique is especially useful to characterise metal supported nanoparticles, since usually particle with a diameter > 1 nm can be observed. The processing of several images of each sample allows a statistical analysis to be performed, allowing the particle size distribution and the average particle size of the supported nanoparticles to be determined.

2.6.3.2.1 Experimental details

Samples were prepared by dispersing the catalyst powder in ethanol *via* ultra-sonication. 50 μ L of the suspension was dropped on to a holey carbon film supported by a 300 mesh copper TEM grid, followed by evaporation at room temperature. TEM images were obtained using a JEOL JEM-1200EX, operating at 300 kV.

The analysis of the particle size distribution of each sample was carried out by measuring 300 particles and performing the statistical analysis of this data set to build a histogram. This permitted the particle size distribution, the average particle size and the standard deviation of the sizes to be determined.

2.6.4 Diffuse Reflectance Infrared Fourier Transformed (DRIFT) spectroscopy

Diffuse Reflectance IR Fourier Transformed (DRIFT) spectroscopy is a suitable technique to analyse powders, due to its simple operational procedure. Following the same principle previously described in Section 2.5.4, DRIFTS occurs due to the capability of molecules to absorb IR radiation when the energy of the beam matches the energy necessary to excite a particular vibration mode of the chemical bonds present in the molecule.

In the diffuse reflectance mode, the IR beam illuminates the catalyst sample, which is placed loosely in a small basket, and the scattered ray resulting from the illumination is collected with suitable optics for analysis. Furthermore, with the proper setup, the sample cell can be heated

up and / or flushed with different atmosphere gases, which can contain also a probe molecule to perform a variety of *in situ* experiments.

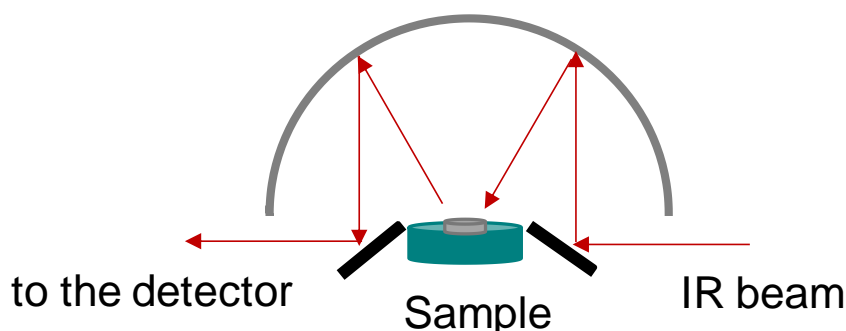


Figure 2.10. Representation of the IR beam diffusion on the sample in a DRIFT cell.

In catalysis, the adsorption of probe molecules to the catalytic material can provide precious information about the type and the strength of the active site, as well as the strength of acidity and basicity properties.^{11,12} The intensity of this signal indicates the quantity of surface coverage and the type of interaction, in addition to the strength of the interaction(s), between the probe and the catalytic surface. The IR spectra is unique to every adsorbate and is highly sensitive to the probes bonding to the surface sites and to the local environment surrounding the molecule. Many different molecules can be used as probe molecules, *e.g.* carbon monoxide, deuterated acetonitrile and pyridine, and the choice of probe depends on the kind of study desired.¹³

For instance, pyridine is a useful probe molecule to study the acidity of the material.¹⁴ In fact, pyridine can bond with both kind of acid sites, *i.e.* Lewis and Brønsted. In doing so, pyridine generates characteristic vibrations at 1595 and 1450 cm^{-1} , assigned to Lewis acid interactions, and vibrations at 1643 and 1540 cm^{-1} that are assigned to Brønsted acid interactions.¹⁵ Semi-quantitative comparison of the degree of Lewis and Brønsted acidity between different materials can be done by measuring the area of the signals at gradually increasing desorption temperatures, in order to remove the contribution of the physisorbed molecules and evaluate how fast the probe molecule desorbs.

2.6.4.1 Experimental measurement

A Bruker Tensor spectrometer equipped with a Harrick praying mantis cell was utilised for DRIFT measurements. Spectra were recorded between 4000 – 600 cm^{-1} .

Pyridine measurements were performed on pre-treated alumina materials (200 °C, 2 h under flowing N_2 , 60 mL min^{-1}) used as sample background. Dosing of the probe molecule was carried out at room temperature for 15 min, by bubbling N_2 (40 mL min^{-1}) through liquid pyridine held at 30 °C. Subsequently, samples were gradually heated up to 50, 100, 150, 200, 300,

400 and 500 °C and the IR spectra of the samples were recorded *in situ* after each heating step.

2.6.5 Magic Angle Spinning NMR (MAS NMR) spectroscopy

When classic NMR, described in Section 2.5.2, is applied to solid samples, the resulting spectra typically possess very poor quality, since samples in a solid state possess constrained molecules. This causes anisotropy of the local magnetic field of the nuclei present, resulting in broad signals and poor signal-noise (S/N). However, by spinning the sample (usually at a frequency of 1 to 130 kHz) at the magic angle, θ_m (ca. 54.74° , where $\cos^2\theta_m = 1/3$) with respect to the direction of the magnetic field, the normally broad lines become narrower, increasing the resolution for better identification and analysis of the spectrum. This type of NMR technique is known as Magic Angle Spinning NMR (MAS NMR).¹⁶

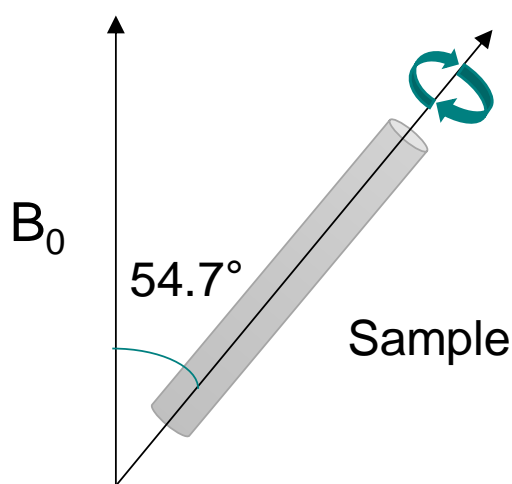


Figure 2.11. Representation of MAS NMR spinning rotor placed at 54.7° (magic angle) respect to the applied magnetic field (B_0).

Accordingly, ^{119}Sn MAS NMR can be used to study the local environment of the nucleus, giving information on the coordination of the Sn in the zeolites employed for this work. For instance, in a ^{119}Sn MAS NMR spectrum, a band at a chemical shift of - 688 ppm is indicative of hydrated isomorphously substituted Sn (IV) species (hexacoordinated) while a band at a chemical shift of - 602 ppm is indicative of octahedral Sn, such as in SnO_2 . Fig 2.14 illustrates how the ^{119}Sn MAS NMR spectrum of 2Sn- β confirms the presence of hydrated Sn (IV) sites in the framework, since only the band at - 688 ppm is observed and the band at - 602 ppm, which corresponds to SnO_2 extra-framework, is negligible.

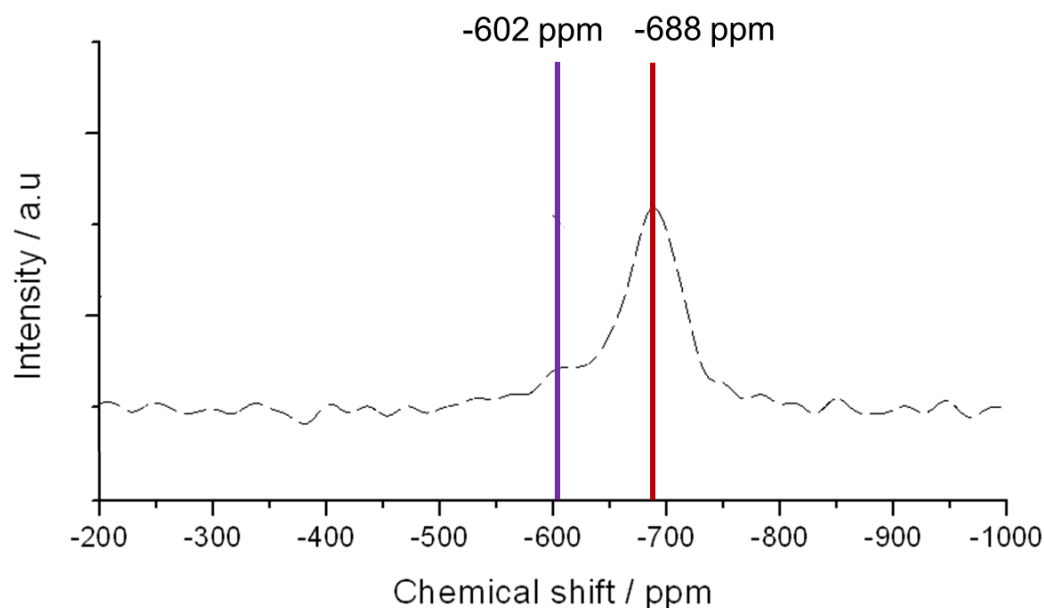


Figure 2.12. ^{119}Sn MAS NMR spectrum of $2\text{Sn-}\beta$.

2.6.5.1 Experimental details

MAS NMR experiments of Sn-catalysts were performed at Durham University through the EPSRC UK National Solid-state NMR Service, with a 400 MHz (9.4 T) solid state NMR spectrometer. ^{119}Sn MAS NMR spectra of the samples employed in this study, were measured under identical conditions to those reported by Bermejo-Deval *et al.*¹⁷ Approximately 60 - 100 mg of sample was packed into a 4 mm rotor. Measurements were performed in direct excitation mode using a Larmor frequency of 149 MHz, with a recycle delay of 2s. The rotor spinning frequency was set on 10 KHz.

2.6.6 X-Ray Photoelectron Spectroscopy (XPS)

X-ray Photoelectron Spectroscopy (XPS) is a surface-sensitive quantitative spectroscopic technique that measures the elemental composition at the parts per thousand range. It also allows the empirical formula, chemical state and electronic state of the elements that exist within a material to be identified.

A surface is irradiated with X-rays (commonly Al K_{α} or Mg K_{α}) in vacuum. When an X-ray photon hits and transfers its energy to a core-level electron, it is emitted from its initial state with a kinetic energy dependent on the incident X-ray and binding energy of the atomic orbital from which it has been originated. The energy and intensity of the emitted photoelectrons are analysed to identify and determine the concentrations of the elements present in the analysed material. These photoelectrons originate from a depth of < 10 nm, therefore, this technique

provides only information about the elements present within this depth. An XPS instrument is commonly composed of a high vacuum system, a source of radiation, an ionisation chamber, an electron analyser (typically hemispherical) and an electron detector, which transforms the signal accordingly to generate the corresponding XPS spectrum.

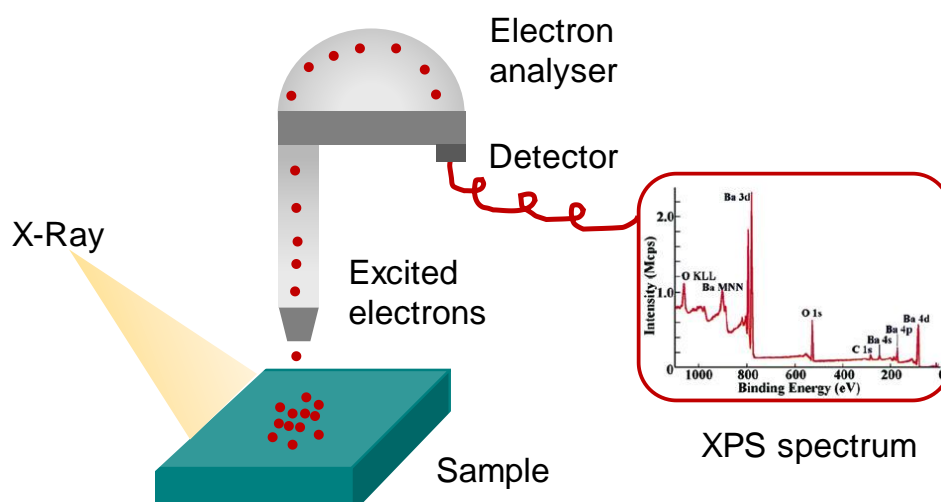


Figure 2.13. Schematic of a typical XPS instrument.

The interpretation of an XPS spectrum is based on the fact that each element possesses characteristic binding energies depending on its chemical state. For instance, metallic Pd has a binding energy of 335.0 eV, whilst Pd oxide has a binding energy of 336.7 eV. The deconvolution of the bands characteristic of each element allows determination and quantification of the oxidation state of the metal(s) present on the samples giving valuable information on the chemical nature of the metal supported nanoparticles. This technique is also very useful to analyse the changes that occurs after a certain treatment (*i.e.* reduction heat treatments) or after a reaction.

2.6.6.1 Experimental details

XPS analyses were performed on a Thermo Scientific K-alpha⁺ spectrometer by Davide Motta. Samples were analysed using a monochromatic Al X-ray source operating at 72 W (6 mA x 12 kV), with the signal averaged over an oval-shaped area of approximately 600 x 400 microns. Data was recorded at pass energies of 150 eV for survey scans and 40 eV for high resolution scan with a 1 eV and 0.1 eV step size respectively.

Charge neutralisation of the sample was achieved using a combination of both low energy electrons and argon ions (less than 1 eV), which gave a C (1s) binding energy of 284.8 eV. All data was analysed using CasaXPS (v2.3.17 PR1.1) software using Scofield sensitivity factors and an energy exponent of -0.6.

2.7 Computational studies

Density Functional Theory (DFT) is an alternative procedure for the solution of the Schrödinger equation, where the functional of the electronic energy is minimised with respect to the electronic density. The DFT method is one of the most commonly used computational tools to study and predict the properties of isolated molecules, bulk solids, and material interfaces, including surfaces.

This kind of calculation can be used to obtain very varied information regarding the molecular properties such as molecular structures, vibrational frequencies, ionisation energies, electric and magnetic properties of a species, as well as reaction pathways and evaluation of the thermodynamics of the reaction.

The fundamental idea of DFT is to replace the complete many-electron wave function with the much simpler ground-state electron density as the main variable. This is an enormous simplification because the density depends only on position (*i.e.* three variables). The electron density is an observable and the orbitals are just a mathematical construction, hence, they can be used to calculate all ground-state molecular properties. However, the exact DFT functional is unknown, thus the reliability of such calculations depends on the development of a series of approximations in order to simplify and resolve the energy functional.¹⁸

The level of complexity of the basis set to describe the density and the applied functionals elevates the time as well as the accuracy of the DFT calculations performed.

2.7.1 Experimental details

The thermodynamic of BVO of CyO and 4-R-CyO reactions was evaluated using DFT calculations performed by Dr Antoine Buchard (University of Bath). Calculations were performed with Gaussian 09 software. Geometry optimisations were performed at the ω B97XD level and 398.15 K, using a mixed valence triple ζ basis set 6-311++g(2d,p) for all atoms, and a conductor-like polarisable continuum model of 1,4-dioxane. Calculations were carried out on the (S)- enantiomers, with the alkyl substituent in equatorial position.

The decreased intrinsic reactivity of 4-R-Capr against Capr was also evaluated by using DFT by calculating the thermodynamics of the hydrolysis reaction for each substrate. Geometry optimisations was performed at the ω B97XD and B3LYP-D3 levels and 398.15 K, using a mixed valence triple ζ basis set 6-311++g(2d,p) for all atoms, and a conductor-like polarisable continuum model of 1,4-dioxane. The smallest value found from both enantiomers (if any) was reported.

References

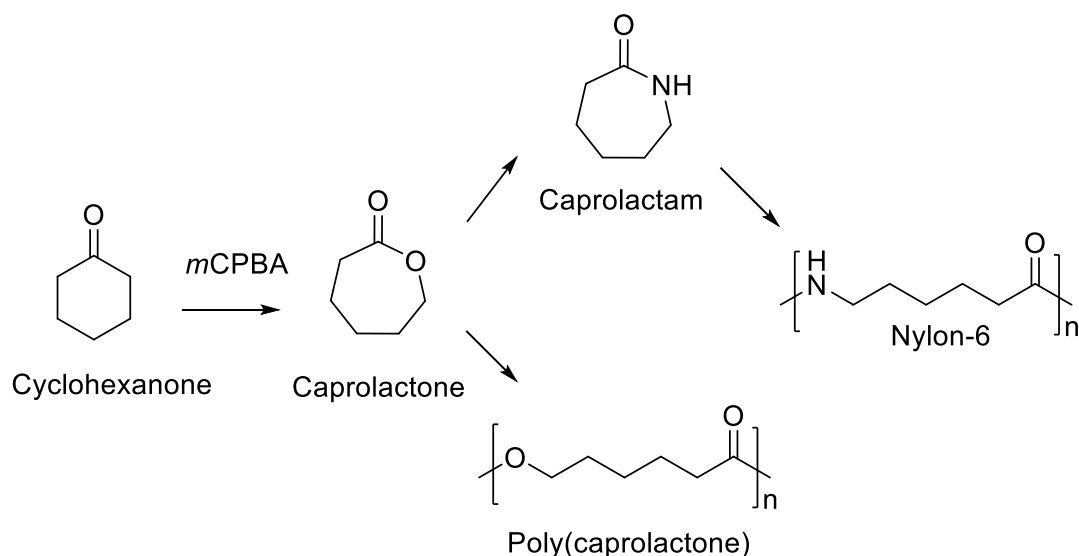
- (1) Agilent technologies, “*An Introduction to Gel Permeation Chromatography and Size Exclusion Chromatography*”
- (2) H. Günther, “*NMR Spectroscopy*”, 3rd edition, Wiley-VCH, 2013
- (3) W. J. Potts, “*Chemical infrared spectroscopy*” / Vol. 1, Techniques. New York: Wiley 1963
- (4) C. Suryanarayana, M. Grant Norton, “*X-Ray Diffraction: A practical Approach*”, New York; London: Plenum Press 1998
- (5) W.H. Bragg, W.L. Bragg, *Proc. R. Soc. Lond. A.*, 1913, **88** (605), 428 – 38
- (6) J. Gregg, K. S. W. Sing, “*Adsorption, Surface area and Porosity*”, 2nd edition Academic Press, 1982
- (7) S. Brunauer, P. H. Emmett, E. Teller, *J. Am. Chem. Soc.*, 1938, **60**, 309 - 319
- (8) E. P. Barrett, L. G. Joyner, P. P. Halenda, *J. Am. Chem. Soc.*, 1951, **73**, 373 - 380
- (9) B. C. Lippens, B. G. Linsen, J. H. de Boer, *J. Catal.*, 1965, **3**, 319 - 323
- (10) Y. Lin, J. A. McCarthy, K. R. Poeppelmeier, L. D. Marks, “*Applications of Electron Microscopy in Heterogeneous Catalysis*”, 2015
- (11) J. W. Niemantsverdriet, “*Spectroscopy in Catalysis an Introduction*”, 3rd edition, Wiley-VCH, 2007
- (12) A. Drochner, M. Fehlings, K. Krauß, H. Vogel, *Chem. Eng. Technol.*, 2000, **23**, 319 - 322
- (13) M. Boronat, P. Concepcion, A. Corma, M. Renz, S. Valencia, *J. Catal.*, 2005, **234**, 111 – 118
- (14) G. Busca, *Catal. Today*, 1998, **41**, 191 - 206
- (15) J. W. Harris, M. J. Cordon, J. R. Di Iorio, J. C. Vega-Vila, F. H. Ribeiro, R. Gounder, *J. Catal.*, 2016, **335**, 141 - 154
- (16) M. Hunger, *Catal. Rev.*, 1997, **39**, 345 - 393
- (17) R. Bermejo-Deval, M. Orazov, R. Gounder, S. J. Hwang, M. E. Davis, *ACS Catal.*, 2014, **4**, 2288 – 2297
- (18) D. S. Sholl, J. A. Steckel, “*Density functional theory: A practical introduction*”, Hoboken, N.J., Wiley c, 2009

3. Selectivity and lifetime effects in zeolite-catalysed Baeyer–Villiger Oxidation reaction

3.1. Introduction

As described in Section 1.3.1.1, the Baeyer Villiger Oxidation (BVO) reaction has been widely studied over the past 100 years, since its discovery in 1899.¹ It has demonstrated itself to be an especially profitable method to convert ketones, readily available building blocks in organic chemistry, into more complex and valuable esters and lactones.^{2,3} A key example of this chemistry is the industrially employed BVO of cyclohexanone (CyO) to ϵ -caprolactone (or simply caprolactone, Capr),⁴ produced at about 50,000 tonnes per year and used for the synthesis of caprolactam, a precursor of Nylon-6,⁵ and poly(caprolactone),^{6,7} a renewable polymer (Scheme 3.1).

Traditionally, BVO chemistry has been performed using peroxyacid-based oxidants, such as *meta*-chloroperbenzoic acid (*m*CPBA) or peroxyacetic acid. However, such oxidants possess several drawbacks, including the co-production of by-products (carboxylic acids), low active oxygen content, potential explosiveness and a requirement for undesirable chlorinated solvents.^{8,9} Additionally, peroxyacid-based oxidants typically exhibit poor levels of selectivity for oxidation reactions when other functional groups, such as C=C double bonds, are present in the substrate.

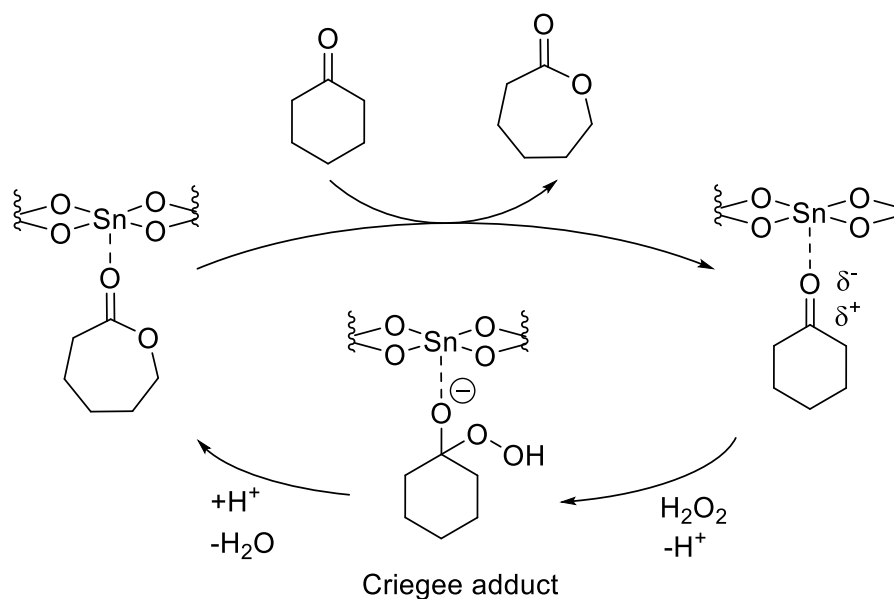


Scheme 3.1. Relevant industrial pathways of Capr obtained from BVO of CyO.

To overcome these problems, much effort has been made towards replacing peroxyacid-based oxidants for greener and potentially less expensive oxidants,¹⁰⁻¹² such as hydrogen peroxide (H_2O_2).¹³⁻¹⁶ In this case, a suitable catalyst is required to allow H_2O_2 to interact appropriately with the ketone substrate and proceed with the transformation. Amongst several potential catalytic materials, the Lewis acidic zeolite, Sn- β , has been conclusively reported by Corma *et al.*¹³ to be the most active, selective, and suitable catalyst for this BVO transformation. The excellent catalytic performance of this material arises from its ability to activate the substrate, without the need of activating H_2O_2 . Indeed, the Lewis acid sites present in the material, are able to polarise the carbonyl group of the substrate, thus making it more reactive to the nucleophilic attack of the oxidant, H_2O_2 .

Although the reaction mechanism has not been truly elucidated yet, the most widely accepted mechanism for this reaction, described in Scheme 3.2, proceeds through the formation of an intermediate known as Criegee adduct. This adduct is formed after nucleophilic attack of the oxidant, and its subsequent rearrangement by the elimination of a molecule of H_2O leads to the obtainment of the lactone.¹⁷

Additionally, this reaction has been shown to be regio-selective, meaning that the insertion of oxygen takes place between the carbonyl and the more substituted carbon atom neighbour, achieving high levels of chemo-selectivity even when multiple functional groups are present. This fact acquires especial importance when a more complex ketone is used as substrate, as it will be shown in more detail in Chapter 4.



Scheme 3.2. Simplified reaction mechanism for the BVO of CyO catalysed by Sn- β .

Although at the time of this study, much work has been devoted in academic research circles towards to scalable synthesis of Sn- β ,¹⁸⁻²² and the development of novel catalytic processes catalysed by the same (or similar) material(s), research focusing on the Sn- β catalysed BVO reaction itself lacked behind, despite the considerable industrial potential. Consequently, several questions and challenges still remain, such as:

- i) The need to identify and optimise all the kinetic parameters of the reaction.
- ii) The requirement to identify the by-products, and hence, close the low carbon balance.
- iii) The study of potential scalability of the system, particularly in the continuous regime.

Therefore, the investigation of these three challenges by taking the BVO of CyO to Capr as model reaction constitutes the focus of this chapter. The BVO of CyO to Capr was selected as first target of investigation for several reasons including i) the practicality of the substrate, with only one functional group involved in the substrate ii) its suitable size (kinetic diameter of 6 Å) allowing it to freely diffuse through the Sn- β pores (7 Å), and iii) the industrial relevancy of the lactone obtained. Herein, understanding of kinetics and mechanism of this model reaction is crucial to move forward to more complex ketones.

3.2 The catalyst: Sn- β

Solid Lewis acid catalysts, such as zeolites, especially those containing small amounts of metals (e.g. Zr, Ti and Sn) in the framework, are increasingly employed for biomass valorisation and other sustainable processes.²³⁻²⁷ These materials combine the advantages of molecular catalysts, such as site isolation and high intrinsic activity, along with the practical

advantages of heterogeneous catalysts, *i.e.* easy separation. Amongst these materials, Sn- β , a medium pore size zeolite possessing isolated Sn (IV) sites and BEA (β) topology, has garnered tremendous levels of academic and industrial interest and has been reported as suitable catalyst to carry out the reaction of study, BVO of CyO.^{13,28}

According to the optimised synthesis protocol described in detail in Section 2.3.1.1, a range of Sn- β catalysts was prepared from a commercially available Al- β precursor material ($\text{SiO}_2/\text{Al}_2\text{O}_3 = 38$). Sn loadings of 1, 2, 5 and 10 wt. % were achieved by incorporating Sn into the vacant framework sites by Solid-State Incorporation (SSI). These catalysts were simply denoted 1, 2, 5 or 10Sn- β , respectively. Additionally, when required, 2 wt. % Sn- β catalysts were also prepared following the same procedure, using different starting β zeolites ($\text{SiO}_2/\text{Al}_2\text{O}_3 = 25$ and 300), denoted 2Sn- β (25) and 2Sn- β (300), respectively.

Sn- β materials were extensively characterised by various techniques in order to determine their structure and successful incorporation of the Sn in the zeolite framework. Firstly, X-Ray Diffraction (XRD) analysis of fresh zeolite β , dealuminated β (deAl- β) and 2Sn- β were performed to evaluate the effect of the preparation treatments to the original structure. As can be seen in Fig 3.1, all XRD patterns obtained presented the same characteristic diffraction peaks of zeolite β , and showed comparable intensity, demonstrating the preservation of the structure as well as high crystallinity of the original material throughout the different stages of synthesis of Sn- β .

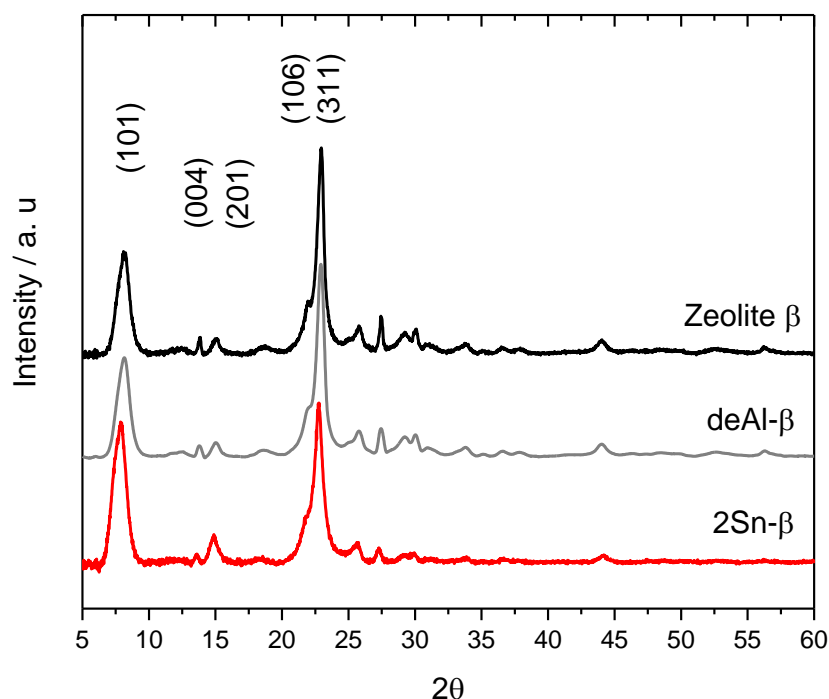


Figure 3.1. XRD patterns of commercial zeolite β , deAl- β and 2Sn- β .

Similarly, Transmission Electron Microscopy (TEM) images (Fig 3.2) of zeolite β and 2Sn- β displayed the same characteristic morphology. Hence, the channels are conserved after the post-synthetic treatments to form 2Sn- β , emphasising the success of the material preparation.

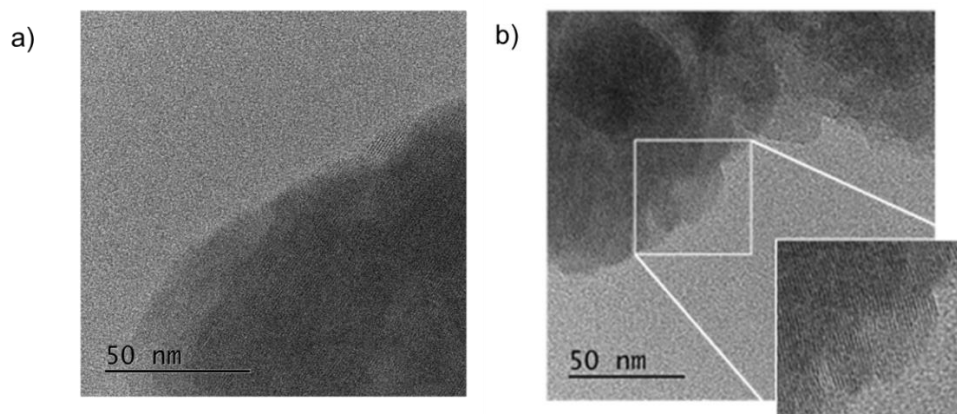


Figure 3.2. TEM images of a) commercial zeolite β and b) 2Sn- β .

Additionally, Hammond *et al.*²⁹ previously confirmed by Magic Angle Spinning (MAS) Nuclear Magnetic Resonance (NMR) analysis that isomorphously-substituted Sn (IV) sites can be almost exclusively observed in Sn- β samples up to a loading of 5 wt. %. Beyond this loading, inactive, extra-framework Sn_xO_y sites can be also present as consequence of the intrinsic limitation of the material to accommodate such high amount of Sn in the framework. Accordingly, the primary catalyst, 2Sn- β was analysed by ^{119}Sn MAS NMR and compared with extra-framework cluster of Sn_xO_y ($10\text{SnO}_2\text{-deAl-}\beta$, physical mixture) and bulk SnO_2 (Fig 3.3).

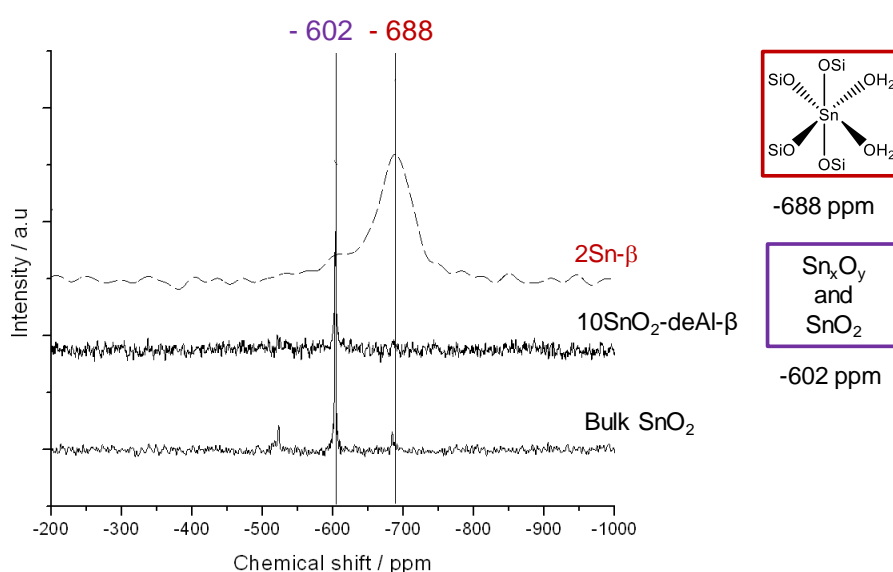


Figure 3.3. MAS NMR spectra of 2Sn- β , $10\text{SnO}_2\text{-deAl-}\beta$ and bulk SnO_2 .

^{119}Sn MAS NMR analysis revealed a main resonance at - 688 ppm which corresponds to isomorphously substituted hydrated Sn (IV) sites, demonstrating the successful incorporation of Sn (IV) sites in the zeolite framework, whilst the resonance corresponding to extra-framework Sn clusters, at - 602 ppm was negligible at the 2 wt. % loading used.

Accordingly, the primary catalyst of this chapter corresponds to 2Sn- β , as this loading is consistent with a material possessing highly active, isolated Sn (IV) sites and negligible amounts of inactive extra-framework Sn.

3.3 Results and discussion

3.3.1 Impact of kinetic parameters

3.3.1.1 Standard BVO reaction

Over the past years various examples using Sn- β catalyst have been successfully reported for BVO of CyO to Capr, with the results obtained by Corma *et al.*¹³ and by Hammond *et al.*,²⁸ being of particular interest. Corma *et al.* reported that the catalytic performance of Sn- β catalyst, prepared by the typical fluoride medium approach, provided up to 52 % of Capr yield with selectivity > 98 % after 3 h of reaction in 1,4-dioxane at 90 °C. In parallel to these results, Hammond *et al.* demonstrated that a Sn- β , prepared by a similar post-synthetic procedure than the one employed in this work, provided up to 41 % of conversion with selectivity up to 93 % after 4h of reaction using also 1,4-dioxane as solvent at 100 °C.

Accordingly, a preliminary test to benchmark the catalytic activity of the 2Sn- β for the BVO of CyO was carried out under a combination of the reaction conditions stated above, following the experimental procedure described in detail in Section 2.4.1. A standard BVO reaction was then performed using a solution of 0.33 M CyO in 1,4 dioxane and 1 mol. % Sn relative to the ketone (2Sn- β) at 100 °C, with the addition of H_2O_2 at a final concentration of 0.5 M (H_2O_2 :CyO = 1.5) for 6 h. The reaction was repeated several times, and an experimental error of 8 % was calculated from the obtained results (Annex). Thus, an error bar of 8 % was added to all kinetic parameters (*i.e.* conversion (X), yield (Y), selectivity (S) and carbon balance (C Bal)) in each experiment.

As can be seen in Fig 3.4, left, under the chosen reaction conditions, 2Sn- β was a highly active catalyst, with CyO conversion values reaching > 60 % in 1 h, and > 90 % in < 6 h. Initially, the system was highly selective (\pm 80 %) to Capr, demonstrating this to be the primary reaction product, however, a remarkable decrease in Capr selectivity and total carbon balance was observed as the conversion increased beyond 60 % (Fig 3.4, right).

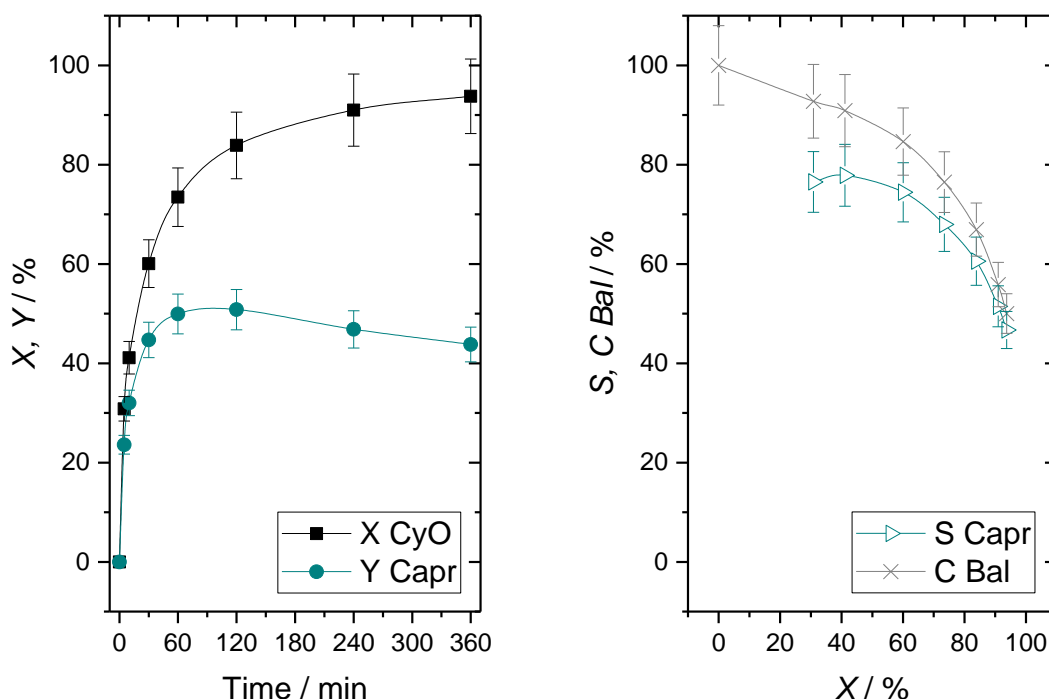


Figure 3.4. Catalytic activity of 2Sn- β for BVO of CyO. (Left) Conversion and Capr yield vs. time and (Right) selectivity towards Capr and total carbon balance as function of CyO conversion. Reaction conditions: 10 mL of 0.33 M CyO in 1,4-dioxane, 1 mol. % Sn respect to CyO, 1.5 H₂O₂:CyO, at 100 °C.

According to this kinetic profile, Capr yield very quickly reached ± 40 %, but then stagnated and eventually decreased slightly at the highest levels of conversion. This observation, coupled with the corresponding decrease in carbon balance at elevated conversion, strongly points towards the formation of consecutive by-products throughout the reaction period. However, no additional products could be detected by Gas Chromatography with Flame Ionisation Detector (GC-FID), used as primary analytical technique for the kinetic evaluation of CyO and Capr. The identity of these by-products is discussed in detail later in this chapter. Subsequently, a range of experiments was performed to optimise all parameters and catalyst features in the attempt to improve the initial catalytic results and get a deeper understanding of the reaction mechanism and its kinetics.

3.3.1.2 Impact of initial aluminium content of parental β zeolite

The first parameter investigated was the catalyst itself. Initial Al content of parental zeolite β used for Sn- β preparation may impact the catalytic performance of the material since the different Al content present in the material may lead to different levels of hydrophobicity/hydrophilicity after the dealumination step and the formation of the free silanol

sites (Si-OH). In regards of this, Corma *et al.*³⁰ reported that in materials such as Ti-MCM-41 or Ti- β , the hydrophobic/hydrophilic properties of the surface are just as important as the number of active sites and that the control of it significantly impacts the adsorption of reactants and products. In view of this, it may be hypothesised that, for example, zeolite β 300 (0.3 % of Al) with a poor Al content should present much less Si-OH groups once dealuminated, which likely leads to a more hydrophobic final material. In the other hand, the higher is the initial Al content, the higher is hydrophilicity after dealumination and the final material.

In order to evaluate how the hydrophilicity may affect the reaction, three parental zeolites with different Al content ($\text{SiO}_2/\text{Al}_2\text{O}_3$ molar ratios of 25, 38 and 300) were used to prepare 2Sn- β materials. Catalysts were tested, and their catalytic performances were compared in Fig 3.5.

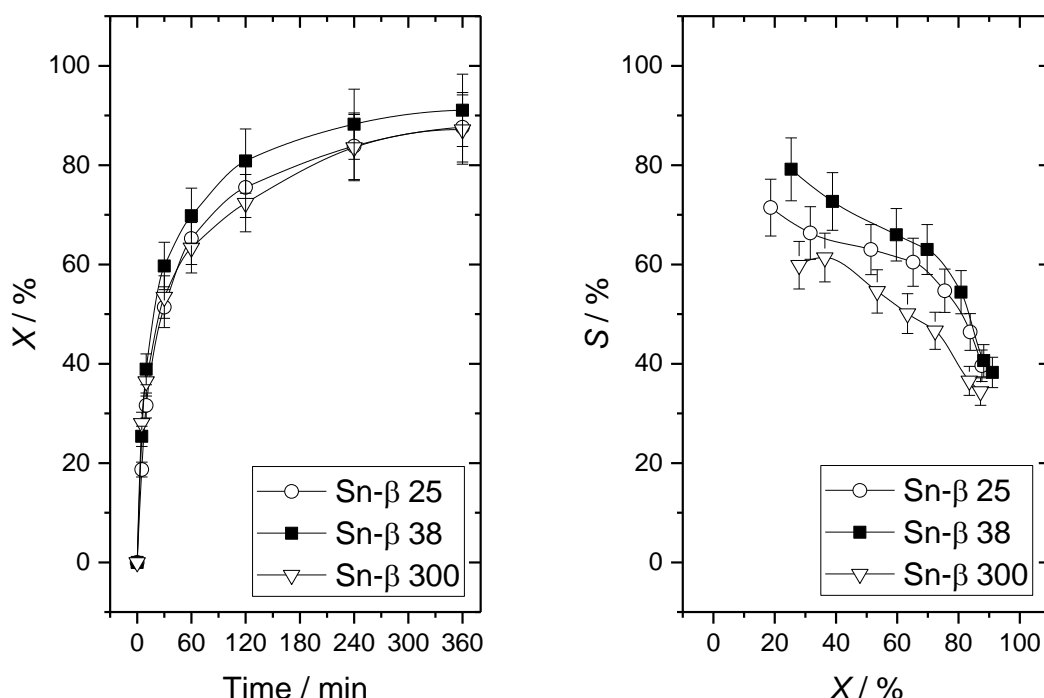


Figure 3.5. Catalytic activity of Sn- β starting from different β zeolites. (Left) Conversion vs. time and (Right) Capr selectivity trends as function of CyO conversion.

As shown in the figures above, zeolite β with higher initial Al content (25 and 38), hence higher acidity and hydrophilicity, presented higher selectivity to Capr, between 10 - 20 % higher than 2Sn- β (300) at all overlapping levels of conversion. Note that selectivity of 2Sn- β (25) was slightly lower than 2Sn- β (38), although the difference was within the applied experimental error. Contrarily, 2Sn- β (300) presented lower selectivity to the lactone, suggesting a major extension of by-products formation potentially due to the lower hydrophilicity of this material. This observation is in good agreement with the recently published study by Conrad *et al.*,³¹

where the best catalytic performance for BVO of CyO in aqueous H_2O_2 was achieved with a Sn- β catalyst with moderate hydrophilicity. Given its higher levels of activity and selectivity, 2Sn- β starting from zeolite β ($\text{SiO}_2/\text{Al}_2\text{O}_3$ molar ratio = 38) was selected to be used for the rest of the study.

3.3.1.3 Impact of the Sn loading

The next catalyst feature to have in mind was the Sn loading. Utilisation of high Sn loadings can be beneficial to obtain high Space Time Yield (STY) values and enhance the process profitability. STY refers to the quantity of product produced per quantity of catalyst per unit time. Therefore, if the same catalytic performance can be observed even at high Sn loading, the mass of catalyst used for the same productivity can be significantly reduced when using the highest Sn loading. With the aim to investigate this aspect, various samples of Sn- β , containing 1, 2, 5 and 10 wt. % of Sn, were tested at a fixed amount of Sn relative to CyO, *i.e.* catalyst mass was adjusted so that the same amount of Sn was employed in the reactor (1 mol. %) (Fig 3.6).

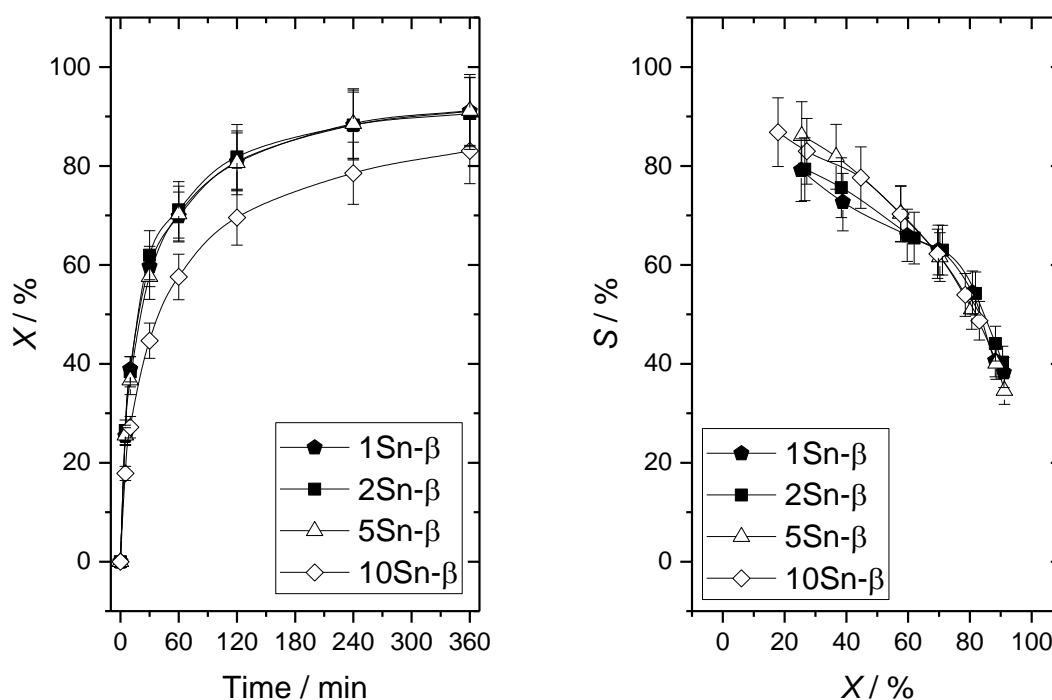


Figure 3.6. Catalytic activity of various Sn- β samples containing 1 - 10 wt. % Sn for BVO of CyO. (Left) Conversion vs. time and (Right) selectivity towards Capr as function of CyO conversion.

As already mentioned in Section 3.2, there is a limited theoretical amount of Sn able to be incorporated into dealuminated zeolite. For instance, for deAl- β 38 this value is approximately 9 wt. %, although in practice only loadings up to 5 - 6 wt. % have been accommodated of all Sn in the zeolite framework. In the set of catalysts investigated, catalysts of loadings below and beyond the limit were used, hence, the selectivity trends towards Capr may differ. However, as observed in Fig 3.6, reactions performed using 1Sn- β , 2Sn- β and 5Sn- β presented almost identical catalytic activity in terms of conversion, whilst 10Sn- β presented slightly lower activity. Subsequently, to better see the effect of the wt. % Sn loading on the initial rate, comparison of initial turnover frequency (TOF) (at 5 min) of the four materials is reported in Fig 3.7. TOF values were calculated as described in Equation 2.5.

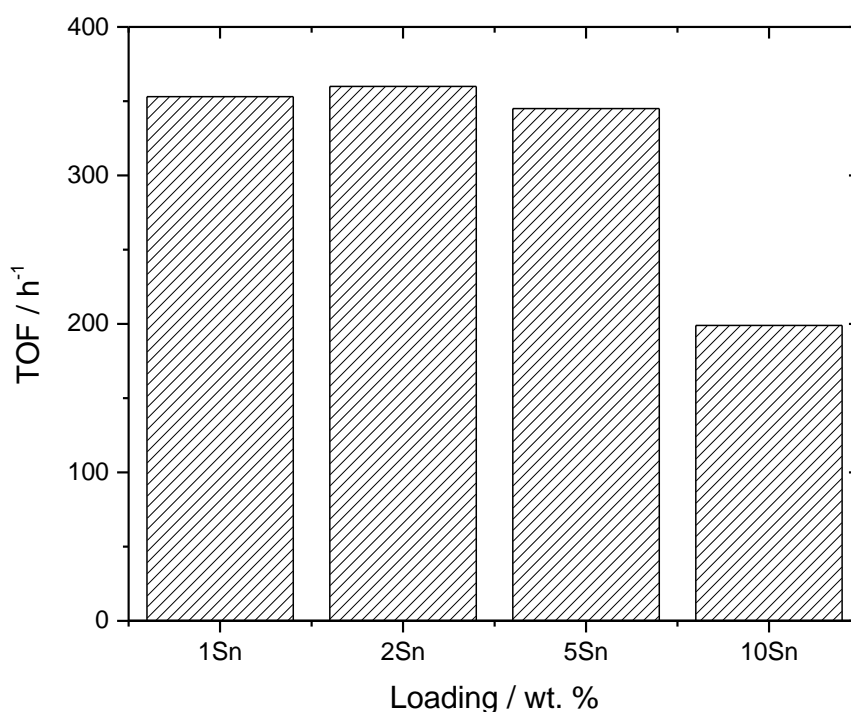


Figure 3.7. Initial TOF obtained for catalysts with different Sn wt. % loadings. Initial TOF was calculated at 5 min of reaction as moles of CyO converted per moles of Sn per time.

This comparison revealed a clear decrease in activity and TOF as the Sn loading of the catalyst was increased to 10 wt. %, from 360 h⁻¹ for 2Sn- β to 199 h⁻¹ for 10Sn- β . Such decrease in activity with the highest Sn loading tested agrees with the formation of inactive SnO₂ clusters when loadings above the intrinsic material limitation are prepared. In fact, Hammond *et al.*²⁹ observed by MAS NMR analysis that at 10Sn- β possesses non-negligible amounts of extra-framework clusters of SnO₂. Said clusters are not active for typical Sn- β reactions, such as

transfer hydrogenation and glucose isomerisation reactions. Hence, the use of high loadings of Sn in Sn- β catalysts results detrimental for the catalytic activity of the material.

Additionally, at all levels of conversion, each catalyst exhibited comparable selectivity, showing that the formation of spectator Sn sites does not negatively contribute to the reaction or consecutive reaction products.

As a result of these experiments, 2Sn- β was determined as primary catalyst and used for the rest of this study. In view of this, selectivity improvement by catalyst modification appears unlikely and the quest of selectivity improvement should be investigated through optimisation of other parameters such as oxidant concentration, mass of catalyst and reaction temperature.

3.3.1.4 Effect of H₂O₂ concentration

Once the optimal catalyst design was identified, other parameters involved in the reaction performance were investigated, starting with the study of the effect of oxidant concentration. To do so, a series of experiments with different H₂O₂:CyO ratios (*i.e.* different initial oxidant concentration) was performed. These experiments allow to evaluate the effect of H₂O₂ concentration on the catalytic rate, with all other parameters *e.g.* Sn content (1 mol. %), reaction temperature (100 °C) and catalyst choice (2Sn- β) remaining unchanged. The initial H₂O₂ concentration was varied from 0.035 to 1 M, representing a range of H₂O₂:CyO ratios from 0.1 to 3.0 (under typical conditions, a ratio of 1.5 (0.5 M) was employed).

To better comprehend this effect, the initial reaction rate of each experiment was calculated. In regard of this, first order and second order kinetic adjustments were considered for the fitting, as described in Equation 3.1 and Equation 3.2, respectively:

$$\text{First order:} \quad \ln[\text{CyO}] = \ln[\text{CyO}]_0 - kt \quad [\text{Equation 3.1}]$$

$$\text{Second order:} \quad \frac{1}{[\text{CyO}]} = \frac{1}{[\text{CyO}]_0} - kt \quad [\text{Equation 3.2}]$$

Where k represents the initial kinetic constant of a reaction according to these two equations. Representative first and second order kinetic plots for the using BVO reaction of CyO at the typical H₂O₂:CyO ratio of 1.5, shown in Figure 3.8, left and right, respectively, revealed a better kinetic adjustment as second order respect to the ketone for the evaluation of the reaction rate of this system. Herein, the apparent rate constant, corresponding to a second order fitting (k_{app} , units M⁻¹ s⁻¹), at each H₂O₂:CyO ratio was determined at the very initial stages of the reaction according to Equation 3.2, and represented in Fig 3.9, left.

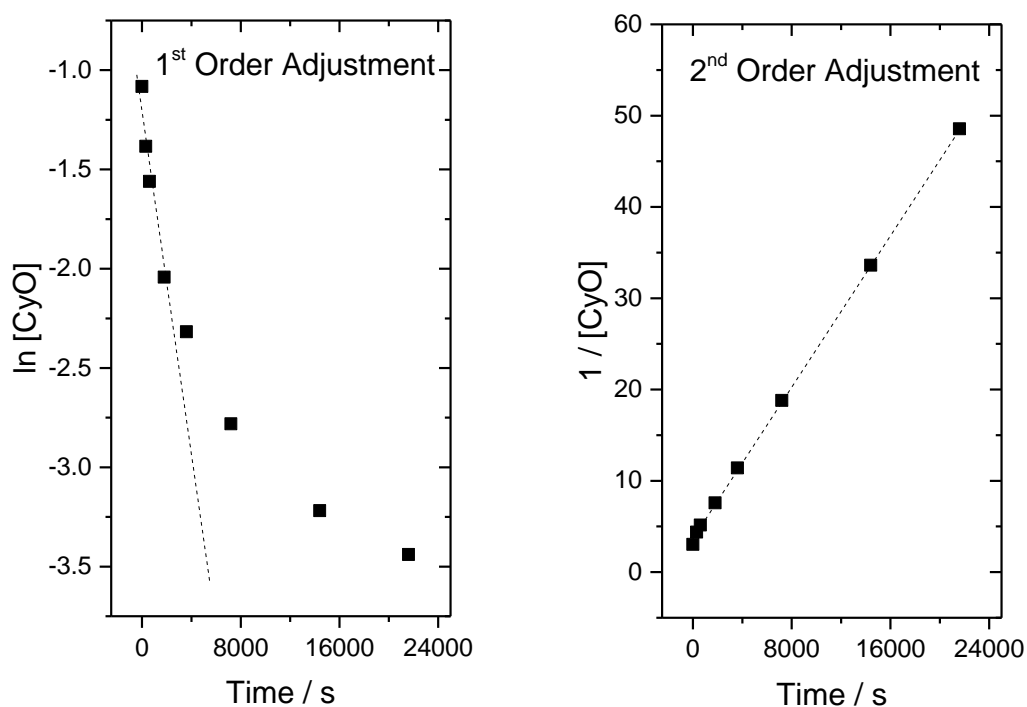


Figure 3.8. Kinetic adjustments for BVO of CyO using a 1.5 H_2O_2 :CyO as (Left) first order adjustment respect to CyO and (Right) second order adjustment respect to CyO.

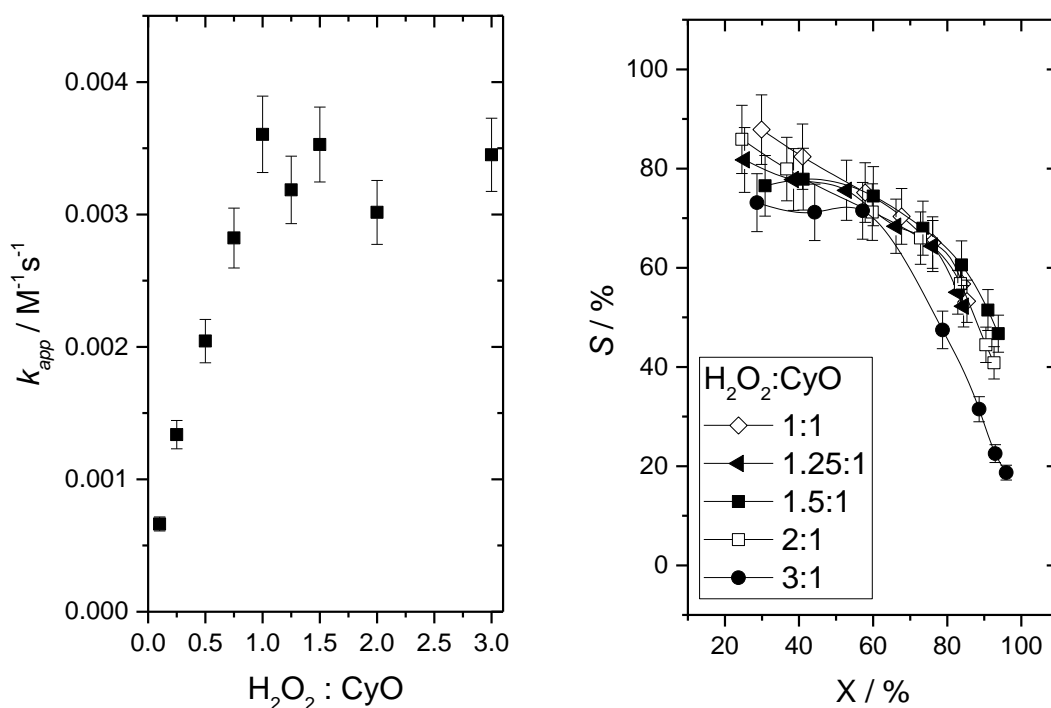


Figure 3.9. (Left) Effect of H_2O_2 :CyO on the catalytic rate and (Right) selectivity trend obtained at different initial H_2O_2 concentrations (stated as H_2O_2 :CyO molar ratio).

As reported in Fig 3.9, left, for H_2O_2 :CyO ratios in the range from 0.1 to 0.75, a first order dependence on H_2O_2 can be observed, with k_{app} increasing linearly with the oxidant concentration. However, above this ratio, k_{app} reached a plateau, within experimental error, and the reaction becomes zero order with respect to the oxidant.

It is worth mentioning that at ratio 0.75, the oxidant was added at sub-stoichiometric quantities, and the reaction could never reach full conversion. However, the initial stage of the reaction remained unaffected by the limitation of H_2O_2 and the k_{app} obtained can be considered in the borderline of the zero order regime range. Once in the zero order regime range, an excess of H_2O_2 did not overly interfere with the intrinsic kinetics of the system, except for the highest oxidant ratio tested where the selectivity towards Capr decreased considerably (Fig 3.9, right). It should be noted that, since H_2O_2 was used as an aqueous solution (50 wt. %), the concentration of H_2O also changed during these experiments and at the highest ratio tested (3:1) the amount of H_2O added was doubled the typically used. This observation suggests that H_2O_2 and/or H_2O may be involved in a consecutive reaction that may cause the observed decrease of total carbon balance observed in Fig 3.4, right. Given the results obtained, a ratio of 1.5 H_2O_2 :CyO was employed for the rest of the optimisation study to ensure no dependence of the oxidant concentration on the reaction rate,.

3.3.1.5 Effect of mass of catalyst

Being in the kinetic regime *i.e.* under catalyst control, is of great importance to obtain reliable catalytic data free of interferences such as mass transfer limitations, which can occur when the limiting reaction step is the diffusion of the reactants to the active sites of the catalyst, instead of being the reaction itself. Therefore, the effect of the mass of catalyst employed was investigated in order to ensure performance in a purely kinetic system.

Typically, usage of catalyst quantities comprised between 0.5 - 2 mol. % of Sn respect to the substrate, can be found in literature when using Sn- β catalyst. For instance, Corma *et al.*,¹³ reported a usage of Sn contents of 1 mol. % (respect to CyO). With the aim of identifying the optimal mass of catalyst, the mass of 2Sn- β was varied so that Sn contents of 0.1 - 3 mol. % Sn relative to CyO were utilised, corresponding to a range of mass of catalyst between 0.02 and 0.6 g. All other reaction parameters were unchanged, and reactions carried out for 6 h. Selectivity to Capr trends obtained as function of CyO conversion for all the reactions are represented in Fig 3.10, left.

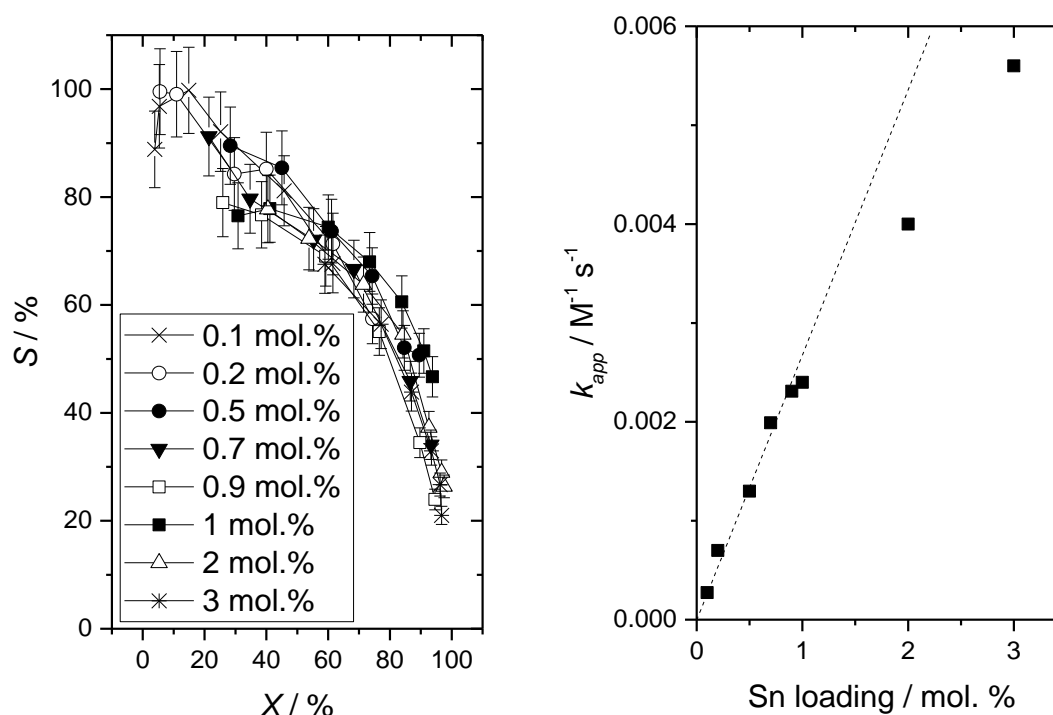


Figure 3.10. (Left) Capr selectivity as function of CyO conversion for all mol. % of Sn tested and (Right) impact of relative Sn content on the rate of BVO of CyO at 100 °C.

As observed in Fig 3.10, the selectivity trend was maintained throughout all experiments, and the differences can be considered within the experimental error. Therefore, varying the Sn content employed does not massively impact selectivity at any level of conversion. In terms of catalytic activity, the increment of mass of catalyst should, in principle, lead to a proportional increment of conversion (at the same reaction conditions used). However, although a slight improvement was observed with increasing mass of catalyst, the improvement was lower than expected. This fact can be better noticed in Fig 3.10, right, where the k_{app} is shown as a function of mol. % of Sn. At low mol. % of Sn, up to 1 mol. % Sn, a linear relationship between k_{app} and Sn content is observed. However, at very high Sn loadings, k_{app} was lower than anticipated, indicating that some mass transfer limitations occurred at higher Sn loadings, diminishing the reaction rate, as consequence of the large mass of catalyst used. Accordingly, to ensure the reaction to be in the kinetic regime, all further experiments were conducted at Sn contents of 1 mol. %.

3.3.1.6 Effect of reaction temperature

Subsequently, the effect of the reaction temperature on the catalytic activity, selectivity and carbon balance, was investigated, with the aim to maximise the lactone production, by varying the reaction temperature from 100 to 40 °C, as reported in Fig 3.11.

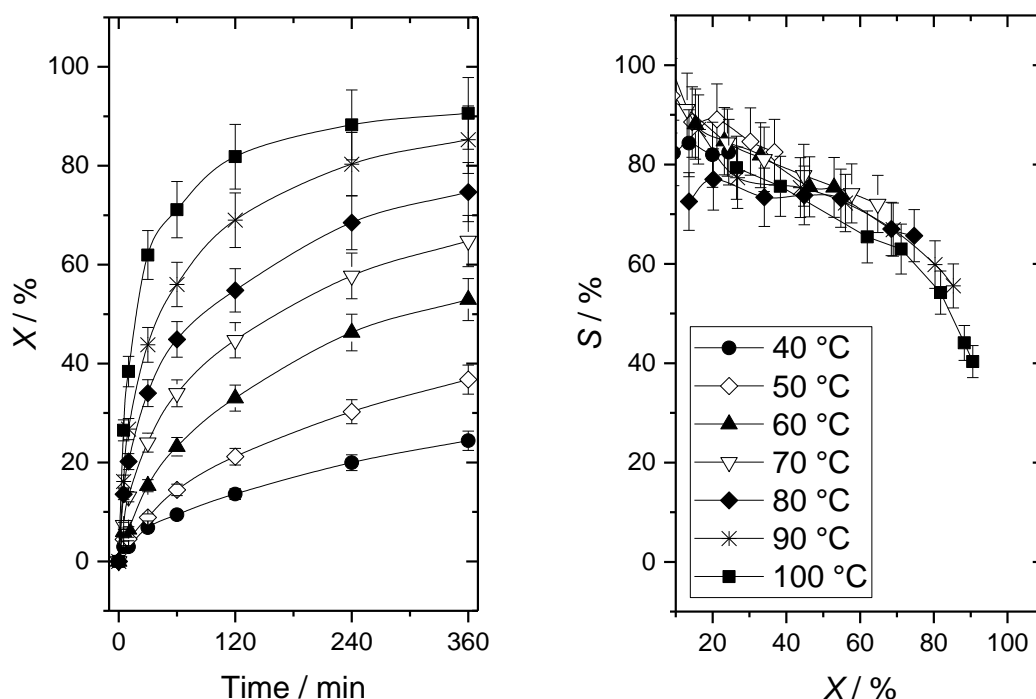


Figure 3.11. BVO of CyO performed at various reaction temperatures. (Left) CyO conversion evolution with time and (Right) Capr selectivity as function of conversion.

As shown in Fig 3.11, left, the conversion per unit time decreased with lower temperature employed. For instance, the conversion reached after 6 h of reaction at 100 °C was about 90 %, while only about 20 % could be achieved at 40 °C. In terms of selectivity trends, as it can be seen in Fig 3.11, right, regardless of the reaction temperature, high selectivity to Capr ($> 70 \%$) was only observed when CyO conversion levels were $< 50 - 60 \%$. However, at higher conversion levels, selectivity towards Capr and total carbon balance, dropped noticeably. Selectivity trends were clearly comparable at all reaction temperatures, within experimental error, hence, selectivity seems to depend only on the extent of conversion. This fact suggests that the side reactions or consecutive reactions involved may have comparable activation energies to the BVO reaction, and that high(er) levels of selectivity cannot be obtained through kinetic control.

Subsequently, advanced kinetic analysis of the data obtained, already mentioned in Section 3.3.1.4 to better fit as a second order reaction with respect to ketone, allowed calculation of the k_{app} of each experiment. Notably, the slope of each linear fit (Fig 3.12, left) corresponded to the k_{app} at each temperature calculated from Equation 3.2.

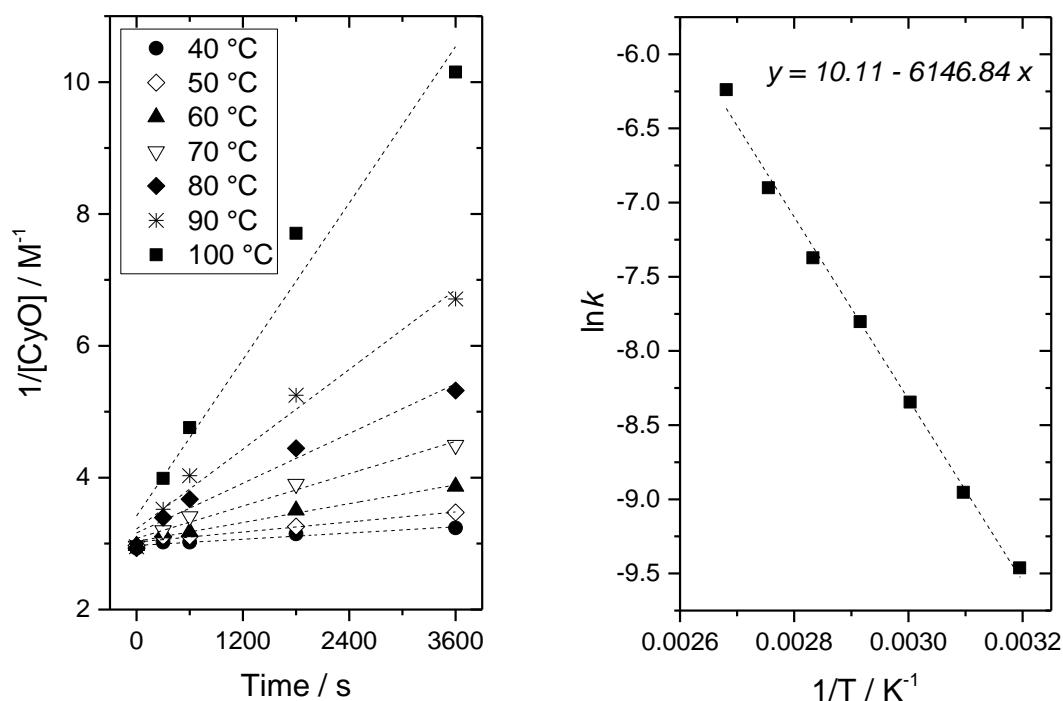


Figure 3.12. (Left) Kinetic adjustment as second order respect CyO of reactions at different reaction temperatures and (Right) the corresponding Arrhenius plot obtained.

The kinetic constant of each reaction can be used to calculate the energy of activation of the reaction using the Arrhenius equation (Equation 3.3):

$$\ln k = \ln A - \frac{E_{act}}{RT} \quad [Equation 3.3]$$

From the slope obtained from the Arrhenius plot (Fig 3.12, right), the activation energy (E_{act}) of the system was determined to be 51.1 kJ mol^{-1} , which represents the minimum energy required to allow the reaction to occur. This value is comparable to the value reported by Boronat *et al.*³² (45 kJ mol^{-1}) for analogous materials under similar reaction conditions.

Following the detailed study of all these parameters and the definition of the optimal reaction conditions for the BVO / Sn- β / H_2O_2 system, the excellent performance of the material for a greener production of renewable lactone monomers, as Capr, is highlighted. However, general selectivity trend, which decreased alongside the carbon balance as CyO conversion increased evidences the need for further investigating the reaction network, and the need to identify all by-products to better understand the limitation of high selectivity to the lactone at high conversion observed.

3.3.2 Identification of by-products and closing the carbon balance

At the time of this work, very few studies had been focused on the detail analytics of the BVO reaction, *i.e.* the full disclosure of the overall reaction network had not been achieved. Hence, attention was focused on the full elucidation of the nature of the unknown by-products that must be present, accounting for the missing carbon balance.

From the literature it is known that the most likely by-products include 6-hydroxyhexanoic acid (6-HHA), formed from the opening of Capr by hydrolysis, and adipic acid (AA), formed *via* oxidation of 6-HHA.³³⁻³⁵ Unfortunately, 6-HHA is a non-volatile compound, not detectable by GC-FID, the analytic technique typically employed for the catalytic evaluation of the system. In view of this, other techniques available such as High Performance Liquid Chromatography (HPLC) and Attenuated Total Reflectance Infrared (ATR-IR) spectroscopy, were then used in order to identify the by-products. However, the analysis was unsuccessful. For instance, HPLC analysis of the standards (CyO, Capr, 6-HHA and AA), showed overlapping of Capr and 6-HHA signals, making them indistinguishable. In the same way, as observed in Fig 3.13, IR spectra of the four potential reactant species displayed a relative overlap of each C=O signal which prohibited the identification and quantification of those presents in the reaction mixture. The monitoring of reaction time online by these techniques was hence not feasible.

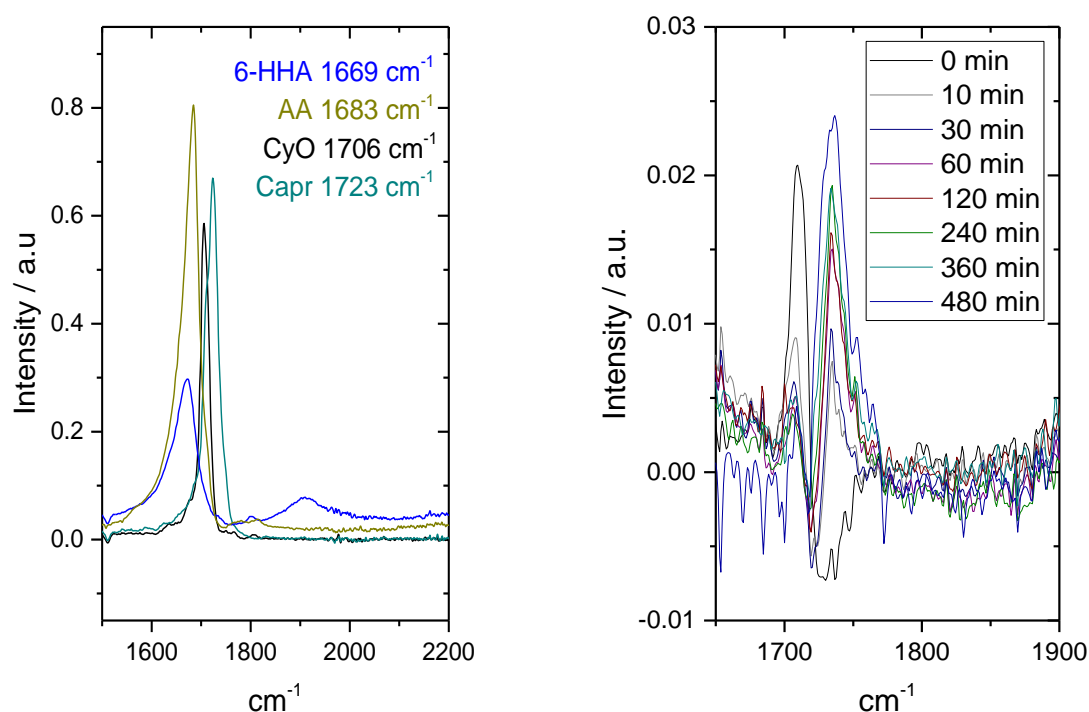


Figure 3.13. ATR-IR analysis. (Left) Spectra of CyO, Capr, 6-HHA and AA standards and (Right) time online analysis of a typical BVO reaction. Reaction conditions: 10 mL of 0.33 M CyO in 1,4-dioxane, 1 mol. % Sn respect to CyO, 1.5 H₂O₂:CyO, at 100 °C.

The next technique considered for the identification of by-products was ^1H NMR spectroscopy. Although the presence of the solvent inhibited identification of all potential species within the reaction solution under normal conditions, the relatively high boiling points of CyO and all the potential products allowed almost complete evaporation of the solvent (1,4-dioxane, boiling point of $101\text{ }^\circ\text{C}$) prior to the analysis, and consequently satisfactory qualitative data to be obtained. Analysis of the four standards, including CyO, Capr, 6-HHA and AA, by ^1H NMR are reported in Fig 3.14.

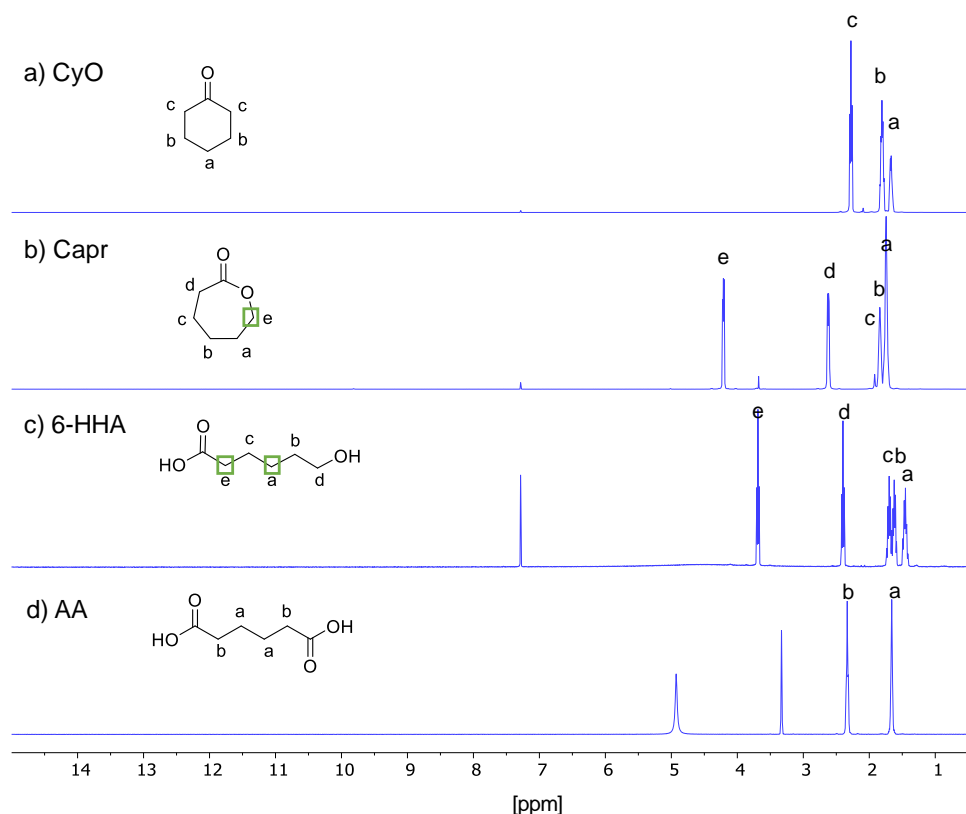


Figure 3.14. ^1H -NMR spectra of a) CyO, b) Capr, c) 6-HHA and d) AA standards.

Unfortunately, all ^1H NMR resonances of CyO and AA overlapped in some way with the rest of the potential reactants. For instance, the ^1H NMR resonance at 2.3 ppm was commonly observed for CyO, 6-HHA and AA. These overlapping resonances complicated identification of CyO and AA and hence they could not be conclusively quantified by ^1H NMR. Only resonances at 4.2 and 1.4 ppm (or 3.6 ppm) of Capr and 6-HHA respectively (marked in green in Fig 3.14), could adequately be used for the analytical quantification of these species.

Quantification of Capr and 6-HHA, formed during the BVO reaction was then carried out by ^1H NMR using a capillary filled with tetramethylsilane in deuterated chloroform (1% TMS/ CDCl_3), previously calibrated against 6-HHA, as described in Section 2.5.2.1.

To verify the validity of this approach, quantification of Capr was carried out using ^1H NMR with the TMS insert and the concentrations obtained were compared with the results

determined by GC-FID. As shown in Table 3.1, all values were found to be within < 6 % of error, verifying the use of this approach. As already mentioned, the presence of overlapping signals prevents quantification of CyO by this method, and its concentration was solely monitored by GC-FID. A typical time online analysis by ^1H NMR is reported in Fig 3.15.

Table 3.1. Capr concentration during the BVO reaction obtained by GC-FID and ^1H -NMR.

Time / min	[Capr] by GC-FID / M	[Capr] by ^1H NMR / M	Standard deviation / %
0	0	0	0
30	0.132	0.131	0.5
60	0.137	0.132	2.6
120	0.129	0.126	1.7
360	0.098	0.090	6.0

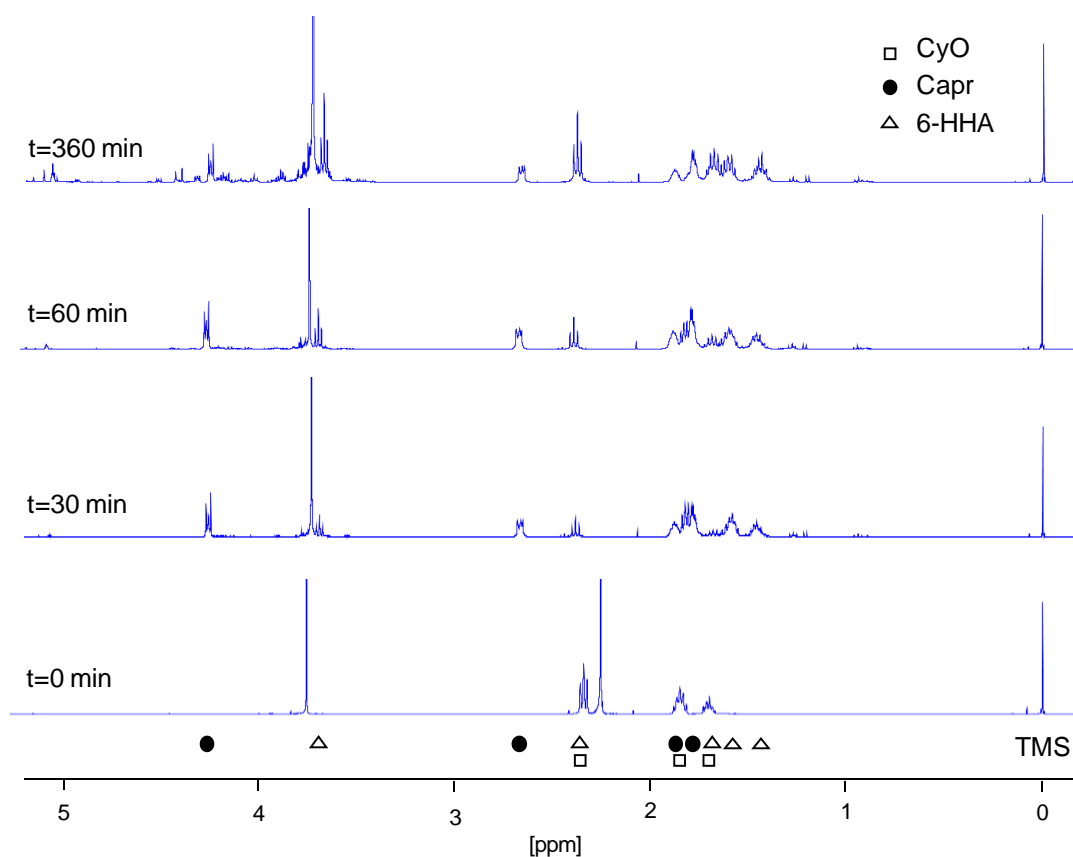


Figure 3.15. Time online analysis of BVO of CyO at 100 °C monitored by ^1H NMR. Reaction conditions: 10 mL of 0.33 M CyO in 1,4-dioxane, 1 mol. % Sn respect to the ketone, 1.5 H_2O_2 :CyO, at 100 °C.

By utilising both GC-FID and ^1H -NMR, a complete kinetic evaluation of the BVO of CyO could be obtained (Fig 3.16).

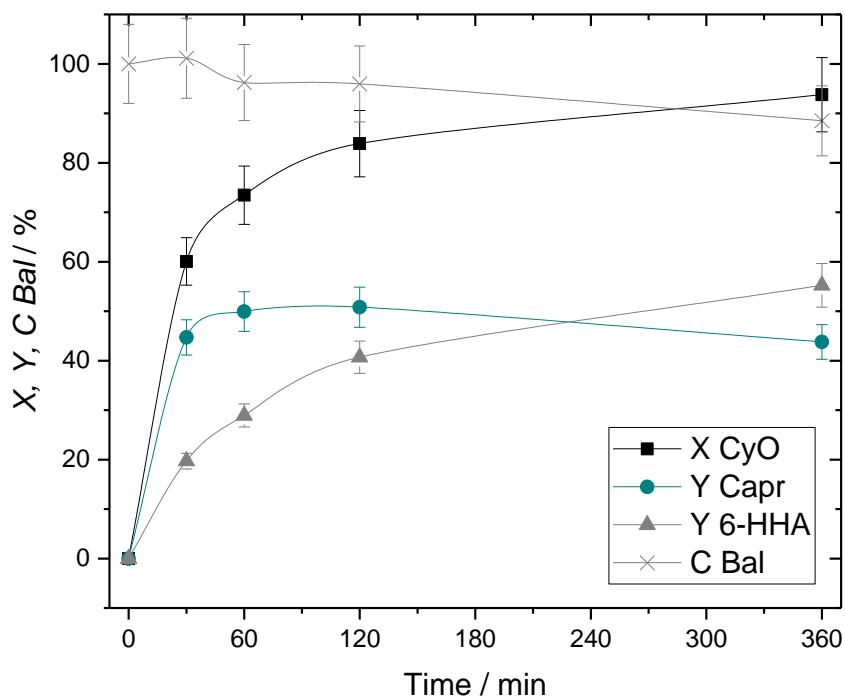


Figure 3.16. Time online analysis of BVO of CyO catalysed by 2Sn- β , at 100 °C, monitored by GC-FID and ^1H NMR.

Following quantification of 6-HHA, carbon balance improved from 54 % to 88 % at the highest levels of conversion. This clearly demonstrates that as CyO conversion increases, selectivity towards 6-HHA dramatically increases, indicating that the overall reaction contains two consecutive steps: 1) BVO of CyO to Capr, and 2) hydrolysis of Capr to 6-HHA.

To fully rule out the presence of AA in the reaction mixture, ^{13}C NMR analysis were performed, since AA possesses a distinct ^{13}C resonance at 175.82 ppm, which can be differentiated from the rest of the reaction components. A representative example of ^{13}C NMR analysis of BVO reaction of CyO after 6 h is shown in Fig 3.17.

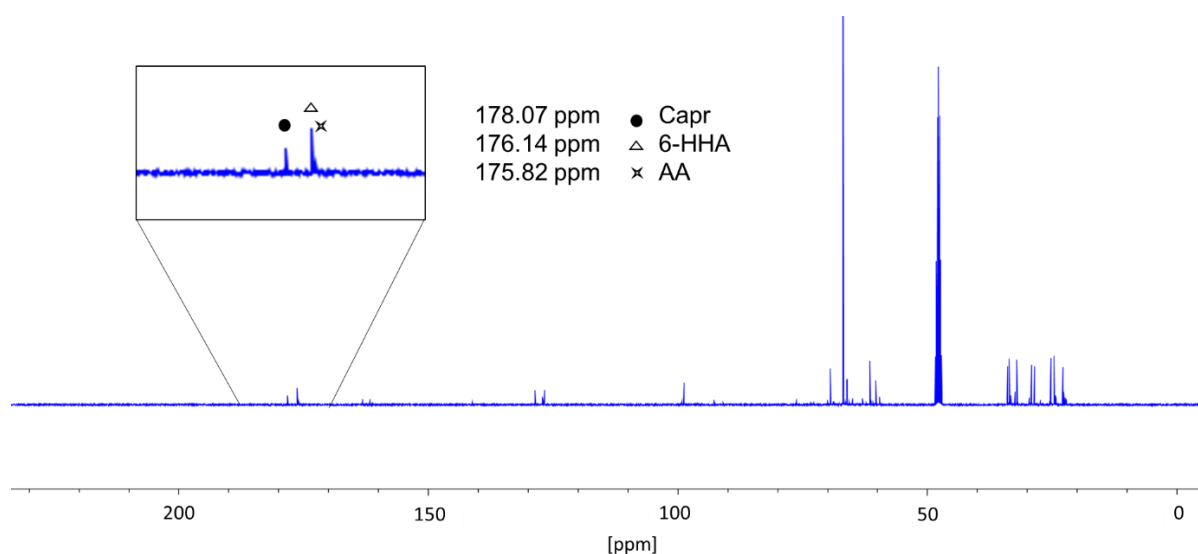


Figure 3.17. ^{13}C -NMR analysis of the final reaction mixture after 6 h of BVO reaction. Reaction conditions: 10 mL of 0.33 M CyO in 1,4-dioxane, 1 mol. % Sn respect to the ketone, 1.5 H_2O_2 :CyO, at 100 $^\circ\text{C}$.

As revealed by ^{13}C NMR analysis, only traces of this by-product could be observed during the entire reaction period. It was previously reported by Cavani *et al.*³⁶ that AA can be formed as a deep oxidation product during the BVO of CyO with titanium silicalite-1 as catalyst, since titanium silicalite-1 is a catalyst which is well known to produce $\cdot\text{OH}$ radicals that may readily oxidize 6-HHA. However, in this study, the 1,4-dioxane employed as solvent can act as an $\cdot\text{OH}$ radical scavenger and Sn- β has a poor ability to generate $\cdot\text{OH}$ radicals. Therefore, the low amounts of AA observed in this work are consistent with the catalyst choice and solvent, which prevent the oxidation reaction to go further.

To further close the final carbon balance, the used catalytic materials extracted from the reactor after reaction was analysed by Thermogravimetric Analysis (TGA). This technique is very useful to identify and quantify the species adsorbed onto the catalyst during the reaction. Firstly, preliminary analysis of the catalyst pre-treated with pure 1,4-dioxane and solutions of CyO, Capr and 6-HHA in 1,4-dioxane, were analysed to determine the grade of adsorption of each compound onto the material. The first derivatives obtained for TGA of each pre-treated sample are collected in Fig 3.18 where it can be observed that each standard could be distinguished by its time of desorption from 2Sn- β .

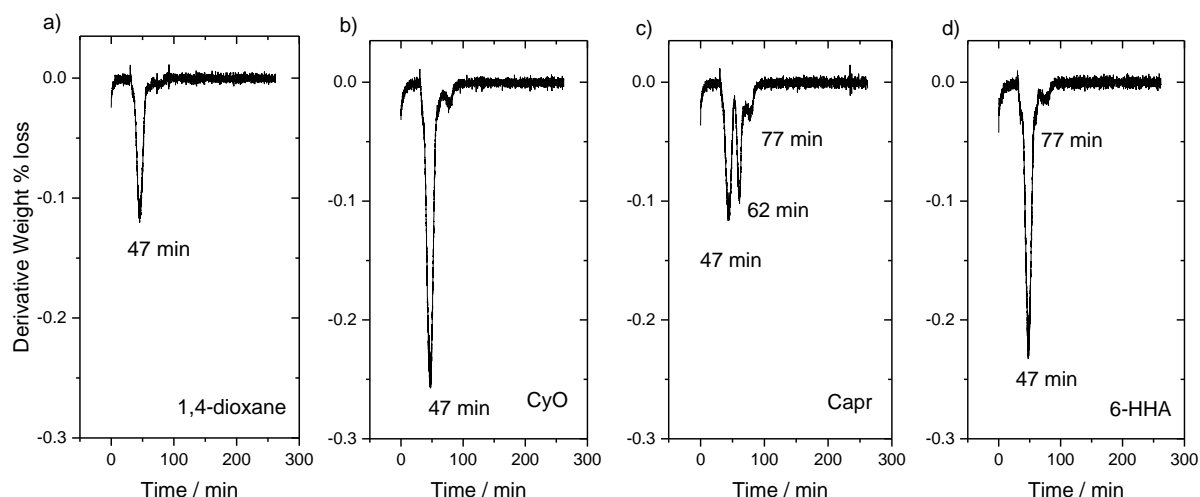


Figure 3.18. TGA of 2Sn- β pre-treated with a) 1,4-dioxane, b) CyO, c) Capr and d) 6-HHA standards in 1,4-dioxane.

The TGA of the used 2Sn- β after a typical BVO reaction of 6 h was compared with the mass losses corresponding to the 4 pre-adsorbed standards. This allowed the type (from the desorption time) and quantity (by the mass loss observed at said time) of adsorbed reactant on the material to be established (Fig 3.19).

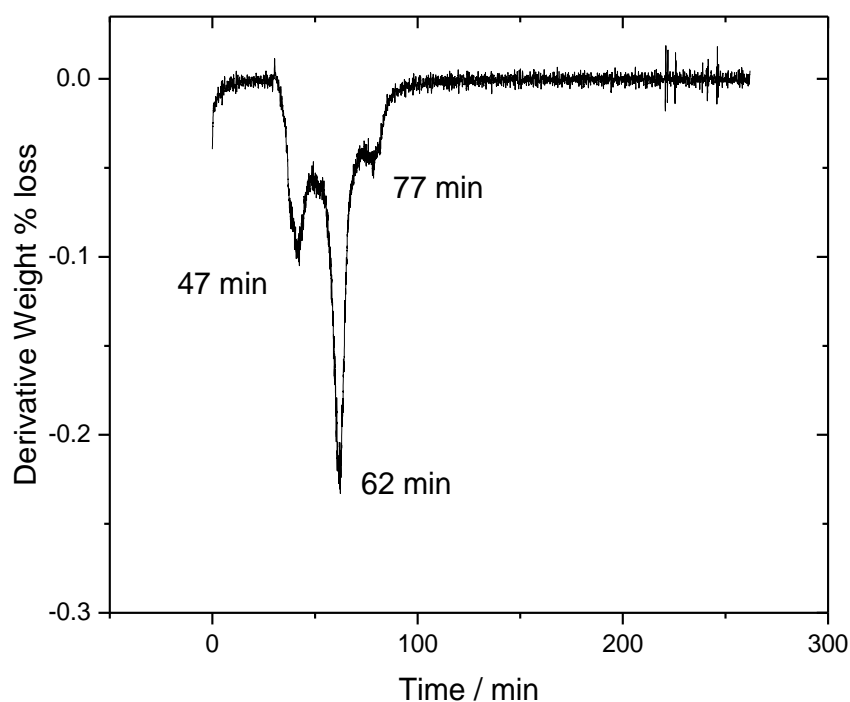


Figure 3.19. TGA of used catalyst after BVO reaction. Reaction conditions: 10 mL of 0.33 M CyO in 1,4-dioxane, 1 mol. % Sn respect to CyO, 1.5 H₂O₂:CyO at 100 °C.

In addition to some residual solvent (which desorbed at a distinct, low temperature), a considerable amount (11 wt. %) of Capr, and a small amount (3 wt. %) of 6-HHA were detected. In total, this corresponded to approximately $\pm 5\%$ of the original carbon species introduced into the reaction at the start of the process, and thus raised the final carbon balance to 93 %.

It should be noted from the ^1H NMR time online analysis (Fig 3.15) that, at extended times, a new set of resonances arose between 3.7 - 4.5 ppm, which suggests the possible formation of oligomeric and polymeric products. With the aim of bringing the carbon balance to 100 %, final reactant solution was analysed by Gel Permeation Chromatography (GPC) as shown in Figure 3.20.

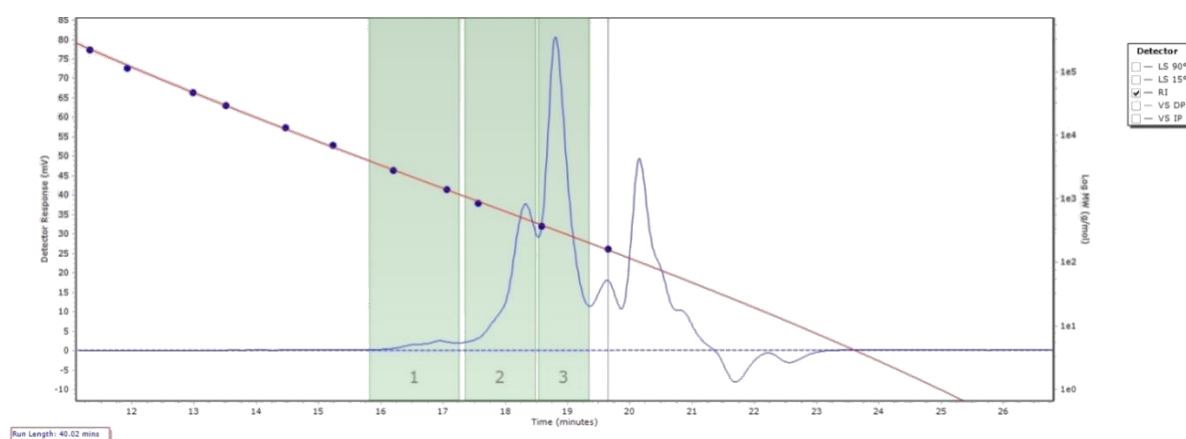


Figure 3.20. GPC analysis of oligomers traces formed after 6 h of reaction.

Preliminary GPC analysis of final reaction mixture (6 h of reaction) revealed these polymeric species to be oligomers of Capr, possessing between 2 and 3 Capr units, although its precise quantification was not possible at this stage of the project. Peak 1 corresponded to species with an average molecular weight (M_n) of 1704 Da and a polydispersity index dispersity (PDI) of 1.08; Peak 2 corresponded to M_n of 534 Da and PDI of 1.04; and Peak 3 corresponded to M_n of 302 Da and PDI of 1.03. Lower molecular-weight species, outside of the calibration zone, are likely monomeric species, including CyO, Capr and 6-HHA. Although not quantitative, the degree of Capr oligomerisation likely fully closes the carbon balance at high levels of conversion and allows to consider the full reaction pathway disclosed. The confirmation of oligomeric products at extended levels of conversion indicates that performing the reaction continuously at high conversion should be avoided, so as to minimise the opportunity of fouling by oligomer formation.

3.3.3 Caprolactone conversion studies

In the previous section, the identity of the main by-product of the BVO reaction of CyO was confirmed to be 6-HHA, co-produced besides the desired lactone, especially at high levels of conversion. Having this fact in mind, a detailed study on its formation was carried out for a better understanding of the reaction network and the nature of the side reaction(s), to evaluate the opportunities to improve the Capr selectivity along the whole reaction period.

It is worth mentioning that even though dehydration of 6-HHA to Capr can be performed in a second step to convert all products in the desired one, obtaining high Capr selectivity would lead to improved efficiency and would minimise downstream processing, if a more direct solution, such as the complete removal of the side reaction, is not viable during the reaction itself.

Accordingly, the role of the catalyst in the hydrolysis reaction of Capr was investigated separately to BVO of CyO. To do so, two preliminary experiments were performed starting from a solution of Capr in 1,4-dioxane in the absence of CyO and H₂O₂ (Table 3.2).

Table 3.2. Extent of Capr hydrolysis observed under various reaction conditions.

Entry	Catalyst	H ₂ O / mL	Conversion / %
1	-	0.15	0
2	2Sn-β	0.15	25
3	deAl-β	0.15	1.8
4	5Sn-β	0.15	23
5	10Sn-β	0.15	13
6	2Sn-β	0.3	36
7	deAl-β	0	1.1
8	2Sn-β	0	8
9	5Sn-β	0	7
10	10Sn-β	0	4
11	2Sn-β Recalcined	0	4
12	2Sn-β	0.3 (50 wt % H ₂ O ₂)	62

Reaction conditions: 10 mL of 0.2 M of Capr in 1,4-dioxane at 100°C, with 1 mol. % Sn respect to Capr (or equivalent mass of deAl-β) and the stated H₂O added, 4 h of reaction.

In the first reaction (Entry 1), the typical amount of H₂O only (added by necessity when using the required amount of 50 wt. % aqueous H₂O₂ as oxidant) was added to the vessel. In the second experiment (Entry 2), 2Sn-β was also added to the reactor, in addition to H₂O. These control experiments were aimed to verify whether hydrolysis of Capr proceeds in an uncatalysed manner, or whether the heterogeneous material promotes the reaction. In both cases, consumption of Capr and formation of 6-HHA were monitored by GC-FID and ¹H NMR, respectively. As detailed above, in the absence of catalyst (Entry 1), no conversion of Capr was observed. In contrast, in the presence of the catalyst, 25 % of Capr conversion to 6-HHA with up to 95 % of selectivity was obtained. This fact strongly indicates that some catalyst functionality (potential Lewis acidity, Brønsted acidity, or defect sites) is required to catalyse the hydrolysis of Capr, forming the undesired 6-HHA by-product.

Since the catalyst was clearly involved in the hydrolysis of Capr, various samples of Sn-β were tested to discern the nature of the catalyst functionality responsible to catalyse this unwanted reaction. Notably, in the absence of Sn (Entry 3), dealuminated zeolite β (deAl-β) showed extremely low reactivity for the hydrolysis of Capr, indicating that defect sites and residual Brønsted acid sites of the zeolite framework alone were not responsible for Capr hydrolysis, *i.e.* the presence of Sn is essential to catalyse this reaction. In contrast, experiments using different Sn-β (possessing between 2 and 10 wt. % Sn, Entries 2, 4 and 5) presented relatively good activity for the hydrolysis of Capr, with up to 25 % of conversion over 4 h reaction time. Interestingly, the relative activities of 2, 5 and 10Sn-β samples for Capr hydrolysis were identical to the relative activities exhibited with these samples for the BVO reaction itself (Fig 3.6), with 2 and 5 wt. % being practically identical in activity, and 10 wt. % Sn loading being significantly lower in activity. Unfortunately, this fact strongly points out that the same Sn (IV) sites are responsible to carry out both reactions, the BVO of CyO and the hydrolysis of Capr. Thus, catalyst modification methodologies are unlikely to be able to remove the hydrolysis side reaction, and 6-HHA formation is likely unavoidable under these reaction conditions.

Furthermore, analysis of Capr hydrolysis reaction was also monitored by ¹H NMR as shown in Fig 3.21. ¹H NMR analysis confirmed the presence of 6-HHA as main product and allowed its quantification by the same methodology of the TMS capillary than for the BVO, resulting in a 6-HHA selectivity > 90 % throughout all the reaction period. Once again, as observed for standard BVO in Fig 3.16, unquantified trace amounts of oligomers could also be detected at extended reaction periods.

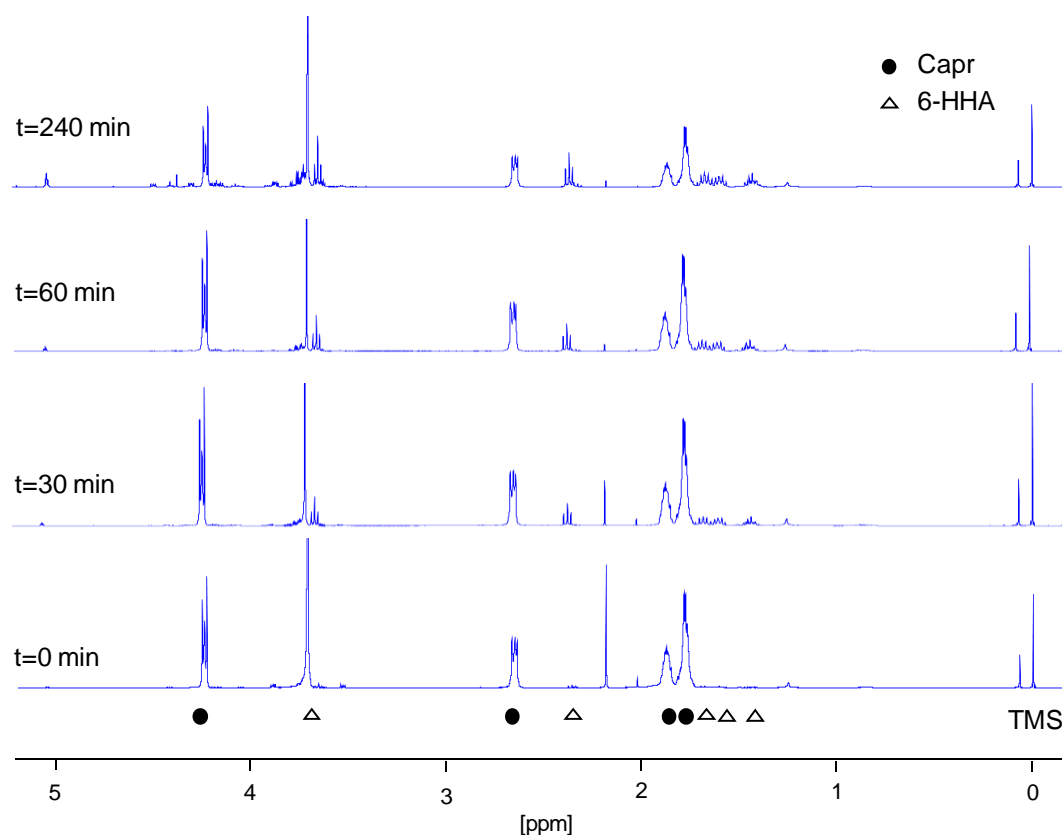


Figure 3.21. ^1H NMR time online analysis of hydrolysis of Capr performed at 100 °C when adding 0.15 mL of H_2O , corresponding to Entry 2, Table 3.2.

Surprisingly, even in the absence of additional H_2O , conversion up to 8 % of Capr to 6-HHA was still observed when using different Sn- β catalysts (Entries 7 to 10). In view of this, an additional experiment using freshly calcined Sn- β (Entry 11) was performed. Catalysts are sometimes not used straight after their preparation and they are commonly stored at ambient conditions for a few days prior using them. During this period, humidity from the environment, *i.e.* H_2O , is likely to get adsorbed onto the catalyst and this may affect the hydrolysis of Capr. Indeed, recalcined catalyst showed a decrease in conversion, although it was not completely eliminated, suggesting that even trace amounts of H_2O coming from the catalyst and/or non-anhydrous solvent lead to hydrolysis.

Subsequently, attention was focus on the effect of H_2O . As shown in Entry 12, higher conversion of Capr was reached when H_2O_2 (typical amount added for standard BVO of CyO) was present alongside H_2O , reaching 62 % after 4 h of reaction while only 36 % of conversion of Capr was observed using analogous amount of H_2O (0.3 mL, Entry 6), *i.e.* in the absence of H_2O_2 , after the same period. Notably, in both reactions (Entries 6 and 12) selectivity to 6-HHA was > 90 % along all the reaction period. For instance, Fig 3.22 illustrates the time online analysis of Entry 12 monitored by ^1H -NMR, where it is shown how only Capr and 6-HHA characteristic resonances could be detected.

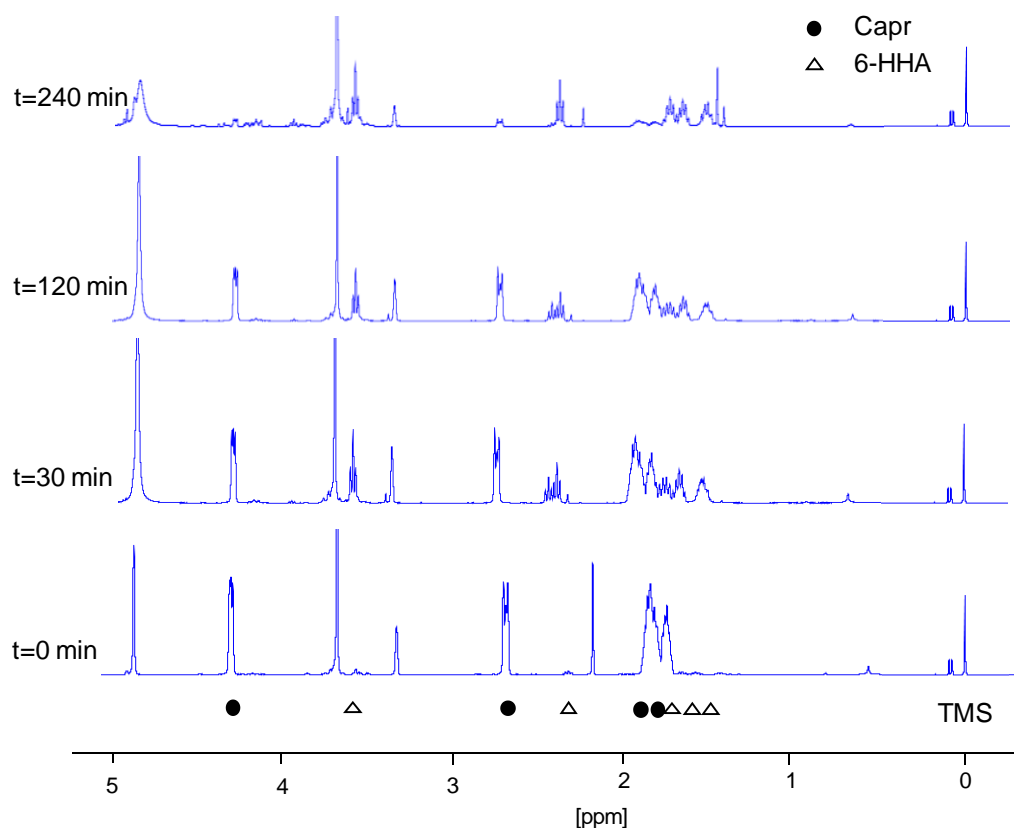


Figure 3.22. ^1H NMR time online analysis of hydrolysis of Capr at 100°C when adding 0.3 mL of 50 wt. % H_2O_2 in aqueous solution, corresponding to Entry 12, Table 3.2.

Indeed, ^1H NMR analysis in Fig 3.22 did not show AA present in any of the aliquots of the reaction, indicating that even in the addition of larger amount of oxidant, no over-oxidation of the 6-HHA to AA occurred, despite the extension of level of conversion of Capr.

With the aim to fully discard AA formation during hydrolysis of Capr, reaction solutions corresponding to a) typical hydrolysis reaction (*i.e.* in the absence of H_2O_2) and b) following addition of H_2O_2 (Entries 2 and 12), were analysed by ^{13}C NMR (Fig 3.23). In both cases no clear evidences of AA were observed. Although the total absence of AA is likely due to the low sensitivity of the analytical methodologies *i.e.* its concentration was too low for detection, the high selectivity towards 6-HHA observed, even in this last case, where H_2O_2 was also present as oxidant, strongly indicates that ring opening (yielding to 6-HHA), and not deep oxidation (yielding to AA), remains the dominant consecutive reaction. The increased rate of ring opening in the presence of H_2O_2 may be due to the lower pH/ pK_a of the solution (pK_a of 11.7) and/or the presence of cationic stabilizers in the aqueous solution of H_2O_2 , both of which may increase the rate of the ring opening reaction relative to H_2O alone.

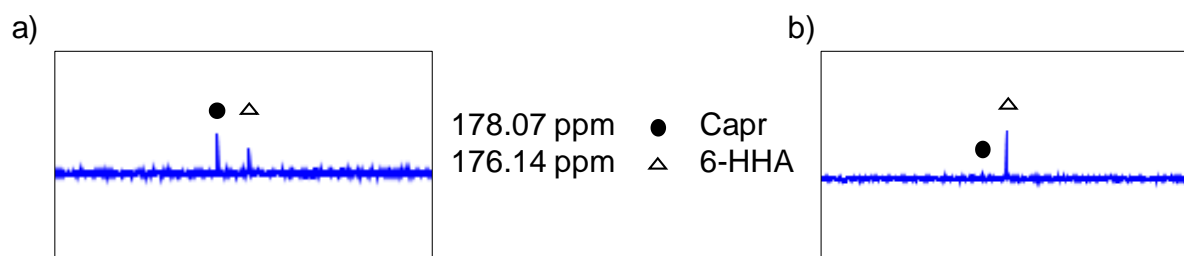


Figure 3.23. ^{13}C -NMR analysis of the final reaction mixture of hydrolysis of Capr at 100°C a) when adding 0.15 mL of H_2O (Entry 2) and b) when adding 0.3 mL of aqueous H_2O_2 (50 wt. %) (Entry 12) after 4 h of reaction.

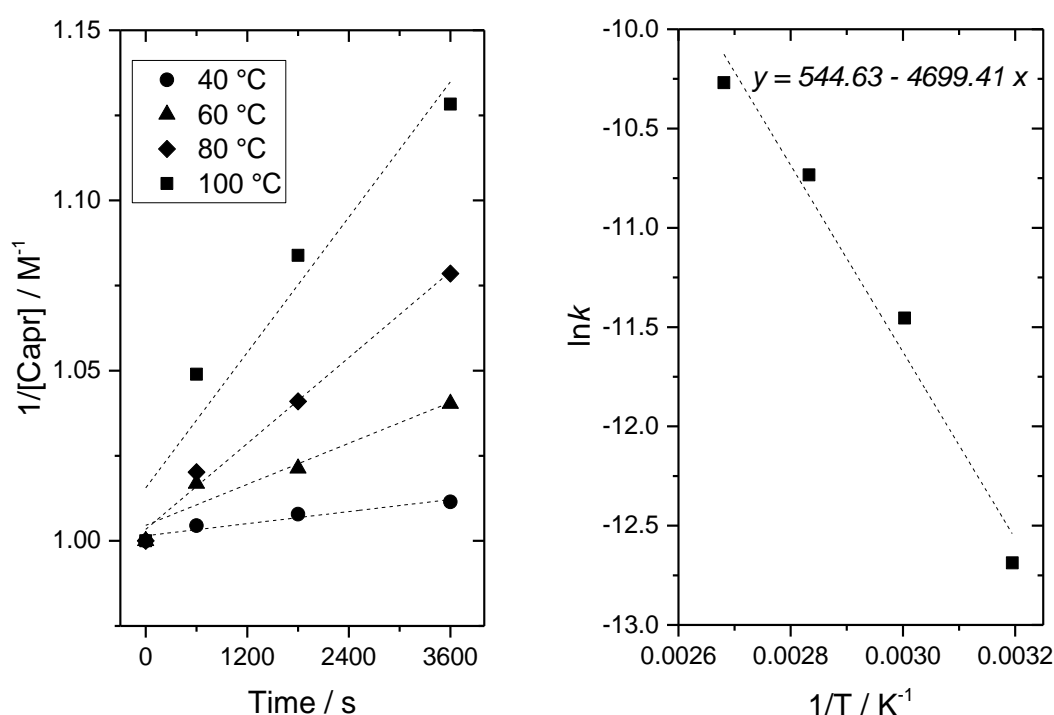


Figure 3.24. Kinetic analysis of hydrolysis of Capr. (Left) Adjustment as second order respect to lactone for 2Sn- β at different reaction temperatures and (Right) the corresponding Arrhenius plot obtained.

As final point of this study, the temperature dependence of the hydrolysis of Capr catalysed by Sn- β was also investigated. Kinetic data from experiments varying T from 100 to 40°C could be adjusted as second order reaction respect to the lactone (Equation 3.2), by use of the Arrhenius plot (Fig 3.24), an E_{act} value of 37 kJ mol^{-1} was calculated. This value obtained is comparable to the E_{act} of BVO, of 51 kJ mol^{-1} . Since these two reactions are consecutive, effort should be made to control the extent of conversion of CyO during BVO, and to use the conversion vs. selectivity relationship to maximise selectivity to Capr.

3.3.4 Intensification and catalyst stability in continuous flow

Having understood the kinetics of the reaction and elucidated the nature of the by-products formed during BVO, potential scalability of this process was explored.

One of the best options to study the potential scalability of a system and enhance its appeal to industry is moving from batch to continuous operation. Continuous flow operation allows to increase notably the productivity of a system, as well as allowing study of the catalysts stability, which plays an important role for all industrial processes and is vital to ensure the success of the catalytic reaction, by evaluating its performance through longer reaction period compared with batch mode.

The first point to tackle, prior to explore the activity of the system in continuous operation, was the investigation of the potential role of each of the (by-)products to poison and deactivate the catalyst (product induced poisoning), since longer contact times between the catalyst and the products in continuous mode may negatively affect to the catalytic performance of the material. As shown in Fig 3.4, standard BVO reaction carried out in batch mode suffers from a large decrease in catalytic rate after 1 h of reaction when high levels of CyO conversion were reached, indicating product-induced poisoning, which may be even more magnified in continuous regime.

Accordingly, the standard BVO reaction at 100 °C (Fig 3.4) was repeated in the presence of various quantities of the reaction (by-)products (Capr, H₂O and 6-HHA), *i.e.* 10, 25 and 50 mol. % of each product. It should be mentioned that H₂O₂ was always used as an aqueous solution (50 wt. %), therefore, a 3.02:1 mole ratio (*i.e.* 302 mol. %) of H₂O relative to CyO was already inevitably present at the beginning of the standard reaction. Hence, in these poisoning studies, the initial 302 mol. % of H₂O was still present. Furthermore, up to an additional 100 mol. % could be formed during the reaction if a totally selective oxidation process occurs transforming all the CyO present into Capr by the formation of H₂O from H₂O₂. This co-produced H₂O was the mol. % H₂O by-product added for the poisoning studies.

In each case, the conversion of CyO was used to determine the kinetics of the reaction as a function of the amount of (by-)product added. By plotting the inverse of each initial reaction rate against the mol. % of each by-product added (Fig 3.25), it could be easily appreciated which by-product has the most effect on the original initial rate, *i.e.* without the addition of any extra by-product.

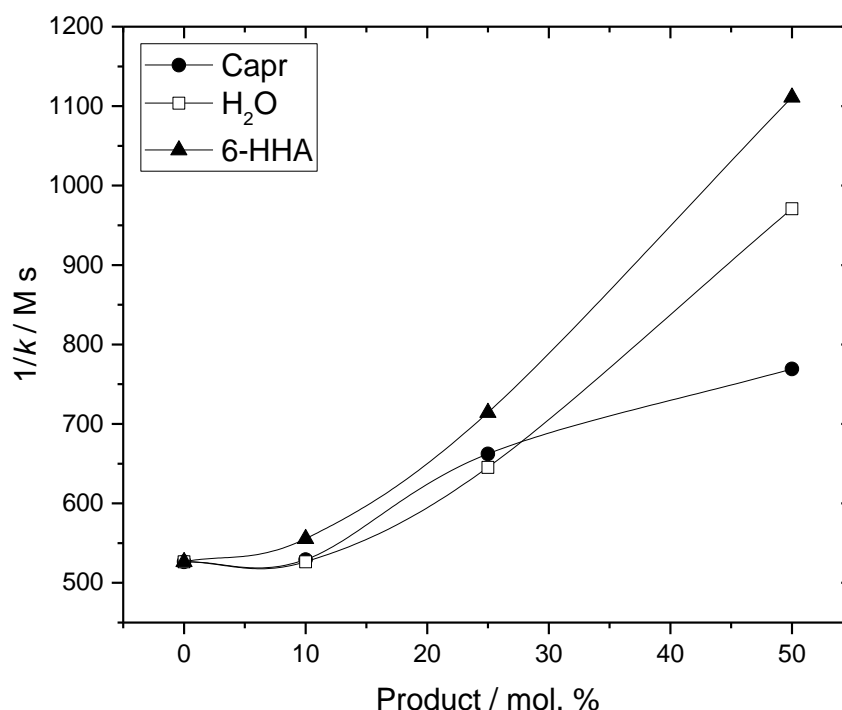


Figure 3.25. Effect of by-product addition on the initial rate of BVO observed.

As reported in Fig 3.25, each of the products added influenced the initial reaction rate to some extent. For instance, Capr, the desired product, showed the lowest effect in the initial rate, even at relatively high amounts, *i.e.* at 50 mol. % relative to CyO, only approximately 20 % of decrease in the initial rate could be observed. On the other hand, influence of H₂O and 6-HHA in the initial catalytic activity were more noticeable. In these cases, the initial rate of reaction was found to decrease significantly, by approximately 40 % when adding 50 mol. % of H₂O, and about 50 % when adding 50 mol. % of 6-HHA.

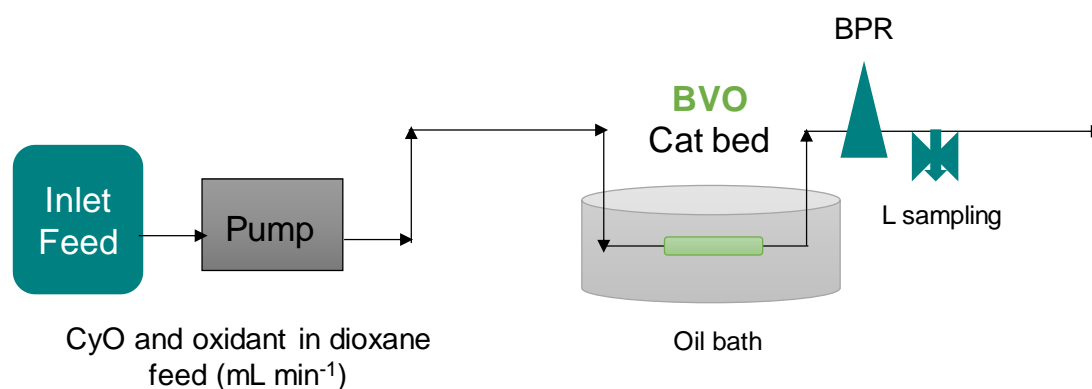
However, it was noticed that low amounts of 6-HHA (< 25 mol. %) do not overly decrease the initial rate. Having in mind the previous results, a CyO conversion level of approximately 50 - 60 % (corresponding approximately to a 6-HHA level of 15 - 25 mol. %, and a decrease in rate of ± 20 %) appears to be a good target. The strong decrease in reaction rate observed at 6-HHA levels of ± 50 mol. % corresponded well to the decrease in catalytic rate observed in the initial batch experiments at CyO conversion levels of 60 % and above, where 6-HHA begin to become the major reaction product, originating a significant drop in Capr selectivity.

Herein, these experiments allowed to identify the main cause of deactivation in batch mode to be mostly due to poisoning by 6-HHA. This study clearly demonstrates that the continuous reactor should be held at a level of CyO conversion consistent with as little 6-HHA and H₂O present as possible to minimise poisoning, *i.e.* around 60 % of CyO conversion.

Once the impact of the potential reaction products on the reaction rate were determined, and the optimal range of product concentration to diminish the poisoning identified, the activity of this system in continuous flow was subsequently explored.

The kind of reactor selected to investigate the viability of BVO of CyO in continuous operation was a continuous Plug Flow Reactor (PFR). A PFR offers major advantages over a slurry reactor, including: i) improved process control and safety, ii) excellent mass- and heat-transfer, iii) shorter reaction times, iv) smaller reactor volumes, v) scalability and vi) increased STYs.³⁷ In addition, as already mentioned, continuous PFR allows critical evaluation of a catalysts stability and lifetime under steady state conditions.

The reactor employed (Scheme 3.3) was adapted from a kinetically relevant PFR optimised for the Sn- β catalysed isomerisation of glucose to fructose and the transfer hydrogenation of carbonyl compounds.^{38,39} The liquid feed was delivered into the system by an HPLC pump to the packed catalyst bed, which was placed in an oil bath maintained at the required reaction temperature. The whole system was kept under pressure by means of a Back Pressure Regulator (BPR). This allowed operation above the boiling point of the solvent to proceed, and hence, accelerated the reaction rate. The reactor was also connected to a sampling valve, from which the reacted solution was periodically taken and analysed by GC-FID and ¹H NMR, following analogous procedures to the BVO batch reactions.



Scheme 3.3. Simplified scheme of the continuous flow reactor.

From the batch kinetic studies, it was determined that BVO best fitted the second order rate equation with respect to CyO (Equation 3.2), which applied to the PFR design equation, allowed to appropriately calculate the value for the contact time, τ , that can also be calculated as:

$$\tau = \frac{V \text{ (cm}^3\text{)}}{Q \text{ (cm}^3\text{min}^{-1}\text{)}} \quad [\text{Equation 3.4}]$$

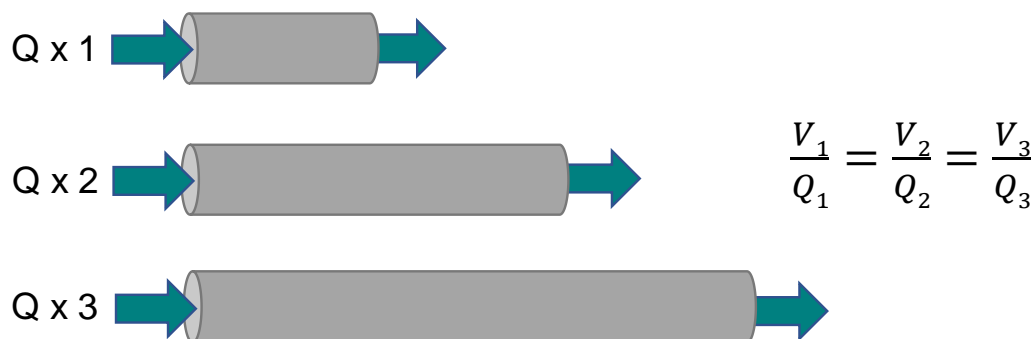
Where V is the volume of the catalyst bed and Q is the volumetric flow rate at the start of the reaction.

To rule out potential external mass transfer limitations, the effect of linear velocity was first investigated. The linear velocity (v) is defined in Equation 3.5 as:

$$v \text{ (cm min}^{-1}\text{)} = \frac{Q \text{ (cm}^3\text{min}^{-1}\text{)}}{S \text{ (cm}^2\text{)}} \quad [\text{Equation 3.5}]$$

Where Q is the volumetric flow rate and S is the reactor section.

The study of the linear velocity is based on a set of experiments that allow to define when external diffusion (also named film diffusion) is the limiting regime. For these experiments, catalyst columns of various length (Scheme 3.4) were prepared and flow rate of reactant was proportionally varied so that the overall contact time was kept constant, while the linear velocity increases, since the section of the reactor is constant. It should be mentioned that the contact time is directly proportional to the conversion, therefore, at same contact time, and under kinetic regime, the conversion of the reaction should be the same at each linear velocity. Thus, in the absence of film diffusion the conversion is independent from the flow rate (at constant contact time). On the other hand, when film diffusion is the dominant regime, the conversion decreases proportionally to the flow rate.



Scheme 3.4. Simplified scheme for the linear velocity experiments.

As shown in Figure 3.26, the set of experiments reached the same levels of conversion, indicating a lack of interphase limitations of the flow rates explored. Linear velocity experiments, which showed similar levels of conversion of CyO achieved at the flow rates tested, confirmed the optimal range of catalyst bed volume - flow rate needed to operate in the kinetic regime, without any mass transfer limitations caused by the reactor itself.

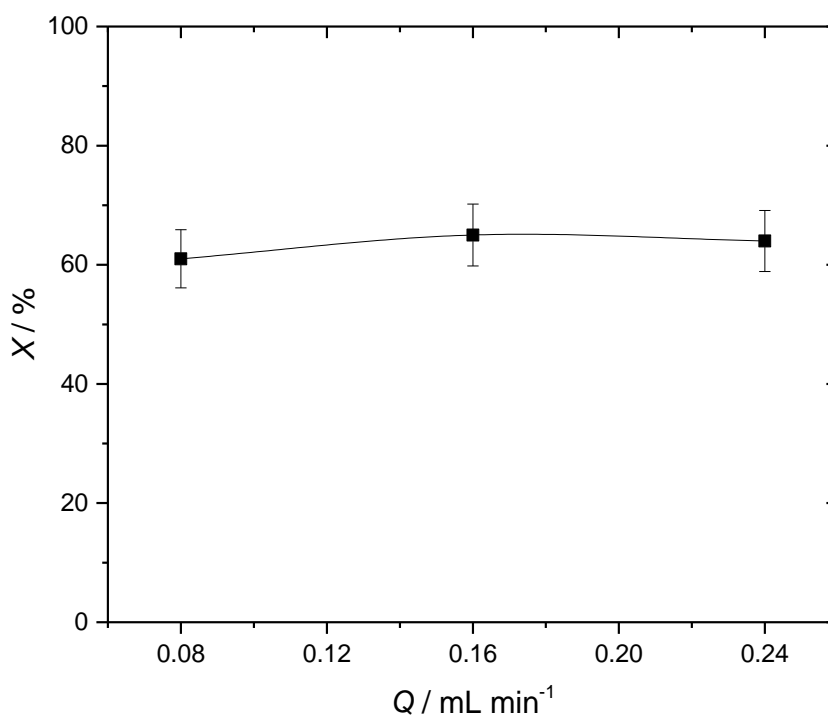


Figure 3.26. Impact of linear velocity (*i.e.* flow rate at fixed contact time) on the catalytic activity of BVO of CyO using 2Sn- β in the continuous regime.

Having ensured a performance in the kinetic regime, a reaction consistent with the standard reaction conditions typically used in batch experiments was carried out, following the procedure described in detail in Section 2.4.4, and its catalytic evolution is represented in Fig 3.27. Apart from a very short induction period (Fig 3.27, left), catalytic activity remained relatively constant over a period of 180 h, with a steady state CyO conversion of $\pm 60\%$ being observed. Furthermore, no major modifications in selectivity were observed upon moving into the continuous reactor, and the conversion vs. selectivity trend sat on the same profile as found for the batch reactor at the same H_2O_2 :CyO ratio of 1.5 (Fig 3.27, right).

Clearly, the Sn- β / H_2O_2 / BVO system possessed good levels of stability. Over the course of 180 h, the catalyst performed > 5000 substrate turnovers, equivalent to over 50 complete batch reactions. Notably, the TON values observed were an order of magnitude higher than those previously observed for the same catalytic system. Overall, a relative loss of approximately 15.4 % of the maximal activity (from 65 to 55 %) was observed during this period, even without periodic catalyst regeneration being performed. However, as reported in Fig 3.27, left, regeneration of the catalyst bed after 180 h by re-calcination treatment (3 h at 550 °C in air) restored the initial activity, demonstrating the slight decrease in activity to be reversible *i.e.* deactivation is not permanent.

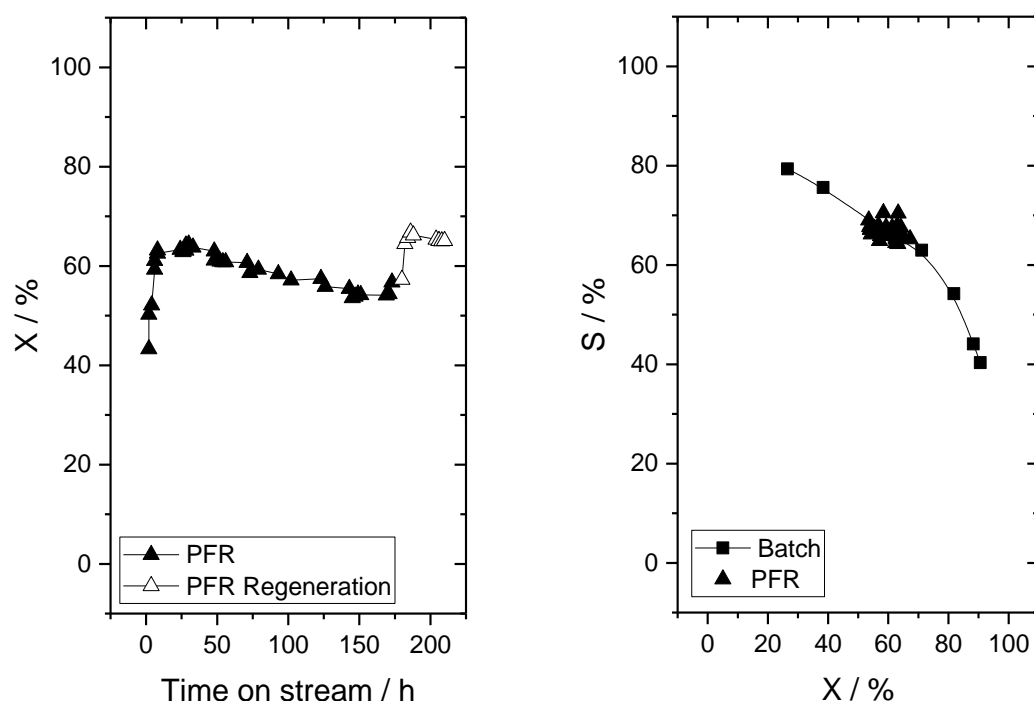


Figure 3.27. (Left) Conversion vs. time on stream during BVO of CyO in the continuous regime at 100 °C and (Right) selectivity towards Capr as function of CyO conversion in both regimes, batch and continuous. Reaction conditions: Reactant feed of 0.33 M CyO and 0.5 M H₂O₂ in 1,4-dioxane with a contact time of 5.5 min under a pressure of 10 bar, at 100°C.

Given that also H₂O showed some ability to poison the catalyst (Fig 3.25) and it was demonstrated in Section 3.3.3 that presence of H₂O enhances the ring opening consecutive reaction to 6-HHA, a reduction of the H₂O present in the system was considered due to the potential benefits that may entail.

To do so, the viability of the system to operate continuously in an oxidant-limited regime was explored, since from the batch studies (Fig 3.9, right), it was shown that similar initial reaction rates could be obtained at a H₂O₂:CyO ratio of 0.75 as for the typical 1.5 ratio *i.e.* the BVO reaction is zero order with respect H₂O₂ concentration in both cases. Although operating in an oxidant-limited regime limits the system to < 75 % CyO conversion, the target level of conversion (50 - 60 %) was still achievable, and the decrease in H₂O may reduce the hydrolysis of Capr and product induced poisoning.

Accordingly, the BVO of CyO was carried out in a PFR at the lower H₂O₂:CyO ratio of 0.75, keeping all other experimental parameters, including temperature, flow rate, catalyst mass, and reactor volume, identical to the previous experiment. Its comparison with the initial experiment carried out at the typical 1.5 ratio of oxidant is reported in Fig 3.28.

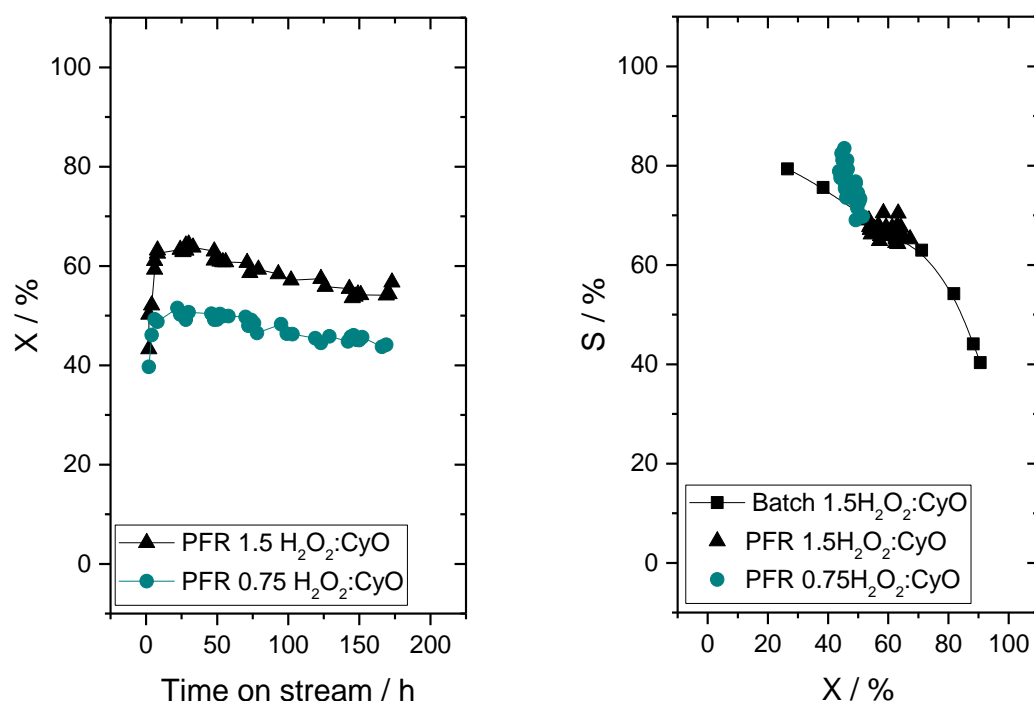


Figure 3.28. Comparison between PFR using 1.5 and 0.75 H₂O₂:CyO ratios. (Left) Conversion vs. time on stream and (Right) Capr selectivity as function of CyO conversion in both regimes, batch and continuous. Reaction conditions: Reactant feed of 0.33 M CyO and 0.5 M or 0.25 M H₂O₂ in 1,4-dioxane with a contact time of 5.5 min under a pressure of 10 bar, at 100°C.

In this comparison, it can be clearly appreciated the good agreement of both experiments in terms of catalytic activity and stability. A high level of stability was observed in the oxidant-limited regime, although CyO conversion was approximately 10 % lower across the entire reaction period (± 65 vs. ± 50 %, respectively). In terms of activity, the maximum conversion obtained was 51 %, dropping to 44 % after 180 h, which represented a relative decrease in activity of 13.7 %. As such, stability was slightly improved in the oxidant-limited regime when compared with the typical oxidant-excess, where the relative loss of activity was approximately 15.4 %. This may be due to the lower amount of H₂O present in the system, or the slightly lower level of conversion in this system, which led to less 6-HHA formation. Worth to be highlighted, the decrease of the oxidant concentration also led to a slight improvement in Capr selectivity at all overlapping CyO conversion levels. Indeed, as can be seen in Fig 28, right, Capr selectivity increased when compared with the typical batch and flow experiments using excess of oxidant. A maximum selectivity of 85 % was achieved in the oxidant-limited regime, while the maximum selectivity reached using 1.5 ratio of oxidant was about 70 %. However,

given the minimum amount of H_2O required for ring opening, the complete suppression of ring opening under these conditions is quite unlikely.

Subsequently, H_2O_2 -based selectivity of the three reactions was investigated in Fig 3.29.

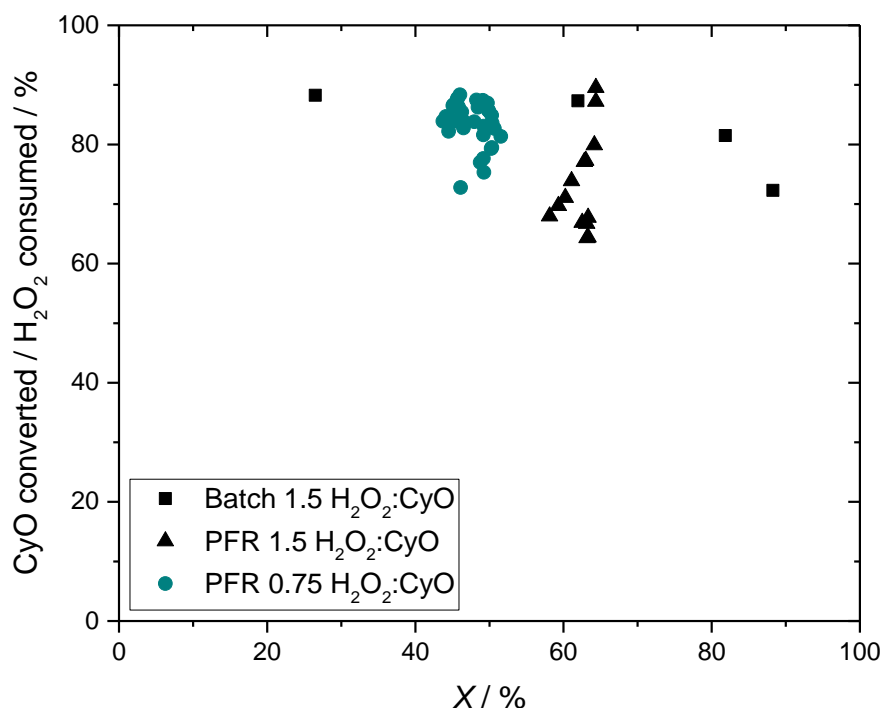


Figure 3.29. H_2O_2 -based selectivity as a function of conversion for BVO of CyO.

As shown above, in addition to leading to higher lactone selectivity at overlapping levels of conversion, operating at oxidant-limited regime in continuous flow also displayed significant differences in terms of oxidant efficiency respect to PFR in oxidant-excess, obtaining major improvements in H_2O_2 -based selectivity that matched the batch results. At a H_2O_2 :CyO ratio of 0.75, a H_2O_2 -based selectivity (*i.e.* moles CyO converted / moles H_2O_2 consumed) of about 85 % was obtained, indicating that most of the oxidant is more effectively used. In contrast, H_2O_2 -based selectivity obtained with H_2O_2 :CyO ratio of 1.5 was generally lower, indicating a poorer usage of the oxidant. This decrease in oxidant efficiency when operating in continuous flow at 1.5 oxidant ratio may be caused by the lowering of the stability of H_2O_2 in the PFR itself, made of stainless steel, and by the operation in higher pressure with respect to the batch experiments, which can lead to some H_2O_2 decomposition.

It should be mentioned that preliminary stability tests of H_2O_2 performed in batch mode revealed that, at the typical BVO reaction conditions employed (100 °C, in 1,4-dioxane and catalyst), about 5 % of H_2O_2 decomposition can be observed after 6 h of reaction. Although analogous experiments were not performed in the continuous PFR, it is though that the extent

of the decomposition may likely be magnified when operating in continuous flow by the reasons stated above, thus leading to a lower H_2O_2 efficiency than for the batch experiment. Clearly, decreasing the concentration of H_2O_2 leads to noticeable improvements in H_2O_2 utilisation, without overly compromising the BVO process itself, achieving comparable levels of activity, stability and productivity. Such improvements are of tremendous importance to both process economics and reaction sustainability, particularly given the cost of H_2O_2 . This set of experiments demonstrates the excellent viability of this system to operate in continuous flow. In addition to the high levels of stability, performing the reaction in plug flow mode also led to tremendous improvements in the productivity of the system respect to single batch operation. For a better direct comparison, STY of the three experiments were calculated at their maximum CyO conversion, as amounts of CyO converted (g) per reactor volume (cm^3) per time (h) per amount of catalyst (kg) (Table 3.3).

Table 3.3. Relative performance of 2Sn- β for BVO chemistry in batch and flow.

Reactor type	STY ^a / g(CyO) cm^3 kg(cat) ⁻¹ h ⁻¹	Relative STY	Capr selectivity at max STY
Batch ^b	24.5	1	39
PFR ^c 1.5 H_2O_2 :CyO	1123	46	66
PFR ^c 0.75 H_2O_2 :CyO	896	37	70

^a STYs were calculated at maximum conversion as g of reactant converted per cm^3 reactor volume, per hour and per kg of catalyst. ^b Only the liquid volume was used as reactor volume. ^c Volume of catalyst bed used as reactor volume.

As can be observed, STY at 100 °C in the continuous reactor increased by two order of magnitude relative to the batch reactor system at the same H_2O_2 :CyO ratio and the relative performance was also highly improved. Notably, Capr selectivity obtained at the maximum STY of each reactor was also substantially higher in the PFR (70 vs. 39 %).

Despite no substantial improvements were observed as a function of conversion at the same H_2O_2 :CyO ratio, it should be highlighted that a remarkable improvement was obtained when working at oxidant-limited regime, manifesting the benefit to operate with lower oxidant concentration without compromising too much the overall catalytic performance.

3.4 Conclusions

The BVO of CyO by Sn- β / H₂O₂ was studied in batch and continuous mode with the aim of understanding the mechanistic aspects of the reaction and identifying its potential scalability. This chapter shows that the BVO of CyO by Sn- β / H₂O₂ is a challenging reaction, especially in terms of maintaining high selectivity to Capr at late stages of reaction, since a significant selectivity drop is observed at conversion > 60 %. The detailed study of the different parameters involved in the BVO reaction does not lead to an improvement of selectivity. Selectivity to Capr decreases with conversion, and this trend is maintained throughout all experiments. Herein, the investigation of hydrolysis of Capr by its own was crucial to reveal that this consecutive reaction to 6-HHA is also catalysed by Sn- β and, therefore, occurs simultaneously to BVO at standard conditions used, substantially decreasing the efficiency (selectivity) and activity (rate) of the process, deactivating the catalyst by poisoning.

It should be noted that at the time of this work, this was the first time that the by-product identification and quantification was analysed in such detail, 6-HHA being the main by-product of the reaction. This achievement, alongside the traces of AA and some oligomers of 2 - 3 Capr units, allows the final carbon balance of the reaction to be closed, from 54 % to almost 100 %, and it is a clear insight to better understand the reasons behind the selectivity drop, at the studied reaction conditions.

Nevertheless, optimising the reaction conditions in order to minimise 6-HHA formation shows the potential scalability of this system in the continuous regime. Operating the reaction at conversion levels < 60 %, at which point 6-HHA formation is less pronounced, the system presented good stability, operating for 180 h without major loss in activity, yielding to turnover numbers > 5000, and a volumetric productivity of 1123 g(CyO converted) cm⁻³ (reactor volume) kg(cat)⁻¹ h⁻¹. In addition to being up to two orders of magnitude more productive on a STY basis than batch experiments, the continuous system is also more selective to Capr at these elevated productivities (70 % vs. 39 %). Finally, a remarkable improvement in lactone selectivity is obtained when using the minimum oxidant required to maintain the same reaction rate, leading also to improved H₂O₂ – based selectivity, thus demonstrating the major advantages of the continuous system.

The successful results presented in this chapter using BVO of CyO as model reaction, set the basis to evaluate the general applicability of the system beyond this typical substrate. In Chapter 4, attention is focused on the exploration of more complex ketones as substrates for BVO as part of a sustainable route for the synthesis of renewable monomers.

This chapter contributed to the following paper:

K. Yakabi, K. Milne, A. Buchard, C. Hammond, *ChemCatChem*, 2016, **8**, 3490 – 3498

References

- (1) A. Baeyer, V. Villiger, *Ber. Dtsch. Chem. Ges.*, 1899, **32**, 3625 – 3633
- (2) M. Renz, B. Meunier, *Eur. J. Org. Chem.*, 1999, 737 – 750
- (3) C. Jiménez-Sanchidrián, J. R. Ruiz, *Tetrahedron*, 2008, **64**, 2011 – 2026
- (4) E. Ohara, K. Kawazumi, 2005, *US 6936724 B2*
- (5) G. Dahlhoff, J. P. M. Nierderer, W. F. Hoelderich, *Cat. Rev.-Sci. Eng.*, 2001, **43**, 4, 381 - 441
- (6) M. Labet, W. Thielemans, *Chem. Soc. Rev.*, 2009, **38**, 3484 – 3504
- (7) C.H. Huang, F.C. Wang, B.T. Ko, T.L. Yu, C.C. Lin, *Macromolecules*, 2001, **34**, 356 - 361
- (8) G. Strukul, *Angew. Chem. Int. Ed.*, 1998, **37**, 1198 – 1209
- (9) M. Renz, T. Blasco, A. Corma, V. Fornes, R. Jensen, L. Nemeth, *Chem. Eur. J.*, 2002, **8**, 4708 – 4717
- (10) T. Katsuki, *Chem. Soc. Rev.*, 2004, **33**, 437 – 444
- (11) G. J. ten Brink, I. W. C. E. Arends, R. A. Sheldon, *Chem. Rev.*, 2004, **104**, 4105 – 4124
- (12) Y. Imada, H. Iida, S. Murahashi, T. Naota, *Angew. Chem. Int. Ed.*, 2005, **44**, 1704 – 1706
- (13) A. Corma, L. T. Nemeth, M. Renz, S. Valencia, *Nature*, 2001, **412**, 423 – 425
- (14) A. Corma, M. T. Navarro, L. Nemeth, M. Renz, *Chem. Commun.*, 2001
- (15) A. Corma, M. T. Navarro, M. Renz, *J. Catal.*, 2003, **219**, 242 – 246
- (16) Z. Q. Lei, Q. H. Zhang, J. J. Luo, X. Y. He, *Tetrahedron Lett.*, 2005, **46**, 3505 – 3508
- (17) R. Criegee, *Justus Liebigs Ann. Chem.*, 1948, **560**, 127 - 135
- (18) P. Li, G. Liu, H. Wu, Y. Liu, J. Jiang, P. Wu, *J. Phys. Chem. C*, 2011, **115**, 3663 – 3670
- (19) J. Dijkmans, D. Gabriels, M. Dusselier, F. de Clippel, P. Vanelderen, K. Houthoofd, A. Malfliet, Y. Pontikes, B. F. Sels, *Green Chem.*, 2013, **15**, 2777 – 2785
- (20) P. Wolf, C. Hammond, S. Conrad, I. Hermans, *Dalton Trans.*, 2014, **43**, 4514 – 4518
- (21) P. Y. Dapsens, C. Mondelli, J. Jagielski, R. Hauert, J. P. Ramirez, *Catal. Sci. Technol.*, 2014, **4**, 2302 – 2311
- (22) W. N. P. van der Graaff, G. Li, B. Mezari, E. A. Pidko, E. J. M. Hensen, *ChemCatChem*, 2015, **7**, 1152 – 1160
- (23) A. Corma, M. E. Domine, L. Nemeth, S. Valencia, *J. Am. Chem. Soc.*, 2002, **124**, 3194 - 3195
- (24) M. Boronat, P. Concepción, A. Corma, M. Renz, *Catal. Today*, 2007, **121**, 39 – 44
- (25) J. M. R. Gallo, D. M. Alonso, M. A. Mellmer, J. Dumesic, *Green Chem.*, 2013, **15**, 85 - 90
- (26) P. Y. Dapsens, C. Mondelli, B. T. Kusema, R. Verel, J. Perez-Ramirez, *Green Chem.*, 2014, **16**, 1176 - 1186
- (27) B. Tang, W. Dai, X. Sun, N. Guan, L. Li, M. Hunger, *Green Chem.*, 2014, **16**, 2281 - 2291
- (28) C. Hammond, S. Conrad, I. Hermans, *Angew. Chem. Int. Ed.*, 2012, **51**, 11736 – 11739
- (29) C. Hammond, D. Padovan, A. Al-Nayili, P. P. Wells, E. K. Gibson, N. Dimitratos, *ChemCatChem*, 2015, **7**, 3322 – 3331
- (30) A. Corma, M. Domine, J. A. Gaona, J. L. Jorda, M. T. Navarro, F. Rey, J. Perez-Pariente, J. Tsuji, B. McCulloch, L. T. Nemeth, *Chem Commun.*, 1998, **20**, 2211 - 2212
- (31) S. Conrad, P. Wolf, P. Müller, H. Orsted, I. Hermans, *ChemCatChem*, 2017, **9**, 175 – 182
- (32) M. Boronat, A. Corma, M. Renz, J. Sastre, P. M. Viruela, *Chem. Eur. J.*, 2005, **11**, 6905 – 6915
- (33) R. A. Steffen, S. Teixeira, J. Sepulveda, R. Rinaldi, U. Schuchardt, *J. Mol. Catal. A*, 2008, **287**, 41 – 44
- (34) P. Li, G. Liu, H. Wu, Y. Liu, J. Jiang, P. Wu, *J. Phys. Chem. C*, 2011, **115**, 3663 – 3670
- (35) C. Xia, L. Ju, Y. Zhao, H. Xu, B. Zhu, F. Gao, M. Lin, Z. Dai, X. Zou, X. Shu, *Chin. J. Catal.*, 2015, **36**, 845 – 854
- (36) F. Cavani, K. Raabova, F. Bigi, C. Quarantelli, *Chem. Eur. J.*, 2010, **16**, 12962 – 12969
- (37) O. Levenspiel, “*Chemical Reaction Engineering*”, John Wiley & sons, New York, 3rd edition, Chapter. 21
- (38) D. Padovan, C. Parsons, M. Simplicio, C. Hammond, *Green Chem.*, 2016, **18**, 5041 – 5049
- (39) A. Al-Nayili, K. Yakabi, C. Hammond, *J. Mater. Chem. A*, 2016, **4**, 1373 – 1382

4. Continuous production of bio-renewable, polymer-grade lactone monomers through Sn- β catalysed Baeyer-Villiger Oxidation with H₂O₂

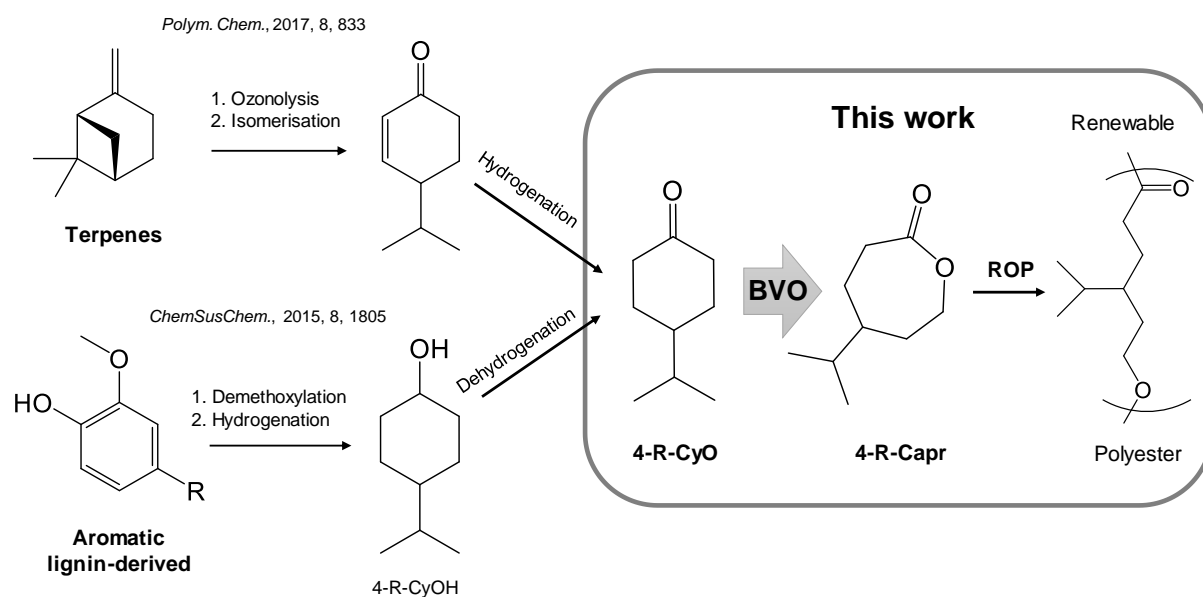
4.1. Introduction

The use of commodity polymers, such as polyesters and polyolefins, is widespread in our society. Their range of applications is highly varied, and includes the textile, agricultural, automotive and healthcare industries, as well as applications in storage and packaging, amongst several other fields. Such materials are highly desired as they are light, strong and cheap. In light of this, over 300 million tonnes of plastics are globally produced every year.¹

At present, almost all polymeric materials are based on fossil feedstocks. However, petroleum-based plastics and polymers have generated increasing concerns regarding their negative impact on the environment, and the depletion of the fossil fuel sources, exposing the need to develop new routes to produce polymeric materials from sustainable sources.^{2,3} Whilst the development of poly(lactic acid), a biodegradable polymer produced from renewable lactic acid, represents a significant breakthrough, such bio-based and biodegradable polymers

currently only account for < 1 % of the polymers produced on an annual basis.⁴ Moreover, their utilisation is strongly limited by their intrinsic properties, particularly their lack of functionalisation, and their cost, since most of these processes still do not stand as solid economic competition for the current industrial processes that use non-renewable sources. Accordingly, the development of greener and more economically profitable processes from biomass derivatives to obtain bio-based polymers with high degrees of functionality, represents a significant challenge.

In view of this, one of the approaches to tackle this challenge and boost the production of biodegradable polymeric material involves the development of new bio-based monomer structures, whose highly oxidized original molecular structure can supply the required functionalities to tailor the physical properties of the final polymeric material. An example of these potential bio-based renewable monomers are substituted ϵ -caprolactones (R-Capr). R-Capr are valuable monomer building blocks to a variety of versatile functional polyesters, as well as elastomers *via* block co-polymerisation with lactic acid,^{5,6} with potential employment in pharmaceutical and medical applications due to their biocompatibility, and favourable mechanical and chemical properties.⁷⁻⁹ A broad palette of biomass sources is suitable for the formation of such renewable monomers. For instance, focusing exclusively on R-Capr formation, naturally available terpenes and terpenoids, such as β -pinene or D-limonene, have successfully been reported as suitable precursors for this kind of monomer.¹⁰ Furthermore, lignin, the largest renewable feedstock for aromatic compounds, has also been revealed to be a promising source for R-Capr.¹¹



Scheme 4.1. Scheme of reaction for biomass derived valorisation to a renewable polyester *via* BVO of substituted cyclohexanone (R-CyO).

As represented in Scheme 4.1, despite their differing pathways, both routes share a common final step, where a substituted cyclohexanone (R-CyO) is converted *via* Baeyer-Villiger Oxidation (BVO) into the corresponding lactone monomer, prior to the ring opening polymerisation yielding the desired polymer. In this kind of sustainable processes where multiple steps are required, optimisation of each step is crucial to minimise costs and maximise productivity and selectivity. Hence, the study of the final step, that is, the BVO of R-CyO and polymerisation of the resulting lactones, represents the focal point of this chapter.

As previously described in Section 3.1, BVO of ketones to lactones and esters has proved to be an efficient chemical transformation,¹² whose sustainability can be increased when using Sn- β as catalyst and hydrogen peroxide (H₂O₂) as a greener oxidant.¹³⁻¹⁵ Since the first report on the Sn- β activity for this reaction, this catalytic system has received increasing attention over the last decades, especially in the academic research. However, the study of this system, at least at the time of this work, seem to be mainly focused to one substrate, cyclohexanone (CyO).¹⁶⁻¹⁸ An example of this is that CyO was the substrate selected to be used as model reaction of BVO in the previous chapter, to elucidate details of the overall reaction network.¹⁹ In Chapter 3, it was confirmed that the control of the lactone selectivity, particularly at high levels of substrate conversion, remains a formidable challenge, due to unavoidable consecutive ring opening hydrolysis of Capr, resulting in 6-hydroxyhexanoic acid (6-HHA) formation, which is also Sn- β catalysed.

Generally, very few publications can be found on other substrates studied for BVO using Sn- β and H₂O₂. For instance, 2-adamantanone, which may be less prone to suffer ring opening side reaction due to its configuration, was successfully transformed into the corresponding lactone by Li *et al.*,²⁰ showing very high selectivity to the lactone when using the appropriate organic solvent. Additionally, BVO of various R-CyO using Sn- β showed a reaction rate trend pointing to increase with bulkier substrates.^{21,22} However, scarce details were given about the justification behind the observed trend.

As an extension of Chapter 3 and in the interest of employing this system as a sustainable step towards the catalytic generation of lactones from biomass, this chapter is aimed for the broadening of the substrate scope for the BVO / Sn- β / H₂O₂ system to a range of R-CyO, whose corresponding lactones can be used as renewable monomers.

Inspired by these challenges exposed above, the main points of the chapter comprise:

- i) The identification of the general applicability of the system for R-CyO.
- ii) The evaluation of lactone selectivity obtained for the different substrates.
- iii) The investigation of the stability of the catalyst and substrate viability in the continuous regime.
- iv) Probe the suitability of the lactones produced for downstream applications.

4.2 The catalysts: Sn- β and Sn- β -H

As discussed in Chapter 3, Sn- β has shown to be an excellent catalyst for the BVO / H₂O₂ system. Accordingly, the same primary catalyst employed in the previous chapter, hence, 2 wt. % Sn- β (SiO₂/Al₂O₃ = 38) denoted 2Sn- β , was prepared following the synthetic procedure described in Section 2.3.1.1 and was used for the detailed studies presented below.

Unfortunately, possessing a microporous structure, Sn- β can sometimes result in susceptibility to the limitations associated with this particular degree of confinement, such as: (i) internal mass transfer limitations, hindering catalytic performance through slow molecular diffusion, (ii) restricted diffusion of bulkier reactants, which limits their scope of reactivity, and (iii) increased rates of deactivation through pore blocking (*i.e.* fouling). Having these limitations in mind, where appropriate, hierarchical Sn- β (Sn- β -H) was also synthesised to evaluate possible mass transfer limitations for BVO reaction of R-CyO. Hierarchical zeolites possess a combination of micro- and meso-pores, resulting in improved molecular transport and greater substrate accessibility. In principle, these materials retain the advantages of purely microporous materials, such as intrinsic reactivity and (hydro)thermal stability, whilst also improving the particular disadvantages associated with overly confined materials, such as mass transfer limitations and increased rates of deactivation.^{23,24} An example of this was reported a few years ago by Al-Nayili *et al.*,²⁵ where Sn- β -H demonstrated its clear advantages as catalyst for the Meerwein–Ponndorf–Verley (MPV) reduction of bulky cycloketones, enhancing the catalytic activity when conventional Sn- β was limited by its pore size. In said study, a key result with Sn- β -H was reported for MPV of cyclododecanone, precursor to lauro lactam and, hence, polyamide 12,²⁶ obtaining a reaction rate one order of magnitude higher than the one reported for Sn- β .

According to the synthesis protocol, described in Section 2.3.1.2, Sn- β -H catalyst was prepared from commercially available zeolite β (SiO₂/Al₂O₃ = 38), by partial desilication (deSi) followed by dealumination (deAl) and Solid-State Incorporation (SSI) of Sn. The final loading of Sn- β -H was also fixed to 2 wt. % and the sample denoted 2Sn- β -H. This protocol allowed to prepare Sn- β -H with hierarchical structure without causing excessive destruction, *i.e.* collapse, of the zeolite framework and successfully incorporating the Sn into the framework after the formation of the mesopores.²⁵

In line with previous research, the Sn- β -H material was extensively characterised by several techniques including X-Ray Diffraction (XRD), microscopy, porosimetry and Magic Angle Spinning Nuclear Magnetic Resonance (MAS NMR). The data for this sample was then compared with the characterisation obtained for the conventional Sn- β catalyst.

As observed in Fig 4.1, XRD patterns of all samples exhibited the main diffraction peaks of β zeolite, indicating that the original crystalline phase structure remained unaltered after the post-synthetic treatments and in the absence of secondary phases. Additionally, although slightly lower, comparable intensity of the diffraction peaks was also observed for Sn- β -H, suggesting that high crystallinity was also maintained.

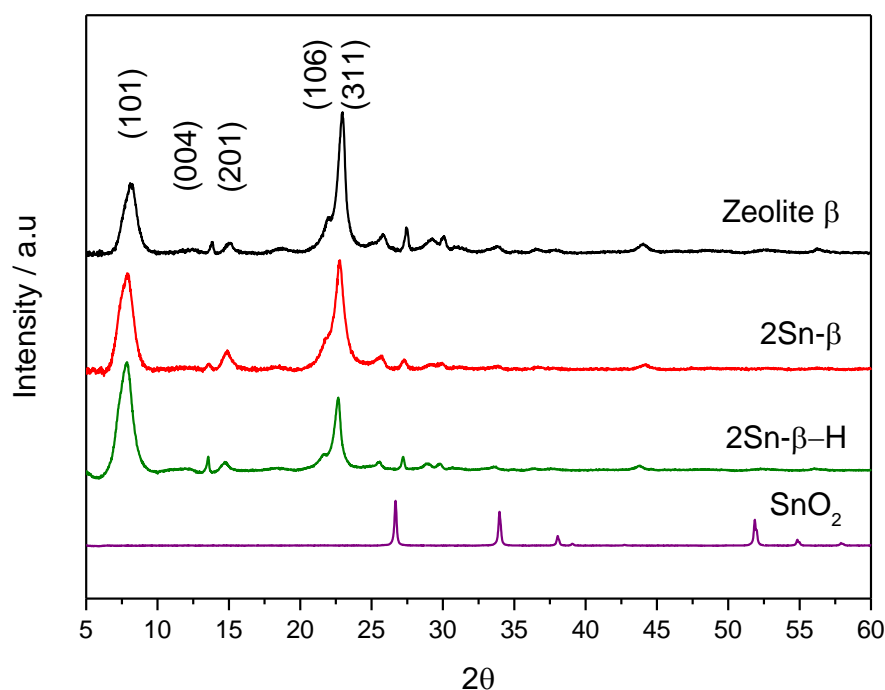


Figure 4.1. XRD patterns for commercial zeolite β , 2Sn- β , 2Sn- β -H and SnO₂.

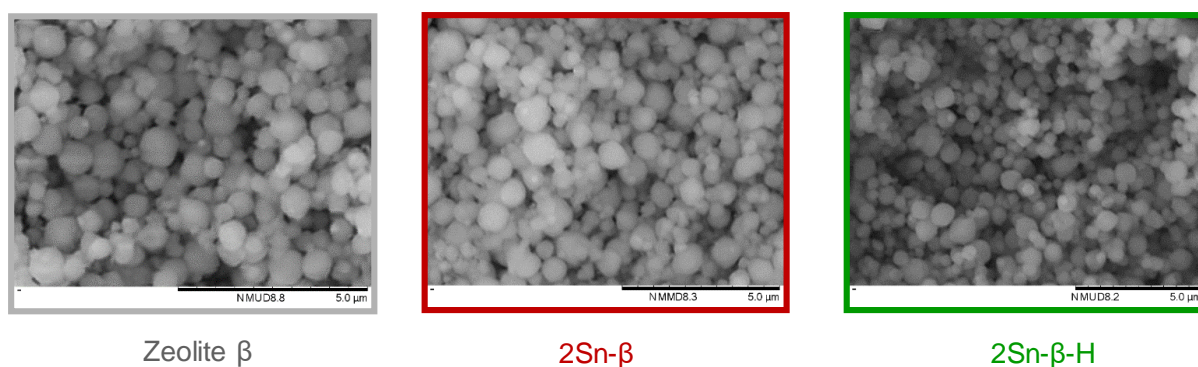


Figure 4.2. SEM images of commercial zeolite β (left), 2Sn- β (centre) and 2Sn- β -H (right).

Furthermore, images obtained by Scanning Electron Microscopy (SEM) (Fig 4.2) showed no significant change in terms of crystal morphology and size. Crystals agglomerates of spherical shape, between 20 to 90 nm of size were maintained after post-synthetic treatments.

Additionally, Energy-Dispersive X-ray (EDX) spectroscopy analysis confirms a uniform distribution of Sn throughout the whole material. The amount of Sn loaded on the conventional and hierarchical zeolite β was indeed 1.9 ± 0.05 wt. % Sn loading. Hence overall, as occurred for microporous 2Sn- β (after deAl), the post-synthetic treatments employed for 2Sn- β -H (deSi followed by deAl) do not overly change the parental zeolite β structure. To further confirm this observation, the extensive textural analysis was carried out by N_2 adsorption.

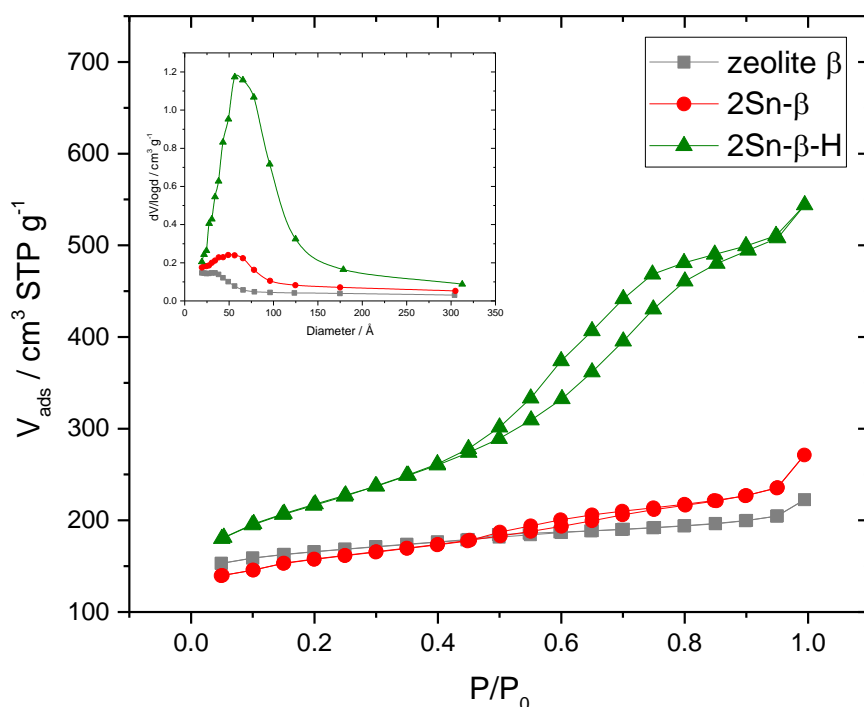


Figure 4.3. Isotherms and pore size distribution of commercial β , 2Sn- β and 2Sn- β -H.

Pore diameter corresponding to the maximum in the pore size distribution was determined by the Barret-Joyner-Halenda (BJH) method as represented in Fig 4.3, left corner, obtaining an average pore diameter of approximately 6 nm for Sn- β -H. However, as mentioned in Section 2.6.2, the BJH method can only be used reliably to analyse mesoporous materials, not microporous materials. The pore size distribution of the other two materials, purely microporous, would require substantially lower relative pressures, the maximum obtained for zeolite β and 2Sn- β not being representative of the real value of their micropores.

According to the Brunauer-Deming-Deming-Teller classification (BDDT),²⁷ parental zeolite β was classified as type I, characteristic of microporous materials, and 2Sn- β -H was classified as type IV, characteristic of mesoporous, with 2Sn- β lying somewhere in between. Porosimetry analysis showed that Sn-catalysts possessed high BET surface area (S_{BET}), characteristic of zeolites, with S_{BET} increasing over the series, the lowest value of $498 \text{ m}^2 \text{ g}^{-1}$

observed for parental zeolite β , then $528 \text{ m}^2 \text{ g}^{-1}$ for 2Sn- β and $614 \text{ m}^2 \text{ g}^{-1}$ for the 2Sn- β -H. As consequence of the demetallation, the total pore volume and the mesopore pore volume also increased notably along the series, from 0.35 and $0.11 \text{ cm}^3 \text{ g}^{-1}$ for parental zeolite β to 0.67 and $0.52 \text{ cm}^3 \text{ g}^{-1}$ for 2Sn- β -H.

To better investigate the active sites of the catalyst, the Sn materials were also analysed by ^{119}Sn MAS NMR spectroscopy to investigate the coordination of the Sn sites. Analogously to Fig 3.3, ^{119}Sn MAS NMR analysis of 2Sn- β -H is compared with 2Sn- β , 10 wt. % SnO_2 on deAl- β (physical mixture) and bulk SnO_2 in Fig 4.4.

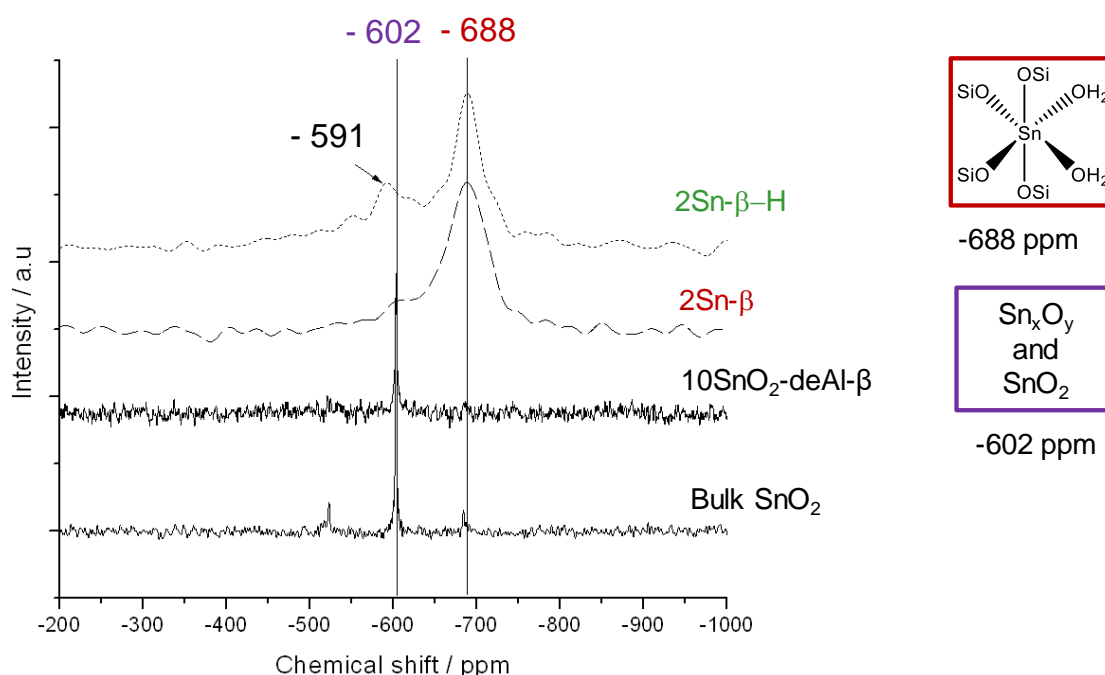


Figure 4.4. MAS NMR spectra of 2Sn- β -H, 2Sn- β , 10SnO₂-deAl- β and bulk SnO₂.

MAS NMR spectrum of 2Sn- β -H revealed a main band at - 688 ppm, attributed to hydrated Sn (IV) sites within the zeolite framework, confirming their predominance among the whole material and proving the successful incorporation of the Sn during the preparation. Additionally, a minor band at - 591 ppm could be appreciated in the hierarchical material, corresponding to the band at - 602 ppm slightly shifted due to asymetry of the resonance. This band corresponds to fractions of extra-framework Sn clusters (Sn_xO_y , not active).²⁸ Therefore, despite that the contribution of Sn_xO_y is not negligible for the hierarchical material, its proportion is significantly lower compared to that of the main band.

Herein, 2Sn- β -H was successfully synthesised, and its intrinsic catalytic activity expected to be comparable with the purely microporous Sn- β . When indicated, 2Sn- β -H catalyst was also employed for the investigations on BVO reaction of R-CyO discussed in this chapter.

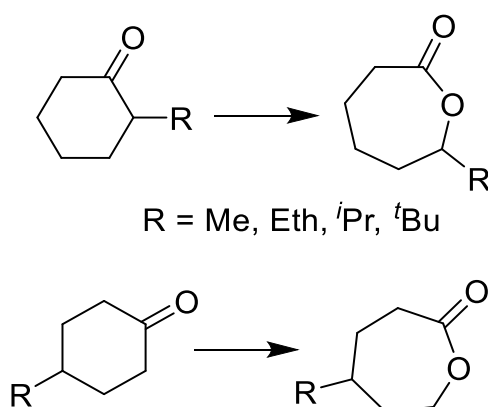
4.3 Results and discussion

4.3.1 Extending the substrate scope

4.3.1.1 Effect of 2- and 4- substitution on catalytic activity of BVO of R-CyO

To evaluate the general applicability of the Sn- β / H₂O₂ BVO system beyond CyO, a range of R-CyO was explored as substrates. Understanding the effect of substituents at different positions (2- and 4-) is of high importance in order to anticipate the viability of the system to convert more complex substrates, such as terpene-derived ketones such as 4-isopropylcyclohexanone, and others with greater levels of substitution, into renewable lactones.

With this aim, the impact of increasing size of the substituent for various alkyl-cyclohexanones (R = -Me, -Eth, -ⁱPr and -^tBu), substituted in position 2 (2-R-CyO) and 4 (4-R-CyO), was first investigated (Scheme 4.2).



Scheme 4.2. Scheme for the BVO reaction of 2-R and 4-R-CyO.

All substrates were evaluated for the BVO reaction under the standard reaction conditions (internal solution temperature 100 °C, 10 mL of 0.33 M substrate in 1,4-dioxane, 1 mol. % of Sn (2Sn- β), 1.5 H₂O₂:ketone ratio, for 6 h) optimised in Section 3.3.1, and their intrinsic activity profiles were compared to the one obtained for non-substituted CyO (Fig 4.5).

As well as for the model reaction (BVO of CyO to Capr), kinetic evaluation was carried out by quantification of R-CyO and R-Capr by GC-FID, and R-6-HHA by ¹H NMR, as described in detail in Section 2.4.1.

Reactions were repeated several times in order to calculate the experimental error of the system (Annex). Hence, a consequent error bar of 8 % was applied to all further experiments to all kinetic parameters (conversion (X), yield (Y), selectivity (S) and carbon balance (C Bal)).

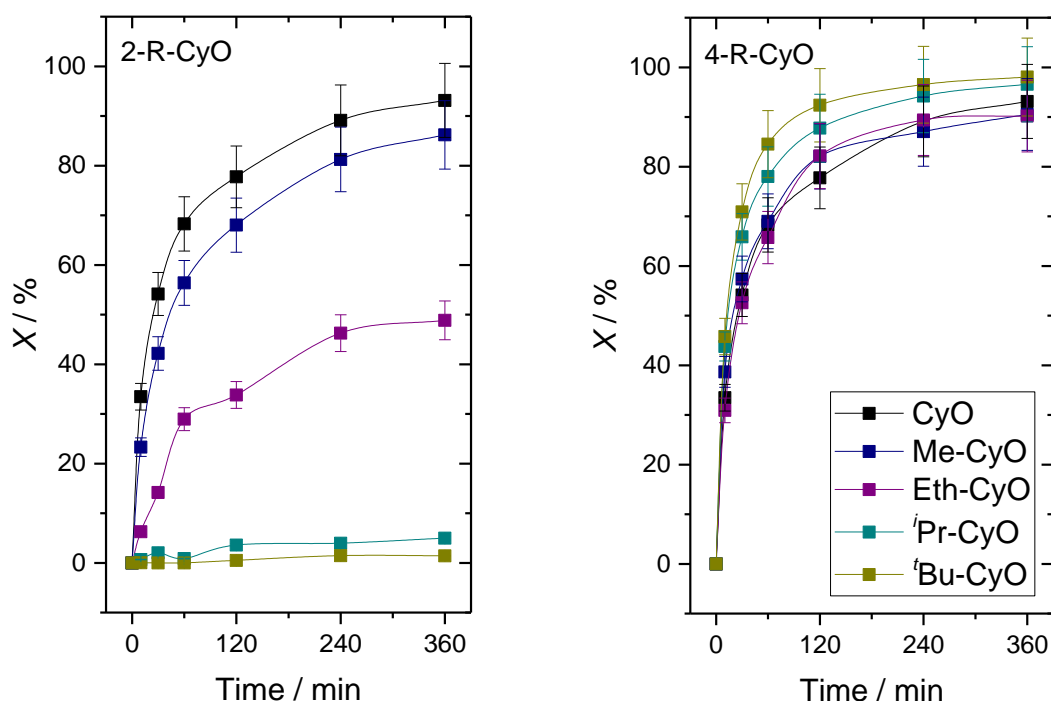


Figure 4.5. Catalytic evolution obtained for the two series of BVO reactions (Left) 2-R-CyO and (Right) 4-R-CyO, where R is defined in the legend. Reaction conditions: 10 mL of 0.33 M of R-CyO in 1,4-dioxane, 1.5 H₂O₂:R-CyO, 1 mol. % Sn respect to R-CyO, at 100 °C.

Despite the similar chemical nature of the substrates tested, large differences in reactivity within each series, and between both series, were observed during the BVO experiments. For the 2-R-CyO series (Fig 4.5, left), catalytic activity for BVO reaction decreased with increasing size of the R group. For instance, BVO of 2-Me-CyO and 2-Eth-CyO reached 84 and 48 % of conversion, respectively, after 6 h, whereas the two bulkiest 2 substituted substrates tested, 2-*i*Pr-CyO and 2-*t*Bu-CyO, showed practically no conversion after the same reaction period. On the contrary, the 4-R-CyO series displayed the opposite trend (Fig 4.5, right), with all substrates converted > 90 % after 6 h with a gradual increase in rate with the size of the R group, reaching 96 % of conversion for the bulkiest substrate tested 4-*t*Bu-CyO.

Subsequently, the initial turnover frequency (TOF) of each substrate of the two series was calculated over the first 10 min of reaction and compared to the one obtained for unsubstituted CyO (Fig 4.6). TOF values were calculated as described in Equation 2.5 as amount of R-CyO converted (mol) per amount of Sn (mol) per unit of time (h).

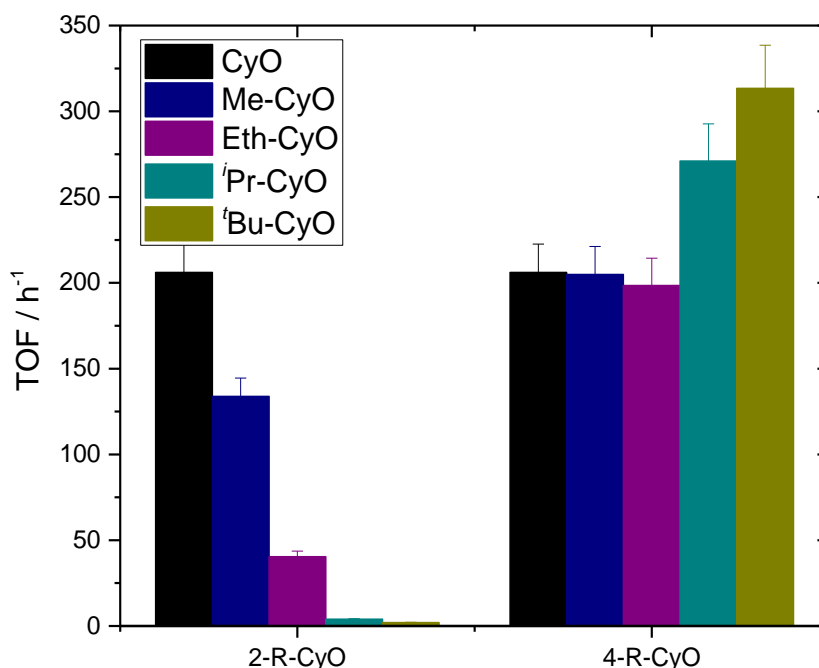


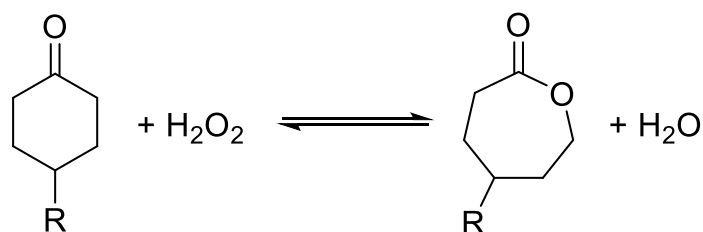
Figure 4.6. Initial TOF (10 min) obtained for the two series of BVO reactions (Left) 2-R-CyO and (Right) 4-R-CyO. Reaction conditions: 10 mL of 0.33 M of R-CyO in 1,4-dioxane, 1.5 H₂O₂:R-CyO, 1 mol. % Sn respect to R-CyO, at 100 °C.

For the 2-R-CyO series, the TOFs values clearly decreased with the increasing size of the R group, from $\pm 200 \text{ h}^{-1}$ for non-substituted CyO to $< 10 \text{ h}^{-1}$ for the bulkiest substrates (R = *i*Pr and *t*Bu). On the contrary, excellent performances were observed for the 4-R-CyO series at all sizes of substituent group. Even though 4-Me-CyO and 4-Eth-CyO initial TOFs were slightly lower than TOF of non-substituted CyO, still within the experimental error applied, as a general trend, initial TOF increased with the size of the R group. Indeed, the initial TOF increased by approximately 50 % across the series, from $\pm 200 \text{ h}^{-1}$ for CyO to $> 300 \text{ h}^{-1}$ for 4-*t*Bu-CyO, the bulkiest substrate tested.

For a better understanding of the increasing reactivity of 4-R-CyO for BVO reaction, some computational studies were carried out. Density Functional Theory (DFT) is a computational quantum mechanical modelling method used in physics, chemistry and materials science to investigate the electronic structure of matter.²⁹ It can be used to predict a variety of molecular properties such as molecular structures, vibrational frequencies, ionisation energies, electric and magnetic properties, as well as reaction pathways and evaluation of the thermodynamics of the reaction.

Given the increasing intrinsic reactivity of 4-R-CyO against CyO observed for BVO reactions using H_2O_2 and Sn- β , DFT calculations were used to evaluate the thermodynamics of each 4-substituted substrates tested. The results of these calculations are summarised in Table 4.1.

Table 4.1. DFT computed Free Gibbs energies for BVO of 4-R-CyO into 4-R-Capr.



4-R-CyO	$\Delta G / \text{kcal mol}^{-1}$ ^a
R = H	– 65.2
R = Me	– 65.0
R = Et	– 65.0
R = ⁱ Pr	– 64.0
R = ^t Bu	– 64.7

^a Protocol: $\omega\text{B97XD/6-311++g(2d,p)}$ / 398.15 K / cpcm = 1,4-dioxane.

DFT calculations show negative values for all Gibbs free energy (ΔG) for the BVO reaction of all 4-R-CyO substrates, indicating that the reactions are thermodynamically favoured. Additionally, the calculated ΔG did not overly change along the series and all the values were comprised between - 64 and - 65.2 kcal mol^{-1} . Accordingly, such small difference points to that the reactions are thermodynamically favoured to a similar extent.

Hence DFT calculations confirm that the BVO reactions of 4-R-CyO into their corresponding lactones are strongly thermodynamically favoured throughout the whole series and the alkyl substitution does not seem to influence the overall thermodynamics of the reaction system. Therefore, kinetic and/or steric factors should account for the observed changes in reactivity.

4.3.1.2 Evaluation of mass transfer limitation through Sn- β

Given the differences in catalytic behaviour obtained for BVO of 2-R-CyO and 4-R-CyO in the series and within the two series, the first effect to consider was the overall steric factor of the substrate when possessing different levels of bulk substituents. Different size and nature (linear or branched) of the substituent group on the ketone may affect the diffusion of the substrate through the catalyst pores, and hence, its intrinsic activity.

It should be reminded that the differences in catalytic activity amongst the same kind of R-CyO in position 2 and 4 were accentuated with increasing size of the R group along the two series. Catalytic activity for BVO of 2-R-CyO drastically decreased with the size of R, while increased for BVO of 4-R-CyO. For instance, 2-Me-CyO and 4-Me-CyO, the two substituted compounds with the smallest R tested, do not massively influence the dynamic diameter of the substrate compared to unsubstituted CyO, displayed different catalytic behaviours (Fig 4.5). 2-Me-CyO reached 10 % less conversion than CyO, whereas 4-Me-CyO showed similar conversion to CyO. Furthermore, 2-ⁱPr-CyO, one of the bulkiest substrates tested in the 2-R-CyO series, has its width enlarged due to the branched nature of the ⁱPr substituent, while the same substituent in position 4, in 4-ⁱPr-CyO, does not influence the width of the molecule but its length. Having this in mind, it can be noticed that not only the position of the R group but also its nature, linear or branched, may modify the overall dynamic diameter of the substrate causing some mass transfer limitation to diffuse through the Sn- β pores, which present a characteristic microporous diameter of 7 Å, and being responsible for the observed differences in activity. Independently from the nature of the R group and its position, employing a catalyst with bigger pores may overcome the limitations, and should mitigate mass transfer limitation if exists.

To evaluate potential mass transfer limitation through the 2Sn- β pores, hierarchical Sn- β with 2 wt. % in Sn loading (2Sn- β -H) was synthesised as described in Section 2.3.1.2 and was employed as catalyst for the BVO reaction at the same standard reaction conditions. For this set of experiments, four representative substrates were selected to be tested with 2Sn- β -H: CyO, 4-Eth-CyO, 4-ⁱPr-CyO and 2-ⁱPr-CyO, with the aim of testing a variety of linear and branched substituents, located in different positions. The use of 2Sn- β -H, which possesses a combination of micropores and mesopores (< 8 nm in diameter) and whose Sn active sites can be successfully incorporated into the zeolite framework after the formation of the mesopores, as it was previously reported,²⁵ should not manifest pore size limitations if previously existed with the original catalyst, reflecting an improvement in the catalytic activity compared with the purely microporous material. Results obtained using the hierarchical material are compared to the activity obtained with the conventional catalyst and reported in Fig 4.7.

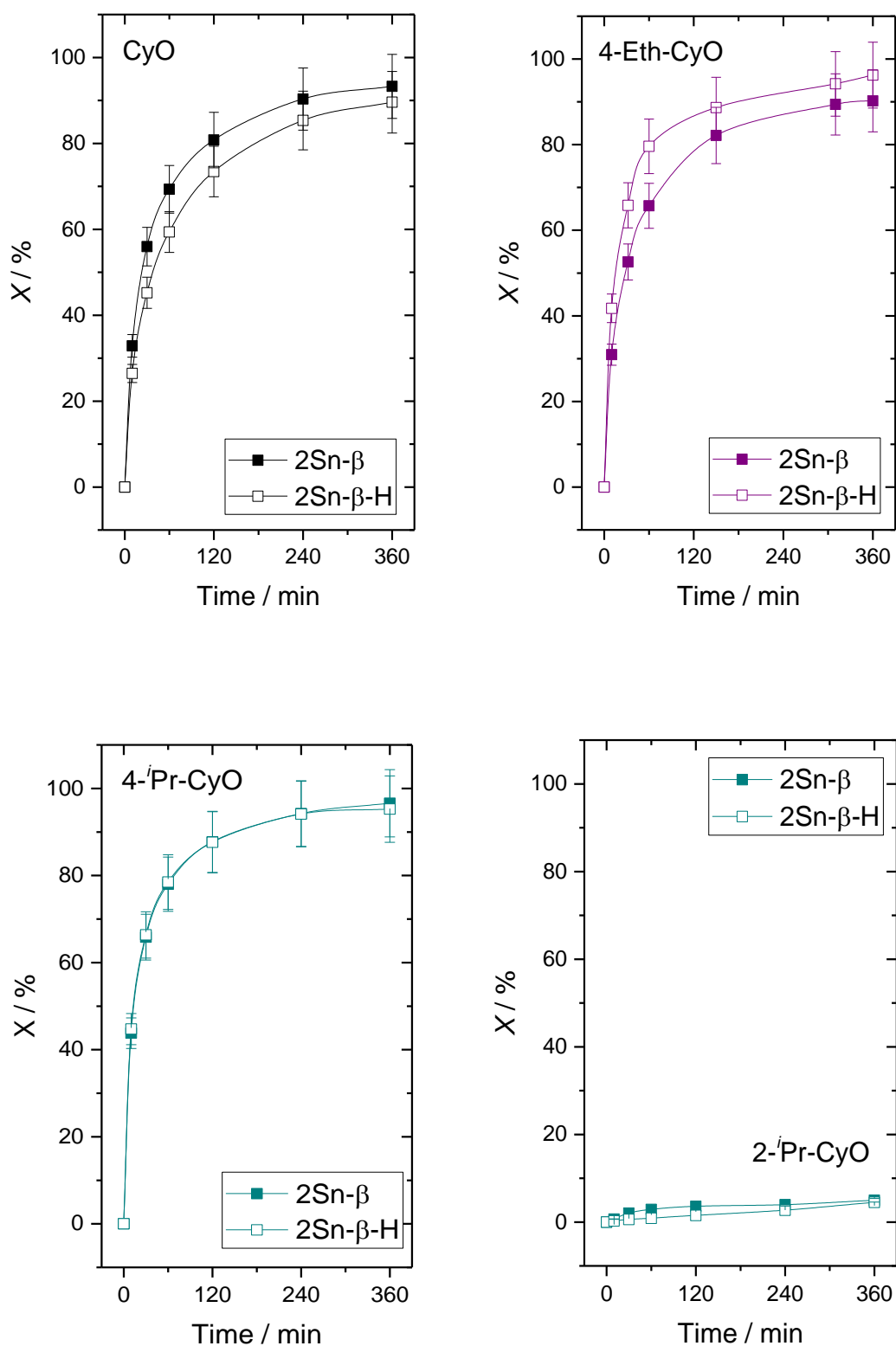


Figure 4.7. Conversion of CyO, 4-Eth-CyO, 4-*i*Pr-CyO and 2-*i*Pr-CyO with 2Sn- β and 2Sn- β -H as function of time. Reaction conditions: 10 mL of 0.33 M of 4-R-CyO in 1,4-dioxane, 1.5 H₂O₂:R-CyO, 1 mol. % Sn respect to R-CyO, at 100 °C.

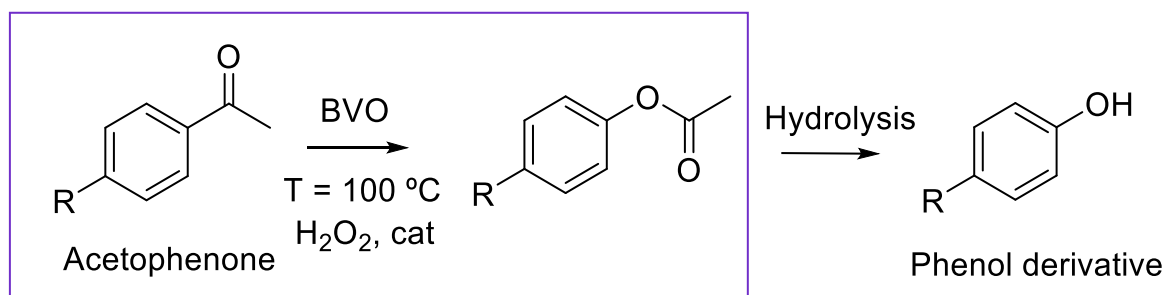
As a general trend, similar levels of catalytic activity were obtained for the three substrates substituted in position 4 for both the hierarchical material and the original catalyst, suggesting no mass transfer limitations being present. It should be noticed that some minor differences can be observed for the BVO reaction of CyO and 4-Eth-CyO (medium size and linear R) using 2Sn- β and 2Sn- β -H, especially at the low levels of conversion. However, identical results were obtained for 4-Pr-CyO (bulky and branched R), the bulkiest substrate tested in this set of experiments, which should be the one presenting the highest diffusion limitation if existed and the one which should display a larger difference in terms of catalytic improvement when using 2Sn- β -H, if the pore size limitation was causing the differences observed in Fig 4.5, right. In the same line of 4-R-CyO, 2-Pr-CyO (bulky and branched R), also manifested no change in terms of catalytic activity observed with 2Sn- β -H as catalyst, maintaining a very low conversion (< 5 %) after 6 h of reaction, as observed with the primary catalyst.

Hence, the use of Sn- β -H does not massively affect the general catalytic evolution of the BVO of R-CyO, independently of the nature and position of the substituent group, obtaining similar results for all substrates tested. This demonstrates that mass transfer limitation through the catalyst pore is not the cause of the differences in reactivity within the two series. However, other more localised effects, potentially accountable for the different catalytic activities observed in Fig 4.5, are investigated in the following sections.

4.3.1.3 Evaluation of the electronic and steric effects on R-CyO

Since diffusion limitation has been proved not to be the reason behind the differences in reactivity for BVO of R-CyO, electronic and localised steric effects were considered. Although not truly conjugated, both effects can contribute to the decrease in activity within the 2-R-CyO series at increasing size of the R group.

To investigate possible electronic contributions in the BVO reaction of the substrates of study, a range of *para*-substituted acetophenones (4-R-AcetoPhO) were selected as model substrates. Such substrates possess an electronically delocalised phenone ring, which can be activated or deactivated by the *para*-substituent. This can enhance or decrease its general activity for the BVO reaction depending on the potential electronic contributions present. In addition to providing a system by which potential electronic effects can be elucidated, the R-phenyl acetates generated by BVO are an attractive source for phenol derivative formation *via* ester hydrolysis (Scheme 4.3).³⁰



Scheme 4.3. BVO of 4-R-AcetoPhO, including potential downstream valorisation of the resulting R-phenyl acetates.

Purely electronic effects can be studied by using the Hammett equation,³¹ commonly used in organic chemistry, which describes a linear Gibbs free energy relationship relating the changes in equilibrium or rate constant with the presence of substituent groups. The basics of this equation (Equation 4.1) rely on the linear change of rate of reaction observed depending on the electron donating/withdrawing ability of the substituent involved:

$$\log \frac{k_R}{k_H} = \sigma \rho \quad [\text{Equation 4.1}]$$

Where k_R is the reaction rate involving the substituted reactant, k_H is the reaction rate involving unsubstituted reactant ($R = H$), σ is the Hammett constant determined for each R and ρ depends only on the type of reaction.

A great variety of organic substituent groups have their Hammett constant value assigned depending on their electron donating ($\sigma < 1$) or electron withdrawing ($\sigma > 1$) capabilities, differentiating also the substituent position (*meta*- or *para*-).³² Bearing this in mind, the effect of various electron-donating substituent groups and electron-withdrawing substituent groups in position *para*- (4-R-AcetoPhO) were studied under standard BVO conditions with microporous 2Sn- β as catalyst.

Considering the most widely accepted reaction mechanism described in Scheme 3.2, based on a two-step reaction first involving the nucleophilic attack of the oxidant to the carbonyl group forming a Criegee adduct, and the subsequent migration resulting in the lactone formation, it was hypothesised a decrease of the BVO reaction rate should be observed when electron-donating R groups are present, due to their presence lowering the electrophilicity of the carbonyl carbon atom, thereby discouraging the nucleophilic attack of the oxidant. Accordingly, electron-donating groups such as NH₂ or alkyl groups are expected to lower the extent of the BVO reaction compared with unsubstituted AcetoPhO at the same reaction conditions.

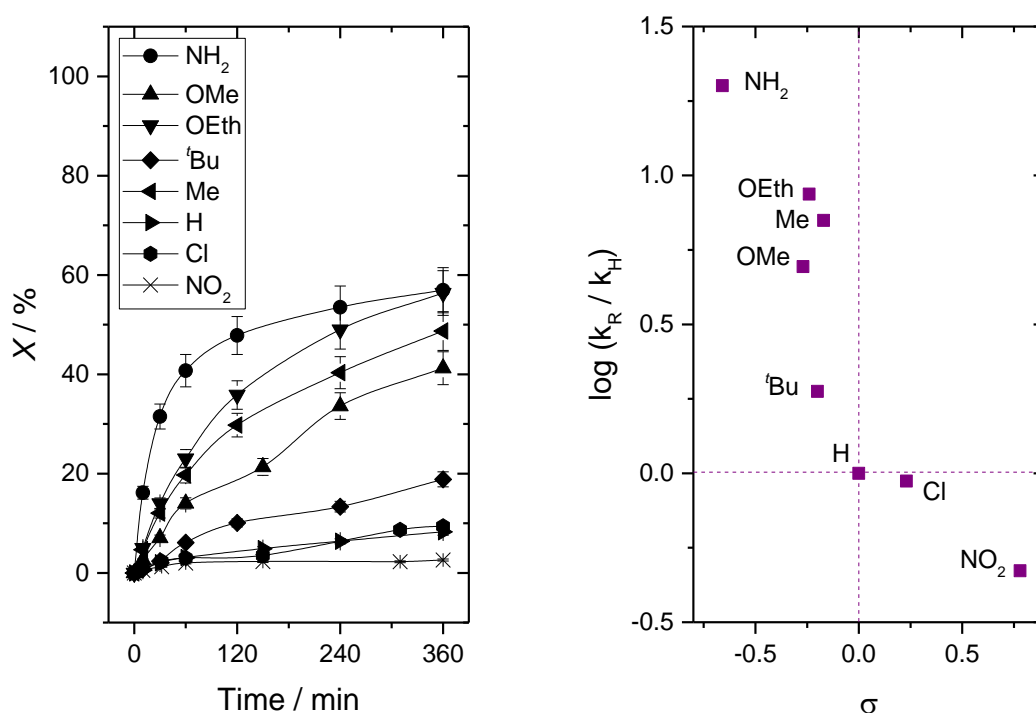


Figure 4.8. (Left) Time online analysis of 4-R-AcetoPhO conversion obtained for BVO reaction of 4-R-AcetoPhO with 2Sn- β , where R is defined in the figure legend and (Right) Hammett plot obtained for this series of BVO reactions. Reaction conditions: 10 mL of 0.33 M of 4-R-AcetoPhO in 1,4-dioxane, 1.5 H₂O₂:4-R-AcetoPhO, 1 mol. %, Sn respect to 4-R-AcetoPhO, at 100 °C, 6 h of reaction.

However, detailed kinetic analysis (Fig 4.8, left) revealed that the opposite trend was observed for all 4-R-AcetoPhO substrates tested. Electron-donating R groups (-NH₂, -OAlkyl and -Alkyl) enhanced activity, whilst electron-withdrawing R groups (-Cl and -NO₂) substantially decreased the reaction rate. For instance, the presence of -NH₂, the strongest electron-donating group of this series, improved conversion of the AcetoPhO substrate from 8 % to 60 % after 6 h of reaction. Contrarily, the presence of -NO₂, the most electron-withdrawing R group, deactivated the substrate completely.

For a better understanding of this effect, a typical Hammett plot, where $\log(k_R / k_H)$ is plotted against the Hammett constant (σ) of each substituent involved, is represented in Fig 4.8, right. Although the trend obtained was not completely linear, in general terms, higher electron-donating ability resulted in higher initial rates of BVO with respect to acetophenone.

To ensure that only purely electronic effects are affecting the reaction rates observed and are responsible for the obtained trend, the same 4-R-AcetoPhO series was also screened employing 2Sn- β -H as catalyst, as additional mesoporous may decrease potential transport contributions for the bulkiest substrates.

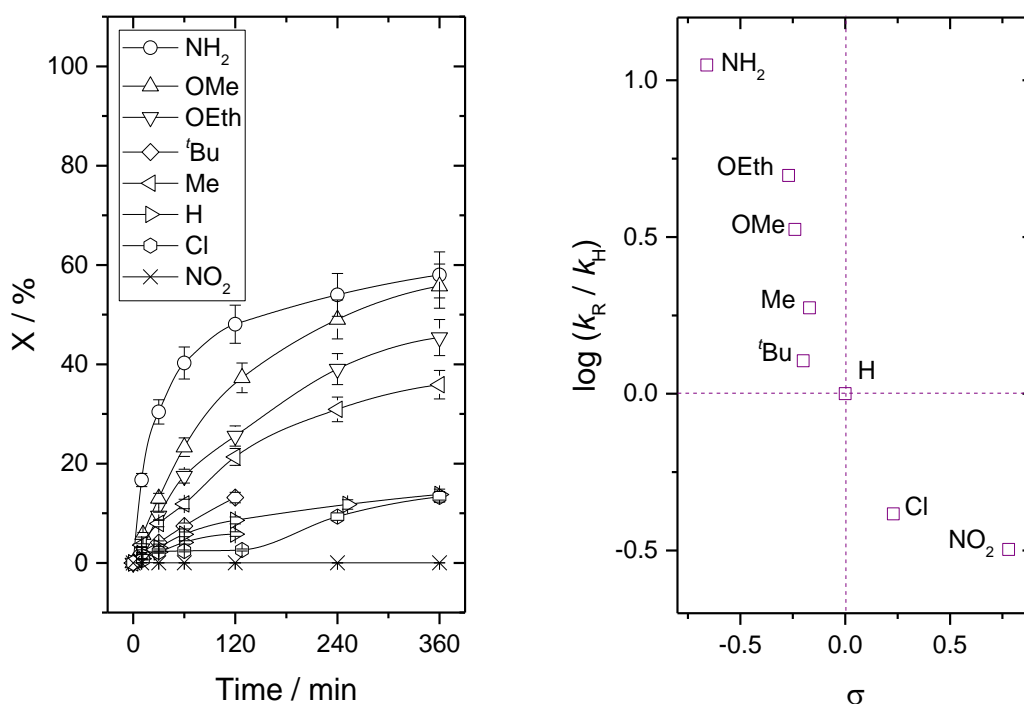


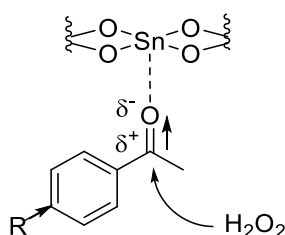
Figure 4.9. (Left) Time online analysis of 4-R-AcetoPhO conversion obtained for BVO reaction, where R is defined in the figure legend and (Right) Hammett plot obtained from BVO of 4-R-AcetoPhO with 2Sn-β-H.

Represented in Fig 4.9, left, the same catalytic trend was obtained for Sn-β-H and, as observed with 2Sn-β (Fig 4.8, left), electron-donating R enhanced catalytic performance of BVO reaction with respect to unsubstituted AcetoPhO. The analogous Hammett plot obtained using 2Sn-β-H (Fig 4.9, right) also shows a similar trend to conventional 2Sn-β, but with slightly improved linearity. Notably, no significant changes were observed in terms of catalytic activity when employing 2Sn-β-H with bulkier substrates, indicating that overall, the substrates tested diffused freely through the 2Sn-β, without significant pore size limitation being involved, in line with previous observations.

Although unexpected based on the accepted reaction mechanism (Scheme 3.2), where the presence of an electron-donating group should decrease the electrophilicity of the carbonyl group discouraging the addition of the peroxide group, the Hammett correlation observed with both Sn-catalysts agrees with previous experimental and theoretical studies of classical BVO chemistry with peroxyacid-based oxidants.³³ In said systems, the presence of an electron-donating group in the *para*-position resulted in two opposite effects; whilst electron-donating groups indeed decreased the electrophilicity of the carbonyl group, they also increased the basicity of the carbonyl oxygen, facilitating its protonation. Once protonated, the electrophilicity

of the carbonyl group dramatically increased, thus favouring the attack by the oxidant. According to these reports,^{30,33} the second effect prevails, and thus electron-donating groups speed up the overall mechanism.

In spite of the differences with the BVO / Sn- β / H₂O₂ system, the same principle can be adopted here; given that the Lewis acid Sn sites of the catalyst need to coordinate to, and subsequently polarise, the C=O bond of the substrate to promote the nucleophilic attack of H₂O₂, it may be that electron-donating R groups enhance the coordination of the substrate to the Sn, facilitating nucleophilic attack of the oxidant to the carbonyl group.



Scheme 4.4. Representation of the effect of electron-donating R groups to enhance polarisation of C=O group by the Sn-catalyst and facilitate the nucleophilic attack.

These results provide a better understanding of the electronic effects of substituents in the kinetics of BVO reaction in aromatic substrates. Regardless of the mechanistic consequences, the AcetoPhO trends observed in Fig 4.8 and 4.9, indicate that in a conjugated system, potential electronic effects of alkyl substituent groups slightly enhance BVO reaction. Therefore, in a non-conjugated system such as R-CyO, it is unlikely that alkyl substituent groups, with a medium electron-donating ability, are responsible of the decrease in activity at increasing size of the R group in the 2-R-CyO series, since, in any case, an increase in BVO rate would be expected across the series based purely on electronic factors.

In view of this, it is likely that the increasing size of the R groups in the second position hindered the reaction through steric contributions. This statement can be better understood through a fundamental organic chemistry principle which describes the nucleophilic attack of carbonyl groups to occur always from a particular angle, known as the Bürgi-Dunitz trajectory.³⁴ This principle reveals that the nucleophile approaches the electrophile with an angle of 107 ° to promote the interaction of the HOMO orbital of the nucleophile and the LUMO orbital of the -C=O group, resulting in the formation of the new σ bond and the breakage of the π bond. When large substituent groups are involved, the repulsive forces between the electrons can disfavour the reaction, causing steric hindrance. Hence, the size of the substituent group plays an important role in many organic reactions and the steric hindrance when large substituent groups are adjacent to the carbonyl group may cause a decrease of the reaction rate.

To better visualise the steric hindrance effect, the substrates of study are represented adopting a chair conformation, the most stable conformation for this kind of compounds. Accordingly, it may be anticipated that the coordination of the C=O group to the Sn sites within the zeolite framework will be greatly hindered by the presence of a bulky R groups in position 2, explaining why for the bulkier 2-CyO tested, the reactions were almost nullified. Hence, the 2-R-CyO series will not be further investigated, as their potential use as substrates for the BVO / H₂O₂ / Sn- β system results of poor interest from a catalytic point of view.

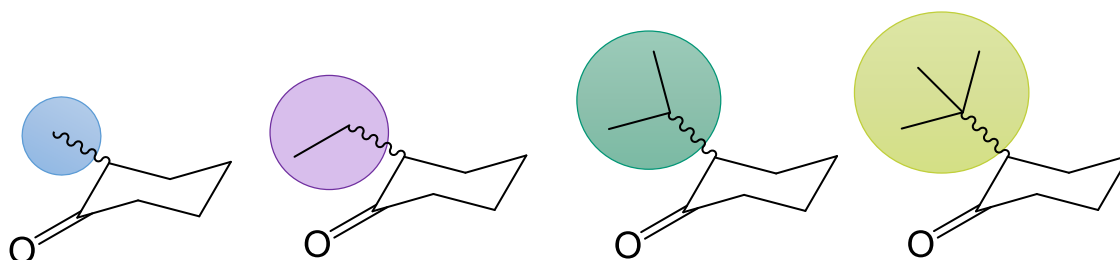


Figure 4.10. Representation of the greater steric hindrance caused by the increment of size of substituent for 2-R-CyO where R = -Me, -Eth, ⁱPr and -^tBu.

In the case of the 4-R-CyO series, it is unlikely that the substituent group at position 4 may cause any electronic effect or steric hindrance, since it is too far from the carbonyl group. Although steric hindrance and electronic effects are not likely to occur, different reaction rates were observed in Fig 4.5. Therefore, the potential reasons accountable to the different reactivity are investigated in detail in the following section.

4.3.2 Effect of 4- substitution on reaction selectivity for BVO of 4-R-CyO

In addition to increased activity, substitution of the cyclohexane ring in CyO resulted in major changes in reaction selectivity for the 4-R-CyO series. In the previous Chapter, focused on the model reaction of BVO of CyO with Sn- β / H₂O₂, it was demonstrated that a decrease in lactone selectivity occurs as the level of CyO conversion increases beyond \pm 60 %. As the reaction progresses, consecutive hydrolysis of the desired lactone leads to the formation of the corresponding hydroxyacid. Along with this decrease in lactone selectivity, 6-HHA formation also was shown to be the main cause of catalyst deactivation by poisoning, if produced in relatively high amounts. Unfortunately, the study performed in Section 3.3.3, also revealed that the consecutive ring opening reaction is unavoidable, at least for CyO, as it is also catalysed by Sn- β and occurs even with trace amounts of H₂O. Therefore, the unavoidable formation of the ring-opened hydroxyacid is in fact the major limitation for the formation of Capr in the BVO of CyO using Sn- β and H₂O₂.

To investigate the impact of the alkyl substitution on reaction selectivity, lactone selectivity of the 4-R-CyO series is represented as a function of substrate conversion.

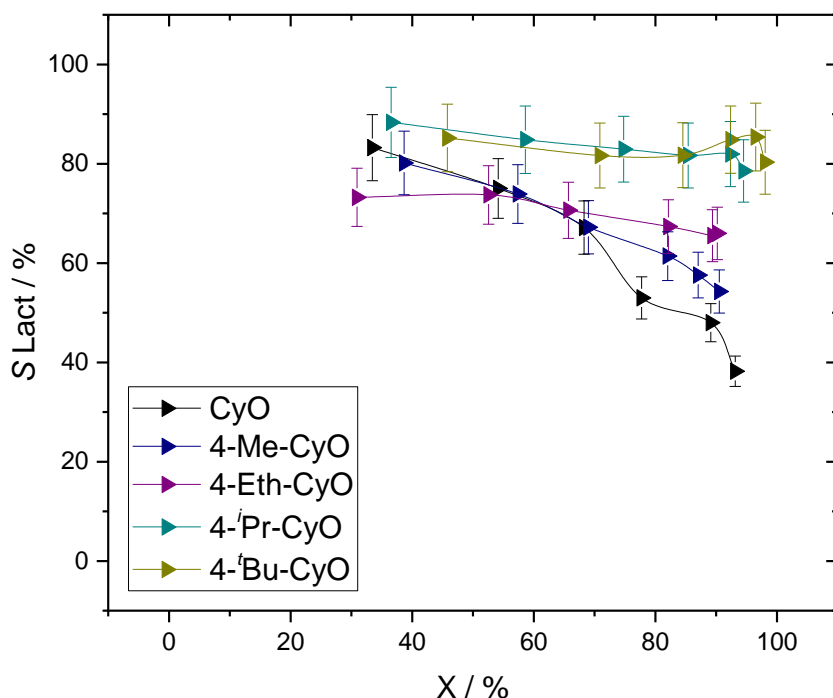


Figure 4.11. Selectivity towards 4-R-Capr as function of 4-R-CyO conversion, where R is defined in the figure legend. Reaction conditions: 10 mL of 0.33 M of 4-R-CyO in 1,4-dioxane, 1.5 H₂O₂:4-R-CyO, 1 mol. % Sn respect to 4-R-CyO, at 100 °C, 6 h of reaction.

As can be seen in Fig 4.11, the lactone selectivity obtained for each substrate was generally higher at all overlapping levels of conversion, following substitution at the position 4. Indeed, comparison of selectivity trends of 4-R-Capr against conversion showed a progressive increase of selectivity towards Capr < 4-Me-Capr < 4-Eth-Capr < 4-Pr-Capr and < 4-tBu-Capr at particular levels of conversion, being more noticeable at extended levels of reaction. This fact implies a decrease of the undesired hydrolysis reaction as a function of size of R, giving higher lactone selectivity as the size of the 4-R substituent group increased. For example, whilst lactone selectivity decreased to < 50 % at 80 % of conversion for CyO, lactone selectivity for both 4-Pr-CyO and 4-tBu-CyO remained above 80 % throughout the reaction profile and becomes independent of the extent of conversion.

Following the analytical procedure described in Section 2.5.2.1, the evolution of the substituted 6-hydroxyhexanoic acids (4-R-6-HHA) formed during BVO of 4-R-CyO was monitored by ¹H NMR, using the previously calibrated TMS insert. 4-R-6-HHA quantified by ¹H NMR (Fig 4.12) represented 42, 20 and 19 % of yield for 4-Eth-, 4-Pr- and 4-tBu-CyO reaction, respectively.

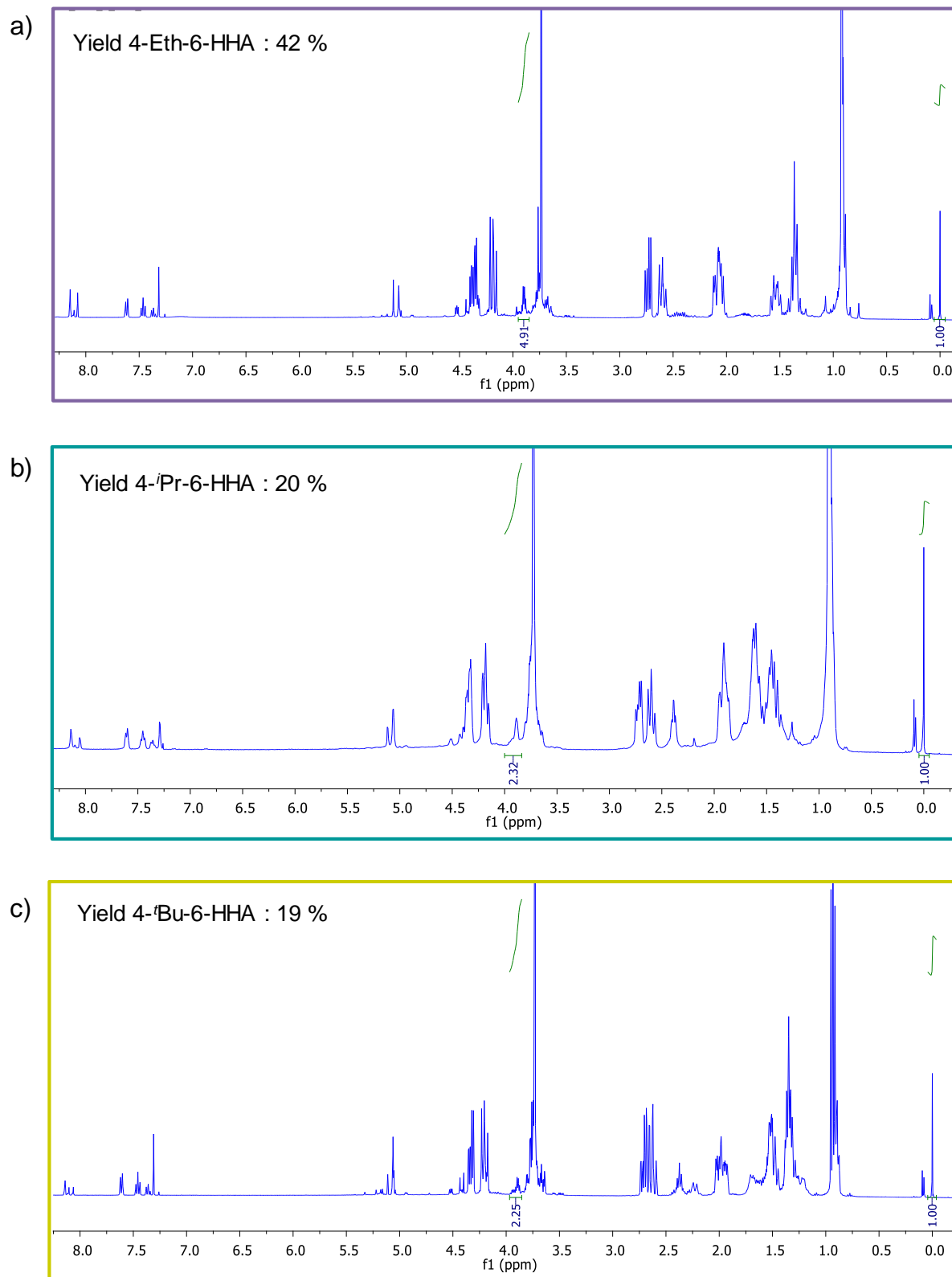


Figure 4.12. ^1H NMR spectra of BVO of a) 4-Eth-CyO, b) 4-*i*Pr-CyO and c) 4-*t*Bu-CyO reaction solution after 6h of reaction used for the quantification of 4-R-6-HHA. Reaction conditions: 10 mL of 0.33 M of 4-R-CyO in 1,4-dioxane, 1.5 H_2O_2 :4-R-CyO, 1 mol. % Sn respect to 4-R-CyO, at 100 $^\circ\text{C}$.

Additional analysis of BVO reaction samples performed by ^{13}C NMR (Fig 4.13), supported the results obtained by ^1H NMR analysis, showing indeed higher relative intensity of the peak corresponding to the lactone carbon peak when 4-R = Eth, than when 4-R = i Pr or t Bu. This is in agreement with lower 4-R-6-HHA yielded for BVO of bulkier 4-R-CyO. Herein, quantification of all the reaction products confirms that ring opening hydrolysis reactions of 4-R-Capr are less pronounced than in BVO of CyO and the ring opened products account for the remaining carbon balance of each reaction.

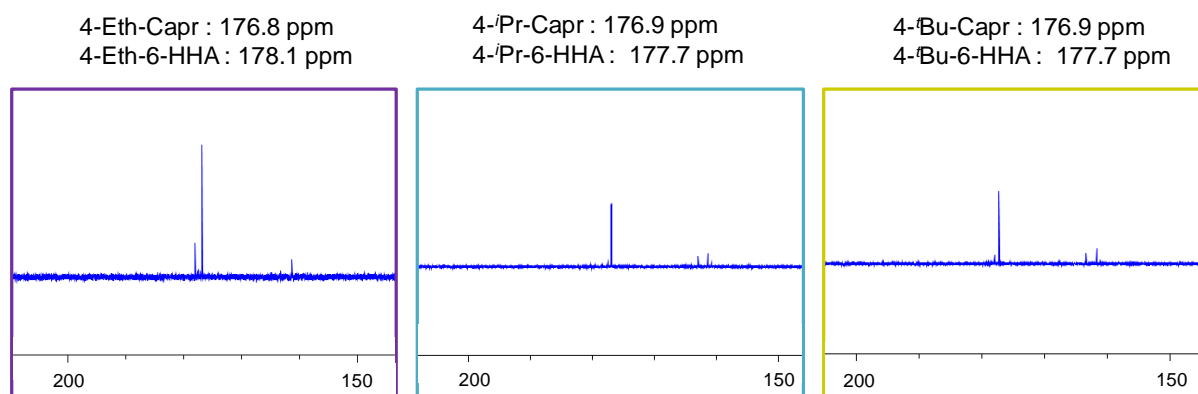


Figure 4.13. ^{13}C NMR spectra of 4-Eth-CyO, 4- i Pr-CyO and 4- t Bu-CyO reaction solution after 6h of reaction.

Analogously to Fig 3.16, where ^1H NMR analysis showed traces of oligomers of 2 - 3 Capr units at the resonances observed between 3.7 - 4.5 ppm, similar resonances can be appreciated in the ^1H NMR analysis of BVO of 4-R-CyO at extended times. Although slightly shifted to the region of 4.5 ppm due to the substitution of the Capr ring, and in considerably minor proportion than for the unsubstituted BVO reaction, some traces of oligomers can be detected after 6 h of reaction (Fig 4.12), which may contribute to < 1 % to the final carbon balance.

The final catalytic evaluations after the 4-R-6-HHA quantification of different 4-R-CyO reactions are represented in Fig 4.14, to give a direct comparison of the product distribution obtained along the 4-R-CyO series. As can be noticed in the following figure, all four substrates reached similar levels of conversion after 6 h of reaction, allowing direct comparison of the lactone selectivity and product distribution at *iso*-conversion levels.³⁵ For all 4-R-CyO, the 4-R-6-HHA yielded contributed to the remaining carbon balance of each substrate to be almost 100 % and the small remaining unaccounted carbon balance can be attributed to the formation of traces of oligomers and analogous substituted adipic acid originated through further oxidation of 4-R-6-HHA.

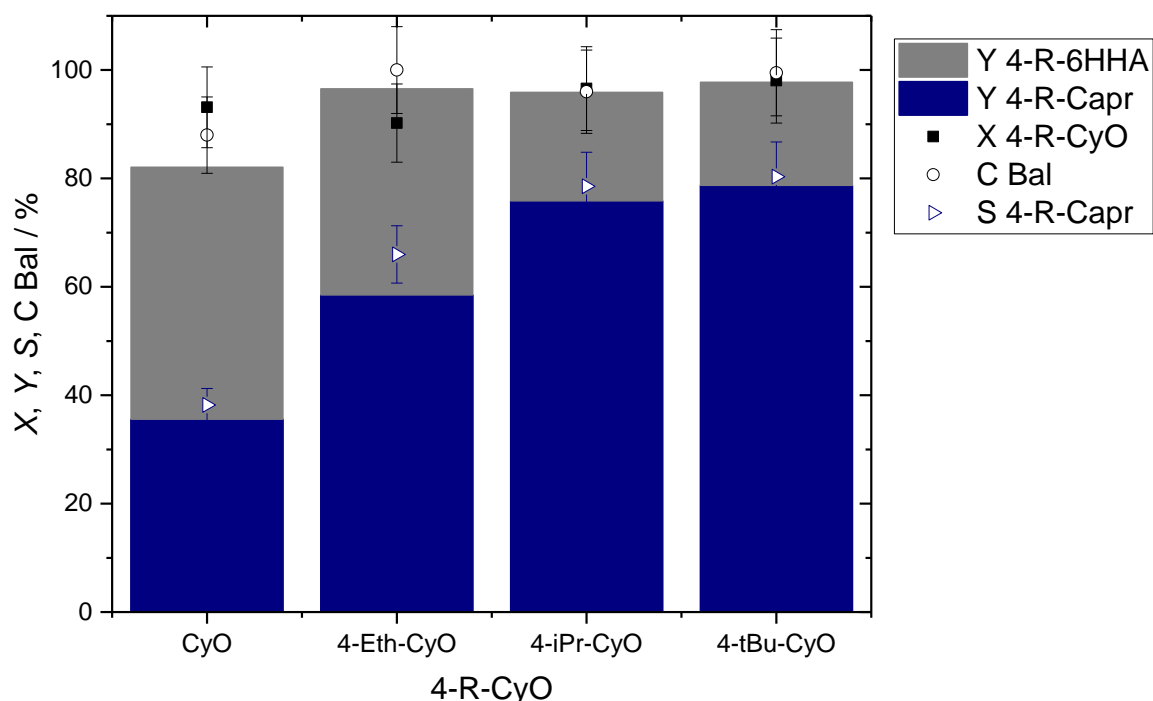


Figure 4.14. Catalytic evaluation of BVO reaction of CyO, 4-Eth-CyO, 4-*i*Pr-CyO and 4-*t*Bu-CyO and product distribution after 6h of reaction.

The outstanding results obtained for 4-R-CyO, especially in terms of high lactone selectivity at high levels of conversion, point towards them as being especially promising substrates for renewable lactone formation, since small amounts of 4-R-6-HHA are formed. Additionally, in Section 3.3.4 it was confirmed the negative role of 6-HHA in the Sn- β / H₂O₂ system, the main cause of catalyst deactivation by poisoning being when it is produced in significant amount. Evaluation of selectivity towards the lactones for BVO of 4-R-CyO showed a clear improvement with increasing size of the 4-R group. However, it should be reminded that as described in the previous chapter (Section 3.3.3), Sn- β also catalyses the consecutive hydrolysis reaction of the lactone formed and this one cannot be avoided with reaction and/or catalyst optimisation, since even traces of H₂O promote the ring opening reaction. In view of this, the key behind this decrease in consecutive hydrolysis reaction should be investigated. In Section 4.3.2.1, it has already been found that pore size limitation does not affect conversion levels reached for BVO of 4-R-CyO, since the use of Sn- β -H does not change the catalytic activity obtained for microporous Sn- β . Therefore, all substrates tested can freely diffuse through the primary catalyst channels and pores to undergo BVO transformation. Nonetheless, during those experiments, only ketone conversion was investigated and compared, whilst changes in the lactones yielded were not deeply evaluated.

Given the improvement in lactone selectivity observed with increasing size of the 4-R group, it was considered the possibility of mass transfer limitation experienced by bulky 4-R-Capr to access again the Sn sites following BVO, thus decreasing consecutive ring opening reaction and leading to a minor formation of 4-R-6-HHA.

To investigate this hypothesis, conversion-selectivity profile obtained for the BVO of CyO, 4-Eth-CyO and 4-*i*-Pr-CyO over the primary catalyst (2Sn- β) and the hierarchical analogue (2Sn- β -H) are compared in Fig 4.15. If confinement and pore size limitations are the key to inhibit the interaction of the lactone formed and the Sn sites, hydrolysis of the lactone should be more dramatic when using the hierarchical catalyst and a change in terms of lactone selectivity should be observed.

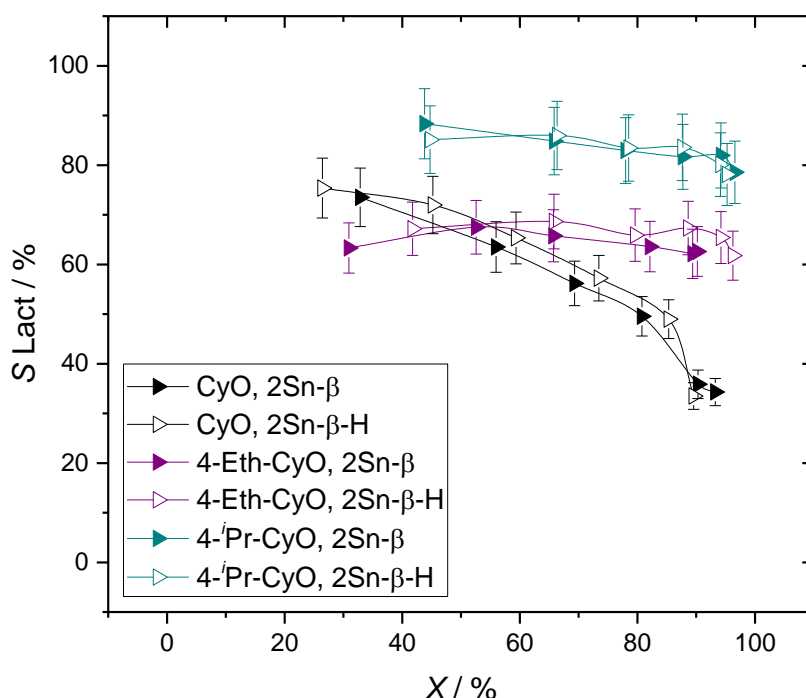


Figure 4.15. 4-R-Capr selectivity as function of 4-R-CyO conversion obtained with 2Sn- β and 2Sn- β -H, where R is defined in the figure legend. Reaction conditions: 10 mL of 0.33 M of 4-R-CyO in 1,4-dioxane, 1.5 H₂O₂:4-R-CyO, 1 mol. % Sn respect to 4-R-CyO, at 100 °C, for 6 h.

Nevertheless, as appreciated in the figure above, no significant differences in terms of activity or selectivity were observed for the three substrates shown when using 2Sn- β -H. The same selectivity trends were observed for the three substrates with both Sn-catalysts. Selectivity towards Capr gradually decreased to 50 % as conversion progressed, while selectivity towards 4-*i*-Pr-Capr was maintained > 80 % throughout all the levels of conversion reached. Selectivity trends to substituted lactones using both materials were identical *i.e.* higher lactone selectivity

is still observed for BVO of bulky 4-R-CyO even when mesopores < 8 nm are present. This means any hypothesis regarding mass transfer limitations of bulky lactones prohibiting access of the lactones to the Sn sites can be discarded.

Having deduced the impact of 4-R groups in the kinetics of the BVO reaction and their electronic and steric effects, and considering the excellent results obtained for BVO of 4-R-CyO, the nature of the promising behaviour of these substrates was explored in more detailed. To do so, a more detailed investigation was focused on 4-*i*Pr-CyO, since it presented excellent catalytic results and its synthesis from β -pinene, a natural terpene, has been successfully reported (Scheme 4.1). The potential obtainment of 4-R-CyO from a renewable origin and the successful optimisation of the catalytic routes derived from this kind of substrates, as they are their BVO reactions to yield the corresponding lactones, are of great importance in order to move towards more sustainable routes to produce bio-polymers.

As already commented above, 4-*i*Pr-CyO was almost fully converted into 4-*i*Pr-Capr after 6 h of reaction with a selectivity > 80% throughout the whole reaction, whilst on the contrary, for unsubstituted CyO, Capr selectivity decreased as conversion increased beyond 60%, suggesting that 4-*i*Pr-Capr may be less prone to be hydrolysed. Furthermore, in the previous section, the use of Sn- β -H demonstrated that mass transfer limitation is negligible as well as the electronic contribution of the isopropyl group.

Compilation of all these facts confirms that 4-*i*Pr-CyO is a very interesting substrate for the BVO reaction to be exploited. Herein, to verify the lower reactivity of 4-R-Capr to be hydrolysed by Sn- β , hydrolysis reaction of 4-*i*Pr-Capr was investigated by its own.

To do so, BVO of 4-*i*Pr-CyO was performed at the usual reaction conditions and the compounds present into the reaction mixture after 6 h of reaction were separated by column chromatography (unconverted 4-*i*Pr-CyO, 4-*i*Pr-Capr and 4-*i*Pr-6-HHA formed). The fractions containing 4-*i*Pr-Capr were isolated and used as substrate for the lactone hydrolysis studies under the standard reaction conditions, adding the equivalent amount of H₂O that would be added for the typical BVO when using the aqueous H₂O₂ solution as oxidant.

The obtained results are compared in Fig 4.16 with the one obtained for the hydrolysis of unsubstituted Capr at the same reaction conditions.

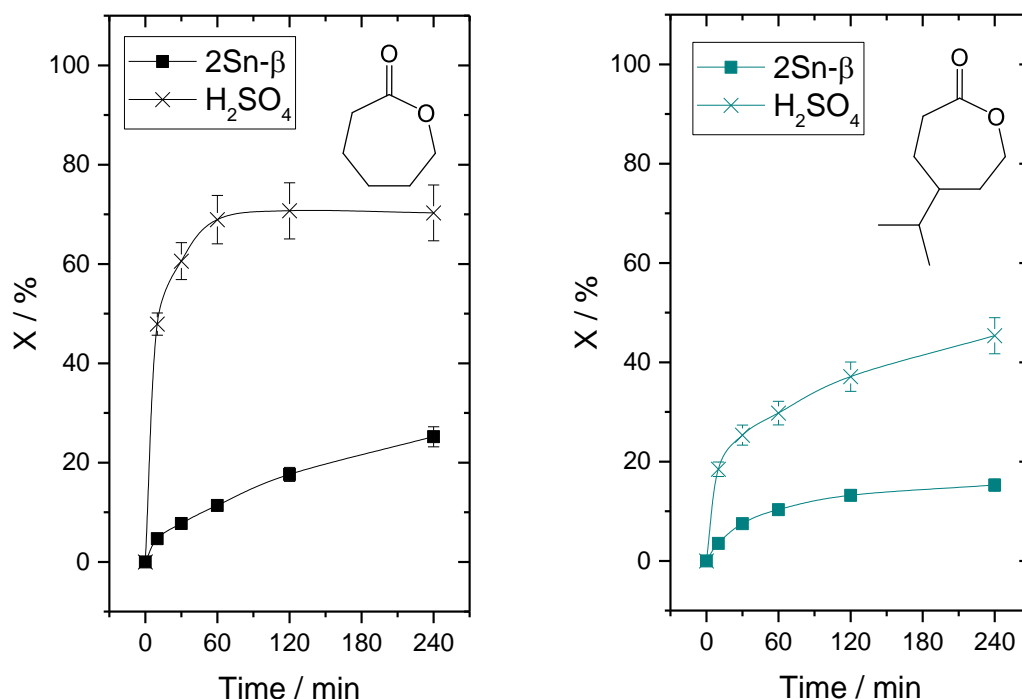


Figure 4.16. Hydrolysis of (Left) Capr and (Right) 4-*i*Pr-Capr performed with 2Sn-β ^a and H₂SO₄ ^b. Reaction conditions: 10 mL of 0.2 M of lactone in 1,4-dioxane, 0.15 mL of H₂O, ^a 1 mol. % Sn and ^b H₂SO₄ equivalent to usual 1 mol. % Sn used, at 100 °C.

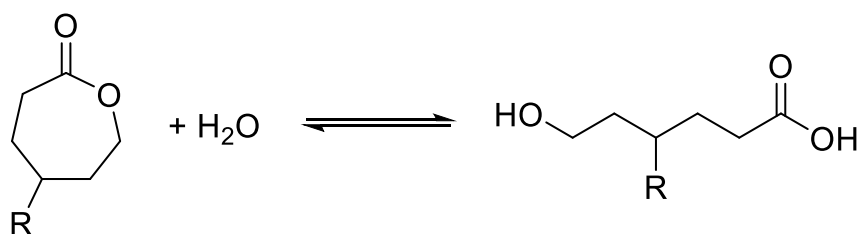
The investigation of the hydrolysis reaction of 4-*i*Pr-Capr with Sn-β revealed a clear decrease of initial reaction rate with respect to the analogous reaction with Capr, indicating a major favourability of the lactone ring to be hydrolysed in the absence of any substituent group. Additionally, to evaluate how the nature of the acid employed (homogeneous H⁺ or heterogeneous Sn (IV) sites) affects the reaction rate, the hydrolysis reactions of Capr and 4-*i*Pr-Capr were studied using a homogeneous Brønsted acid, H₂SO₄ (in the same mol. % respect ketone than the Sn typically used). H₂SO₄ is well known to promote hydrolysis reactions.

As observed in Fig 4.16, for both substrates, conversion to give rise to the ring opened product was more pronounced in the homogeneous system, indicating that the Brønsted acid presented a superior behaviour to hydrolyse the lactone than the Lewis acidic catalyst. Regardless of that, it should be noted that, the increment in final conversion obtained after 4 h of reaction comparing Sn-β and H₂SO₄ reactions was more remarkable with Capr than with 4-*i*PrCapr, from 25 to 70 % and from 15 to 45 %, respectively. Herein, 4-*i*Pr-Capr hydrolysis is always lower than Capr, even with a homogeneous H⁺ with no pore issues involved.

The decrease in the 4-*i*Pr-Capr hydrolysis reaction rate compared with non-substituted CyO is intrinsic of the nature of the substrate and it is in good agreement with the results observed previously for the BVO reaction, where less 4-*i*Pr-6-HHA was yielded due to the less extent of consecutive hydrolysis reaction.

As a complementary study of the experimental work, the intrinsic decreased reactivity of hydrolysis of 4-R-Capr was also evaluated using DFT calculations. Analogously to BVO of 4-R-CyO, the thermodynamics of the hydrolysis reaction of R-Capr were calculated for each substrate. Calculations were performed by using various functionals in order to obtain more accurate results and compared with Capr. These DFT calculations are summarised in Table 4.2.

Table 4.2. DFT computed Free Gibbs energies of the hydrolysis of 4-R-Capr.



4-R-Capr	ΔG / kcal mol ⁻¹ ^a ω B97XD functional	ΔG / kcal mol ⁻¹ ^b B3LYP-D3 functional
R = H	+ 4.9	+ 4.5
R = Me	+ 7.3	+ 6.5
R = Et	+ 7.9	+ 8.3
R = <i>i</i> Pr	+ 7.7	+ 8.4
R = <i>t</i> Bu	+ 11.5	+ 7.7

^a Protocol: ω B97XD/6-311++g(2d,p) / 398.15K/cpcm=1,4-dioxane.

^b Protocol: B3LYP-D3/6-311++g(2d,p) / 398.15K/cpcm=1,4-dioxane.

Despite minor variations depending on the level of complexity of the functional used, as a general trend, increasing size of the substituent group in position 4 is linked to a more thermodynamically unfavoured hydrolysis. This trend is in good agreement with the increasing selectivity to the lactone observed for BVO of 4-R-CyO with increasing size of the substituent group and with the study of the hydrolysis reaction of 4-*i*Pr-Capr by its own, which

demonstrated to be less favourable than the hydrolysis of unsubstituted Capr, for both thermodynamic (DFT) and kinetic (experimental) reasons.

Regardless of this substitution being relatively remote from the lactone functional group, its effect is significant enough to affect the thermodynamics, making it the key point to explain the increment of the lactone selectivity within these substrates.

Herein, both experimental and computational results demonstrate that 4-R-Capr are less prone to be hydrolysed, leading to higher selectivity towards the lactone during BVO reaction.

4.3.3 Intensification of 4-*i*-Pr-CyO BVO in continuous flow

Given that 4-substituted ketones, such as 4-*i*-Pr-CyO, are more active for BVO, are more resistant to undesirable hydrolysis, and also available from renewable resources such as β -pinene, they appear to be especially promising substrates for BVO chemistry.

In Chapter 3, it was demonstrated that high presence of 6-HHA formed during the consecutive hydrolysis reaction of the lactone is detrimental for the catalyst, causing deactivation by poisoning. Consequently, the viability of the system to operate in continuous mode was carried out at a target conversion of 50 - 60 %, in order to minimise 6-HHA formation and limit deactivation.

Having this in mind, the fact of that 4-R-Capr has proved to be less prone to be hydrolysed and hence, less 4-R-6-HHA is formed during BVO reaction, point to 4-R-CyO as excellent substrates to be explored in continuous operation. Accordingly, the potential scalability of BVO of 4-R-CyO and its adaptation into an industrial process was investigated. To do so, intensification of the BVO of 4-*i*-Pr-CyO was explored in the continuous regime using a Plug Flow Reactor (PFR) with Sn- β as catalyst. Reaction conditions employed were the same as used for the PFR of BVO of CyO at standard conditions, described in Section 3.3.4: 100 °C, 0.33 M of 4-*i*-Pr-CyO in 1,4-dioxane, 1.5 H₂O₂:ketone, catalyst bed containing 0.2 g of 2Sn- β and a contact time of 5.5 min.

Performance, in terms of stability and lactone productivity, calculated as amount of lactone produced (g) per amount of catalyst (kg) per reactor volume (cm³) per unit of time (h), are compared in Fig 4.17 to the results obtained during BVO of CyO.

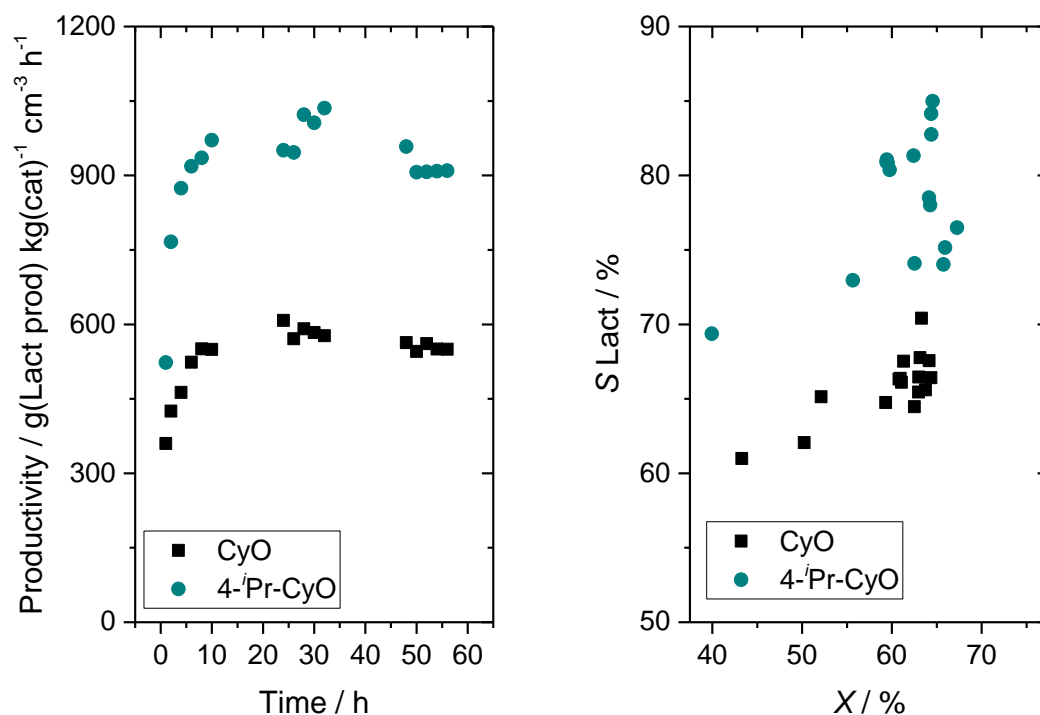


Figure 4.17. Comparison of PFR for BVO of CyO and 4-ⁱPr-CyO. (Left) Productivity obtained in continuous operation, calculated as g of lactone produced per kg of catalyst per reactor volume per time and (Right) Lactone selectivity as function of conversion. Reaction conditions: Reactant feed of 0.33 M 4-R-CyO and 0.5 M H₂O₂ in 1,4-dioxane with a contact time of 5.5 min under a pressure of 10 bar, at 100°C.

After a short induction period (approximately the first 12 h) during which both activity and selectivity increased, both systems, BVO of CyO and 4-ⁱPr-CyO reached a steady state level of performance over the reaction period explored (56 h), with little loss of activity being observed. Although both systems exhibited comparable levels of stability, it was notable that under identical reaction conditions, the continuous BVO of 4-ⁱPr-CyO resulted in higher levels of lactone productivity and selectivity (Fig 4.17, right). Selectivity towards 4-ⁱPr-Capr reached a maximum of $\pm 85\%$ during the 50 h of operation, higher than selectivity towards Capr observed at all overlapping levels of conversion. As can be seen in Fig 4.17, right, it could mistakenly be believed that BVO of 4-ⁱPr-CyO in the continuous flow experiment give rise to disperse values of lactone selectivity. Therefore, selectivity towards 4-ⁱPr-Capr as function of time is represented in Fig 4.18. Although selectivity indeed increased slightly during the first 10 h of reaction, then once reached steady state, it was maintained around 80 %, and the differences observed in both figures, 4.17, right and 4.18 can be considered within the applied experimental error.

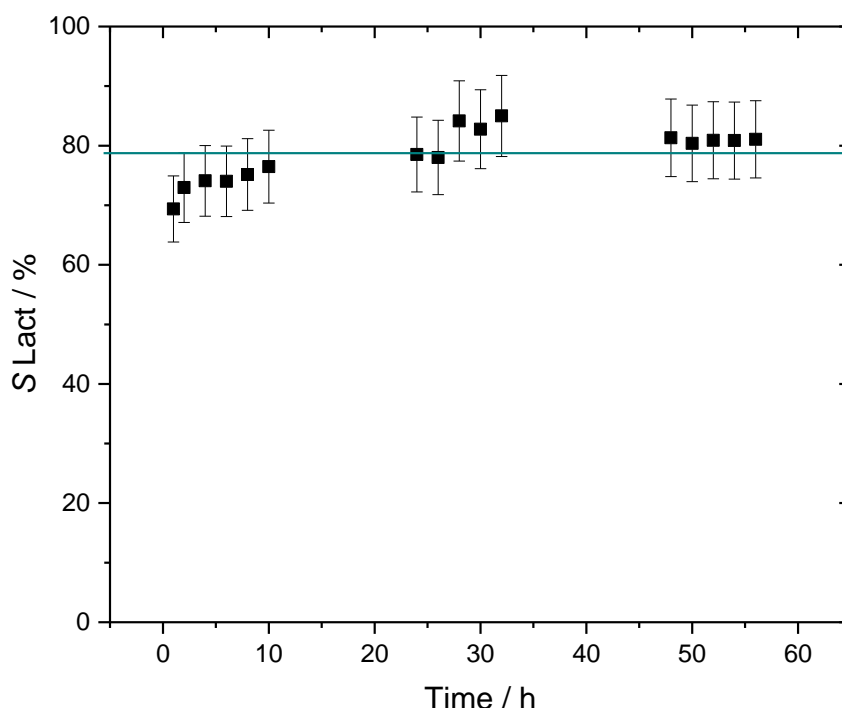


Figure 4.18. Evolution of 4-*i*Pr-Capr selectivity as function of time obtained in continuous mode for BVO of 4-*i*Pr-CyO.

In addition to corroborating the batch results of BVO of 4-*i*Pr-CyO described above, by showing the increased levels of activity and selectivity compared to BVO of CyO, this experiment improved notably the lactone productivity over the reaction period. During this period, > 1000 turnovers (mol. substrate / mol. Sn) are achieved for 4-*i*Pr-CyO, equivalent to > 10 batch reactions under typical conditions. This clearly demonstrates the stability of the Sn- β / H₂O₂ catalytic system for the BVO of more functionalized starting substrates. Indeed, the maximal lactone productivity obtained during the BVO of 4-*i*Pr-CyO is almost two-times higher than the one obtained during the BVO of CyO, 1173 and 607 g(Lact produced) kg(cat)⁻¹ cm⁻³ h⁻¹, respectively. Thus, in addition to be a renewable and sustainable source of carbon for chemical production, 4-substituted ketones such as 4-*i*Pr-CyO are more active, selective and productive substrates for BVO chemistry.

4.3.4 Probing lactone quality: Polymerisation studies

To demonstrate the viability of the lactone produced through this BVO process for polymer formation, preliminary ring opening polymerisation studies were performed on 4-*i*Pr-Capr. To do so, the produced lactone was isolated by simple column chromatography, following the procedure used to obtain the lactone for the study of the ring opening reaction by its own, as

As reported in Fig 4.19, initially, polymerisation of 4-*i*Pr-Capr was performed at room temperature (rt). However, no ^1H NMR signal corresponding to the polymer could be observed even after 16 h. Subsequently, the reaction temperature was increased to 80 °C, achieving some traces of polymer after 4 h, which appeared at 4.0, 3.6 and 3.2 ppm, among other signals overlapping with the monomer. Given the promising improvement observed by increasing the temperature, polymerisation was performed at 110 °C. As can be seen in the ^1H NMR analysis, resonances corresponding to the poly(4-*i*Pr-Capr) increased with time. Conversion of the lactone was calculated by integration of the resonances at 4.1 and 4.25 ppm of the ^1H NMR spectrum, obtaining 30 % after 24 h of reaction.

Subsequently, the polymer obtained at 110 °C after 24 h of reaction was separated from the unreacted monomer and analysed by Gel Permeation Chromatography (GPC) as described in detail in Section 2.5.1.2.1. The resulted chromatograph is reported in Fig 4.20.

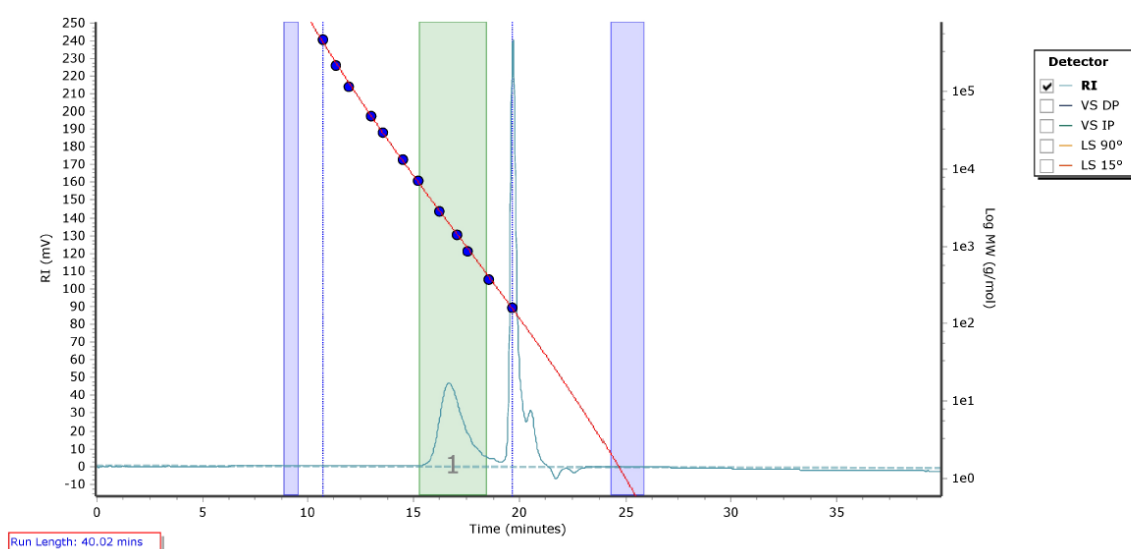


Figure 4.20. GPC analysis of poly-4-*i*Pr-Capr formed at 110 °C after 24 h of reaction.

The GPC analysis showed the formation of a polyester with an average molecular weight number (M_n) of 1384 g mol $^{-1}$, and 1.27 of polydispersity index (PDI), where M_n refers to the total weight of the sample divided by the number of molecules in the sample. The dispersity refers to the heterogeneity of sizes of molecules in the whole polymer and the PDI presents a value equal or greater than 1, the closer to 1 it is, the more uniform polymer chain length. Therefore, the obtained polyester presents a good PDI, even without excessive pre-treatments and / or further lactone purifications being performed.

This preliminary result clearly demonstrates that the lactone produced through BVO using the greener system Sn- β / H $_2$ O $_2$ is suitable for polymer applications obtaining good polymer quality even after a simple column chromatography separation of the monomer.

4.4 Conclusions

Applying the knowledge and the reaction protocol optimised in Chapter 3, BVO using Sn- β / H₂O₂ was successfully performed on a series of alkyl-substituted CyO.

This chapter shows that the study of different 2-R-CyO and 4-R-CyO, from a kinetic and a thermodynamic point of view, reveals a crucial impact of the substituent position and size. Whilst increasing the size of the R group limits the activity for the bulkiest substrates substituted in position 2 due to steric hindrance, excellent catalytic performance is obtained for 4-R-CyO for all sizes of R groups tested, achieving > 90 % of conversion after 6 h of reaction. Additionally, 4-R-Capr selectivity, especially for the bulkiest substrates tested, is higher than Capr selectivity obtained for plain CyO throughout the whole reaction period.

By complementary computational studies, 4-R-CyO are confirmed to be thermodynamically favourable to undergo BVO, being the consecutive hydrolysis reaction thermodynamically and kinetically less favoured in the presence of bulkier 4-substituent. Hence, 4-R-CyO, readily available from renewable sources such as terpenes or lignin, is shown to be more active for BVO and more resistant to hydrolysis than unsubstituted CyO, leading to high selectivity to the lactone, > 80% throughout all the reaction period.

Herein, it has been demonstrated that this kind of substrates, particularly 4-*i*-Pr-CyO, are especially favourable as platforms for BVO, which is a key step in the production of renewable lactone monomers. Furthermore, the potential viability of BVO reaction of 4-*i*-Pr-CyO in continuous operation has been demonstrated, obtaining very good stability, productivity and high selectivity to the lactone (up to 85 %) and > 1000 substrate turnovers. To be highlighted, the maximal lactone productivity from 4-*i*-Pr-CyO is almost the double of the one obtained during BVO of CyO, being 1173 and 607 g(Lact produced) kg(cat)⁻¹ cm⁻³ h⁻¹, respectively.

Finally, the lactone produced by BVO using Sn- β / H₂O₂ has been proved to be polymer-grade, since preliminary experiments led to the obtainment of a good quality polyester *via* ring opening polymerisation mechanism, showing the practical applicability of this catalytic route.

The outstanding results obtained in both batch and continuous mode clearly demonstrates the successful broadening of the substrate scope of the Sn- β / H₂O₂ BVO system. Moreover, it opens a route towards the sustainable production of renewable monomers through the BVO of sustainably derived ketones.

This chapter contributed to the following paper:

K. Yakabi, T. Mathieux, K. Milne, E. M. López-Vidal, A. Buchard, C. Hammond, *ChemSusChem*, 2017, **10**, 1 - 9

References

- (1) Plastics Europe, “*Plastic - The Facts 2016*”, www.plasticseurope.org
- (2) C. Vilela, A. F. Sousa, A. C. Fonseca, A. C. Serra, J. F. J. Coelho, C. S. R. Freire, A. J. D. Silvestre, *Polym. Chem.*, 2014, **5**, 3119 – 3141
- (3) A. Llevot, P. Dannecker, M. von Czapiewski, L. C. Over, Z. Sçyler, M. A. R. Meier, *Chem. Eur. J.*, 2016, **22**, 11510 – 11521
- (4) “*Bioplastics market data*”, www.european-bioplastics.org/market/ (Accessed June 2017)
- (5) A. Watts, N. Kurokawa, M. A. Hillmyer, *Biomacromolecules*, 2017, **18**, 1845 - 1854
- (6) M. Hiljanen-Vainio, T. Karjalainen, J. Seppälä, *J. Appl. Polym. Sci.*, 1996, **59**, 1281 – 1288
- (7) L. Wang, Z. Zhang, H. Chen, S. Zhang, C. Xiong, *J. Polym. Res.*, 2010, **17**, 77 – 82
- (8) R. Lowe, M. T. Martello, W. B. Tolman, M. A. Hillmyer, *Polym. Chem.*, 2011, **2**, 702 - 708
- (9) J. H. Park, B. K. Lee, S. H. Park, M. G. Kim, J. W. Lee, H. Y. Lee, H. B. Lee, J. H. Kim, M. S. Kim, *Int. J. Mol. Sci.*, 2017, **18**, 671 - 686
- (10) H. C. Quilter, M. Hutchby, M. G. Davidson, M. D. Jones, *Polym. Chem.*, 2017, **8**, 833 - 837
- (11) W. Schutsyter, S. Van den Bosch, J. Dijkmans, S. Turner, M. Meledina, G. Van Tendeloo, D. P. Debecker, B. F. Sels, *ChemSusChem*, 2015, **8**, 1805 -1818
- (12) A. Baeyer, V. Villiger, *Ber. Dtsch. Chem. Ges.*, 1899, **32**, 3625 – 3633
- (13) A. Corma, L. T. Nemeth, M. Renz, S. Valencia, *Nature*, 2001, **412**, 423 – 425
- (14) A. Corma, M. T. Navarro, L. Nemeth, M. Renz, *Chem. Commun.*, 2001, 2190 – 2191
- (15) Z. Q. Lei, Q. H. Zhang, J. J. Luo, X. Y. He, *Tetrahedron Lett.*, 2005, **46**, 3505 – 3508
- (16) C. Hammond, S. Conrad, I. Hermans, *Angew. Chem. Int. Ed.*, 2012, **51**, 11736 – 11739
- (17) F. Cavani, K. Raabova, F. Bigi, C. Quarantelli, *Chem. Eur. J.*, 2010, **16**, 12962 – 12969
- (18) S. Conrad, P. Wolf, P. Meller, H. Orsted, I. Hermans, *ChemCatChem*, 2017, **9**, 175 – 182
- (19) K. Yakabi, K. Milne, A. Buchard, C. Hammond, *ChemCatChem*, 2016, **8**, 3490 – 3498
- (20) P. Li, G. Liu, H. Wu, Y. Liu, J. Jiang, P. Wu, *J. Phys. Chem. C*, 2011, **115**, 3663 – 3670
- (21) J. Dijkmans, W. Schutyser, M. Dusselier, B. F. Sels, *Chem. Commun.*, 2016, **52**, 6712 – 6715
- (22) M. Renz, T. Blanco, A. Corma, V. Fornes, R. Jensen, L. Nemeth, *Chem. Eur. J.*, 2002, **8**, 4708 - 4717
- (23) J. Perez-Ramirez, C. H. Christensen, K. Egleblad, C. H. Christensen, J. C. Groen, *Chem. Soc. Rev.*, 2008, **37**, 2530 – 2542
- (24) K. Li, J. Valla, J. Garcia-Martinez, *ChemCatChem*, 2014, **6**, 46 – 66
- (25) A. Al-Nayili, K. Yakabi, C. Hammond, *J. Mater. Chem. A*, 2016, **4**, 1373 – 1382
- (26) W. Griehl, D. Ruestem, *Ind. Eng. Chem.*, 1970, **62**, 16–22
- (27) S. Brunauer, L. S. Deming, W. S. Deming, E. Teller, *J. Am. Chem. Soc.*, 1940, **62**, 1723-1732
- (28) C. Hammond, D. Padovan, A. Al-Nayili, P. P. Wells, E. K. Gibson, N. Dimitratos, *ChemCatChem.*, 2015, **7**, 3322 – 3331
- (29) D. S. Sholl, J. A. Steckel, “*Density functional theory: A practical introduction*”, Hoboken, N.J., Wiley c, 2009
- (30) C. Gambarotti, H. Bjorsvik, *J. Phys. Org. Chem.*, 2015, **28**, 619 - 628
- (31) C. D Johnson, “*The Hammett equation*”, 1952, London: Cambridge University Press, 1973
- (32) C. Hansch, A. Leo, R. W. Taft, *Chem. Rev.*, 1991, **91**, 165 - 195
- (33) L. Reyes, J. R. Álvarez-Idaboy, N. Mora-Diez, *J. Phys. Org. Chem.*, 2009, **22**, 643 - 649
- (34) J. Clayden, N. Greeves, S. Warren, “*Organic Chemistry*”, 2nd edition, 2012, Oxford University Press, Chapter 6, 125 - 127
- (35) F. Schüth, *Chem. Mater.*, 2018, **30**, **11**, 3599 – 3600

5. Upgrading the sustainability of BVO chemistry by coupling *in situ* H₂O₂ production

5.1. Introduction

In Chapter 3, it was demonstrated that the BVO reaction of cyclohexanone (CyO) to caprolactone (Capr), using Sn- β as catalyst and hydrogen peroxide (H₂O₂) as oxidant, was accompanied by the unavoidable consecutive hydrolysis of the desired lactone to 6-hydroxyhexanoic acid (6-HHA), since the latter reaction is also Sn- β catalysed in the presence of some H₂O. Unfortunately, low extents of Capr hydrolysis were observed even without the addition of H₂O in the system (Table 3.2), suggesting that even the minimum amount of H₂O can promote the hydrolysis reaction. Complete elimination of H₂O and consequently the consecutive hydrolysis reaction, therefore seems unlikely, since traces of H₂O can be found in the solvent and the catalyst. Furthermore, the main source of H₂O is the oxidant itself, as H₂O₂ was used in aqueous form (50 wt. %) and H₂O is formed as by-product from H₂O₂ during the BVO reaction. Notwithstanding, promising results were obtained in Chapter 3 in continuous flow mode when operating at oxidant-limited regime (0.75 H₂O₂:ketone, Fig 3.28). In this regime, higher selectivity towards the lactone was achieved (> 70 %), showing that the

decrease of H₂O in the system can indeed benefit the productivity of the system by diminishing the extent of lactone hydrolysis.¹

Herein, attention was focused on the investigation of various approaches to reduce the presence of H₂O in the BVO / Sn-β / H₂O₂ system, in an attempt to find more selective ways of performing BVO of CyO and similar substrates which can suffer ring opening hydrolysis. These approaches include: i) the use of oxidant in higher concentrations, ii) the use of various H₂O traps, iii) the use of solid oxidants, and iv) the *in situ* generation of H₂O₂ from H₂ and O₂.

5.1.1. Preliminary studies for H₂O removal from the BVO / Sn-β / H₂O₂ system

The first approach to be considered was the use of a more concentrated oxidant solution to reduce the initial H₂O content at the start of the reaction, *i.e.* H₂O₂ 70 wt. % in H₂O. However, for safety considerations, which are described in greater detail in the next section, this highly concentrated mixture is rarely used commercially.

Accordingly, H₂O₂ was replaced by a different oxidising agent that can be purchased in higher concentration, *i.e.* *tert*-butyl hydrogen peroxide (TBHP, 70 wt. % in H₂O), resulting in less H₂O being present at the start of the reaction.

Unfortunately, the use of TBHP as oxidant for the BVO reaction of CyO at the standard reaction conditions employed in batch mode (10 mL of 0.33 M CyO in 1,4-dioxane, 1 mol. % Sn respect to the CyO, 0.5 M of oxidant, at 100 °C), led to very poor catalytic performance compared with the performance with 50 wt. % aqueous H₂O₂ as described in Table 5.1.

Table 5.1. Comparison of the catalytic performance obtained for BVO of CyO at the standard reaction conditions using H₂O₂ (50 wt. % in H₂O) and TBHP (70 wt. % in H₂O).

Oxidant used	Conversion / %	Yield Capr / %
H ₂ O ₂	94	44
TBHP	3	2.4

Reaction conditions: 10 mL of 0.33 M CyO in 1,4-dioxane, at 100 °C, with 1 mol. % of Sn respect to CyO, 1.5 oxidant: CyO (0.5 M), 6 h of reaction.

The large differences in catalytic activity observed between the two kinds of peroxides employed as oxidants can be attributed to the combination of two main factors: i) the differences in reactivity of the activated forms of these two oxidants and ii) the poor ability of Sn-β to form these activated species. Firstly, activation of H₂O₂ and TBHP to act as oxidising agents typically requires the formation of M-OOH and M-OO^tBu species, respectively, where

M represents metals such as Ti, V or Mo, which are excellent metal centres to form these hydroperoxo species. However, the reactivity of M-OO^tBu has been proved to be intrinsically lower than the reactivity of M-OOH for various oxidation reactions, such as oxidation of olefins or epoxidation of alkenes.^{2,3} Secondly, Sn has a very poor ability to form hydroperoxo species. For instance, through theoretical studies, Boronat *et al.*⁴ compared the mechanism of Sn- β catalysed BVO using H₂O₂ based on the activation of the carbonyl group proposed by Corma;⁵ and based on the activation of the oxidant by the formation of Sn hydroperoxo species. In said report, formation of Sn-OOH species was found to be less energetically favoured, indicating that the second mechanism was less probable. Indeed, they reported that the BVO of CyO catalysed by Sn- β using H₂O₂ follows the first mechanism, based on the activation of the carbonyl group without the need to activate the oxidant. Therefore, due to the intrinsically lower reactivity of TBHP, the use of this oxidant is likely to require some activation, in order to be effectively used as nucleophile for the BVO reaction, which Sn- β is unlikely to provide.

The second approach to minimise the impact of H₂O during BVO involved the use of H₂O traps such as molecular sieves, which can capture the H₂O molecules present in the reaction mixture. Molecular sieves are synthetic zeolitic materials whose three-dimensional structure forms cavities that can trap molecules of the same and/or smaller size to these cavities and can absorb up to approximately 20 wt. % of H₂O.

Accordingly, an excess of molecular sieves 3A was added to the typical BVO reaction set up, and the results compared to those obtained from the standard BVO reaction in Table 5.2.

Table 5.2. Catalytic performance obtained for the standard BVO of CyO and with the addition of molecular sieves as H₂O trap.

Reaction	Conversion / %	Selectivity Capr / %	H ₂ O ₂ Selectivity / %
Standard BVO	90	47	72
With Molecular Sieves ^a	23	82	11

Reaction conditions: 10 mL of 0.33 M CyO in 1,4-dioxane, at 100 °C, with 1 mol. % of Sn respect to CyO, 1.5 H₂O₂:CyO (0.5 M), 4 h of reaction, ^a with addition of 1 g of molecular sieves 3A. H₂O₂ Selectivity was calculated as CyO converted / H₂O₂ consumed x 100.

As stated in Table 5.2, a drastic decrease in catalytic activity was observed when adding the molecular sieves to the standard BVO reaction. This experiment led to a CyO conversion of 23 % and a Capr yield of 18 %, which corresponded to a Capr selectivity of 82 % after 4 h of reaction. However, the molecular sieves started to dissolve in the reaction mixture after a certain time. These results contrasted with the usual high levels of catalytic activity obtained

at these reaction conditions for the standard BVO in the absence of molecular sieves. Remarkably, selectivity obtained in presence of the molecular sieves matched the selectivity values normally reached at low levels of conversion in the standard BVO reaction (Fig 3.4).

Unfortunately, quantification of H_2O_2 also revealed a high level of decomposition was observed in the presence of the molecular sieves, since after 4 h of reaction practically no oxidant was left in the reaction mixture. Typical H_2O_2 selectivity is around 70 % for the standard BVO whilst only 11 % was obtained with the addition of the H_2O trap, indicating that the oxidant was not efficiently used. Molecular sieves have previously been reported to react with strong oxidising agents,⁶ such as H_2O_2 . This clearly indicates that the presence of molecular sieves was detrimental for the overall catalytic activity of the BVO / Sn- β / H_2O_2 system.

Subsequently, other H_2O traps, such as desiccants, were considered for H_2O removal. Among them, anhydrous sodium sulfate can be used as inert drying agent, as it is known to remove traces of H_2O from organic solutions, and anhydrous calcium chloride is also a well know hygroscopic salt.⁷ However, both candidates present significant drawbacks, *i.e.* anhydrous sodium sulfate loses effectiveness as desiccant at temperatures over 30 °C; and anhydrous calcium chloride is not compatible with ketones, as they form adducts.

A reaction adding anhydrous sodium sulfate to the reaction mixture was carried out at the standard BVO reaction conditions.

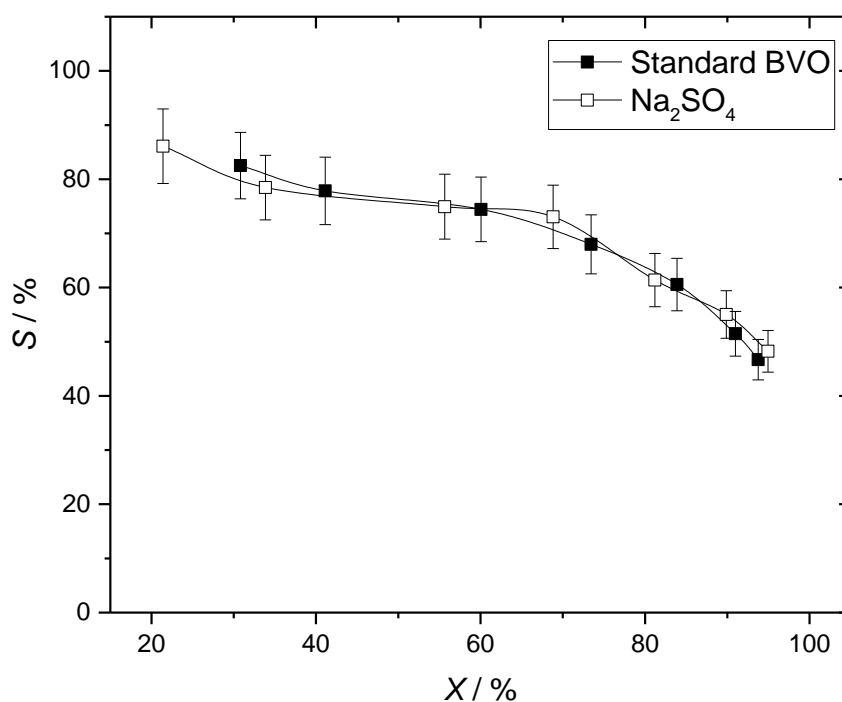


Figure 5.1. Catalytic activity of standard BVO of CyO with and without the addition of the desiccating agent.

However, as can be seen in Fig 5.1, identical results to those observed in absence of the desiccant were observed. The use of the drying agent led to the same catalytic performance and selectivity trend as observed in its absence, reaching 95 % of CyO conversion with 48 % of Capr selectivity after 6 h of reaction. This result demonstrated the poor ability of this desiccant to operate efficiently at such high reaction temperatures, making its use infeasible to remove H₂O from this system. The use of the drying agent led to the same catalytic performance and selectivity trend than in its absence, reaching 95 % of CyO conversion with 48 % of Capr selectivity after 6 h of reaction. This result manifested the poor ability of this desiccant to operate efficiently at such high reaction temperatures, making its use not feasible to remove H₂O from this system.

An alternative approach involves the use of H₂O₂ in solid form, by employing a urea-H₂O₂ adduct. The use of H₂O₂ in solid form suppresses all the extra H₂O typically added at the beginning of the reaction into the reaction medium when using a 50 wt. % H₂O₂ aqueous solution. Therefore, the absence of this initial amount of H₂O may be beneficial in order to reach higher levels of Capr selectivity along all the reaction period if the urea-H₂O₂ adduct can be efficiently used as oxidant for the BVO reaction.

Accordingly, the equivalent amount of urea-H₂O₂ adduct, *i.e.* to obtain 1.5 H₂O₂:CyO ratio, was added to the reaction mixture instead of the aqueous H₂O₂ solution and its catalytic activity was compared with the standard BVO reaction in Fig 5.2. As can be seen in Fig 5.2, the use of urea-H₂O₂ adduct considerably diminished the catalytic activity of this reaction, achieving half of the conversion usually obtained for the standard BVO with aqueous H₂O₂ solution after 4 h of reaction. Given the low catalytic activity observed using the urea-H₂O₂ adduct, an additional test was performed to evaluate the potential poisoning effect of the urea-H₂O₂ adduct, by adding extra 1.5 equivalents of H₂O₂ in solid form to the typical 1.5 equivalents of H₂O₂ in aqueous solution (50 wt. %) employed, representing a total amount of H₂O₂ of 1 M (3 H₂O₂:CyO). According to the results obtained in Chapter 3 in regards of the dependency of reaction rate from the oxidant, above approximately 0.75 H₂O₂:CyO, the initial reaction rate becomes independent of the oxidant (zero order) (Fig 3.9). As such, similar initial reaction rate than for the standard BVO reaction, using 1.5 equivalents of H₂O₂ in aqueous solution (50 wt. %), would be expected, while a decrease in catalytic activity would be indicative of poison.

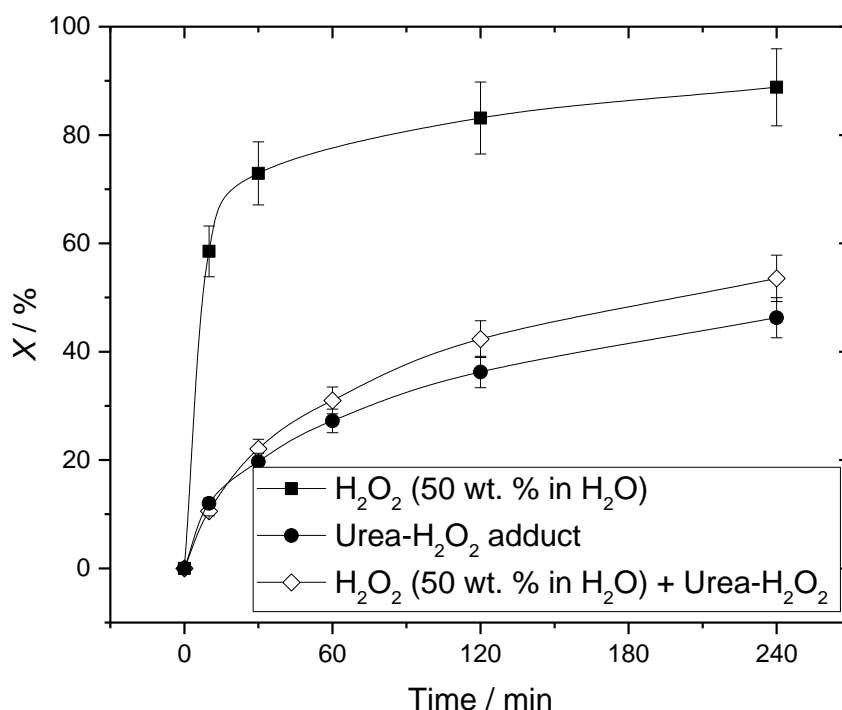


Figure 5.2. Catalytic activity of 2Sn-β for the BVO of CyO using 1.5 H₂O₂:CyO in the form of H₂O₂ (50 wt. % in H₂O), urea-H₂O₂ adduct and using 1.5 equivalents of H₂O₂ (50 wt. % in H₂O) with extra 1.5 equivalents of urea-H₂O₂ adduct. Reaction conditions: 10 mL of 0.33 M CyO in 1,4-dioxane, 1 mol. % Sn respect CyO, at 100 °C.

As can be observed in Fig 5.2, initial reaction rate of the poisoning experiment was considerably lower, displaying a trend similar to the one showed by the use of urea-H₂O₂ adduct only, indicating the negative effect of the solid H₂O₂ which inhibited the BVO from performing as usual.

In view of the difficulties faced for the removal of H₂O from the BVO / Sn-β / H₂O₂ system, attention was focused on alternative obtainment of H₂O₂. In this respect, the *in situ* production of H₂O₂ coupled to the BVO reaction was proposed. This final approach would avoid its dilution in the H₂O required to stabilise it (usually commercialised as 30 or 50 wt. % in aqueous form), and its further dilution in the reaction solution to be used as oxidant for the BVO reaction, since lower targets (0.5 M) are required.

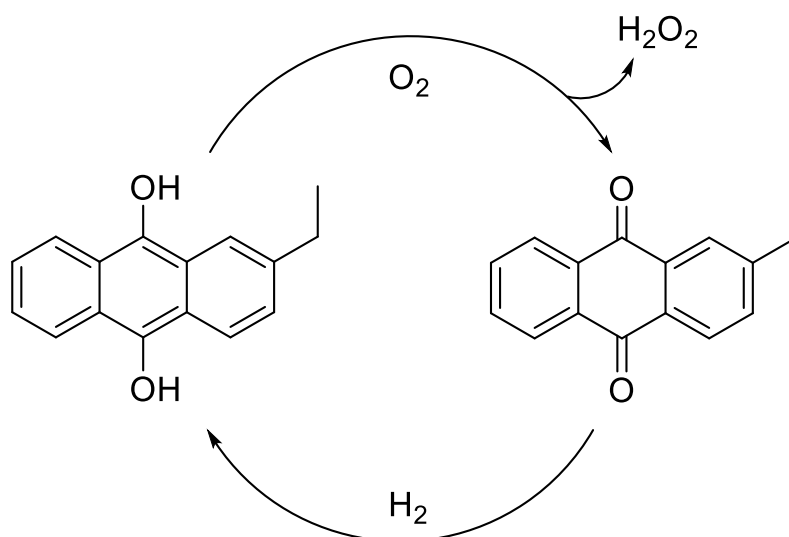
5.2. Hydrogen peroxide (H₂O₂) production

Hydrogen peroxide (H₂O₂) is a very important bulk chemical with a production of over three million tonnes per annum, at an increasing level of demand. It has many practical applications, its most relevant being its use as disinfectant, bleaching agent and oxidising agent.

Furthermore, H_2O_2 is considered to be one of the greenest oxidants since the only by-product of its use as oxidant is H_2O , and it is also one of the most efficient due to its high active oxygen content.⁸

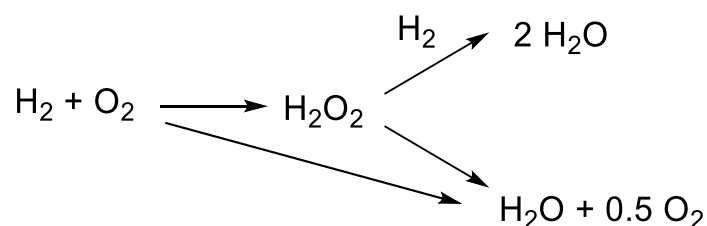
Currently, H_2O_2 is mainly industrially produced *via* the auto-oxidation (AO) of organic compounds. Typically, its synthesis involves indirect reduction of O_2 to H_2O_2 by the oxidation of an alkyl anthraquinol to the corresponding quinone (Scheme 5.1). However, this process presents several drawbacks which include i) the use of complex and toxic solvent system, ii) high cost of the quinone, iii) requirement to reduce back the quinone by hydrogenation, iv) deactivation of the hydrogenation catalyst and v) economic viability only when produced at large scales.

Additionally, its transportation and storage requirements result in many safety regulations, since concentrated H_2O_2 presents low stability and can be explosive, and therefore, it is commonly commercialised only when diluted in an aqueous solution.



Scheme 5.1. Simplified representation of H_2O_2 synthesis via AO process.

In view of this, an alternative method has gathered intense attention in the last decades due to its higher sustainability and reduction of operational costs: the direct synthesis of H_2O_2 from H_2 and O_2 . Unfortunately, this alternative approach comes with some disadvantages attached, such as the need to work with an appropriate H_2 - O_2 mixture, outside the explosion range,⁹ thereby necessitating dilution of the mixture in an inert gas such as N_2 or CO_2 . Moreover, the fact that non-selective oxidation to H_2O ($\Delta G^\circ = -237 \text{ kJ mol}^{-1}$), hydrogenation to H_2O ($\Delta G^\circ = -354 \text{ kJ mol}^{-1}$) and H_2O_2 decomposition ($\Delta G^\circ = -117 \text{ kJ mol}^{-1}$) are thermodynamically more favoured than the selective oxidation of H_2 to H_2O_2 ($\Delta G^\circ = -120 \text{ kJ mol}^{-1}$) (Scheme 5.2), makes imperative to find optimal working conditions and a suitable catalyst selective to H_2O_2 .



Scheme 5.2. Reactions involved in the direct synthesis of H_2O_2 .

Although apparently trivial, the direct synthesis of H_2O_2 from H_2 and O_2 is in fact, more tangled than it seems at first glance. Despite the significant advances in this field, productivity and selectivity towards H_2O_2 need to be further improved to commercially compete with the AO method.¹⁰ Nevertheless, it should be noted that AO method is only viable at large scale and concentrations (usually commercialised as 30 or 50 wt. % aqueous solution) and H_2O_2 is diluted further down in the reactor. Hence, direct synthesis of H_2O_2 opens a possibility to produce H_2O_2 on a small scale and use it *in situ* as oxidant for many different reactions, whose working concentration are lower e.g. the typical 0.5 M of H_2O_2 employed for the BVO reaction, which represents a concentration of only 1.7 wt. %, making the target of *in situ* production lower and more feasible.

In regard to catalysts suitable for the direct synthesis of H_2O_2 , a selection of examples are collected in Table 5.3.

Table 5.3. Productivity values for a selection of catalysts reported in literature.

Catalyst ^a	Solvent	H_2O_2 Productivity / $\text{mol kg(cat)}^{-1} \text{h}^{-1}$	Reference
2.5Au-1.8Pd/HZSM5	MeOH/ H_2O	138	11
1.5Pd/Y	MeOH/ H_2O	84	11
2.5Au-2.5Pd/C	MeOH/ H_2O	160	12
5Pd/ CeO_2	MeOH/ H_2O	97	13
Pd/SBA-15	MeOH	24 ($\text{mg mg}^{-1} \text{cat}$)	14
4.5Pd-0.45Ru-0.05Au/ TiO_2	MeOH/ H_2O	153	15
2.5Au-2.5Pd/ TiO_2	MeOH/ H_2O	135	16
Pd/ HfNb_3O_8 -NS	MeOH	50 ($\text{mmol mmol}^{-1} \text{Pd h}^{-1}$)	17

^a Where the number preceding the metal corresponds to the metal loading in wt. %.

As can be observed in the small sample compiled in Table 5.3, most of the catalysts employed involve noble metals supported on different materials. The most active metals used are Pd and/or Au based, supported in zeolites, mesoporous silicas, C or TiO₂.¹⁸⁻²⁰ However, many other combinations including Pd-Ag, Pd-Ru or Pd-Pt have also been employed.^{21,22} The selection of the examples compiled in the table are based on the fact that Pd is well known to possess a high propensity for dissolution of H₂ and excellent performance in hydrogenation reactions. Hence, it presents itself as a good contender to catalyse *in situ* H₂O₂ production,²³ whilst Au catalysts have been successfully reported for different hydrogenation reactions.²⁴ Notwithstanding, the challenge that still remains is the need to find a catalyst selective towards H₂O₂ that does not promote the rest of the potential reactions (Scheme 5.2), in order to increase selectivity towards H₂O₂ over 95 %. Although significant improvements have been made by addition of promoters and refining the catalyst design,^{25,26} the optimisation of this reaction is still a hot topic.

Given that in Chapter 3, the BVO reaction was proved to operate independently of the amount of oxidant employed when using H₂O₂:CyO above 0.75 (Fig 3.9), the coupling of *in situ* H₂O₂ production with BVO reaction could operate at the same initial reaction rates with concentrations of only 0.85 wt. % of H₂O₂, reducing considerably the targeted H₂O₂ concentration to be formed *in situ*. For instance, it was successfully reported by Santonastaso *et al.*²⁷ that *in situ* generated H₂O₂ can be used for oxidation of benzyl alcohol. Furthermore, *in situ* H₂O₂ production was reported by Cavani *et al.*²⁸ as a tool to upgrade the sustainability of the epoxidation of propene.

Considering these facts, *in situ* generation of H₂O₂ appears to be an attractive solution to reduce the H₂O present in the system and to upgrade the sustainability of the BVO chemistry, as well as potentially increase the lactone selectivity by limiting the hydrolysis step upon reduction of the amount of H₂O in the system.

Nonetheless, coupling of *in situ* H₂O₂ synthesis and the BVO reaction represents a great challenge since initial optimal conditions of both systems present important differences in terms of temperature and reaction media. Whilst *in situ* H₂O₂ synthesis typically demands very low working temperature (2 °C) and a mixture of MeOH/H₂O or similar as solvent,⁸ BVO chemistry requires high temperature (< 70°C) and an organic solvent, commonly 1,4-dioxane, to proceed smoothly.²⁹

In the attempt to couple these two systems, the following parts of this chapter are focused on:

- i) The quest for a suitable catalyst based on previous reports.
- ii) The investigation of suitable solvents for *in situ* production of H₂O₂.
- iii) The investigation of alternative solvents for BVO.
- iv) The study of the compatibility of *in situ* H₂O₂ production and BVO reaction in one pot.
- v) The viability of coupling *in situ* H₂O₂ production and BVO chemistry in two pots.

It should be reminded that the catalyst design and the study of the correlation between the catalyst activity and its characterisation is beyond the scope of this work. The main goal was to investigate the viability of coupling *in situ* H₂O₂ production with BVO. Hence, various previously reported catalysts that can be adequately used for H₂O₂ production were reproduced, so as to identify a useful co-catalyst for the coupling with the BVO reaction.

5.3 Results and discussion

5.3.1 Preliminary studies for coupling *in situ* H₂O₂ production and BVO reaction

An example of working conditions for the direct synthesis of H₂O₂ from H₂ and O₂ found in literature consists of a 2:1 solvent mixture of MeOH/H₂O at 2 °C, in the presence of a Pd-Au/TiO₂ catalyst using 37.5 bar of 5 % H₂ / CO₂ and 25 % O₂ / CO₂ (1:2 molar).¹¹ Since direct synthesis of H₂O₂ and BVO reaction are usually carried out at very different working conditions, the first point to tackle was the evaluation of both systems separately to explore the reaction phase space, to determine whether a potential compromise between the operational conditions of both distinct reactions can be found, even though it means lowering the productivity of the two individual reactions. For instance, the solvent required for *in situ* H₂O₂ production must possess high H₂ solubility, must be able to promote enough H₂O₂ formation to act as oxidising agent for BVO, and ideally, this solvent has to also be compatible with the BVO system.

As the main goal of coupling *in situ* H₂O₂ production with the BVO reaction was reducing the presence of H₂O in the system, the employment of MeOH/H₂O mixture, reported in several publications as one of the most suitable solvent mixtures for this reaction (Table 5.3), was intentionally avoided and pure MeOH was used instead in the preliminary tests. Additionally, having in mind the needs of the BVO reaction, 1,4-dioxane was also tested for *in situ* H₂O₂ production, as well as acetonitrile (ACN), as this is also reported to be a suitable solvent for the BVO reaction.³⁰

Accordingly, preliminary experiments were carried out in a stainless-steel autoclave at 10, 20 and 50 °C, using the three solvents mentioned above, charging it with 40 bar of 2.5% H₂ / 5% O₂ in CO₂ and Pd-Au/TiO₂ as catalyst. The choice of this catalyst was based on a report from Freakley *et al.*,¹⁶ who demonstrated it to be a promising catalyst for this reaction.

The catalyst was prepared with loadings of 1 wt. % Pd and 1 wt. % Au on TiO₂ (P25) by the sol immobilisation (SI) method, using PVA as stabilising agent, following the same methodology reported by Freakley *et al.*, described in Section 2.3.2.1. Prior to use, the catalyst was calcined at 400 °C in static air and was denoted 1Pd-1Au/TiO₂(400).

The preliminary results obtained are summarised in Table 5.4. H₂O₂ production was quantified by titration with Ce(IV) sulfate following the procedure described in Section 2.5.3.1.

Table 5.4. Preliminary results for *in situ* H₂O₂ production.

Solvent	H ₂ O ₂ Productivity at 10 °C / mol kg(cat) ⁻¹ h ⁻¹	H ₂ O ₂ Productivity at 20 °C / mol kg(cat) ⁻¹ h ⁻¹	H ₂ O ₂ Productivity at 50 °C / mol kg(cat) ⁻¹ h ⁻¹
MeOH	97	5	< 1
1,4-dioxane	17	5	< 1
ACN	5	4	< 1

Reaction conditions: 10 mL of solvent, 10 mg of 1Pd-1Au/TiO₂(400), 40 bar of 2.5 % H₂ / 5 % O₂ in CO₂ at the stated temperature after 30 min of reaction. H₂O₂ production was quantified by titration with Ce(IV) sulfate and its productivity was calculated as mol of H₂O₂ produced per kg of catalyst per time.

As it could be already anticipated according to the literature summarised above, lower reaction temperature resulted in higher H₂O₂ productivity being obtained. In contrast, higher reaction temperature strongly disfavoured H₂O₂ production, being practically inexistent at 50 °C for the three solvents tested.

In order to investigate whether the low amounts of H₂O₂ observed at higher temperature were indeed caused by very low reaction rates to H₂O₂ or as consequence of rapid thermal decomposition of the H₂O₂ formed into other products, the thermal stability of H₂O₂ in the reaction system was analysed under inert atmosphere.

To do so, a known amount of commercial H₂O₂ (50 wt. % in H₂O) was placed into the reactor, in addition to the catalyst and the solvent, and the reactor charged with 20 bar of N₂. Subsequently, reactions were carried out at 10 or 20 °C for 30 min, and the thermal stability of H₂O₂ under otherwise inert conditions was evaluated by analysing the final concentration of H₂O₂ in the reaction mixture, as summarised in Table 5.5.

Table 5.5. Thermal stability studies of H₂O₂ at 10 and 20 °C.

Solvent	% of H ₂ O ₂ loss at 10 °C	% of H ₂ O ₂ loss at 20 °C
MeOH	0.8	18
1,4-dioxane	7	11

Reaction conditions: 10 mL of solvent, 0.1 mL of H₂O₂ (50 wt. % in H₂O) 10 mg of 1Pd-1Au/TiO₂(400), 20 bar of N₂ at the stated reaction temperature after 30 min of reaction. H₂O₂ production was quantified by titration with Ce(IV) sulfate and its % loss was calculated as H₂O₂ consumed / initial H₂O₂ x 100.

The stability studies revealed that although H₂O₂ suffered from thermal decomposition after 30 min at all conditions, decomposition was aggravated with increasing temperature. Considering that commercial aqueous H₂O₂ contains a series of stabilisers in solution, it is likely that H₂O₂ obtained *in situ*, where no stabilisers are present, suffers even greater thermal decomposition at the temperatures investigated. Thus, based on the stability studies, although at 20 and 50 °C some H₂O₂ was produced, at those temperatures it was not thermally stable and it rapidly decomposed, leading to a very poor productivity after 30 min of reaction.

From these initial results, optimal working temperature was established to be 10 °C in order to maximise H₂O₂ production and to diminish its decomposition.

Subsequently, the study was focused on the investigation of different catalysts that could be used for direct synthesis of H₂O₂ and exploring alternative optimal solvents.

5.3.2 Catalysts for *in situ* H₂O₂ production

Given that Pd and/or Au catalysts showed the most promising results (Table 5.3), these two metals were selected as active species in the quest of suitable catalyst for *in situ* H₂O₂ production.

It should be noted that most of the productivity values given in Table 5.3 were obtained at 2 °C, while all the H₂O₂ productivities given in this study were obtained at 10 °C. However, as described above, the aim of this study was to find an adequate catalyst to couple *in situ* H₂O₂ production with BVO to evaluate its potential viability to upgrade the process and to make it more sustainable. Catalyst design or quest for excellence in direct production of H₂O₂ to compete with the relevant achievements in this field is beyond the scope of this chapter.

Accordingly, in addition to bimetallic 1Pd-1Au/TiO₂, monometallic Pd (1 wt. %) and monometallic Au (1 wt. %) on TiO₂, denoted 1Pd/TiO₂ and 1Au/TiO₂, respectively, were prepared by the SI method, and were subjected to different heat treatments to evaluate their impact on the target reaction. This synthesis methodology, based on colloid formation prior to

immobilisation on the support, has shown to be very efficient to obtain small metal nanoparticle, with a narrow particle size and uniform distribution throughout the whole support, since the surfactant prevents particle sintering and agglomeration.³¹ Additionally, it was reported by Pritchard *et al.*³² that catalysts prepared by SI were considerably more active for *in situ* H₂O₂ production than those analogous prepared by impregnation (IMP).

The results obtained for *in situ* production of H₂O₂ with this set of catalysts are summarised in Table 5.6.

Table 5.6. Catalyst screening for *in situ* H₂O₂ production.

Catalyst	Preparation method and heat treatment	H ₂ O ₂ Productivity / mol kg(cat) ⁻¹ h ⁻¹	H ₂ O ₂ Productivity / mol kg(metal) ⁻¹ h ⁻¹
1Au/TiO₂	SI, untreated	16	1615
	SI, 400 °C Air	24	2350
1Pd-1Au/TiO₂	SI, untreated	36	1819
	SI, 400 °C Air	97	4843
	SI, 400 °C Air + 200 °C Red	89	4450
1Pd/TiO₂	SI, untreated	19	1920
	SI, 400 °C Air	28	2750

Reaction conditions: 10 mL of MeOH, 10 mg of catalyst, 40 bar of 2.5 % H₂ / 5 % O₂ in CO₂ at 10 °C after 30 min of reaction. H₂O₂ production was quantified by titration with Ce(IV) sulfate and its productivity was calculated as mol of H₂O₂ produced per kg of catalyst per time and mol of H₂O₂ produced per kg of metal per time.

As it can be appreciated from Table 5.6, the results obtained agree to those reported in the literature. Moreover, it is clear that the combination of the two metals in the bimetallic alloy catalyst boosted H₂O₂ formation compared with the monometallic alloys, resulting in higher productivity.³² The synergistic effect between Pd-Au remarkably improved the productivity by over two times more than the individual performances, from ± 2500 mol kg(metal)⁻¹ h⁻¹ for the monometallic catalysts, to 4800 mol kg(metal)⁻¹ h⁻¹ for 1Pd-1Au/TiO₂.

Noticeably, catalysts subjected to heat treatments displayed greater productivity than untreated samples tested as synthesised (only dried in the oven at 110 °C). Although the benefit was lower for monometallic catalysts, the productivity of 1Pd-1Au/TiO₂ was

significantly improved, to the point that the catalyst achieved comparable levels of productivity to those summarised in Table 5.1, despite the fact reactions were performed at higher temperature (2 °C vs. 10 °C).

In view of the promising results obtained for 1Pd-1Au/TiO₂₍₄₀₀₎ at 10 °C and guided by some reports where the catalyst reactivity was improved by calcination-reduction cycles,¹⁶ an additional experiment was performed with 1Pd-1Au/TiO₂ after calcination at 400 °C in static air followed by reduction at 200 °C. Nevertheless, even though the productivity obtained was still high, at 4450 mol kg(metal)⁻¹ h⁻¹, it did not surpass the one obtained with the calcined catalyst.

Notably, all reactions were performed employing 10 mg of catalyst, independently of the metal loading. As such, productivity values normalised as mol H₂O₂ produced kg(metal)⁻¹ h⁻¹ provide a more accurate quantification allowing direct comparison of the catalysts reactivity, as the reaction is driven by the metal. However, since most of the publications expressed productivity values as mol of H₂O₂ kg(cat)⁻¹ h⁻¹, values expressed in these units were shown to prove that productivity values in the same range of the ones already reported in literature could be obtained, although from this point on, only productivity based on the metal is used for further comparisons.

As can be appreciated from Table 5.3, the other important block of materials successfully reported for this reaction were Au and/or Pd supported on different zeolites. Therefore, considering the possibility to couple it with the BVO reaction in one pot, which was demonstrated to be efficiently catalysed by Sn-β in previous chapters, a series of catalysts composed of Au and/or Pd supported on 2Sn-β 38 were explored for *in situ* H₂O₂ production. In this case, 2.5 wt. % loadings of monometallic Au and Pd and 0.5 wt. % of each metal for the bimetallic analogue, were supported on 2Sn-β 38 by wet impregnation (IMP) following the synthetical procedure described in Section 2.3.2.2. This kind of synthetic method was chosen based on the successful employment of Pd/Y prepared by IMP for H₂O₂ synthesis, as reported by Li *et al.*¹¹

Samples were tested as synthesised and after calcination at 400 °C in air, using the same reaction conditions stated above and the results obtained are summarised in Table 5.7.

Table 5.7. Au and/or Pd supported on 2Sn- β for *in situ* H₂O₂ production.

Catalyst	Preparation method and heat treatment	H ₂ O ₂ Productivity / mol kg(cat) ⁻¹ h ⁻¹	H ₂ O ₂ Productivity / mol kg(metal) ⁻¹ h ⁻¹
2.5Au/2Sn-β	IMP, untreated	8.5	342
	IMP, 400 °C Air	9.5	370
2.5Pd/2Sn-β	IMP, untreated	25	987
	IMP, 400 °C Air	32	1268
0.5Au-0.5Pd/2Sn-β	IMP, untreated	24	2408
	IMP, 400 °C Air	28	2768

Reaction conditions: 10 mL of MeOH, 10 mg of catalyst, 40 bar of 2.5 % H₂ / 5 % O₂ in CO₂ at 10 °C after 30 min of reaction. Productivity was calculated considering only the noble metal loading, without accounting the 2 wt. % of Sn already incorporated into the zeolite framework.

In this case, significant differences were observed between monometallic Pd and Au catalysts, with the productivity being almost 4 times higher for 2.5Pd/2Sn- β than 2.5Au/2Sn- β . Analogously to the effect observed for the TiO₂ supported materials, monometallic Pd and Au on 2Sn- β displayed lower H₂O₂ productivity than the bimetallic catalyst, with the synergistic effect improving H₂O₂ productivity from 370 and 1268 mol kg(metal)⁻¹ h⁻¹ for 2.5Au/2Sn- β and 2.5Pd/2Sn- β , respectively, to 2768 mol kg(metal)⁻¹ h⁻¹ for 0.5Au-0.5Pd/2Sn- β after 30 min of reaction.

As happened for the TiO₂ supported materials, catalyst reactivity towards H₂O₂ production was improved after the calcination treatment, although the differences were not as dramatic in this case. The set of catalysts tested presented higher H₂O₂ productivity values when calcined at 400 °C. For a better comparison, the H₂O₂ productivity values obtained are reported in Fig 5.3.

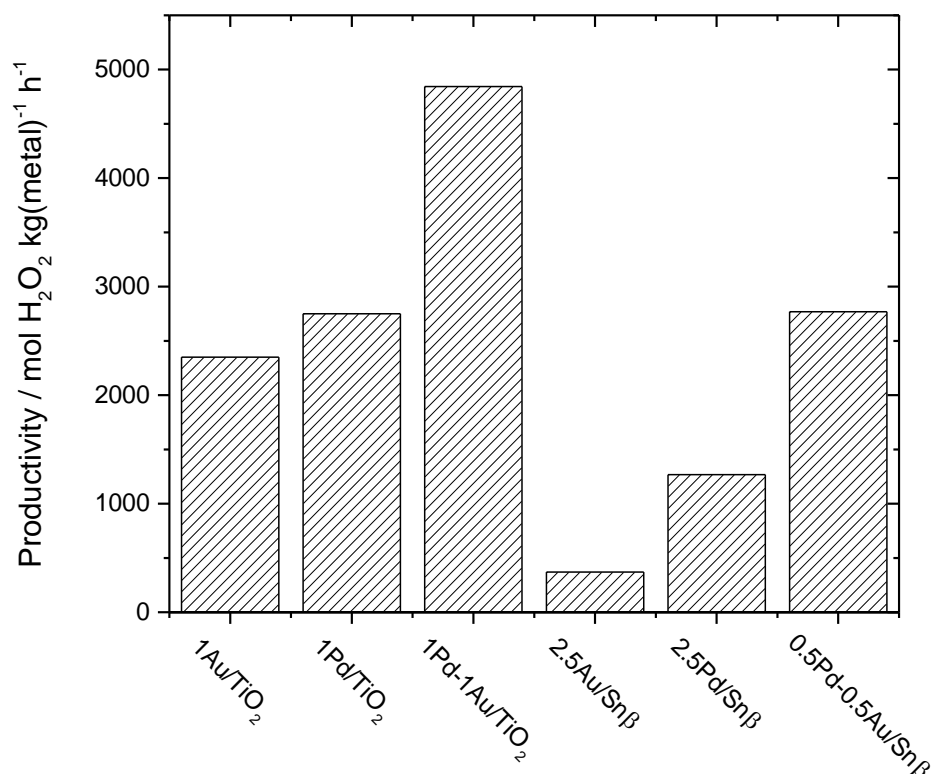


Figure 5.3. Comparison of H₂O₂ productivity obtained for the catalysts calcined at 400 °C, after 30 min of reaction at 10 °C in MeOH.

By this comparison, the reactivity trend Au < Pd < Pd-Au confirmed the positive effect obtained by employing a bimetallic catalyst through the reported synergistic effect. Additionally, the TiO₂ supported series showed to be generally more active than the 2Sn-β series, with 1Pd-1Au/TiO₂₍₄₀₀₎ being the best catalyst considered in this study. Accordingly, 1Pd-1Au/TiO₂₍₄₀₀₎ was selected as catalyst to be used in the following sections for *in situ* H₂O₂ production.

Nevertheless, 0.5Au-0.5Pd/2Sn-β achieved the second greatest productivity, exhibiting a productivity approximately half that of 1Pd-1Au/TiO₂₍₄₀₀₎. Yet, as this catalyst was formed by IMP of the catalyst typically used for BVO reaction, this combination was evidently very promising and highly convenient for one pot coupling of *in situ* H₂O₂ with BVO chemistry. Thereby, it must be taken into account for future experiments.

5.3.3 Solvents for *in situ* H₂O₂ production

Subsequently, once the most suitable catalyst to be used for direct production of H₂O₂ was determined, solvent screening was carried out in the quest for an optimal solvent to be used.

Table 5.8. Solubility of H₂ and O₂ in various solvents at room temperature.⁸

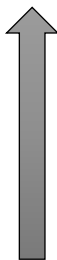
Solvent	Solubility of H ₂ / mg L ⁻¹	Solubility of O ₂ / mg L ⁻¹	Polarity
MeOH	7.91	324	
EtOH	7.50	320	
IPA	6.92	323	
1,4-dioxane	4.12	231	
Acetone	8.15	364	

Table 5.8 compiles some of the properties of the different solvents selected for the screening. It includes MeOH and 1,4-dioxane, already employed in the preliminary studies to evaluate the optimal reaction temperature, in addition to acetone, ethanol (EtOH) and isopropanol (IPA). The selection of these solvents was based on their ability to solubilise H₂ and O₂ and their polarity, which was reported to be beneficial for the promotion of direct H₂O₂ synthesis.⁸ Since the direct synthesis of H₂O₂ occurs in a three-phase system (catalyst / solvent / gases), a higher ability to solubilise H₂ and O₂ is desirable to increase the diffusion of the gas reactants to the catalyst surface.

All solvents were tested for 30 min using 1Pd-1Au/TiO₂₍₄₀₀₎, and 40 bar of 2.5 % H₂ / 5 % O₂ in CO₂. The H₂O₂ productivity values obtained in each solvent are summarised in Table 5.9.

Table 5.9. Solvent screening for *in situ* H₂O₂ production.

Solvent	H ₂ O ₂ Productivity / mol kg(metal) ⁻¹ h ⁻¹
MeOH	4843
EtOH	1884
IPA	1051
1,4-dioxane	848
Acetone	969

Reaction conditions: 10 mL of solvent, 10 mg of 1Pd-1Au/TiO₂₍₄₀₀₎, 40 bar of 2.5% H₂ / 5% O₂ in CO₂ at 10 °C after 30 min of reaction. H₂O₂ production was quantified by titration with Ce(IV) sulfate and its productivity was calculated as mol of H₂O₂ produced per kg of metal per time.

From this set of experiments, it was clearly shown that MeOH was the most efficient solvent tested by far, producing 4843 mol H₂O₂ kg(metal)⁻¹ h⁻¹. Whereas the second highest productivity value, obtained in EtOH, was about the half of the one obtained in MeOH. Unfortunately, 1,4-dioxane, the solvent typically used for BVO reaction, gave one of the lowest H₂O₂ productivity values. This fact strongly demonstrated the importance of the reaction solvent in the optimisation of direct H₂O₂ formation, since the same catalyst and conditions were employed to perform all the reaction series.

Accordingly, MeOH was selected as the most suitable solvent for *in situ* H₂O₂ production, given that the MeOH/H₂O mixture was deliberately excluded from the screening due to the negative role played by H₂O in the BVO system, since as described in Section 3.3.3, even traces of H₂O can promote hydrolysis of the desired lactone to 6-HHA.

After the determination of the most suitable catalyst (1Pd-1Au/TiO₂₍₄₀₀₎) and solvent (MeOH) for *in situ* H₂O₂ production, supported by the experimental studies described in this and the previous section, attention was focused on the investigation of potential modification of BVO reaction conditions with the aim of increasing its compatibility for the coupling.

5.3.4 Alternative solvents for BVO reaction

Unfortunately, 1,4-dioxane, the typical solvent employed for BVO reactions, showed very poor capability to be used as solvent in the direct formation of H₂O₂, making the screening of alternative solvents for the BVO reaction essential, in order to increase the compatibility of the two systems to proceed with their coupling.

In regards of this, very few other solvents were successfully reported in literature, at least at the time of this study, for BVO reactions and their efficiency was significantly lower than 1,4-dioxane. Furthermore, ACN, which was one of them, performed very poorly in the preliminary tests for *in situ* H₂O₂ formation (Table 5.4) and hence, discarded from further investigations.

Thus, with the aim of exploring alternative solvents, the same solvents tested for *in situ* H₂O₂ production in the previous section were used as solvents for BVO reaction of CyO to Capr using Sn-β and commercial H₂O₂ (50 wt. % in H₂O). It should be noted that all these solvents presented a lower boiling point than the typical reaction temperatures employed for BVO (100 °C), hence, the following set of reactions was carried out at the standard conditions determined in Section 3.3.3, except the temperature, set up to 50 °C. Reactions were carried out for a period of 4 h and monitored following the procedures described in Section 2.4.1 and kinetic parameters were calculated according to Equations 2.1 to 2.3. The same experimental error of 8 % applied during Chapter 3 and 4 to all BVO reactions was also applied to the kinetic parameters measured for BVO reactions along this chapter. The results obtained are summarised in Table 5.10.

Table 5.10. Solvent screening for BVO reactions.

Solvent	Conversion / %	Yield Capr / %	Capr Selectivity / %	H ₂ O ₂ consumed / %
MeOH	77	7	9	11
EtOH	67	5	7	30
IPA	29	11	39	11
1,4-dioxane	27	22	81	31
Acetone	14	8	54	10

Reaction conditions: 10 mL of 0.33 M CyO in different solvents, 1 mol. % Sn respect to CyO (2Sn- β), 1.5 H₂O₂:CyO, at 50 °C after 4 h of reaction.

As expected from the knowledge gained on the BVO reaction from Chapter 3, the best results in terms of catalytic activity and Capr selectivity were obtained in 1,4-dioxane. It should be mentioned that the selectivity towards Capr obtained was ± 80 %, in agreement with the selectivity trend observed at 50 °C at similar levels of conversion (Fig 3.11, right). Additionally, the H₂O₂ consumed during the reaction in 1,4-dioxane, approximately 30 %, corresponded well to the levels of conversion of CyO achieved, giving a H₂O₂-based selectivity of 87 %, calculated as function of CyO converted per H₂O₂ consumed. Such high H₂O₂-based selectivity indicates a good correlation between the reactivity towards BVO chemistry and the oxidant used.

Unfortunately, the rest of the solvents screened resulted in very poor catalytic activities in terms of selectivity towards Capr, being 54 % in acetone, 39 % in IPA and < 15 % for the others and H₂O₂ consumption which did not correspond to the levels of conversion observed, suggesting that other reactions different to BVO were taking place simultaneously during the experiments. For instance, in IPA some Meerwein Ponndorf Verley (MPV) reaction to cyclohexanol (CyOH) was also observed (9 % CyOH yield). This kind of transfer hydrogenation is well known to be promoted in this kind of solvent and similar catalysts.^{33,34} On the other hand, in MeOH and EtOH media high levels of conversion were achieved, 77 and 67 % respectively, even though only 7 and 5 % of Capr yields were obtained. In both cases, no CyOH was formed, in agreement with the poor performance of both solvents to assist in MPV reaction, which was reported to work better in presence of branched and longer alcohol chain as solvent.³⁵

Thus, in order to elucidate the nature of the high conversion but poor Capr yield observed in MeOH, a detailed analysis on this reaction was carried out as shown in Fig 5.4.

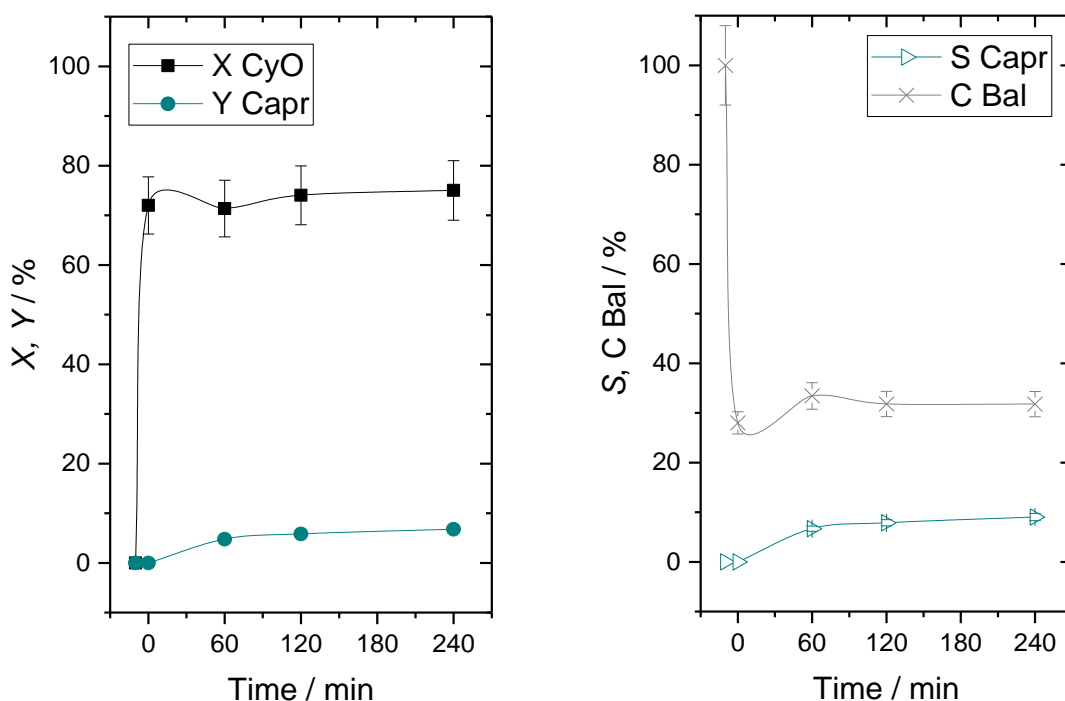


Figure 5.4. Time online analysis of BVO of CyO in MeOH. (Left) Conversion and Capr yield and (Right) selectivity towards Capr and carbon balance as function of time.

The time online analysis of BVO of CyO in MeOH showed that at $t = 0$ (15 min of heating up) very high conversion was already obtained, indicating that during the heating process, and prior to the addition of the oxidant to start the BVO reaction, CyO was already being consumed. After the addition of the oxidant, conversion was maintained $\pm 75\%$ whilst Capr yield slowly increased with time, reaching 7 % after 4 h of reaction. Accordingly, very low selectivity and carbon balance were observed.

In line with the low carbon balance, two unknown peaks were detected by Gas Chromatography equipped with a Flame Ionisation Detector (GC-FID), including at $t = 0$, indicating the presence of other products being formed in the reaction medium prior the addition of H_2O_2 . These two peaks gradually decreased slightly as lactone formation increased.

For a better identification of the products formed, samples at $t = 0$ and 4 h were analysed by proton Nuclear Magnetic Resonance (^1H NMR), as shown in Fig 5.5. ^1H NMR analysis allowed the quantification of 6-HHA by the same methodology of the TMS insert used in Chapter 3 and Chapter 4.

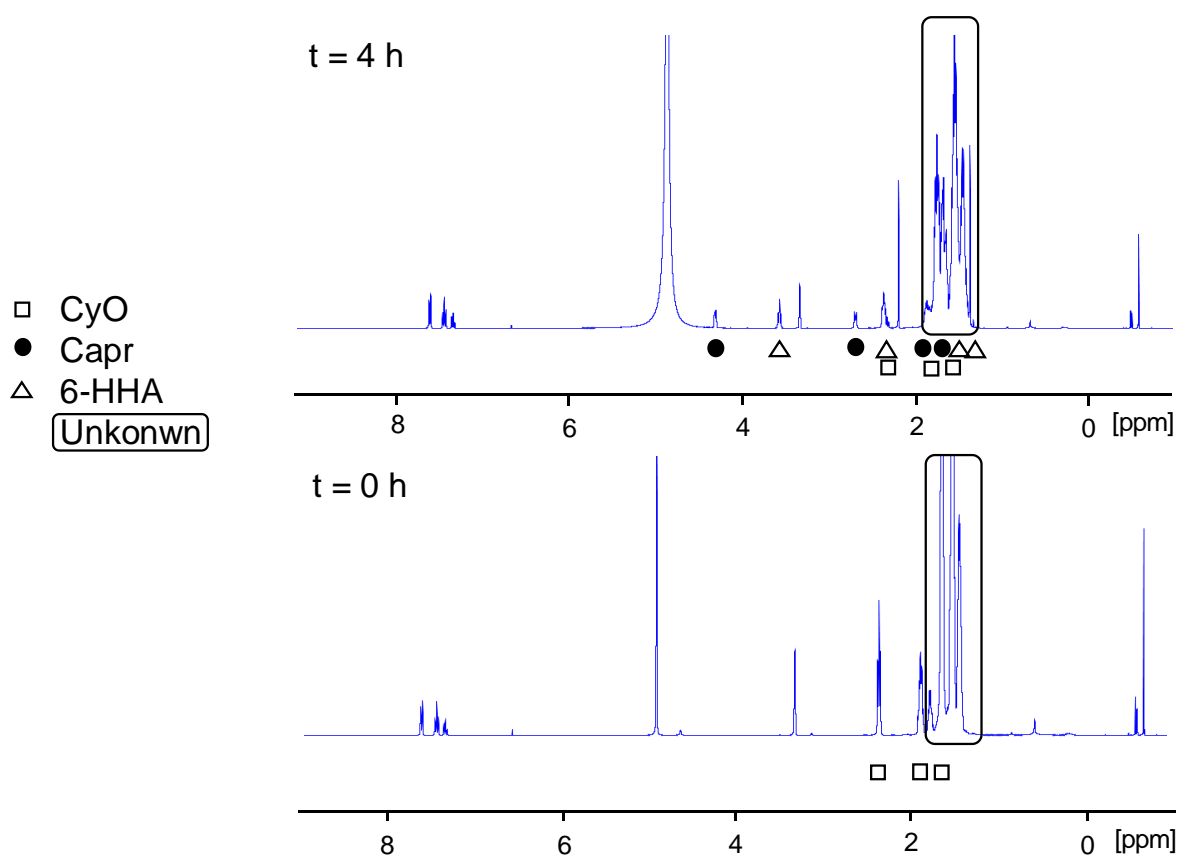
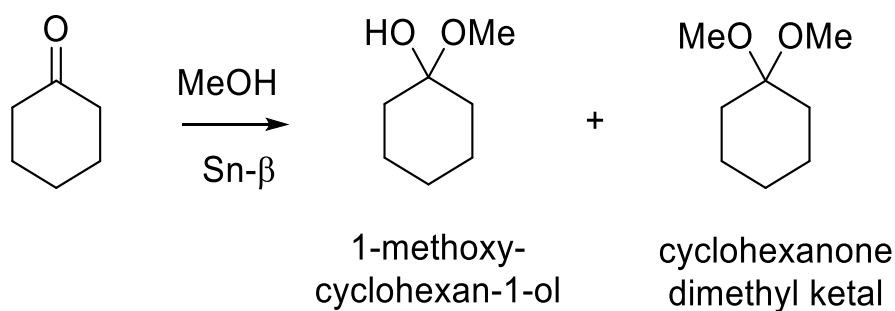


Figure 5.5. ^1H NMR analysis of BVO reaction of CyO in MeOH at $t = 0$ and $t = 4$ h.

Accordingly, 6-HHA yield at 4 h was quantified as 5 % and accounted to increase the final carbon balance only from 32 % to 37 %. This fact suggests that the unwanted parallel reaction taking place is strongly favoured in MeOH.

It was found in literature that CyO can undergo to acetalisation by MeOH in the presence of zeolites, mesoporous silicas or metal organic frameworks to form ketals (Scheme 5.3).^{36,37} Accordingly, it was hypothesised that these two products corresponded to the unknown peaks observed in the GC-FID and ^1H NMR.



Scheme 5.3. Acetalisation reaction of CyO in presence of MeOH and zeolite as catalyst.

Consequently, pure standards of cyclohexanone dimethyl ketal and 1-methoxy-cyclohexan-1-ol were injected in the GC-FID and the identity of the unknown products was confirmed. Acetalisation of CyO to cyclohexanone dimethyl ketal and 1-methoxycyclohexan-1-ol was found to take place during the heating up period, and only following addition of the oxidant was the BVO reaction to Capr found to take place, although in minor proportion in MeOH at 50 °C. Selectivity towards Capr very slowly increased from 7 to 9 %, suggesting that the driving force of BVO was not enough to push the BVO reaction against the acetalisation side reaction. It was hypothesised that the same kind of acetalisation reaction was also taking place in EtOH media, although in minor extension. However, given that the performance of EtOH was significantly lower than MeOH for direct formation of H₂O₂, EtOH was not further investigated. Unfortunately, these experiments show the detrimental effect of MeOH, the best solvent tested for *in situ* H₂O₂ production, as a primary solvent in the BVO system, as it causes a strong decrease in Capr yield with respect to 1,4-dioxane, promoting a side reaction in significant proportions.

5.3.5 Coupling *in situ* H₂O₂ production with BVO in one pot

In the previous sections, it was demonstrated that the best solvents for *in situ* H₂O₂ and BVO reactions performed very poorly in the other system. Very low H₂O₂ productivity was obtained for the *in situ* H₂O₂ system in 1,4-dioxane, whilst very high conversion but low Capr yields were obtained for the BVO of CyO in MeOH, due to the acetalisation of the substrate. In view of this, the replacement of one of the solvents for the other one in the coupling of the two reactions in one pot seemed unlikely to allow to operate in a unique solvent. Furthermore, no other solvents tested for both individual reactions exhibited sufficient suitability for potential coupling of the reactions.

Consequently, attention was focused on the investigation of different mixtures of MeOH/1,4-dioxane that may solve the compatibility issues observed so far.

With this aim, mixtures of MeOH/1,4-dioxane with various ratios, *i.e.* 1:1, 1:3 and 1:9, were tested for *in situ* H₂O₂ production, and the BVO of CyO, and compared with the previous results.

Firstly, solvent mixtures were tested for direct H₂O₂ formation at the determined optimal conditions and compiled in Fig 5.6.

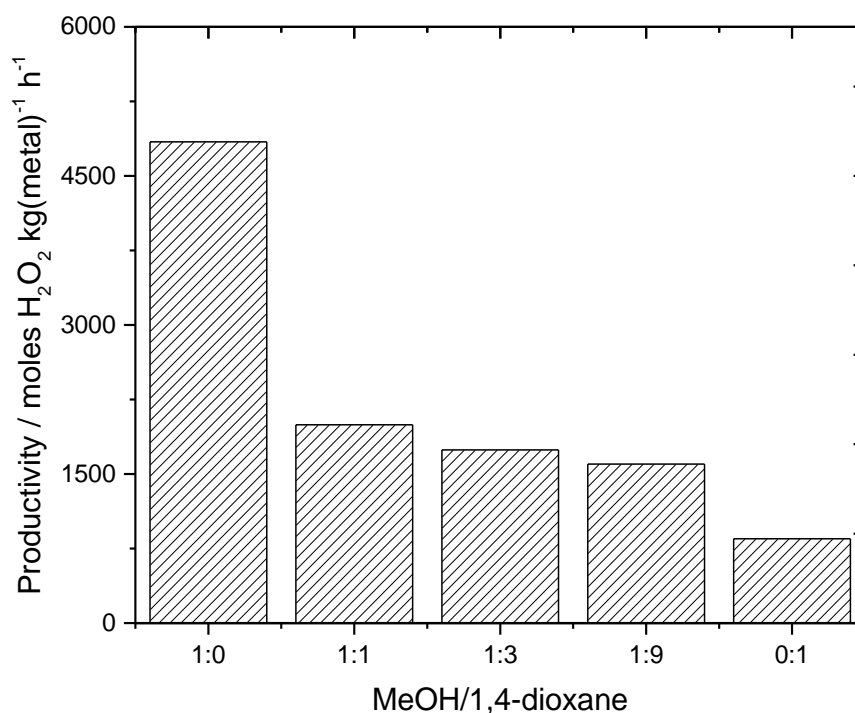


Figure 5.6. Productivity of H₂O₂ obtained in different mixtures of MeOH/1,4-dioxane. Reaction conditions: 10 mL of solvent, 10 mg of 1Pd-1Au/TiO₂(400), 40 bar of 2.5% H₂ / 5% O₂ in CO₂, at 10 °C after 30 min of reaction. H₂O₂ production was quantified by titration with Ce(IV) sulfate and its productivity was calculated as mol of H₂O₂ produced per kg of metal per time.

As can be seen in Fig 5.6, the addition of 1,4-dioxane (1:1) drastically diminished the H₂O₂ productivity by approximately 40 % compared with pure MeOH, from 4843 to 1995 mol H₂O₂ kg(metal)⁻¹ h⁻¹. For the other solvent mixtures, H₂O₂ productivity values gradually decreased, achieving 1742 and 1600 mol H₂O₂ kg(metal)⁻¹ h⁻¹ for 1:3 and 1:9, respectively.

It should be noted that, despite a gradual decrease in productivity caused by the presence of increasing 1,4-dioxane content, mixtures richer in 1,4-dioxane did not overly impact the overall productivity, being only reduced from 1995 to 1600 mol H₂O₂ kg(metal)⁻¹ h⁻¹ for mixtures 1:1 and 1:9 respectively, even though the latter contained very high proportion of 1,4-dioxane.

Furthermore, productivity obtained with 1:9 mixture was significantly higher than with pure 1,4-dioxane, at 1600 and compared to 848 mol H₂O₂ kg(metal)⁻¹ h⁻¹, respectively.

This set of experiments demonstrates again the favourable performance of this reaction in MeOH. The addition of only 10 % of MeOH in the solvent mixtures (1:9), can considerably improve the efficiency of the system respect to pure 1,4-dioxane in the direct synthesis of H₂O₂, by boosting oxidant formation. Despite being three times less productive for direct

formation of H_2O_2 than pure MeOH, the 1:9 mixture may be a good compromise for the coupling of the two systems if this mixture can also perform positively for the BVO reaction. Subsequently, the same solvent mixtures were tested for BVO reaction of CyO with $2\text{Sn-}\beta$ at $50\text{ }^\circ\text{C}$ for a period of 4 h, as shown in Fig 5.7.

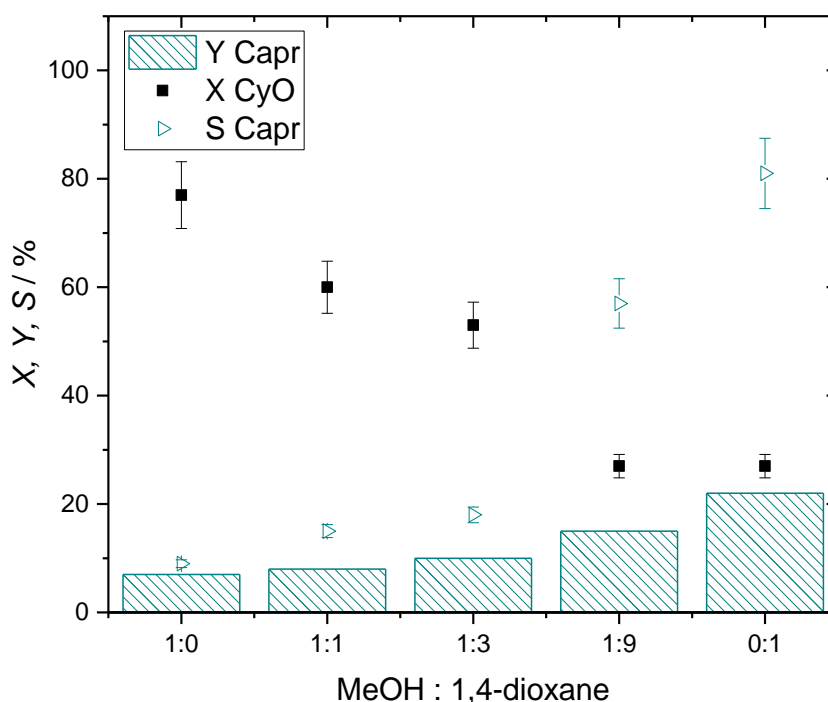


Figure 5.7. Catalytic activity obtained in different mixtures of MeOH/1,4-dioxane for BVO reaction of CyO with $2\text{Sn-}\beta$, at $50\text{ }^\circ\text{C}$, after 4 h of reaction.

As can be seen, conversion gradually decreased with increasing content of 1,4-dioxane present in the reaction medium. For instance, conversion decreased considerably from pure MeOH to 1:1 mixture, from 77 to 60 %, respectively. However, both reactions yielded similar amounts of Capr indicating a significant reduction of the acetalisation side reaction in the presence of some 1,4-dioxane. In fact, from the results it could be noticed that the acetalisation reaction was gradually palliated with increasing 1,4-dioxane content in the solvent mixture, as this side reaction was only able to proceed in MeOH.

Interestingly, the reaction performed using 1:9 mixture displayed the same extent of CyO conversion than the reaction in pure 1,4-dioxane, although the Capr yielded were different. In 1:9 solvent mixture, the BVO reaction proceeded achieving 15 % of Capr yield, whilst in pure 1,4-dioxane, 22 % Capr yield was observed. In view of this, selectivity towards Capr decreased to 57 % in 1:9 solvent mixture, compared with the 81 % achieved in the pure solvent,

suggesting that the 10 % of MeOH present in the reaction mixture was still promoting a certain amount of acetalisation.

Despite this, it should be remarked that selectivity towards Capr was significantly enhanced from < 20 % to 57 % for 1:3 and 1:9 mixture, respectively, highlighting the promising results of the latter. Accordingly, BVO of CyO in 1:9 solvent mixture was analysed in greater detail.

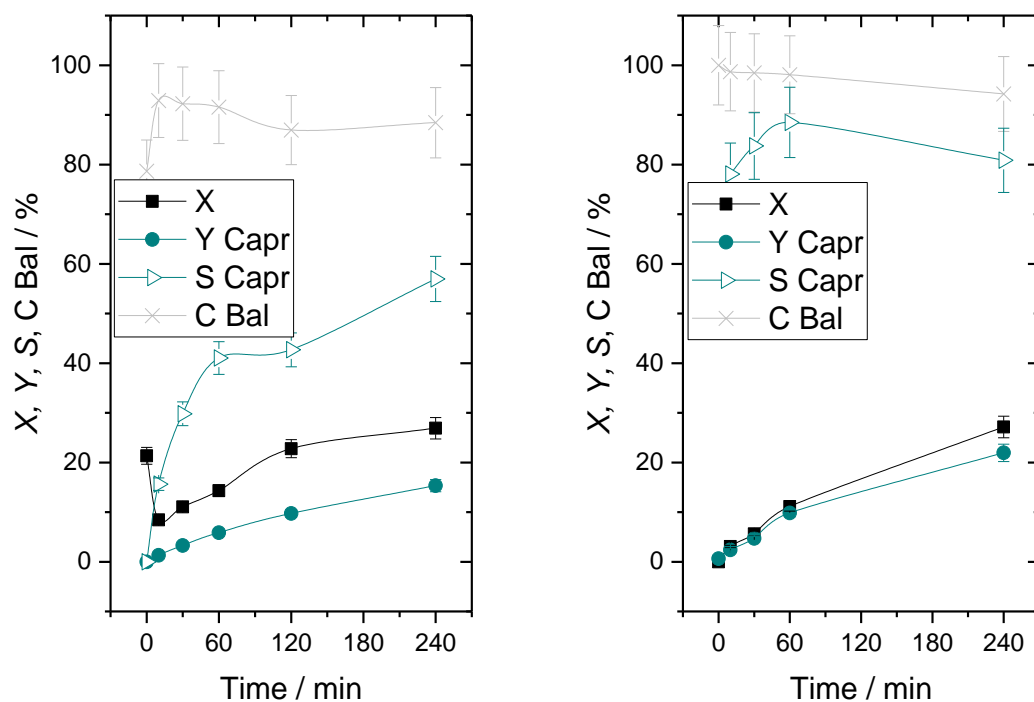


Figure 5.8. Comparison of the catalytic activity obtained for BVO of CyO (Left) in MeOH/1,4-dioxane in a ratio 1:9 and (Right) in pure 1,4-dioxane at 50 °C in 4 h.

As reported in Fig 5.8, left, initial conversion was already 20 %, due to some acetalisation of CyO to ketals occurring during the heating period (analogous to Fig 5.4). Then, following addition of the oxidant, CyO conversion slightly decreased, and the BVO reaction started to take place. In this case, both, Capr yield and its selectivity were increased more notably with time, indicating that in a richer 1,4-dioxane medium, acetalisation of CyO with MeOH was less favoured and the BVO driving force was more able overcome the side reaction. Notably, carbon balance, except at $t = 0$, was maintained close to 90 %, not far from the > 95 % obtained in pure 1,4-dioxane.

Although lower in terms of Capr yield and its selectivity, due to the detrimental effect caused by the presence of some MeOH in the reaction media, compared with reaction in pure 1,4-dioxane (Fig 5.8, right), the results obtained showed potential.

Additionally, final reactant solution in 1:9 mixture was analysed by ^1H NMR in order to quantify the 6-HHA formed, shown in Fig 5.9.

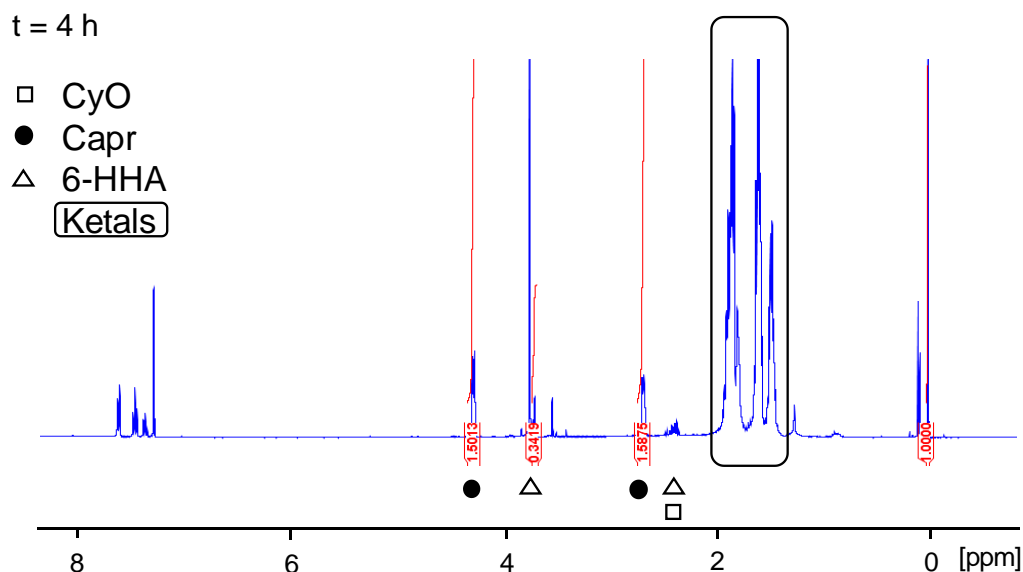


Figure 5.9. ^1H NMR analysis of BVO of CyO in MeOH/1,4-dioxane in a ratio 1:9, after 4 h of reaction.

As shown in Fig 5.9, it could be distinguished the presence of unreacted CyO, Capr, 6-HHA and ketals formed. 6-HHA yield after 4 h of reaction calculated from the analysis was 3 %, corresponding to a selectivity towards 6-HHA of 12 % and contributing to the final carbon balance to increase from 88 % to 92 %. The remaining carbon balance was attributed to ketal formation, although this was not quantified further.

Given the results obtained in the above experiments, the use of a 1:9 mixture of MeOH/1,4-dioxane showed to be the most suitable alternative to couple *in situ* H_2O_2 formation and BVO reaction. Despite lowering the H_2O_2 formed compared with pure MeOH, the effect of the small amount of MeOH introduced in the BVO reaction was justifiable and the results were comparable with pure 1,4-dioxane.

All these experiments thus suggest, that coupling the two systems in one pot requires a high degree of compromise between the most suitable conditions from each individual system, the mixture of solvents being the only viable alternative to proceed and decreasing the typical BVO working temperature.

Nevertheless, it should be reminded that, as was demonstrated in Chapter 3 (Fig 3.11), that the decrease in reaction temperature reduces considerably the reaction rate. Hence, coupling these two systems at low temperature implies a significant decrease in Capr productivity.

Accordingly, a preliminary test in one pot was performed in a stainless-steel autoclave using a physical mixture of 1Pd-1Au/ $\text{TiO}_{2(400)}$ and 2Sn- β in the appropriate amounts, in a 1:9 mixture

of MeOH/1,4-dioxane as solvent, at 40 bar of 2.5 % H₂ / 5% O₂ in CO₂ at 10 °C. This reaction temperature was selected to avoid thermal decomposition of H₂O₂, since it was observed in Section 5.3.1 that higher temperature can significantly affect the thermal stability of H₂O₂. Unfortunately, after 6 h of reaction, no BVO products were detected.

In all likelihood, there were two clear limitations in the coupling of the systems in one pot at the chosen reaction conditions.

Firstly, there was a limitation on the H₂O₂ formed, the higher concentration obtained was 0.05 M for 1Pd-1Au/TiO₂₍₄₀₀₎ in pure MeOH, while in the 1:9 mixture only about 0.017 M was obtained, which was far below the typical oxidant concentration used for BVO reaction (0.5 M). It should be reminded that, as described in Fig 3.9, the BVO initial reaction rate is independent of the oxidant concentration, when using ratio > 0.75:1. However, at lower ratios the initial reaction rate becomes first order dependant respect to the oxidant. Thus, at the concentration reached at the used reaction conditions the initial reaction rate would drastically be decreased.

Secondly, the BVO reaction was highly limited at the chosen working temperature. From the Arrhenius equation reported in Fig 3.12, the reaction time needed to obtain 10 % of CyO conversion (considering the usual 0.5 M of oxidant) could be calculated to be about 17 h, and the reaction was only ran for 6 h. Additionally, batch reactions of *in situ* H₂O₂ formation typically ran for a short period (30 min), since longer reaction times are likely to promote its decomposition as no stabilisers are added to the reaction mixture.

Therefore, when combined, these circumstances likely support the observation that no BVO reaction took place during the attempt to couple the two systems in one pot.

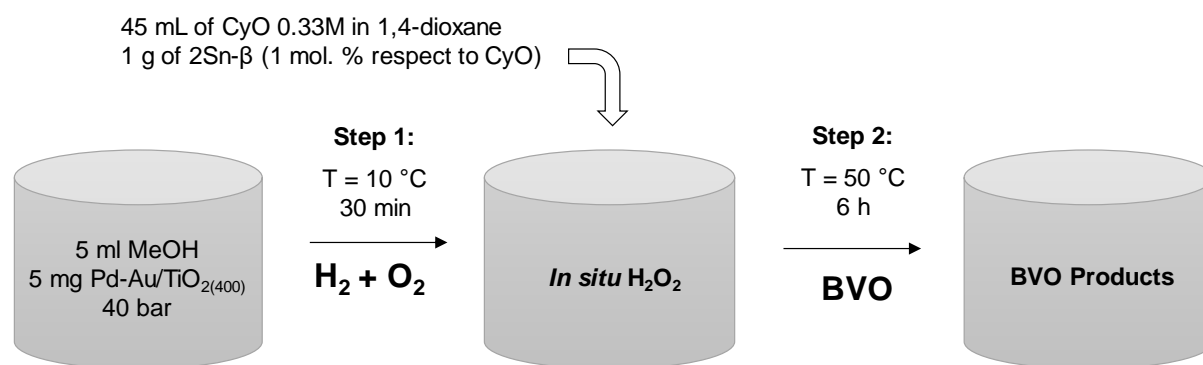
Given that the two reactions required completely different needs, a successful one-pot approach would require scaling up the volume and gas charged to produce higher amounts of oxidant, and the reaction time would need to be extended considerably to be able to detect the lactone product, indicating that coupling *in situ* H₂O₂ formation and BVO reaction in one pot was not possible at this stage.

5.3.5 Coupling *in situ* H₂O₂ production with BVO in two pots

In an alternative approach, the coupling of these two systems can be performed in two pots, by first producing the H₂O₂ *in situ*, and then using it as oxidant for the BVO reaction in a second optimised reaction step.

With the aim of proving the viability of this second approach, the coupling of the two systems was carried out in two individual steps. Firstly, a scaled down version of the *in situ* H₂O₂ reaction was performed (both catalyst and solvent volume were halved) at the reaction conditions optimised along this chapter, *i.e.* using Pd-Au/TiO₂₍₄₀₀₎ in MeOH at 10 °C for 30 min

in a stainless-steel autoclave of 100 mL. Secondly, after H_2O_2 synthesis, the reaction was stopped, the gas released, and the reactor vessel was opened. Subsequently, a solution of the appropriate volume of CyO in 1,4-dioxane, in order to obtain a 1:9 mixture of MeOH/1,4-dioxane (45 ml), and 2Sn- β (1 mol. % respect to CyO) were added into the reactor and the temperature was raised to 50 °C to perform BVO reaction for 6 h.



Scheme 5.5. Representation of the coupling of *in situ* H_2O_2 formation with BVO in two steps.

In this experiment, 15 % of CyO conversion was observed, as in the presence of MeOH some ketal formation occurred. However, 0.1 % of Capr yield was observed after 6 h of reaction, indicating that the H_2O_2 produced *in situ* was indeed able to act as oxidant for the BVO reaction. Herein, despite the very low amount of the desired lactone obtained, this positive result proves the potential of coupling these two reaction systems in two stages. Further discussion of this can be found in Chapter 7.

5.4 Conclusions

Various approaches to reduce the presence of H_2O in the BVO / Sn- β / H_2O_2 reaction system are investigated in this chapter with the aim to boost Capr selectivity by decreasing the hydrolysis reaction of the desired lactone to the corresponding hydroxyhexanoic acid. Upon the difficulties faced for the successful removal of H_2O , *in situ* production of H_2O_2 and its coupling with the BVO / Sn- β are considered, requiring the investigation of both systems separately and the evaluation of the viability to couple them. *In situ* production of H_2O_2 has been successfully reported for the production of low concentrations of H_2O_2 and can avoid the safety transportation and storage issues commonly attached to the commercial aqueous H_2O_2 . Optimisation studies of direct *in situ* H_2O_2 formation from H_2 and O_2 show that high productivity values can be obtained when employing Pd-Au/TiO₂ catalyst in MeOH medium at low reaction temperatures, whilst pure 1,4-dioxane, the most convenient solvent for the BVO reaction, exhibits significantly lower H_2O_2 productivity value during *in situ* H_2O_2 production.

However, a detailed study on MeOH as solvent for the BVO reaction of CyO reveals the detrimental effect of this medium in the BVO reaction rate, since a strongly favoured acetalisation reaction occurs leading to the formation of ketals.

Remarkably, the employment of a solvent mixture MeOH/1,4-dioxane in a ratio 1:9 results in benefits to both systems, improving the H₂O₂ formation compared with pure 1,4-dioxane, and improving the catalytic activity for BVO reaction relative to pure MeOH (at 50 °C), decreasing significantly the acetalisation side reaction without compromising too much the BVO reaction rate obtained in pure 1,4-dioxane.

Accordingly, these results pointed to a solvent mixture MeOH/1,4-dioxane in a ratio 1:9 as the only viable alternative for the coupling of *in situ* H₂O₂ production and BVO reaction, despite implying a big sacrifice on both individual reaction rates.

Unfortunately, coupling the two systems in one pot was unsuccessful, emphasising the very different needs of each reaction system. Nevertheless, a preliminary test in two stages, by first producing the H₂O₂ *in situ* in MeOH at 10 °C and diluting this reaction solution to be 1:9 in 1,4-dioxane for the BVO reaction at 50 °C, successfully proved the feasibility of the overall system to work in two pots.

Although preliminary, this positive last result opens up the possibility to explore this approach in the future. By working in two stages, both systems can be independently optimised in order to increase H₂O₂ productivity and obtain high BVO reaction rates and hence, upgrading the sustainability of the BVO chemistry.

References

- (1) K. Yakabi, K. Milne, A. Buchard, C. Hammond, *ChemCatChem*, 2016, **8**, 3490 – 3498
- (2) A. Corma, P. estev, A. Martinez, S. Valencia, *J Catal.*, 1995, **152**, 18 - 24
- (3) S. Krijnen, P. Sanchez, B. T. F. Jakobs, J. H. C. van Hoof, *Micropor. Mesopor. Mat.*, 1999, **31**, 163 - 173
- (4) M. Boronat, A. Corma, M. Renz, G. Sastre, P. M. Viruela, *Chem. Eur. J.*, 2005, **11**, 6905 – 6915
- (5) A. Corma, L. T. Nemeth, M. Renz, S. Valencia, *Nature*, 2001, **412**, 423 – 425
- (6) Molecular sieves 3A, Alfa Aesar Safety Data Sheet
- (7) A. I. Vogel, B.V. Smith, N.M. Waldron, “*Vogel's Elementary Practical Organic Chemistry 1 Preparations*”, 3rd edition, 1980, London: Longman Scientific & Technical
- (8) C. Samantha, *App. Catal A: General*, 2008, **350**, 133 - 149
- (9) “*Part V. Summary of limits of flammability*”
- (10) J. Garcia-Serna, T. Moreno, P. Biasi, M. J. Cocero, J. Mikkola, T. O. Salmi, *Green Chem.*, 2014, **16**, 2320 - 2343
- (11) G. Li, J. Edwards, A. F. Carley, G. J. Hutchings, *Catal Today*, 2007, **122**, 361 - 364
- (12) J. K. Edwards, B. Solsona, E. Ntainjua, A. F. Carley, A. A. Herzong, C. J. Kiely, G. J. Hutchings, *Science*, 2009, **323**, 1037 - 1041
- (13) E. N. Ntainjua, M. Piccinini, J. C. Pritchard, J. K. Edwards, A. F. Carley, C. J. Kiely, G. J. Hutchings, *Catal. Today*, 2011, **178** (1), 47 - 50
- (14) S. Abate, P. Lanzafame, S. Perathoner, G. Centi, *Catal. Today*, 2011, **169**, 167 - 174
- (15) E. N. Ntainjua, S. J. Freakley, G. J. Hutchings, *Top Catal.*, 2012, **55**, 718 - 722
- (16) S. J. Freakley, Q. He, J. H. Harry, L. Lu, D. A. Crole, D. J. Morgan, E. N. Ntainjua, J. K. Edwards, A. F. Carley, A. Y. Borisevich, C. J. Kiely, G. J. Hutchings, *Science*, 2016, **351**, 965 - 968

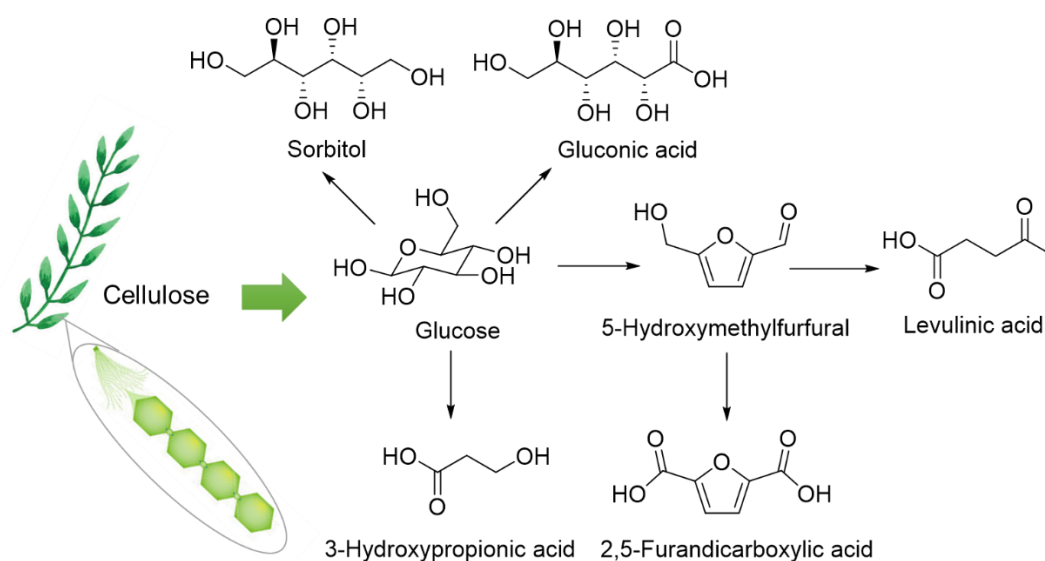
- (17) N. Lee, Y. M. Chung, *Res. Chem. Intermed.*, 2016, **42**, 95 - 108
- (18) G. Li, J. K. Edwards, A. F. Carley, G. J. Hutchings, *Catal Commun.*, 2007, **8**, 247 - 250
- (19) I. Moreno, N. F. Dummer, J. K. Edwards, M. Alhumaimess, M. Sankar, R. Sanz, P. Pizarro, D. P. Serrano, G. J. Hutchings, *Catal. Sci. Technol.*, 2013, **3**, 2425 - 2434
- (20) A. Villa, S. J. Fraekley, M. Schiavoni, J. K. Edwards, C. Hammond, G. M. Veith, W. Wang, D. Wang, L. Prati, N. Dimitratos, G. J. Hutchings, *Catal. Sci. Technol.*, 2016, **6**, 694 - 697
- (21) S. Abate, S. Melada, G. Centi, S. Perathoner, F. Pinna, G. Strukul, *Catal. Today*, 2006, **117**, 193 - 198
- (22) G. Bernardotto, F. Menegazzo, F. Pinna, M. Signoretto, G. Cruciani, G. Strukul, *Appl. Catal. A*, 2009, **358**, 129 - 135
- (23) V. R. Choundhary, C. Samanta, *J. Catal.*, 2006, **238**, 28 - 38
- (24) J. A. Lopez-Sanchez, N. Dimitratos, P. Meiedziak, E. N. Ntainjua, J. K. Edwards, D. Morgan, A. F. Craley, R. Tiruvalam, C. J. Kiely, G. J. Hutchings, *Phys. Chem. Chem. Phys.*, 2008, **10**, 1921 - 1930
- (25) J. Li, T. Ishihara, K. Yoshizawa, *J. Phys. Chem. C*, 2011, **115**, 25359 - 25367
- (26) J. K. Edwards, S. J. Freakley, R. J. Lewis, J. C. Protchard, G. J. Hutchings, *Catal Today*, 2015, **248**, 3 - 9
- (27) M. Santonastaso, S. J. Freakley, P. J. Miedziak, G. L. Brett, J. K. Edwards, G. J. Hutchings, *Org. process Res. Dev.*, 2014, **18**, 1455 - 1460
- (28) F. Cavani, J. H. Teles, *ChemSusChem*, 2009, **2**, 508 - 534
- (29) A. Corma, L. T. Nemeth, M. Renz, S. Valencia, *Nature*, 2001, **412**, 423 - 425
- (30) J. A. Jennings, S. Parkin, E. Munson, S. P. Delaney, J. L. Calahan, M. Isaacs, K. Hong, M. Crocker, *RSC Adv.*, 2017, **7**, 25987 - 25997
- (31) N. Dimitratos, J. A. Lopez-Sanchez, D. Morgan, A. F. Carley, R. Tiruvalam, C. J. Kiely, D. Bethell, G. J. Hutchings, *Phys. Chem. Chem. Phys.*, 2009, **11**, 5142 - 5153
- (32) J. Pritchard, L. Kesavan, M. Piccinini, Q. He, R. Tiruvalam, N. Dimitratos, J. A. Lopez-Sanchez, A. F. Carley, J. K. Edwards, C. J. Kiely, G. J. Hutchings, *Langmuir*, 2010, **26** (21), 16568 - 16577
- (33) C. Hammond, D. Padovan, A. Al-Nayili, P. P. Wells, E. K. Gibson, N. Dimitratos, *ChemCatChem* 2015, **7**, 3322 - 3331
- (34) R. López-Asensio, J. A. Cecilia, C. P. Jiménez-Gómez, C. García-Sancho, R. Moreno-Tost, P. Maireles-Torres, *App. Catal A, General*, 2018, **556**, 1 - 9
- (35) R. A. W. Johnstone, A. H. Wilby, *Chem. Rev.*, 1985, **85**, 129 - 170
- (36) Y. Tanaka, N. Sawamura, M. Iwamoto, *Tetrahedron Letters*, 1998, **39**, 9457 - 9460
- (37) A. Dhakshinamoorthy, M. Álvaro, H. García, *Adv. Synth. Catal.*, 2010, **352**, 3022 - 3030

6. Chemo-selective lactonization of renewable succinic acid with heterogeneous catalysts

6.1. Introduction

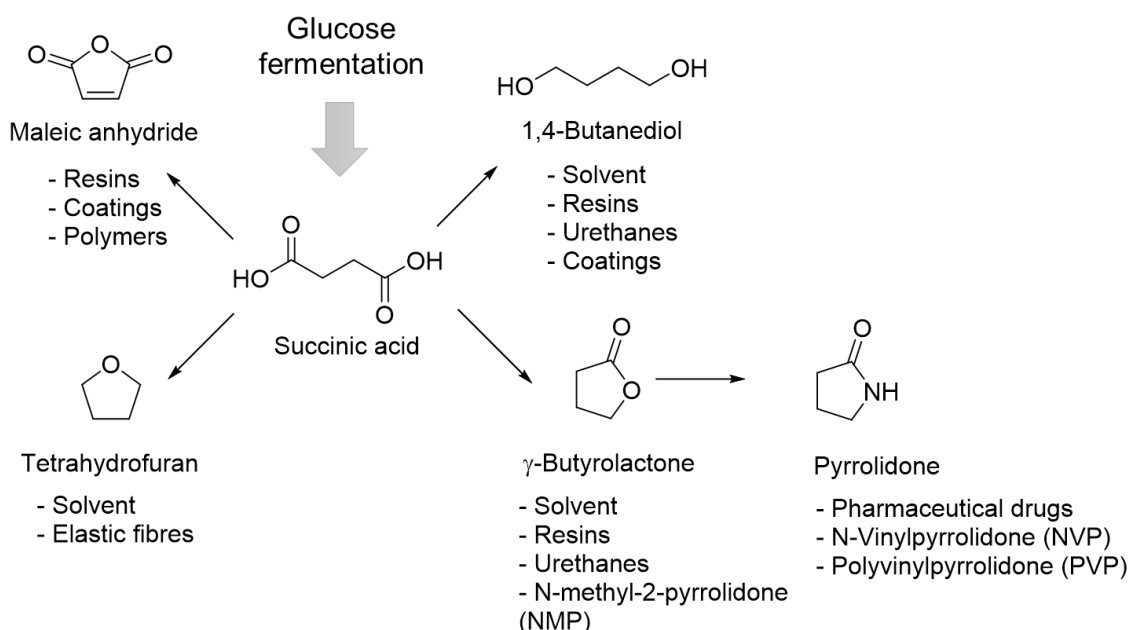
As discussed in Chapter 1, renewable feedstock utilisation has become increasingly demanded as a green alternative in order to replace the limited repository of fossil fuel feedstocks, the most common feedstock in use.^{1,2} In this regard, biomass represents one of the most promising renewable feedstocks to be employed to produce biofuels, commodity chemicals and new bio-based materials such as bioplastics.³⁻⁵ Some of its multiple advantages rely on its high functionality and chemical diversity, which allow a reduction in the number of processing steps for functional group insertions, and permit higher carbon chain length molecules (C4+), typically not present in other emerging feedstocks to be obtained.^{6,7} Moreover, utilisation of second generation biomass, such as lignocellulose, results in a lower lifecycle CO₂ emission, higher productivity in terms of sugar produced per acre and per unit time, no competition with food crops, unlike other first generation biomass such as bio-ethanol, and it can be grown on marginal land.^{8,9} For instance, cellulose, the most abundant component of lignocellulose, accounts for the 60 - 90 % (by weight) of all bio-renewable material, and therefore represents the most viable and sustainable source of carbon chemical production.¹⁰

Amongst possible strategies for converting cellulose into valuable chemicals, catalytic methodologies offer several advantages, particularly in the context of process intensification. Of these strategies, one of the most promising involves the catalytic conversion of various 'platform' molecules, obtained by controlled depolymerisation or fermentation of cellulose.¹¹ Some of the most relevant examples include glucose, fructose, 5-hydroxymethylfurfural, 2,5-furandicarboxylic acid, 3-hydroxypropionic acid and glycerol, amongst others (Scheme 6.1).^{12,13}



Scheme 6.1. Some relevant catalytic routes to convert cellulose into different platform molecules.

In fact, the catalytic conversion of several of these platform molecules has received an enormous amount of attention over the last decade. However, despite the surge of interest in renewable chemical production from these platform molecules, a number of other platforms with high potential have received relatively little attention. A key example is succinic acid (SA).^{14,15} Classically obtained by the hydrogenation of butane-derived maleic anhydride, thanks to biotechnological advances SA can now be produced from renewable biomass *via* enzymatic fermentation of glucose on a kiloton scale, as demonstrated by several companies.¹⁶⁻¹⁹ Its advanced stage of production *via* sustainable processes, and its widely accepted high potential as C4 platform molecule, since it has been included in the top list of building block molecules for the production of high value chemicals²⁰ point to SA as being one of the strategic platform molecules with high interest for future industrial applications.²¹ As a matter of fact, an important number of commodity chemicals, including 1,4-butanediol (BDO), tetrahydrofuran (THF) and γ -butyrolactone (GBL), can be obtained from SA over a suitable catalytic material (Scheme 6.2).



Scheme 6.2. Potential routes for renewable SA valorisation.

Of particular interest is the reductive valorisation of SA to BDO and GBL, which are key monomers in the polymer industry.^{22,23} For instance, GBL was normally considered to be a “non-polymerizable” monomer due to the low strain energy of the five-membered ring. However, it has been recently successfully polymerised through ring opening mechanism and used efficiently as co-monomer to modulate material properties of polyesters.^{24,25} Furthermore, the conversion of SA to GBL has been identified as one of the most technologically attractive processes, as it opens routes towards various commodity compounds and additional downstream monomers, such as 2-pyrrolidone.^{13,26,27}

Typically, hydrogenation of SA to BDO, GBL and THF is carried out with the assistance of heterogeneous catalysts, especially metal supported nanoparticles. Interestingly, the catalytic activity of SA towards these three main products (high selectivity) can be turned by varying both the type of catalyst and the reaction conditions applied. Predominantly, these reactions are conducted in the gas-phase or in organic solvents, such as 1,4-dioxane.^{28,29} However, in the last decades, some interesting examples of SA aqueous hydrogenation, an important medium when using renewable derived compounds, have also been reported.³⁰⁻³³ In terms of reaction conditions, it has been shown that parameters such as temperature or pressure play an important role. Generally, selectivity towards THF increases with pressure and temperature, whilst BDO formation is usually favoured at lower temperatures.

In Table 6.1, some of the most relevant reports regarding SA reductive valorisation to GBL are compiled. There, it can be seen that although classical hydrogenation catalysts, such as supported Ru or Pd nanoparticles, have been shown to be active heterogeneous catalysts for

this reaction, generally, high reaction temperatures (up to 240 °C) and high pressures (up to 80 bar), and usually long reaction times have previously been required in order to reach high levels of product yield.

Table 6.1. Comparison of reaction conditions and GBL productivities reported in the literature.

Entry	T / °C	P / bar	Catalyst GBL productivity / $\text{g g(cat)}^{-1} \text{h}^{-1}$	Reactor GBL productivity / $\text{g cm}^{-3} \text{h}^{-1}$	$S_{\text{GBL}} / \%$	Reference
1	240	40	0.319	1.59×10^{-3}	95	29
2	240	80	0.039	4.38×10^{-4}	66	32
3	220	80	0.465	4.65×10^{-3}	64	33
4	200	60	0.173	1.39×10^{-3}	95	34
5	240	60	0.307	1.23×10^{-3}	72	35
6	240	30	0.364	2.43×10^{-3}	94	36
7	200	80	0.165	3.32×10^{-4}	88	37
8	240	30	0.230	4.61×10^{-3}	65	38
9	160	150	0.082	6.81×10^{-4}	95	39
10	180	80	0.398	9.96×10^{-3}	69	40
11	240	80	0.398	3.98×10^{-3}	61	41

For example, the processes which reported the highest GBL productivity (Table 6.1, Entries 3, 10 and 11) operate with very high pressure, and their selectivity towards GBL was < 70 %. On the contrary, processes which reported high selectivity towards GBL usually display lower productivity values. Therefore, it is clear that investigation of the overall reaction network, and particularly the selective production of one particular reaction product, has not yet been achieved.

Although achieving high levels of selectivity during the upgrading of bio-renewables is especially challenging, given their high levels of functionality and reactivity, it is an essential

task given the economic and energetic cost of downstream separation. In regard of this, the nature of the metal and/or combination of metals present in the catalyst, the type of supporting material and the nature of their interactions, will determine the selectivity towards certain products. The metal loading and preparation method are also likely to be highly influential for catalytic performance.

Herein, this chapter is focused on the investigation of suitable catalysts for SA hydrogenation, with special interest paid to achieving high selectivity towards GBL, by:

- i) The optimisation of the reaction conditions.
- ii) The optimisation of the catalyst design by selecting the proper metal, support and preparation method.

6.2 Results and discussion

6.2.1 Preliminary studies for SA hydrogenation

As already mentioned, the catalytic hydrogenation of SA can result in a variety of important commodity chemicals, including THF, GBL and BDO, amongst others. Given how the reaction conditions can impact the overall activity and selectivity, the choice of reaction conditions including time, temperature, pressure and catalyst loading required optimisation for the highest levels of performance to be achieved.

Based on the reported ability of Ru nanoparticles to hydrogenate SA, preliminary studies for the optimisation of the reaction conditions were performed with a commercially available Ru/Al₂O₃ catalyst (5 wt. % Ru, reduced, henceforth denoted 5Ru/Al₂O₃(COM)). Firstly, a series of experiments varying the reaction temperature from 140 to 270 °C was carried out at different times (from 1 to 4 h) in order to identify the optimal reaction temperature for SA catalytic hydrogenation.

Preliminary reaction conditions involved 15 mL of 0.2 M SA in 1,4-dioxane, 15 bar of H₂, and 1 mol. % of Ru with respect to SA, at different reaction temperatures and times. Reactions were carried out following the experimental procedure described in Section 2.4.8, and were monitored by High Performance Liquid Chromatography (HPLC) and Gas Chromatography (GC). The total product yields obtained as function of the working temperature employed are summarised in Fig 6.1, left.

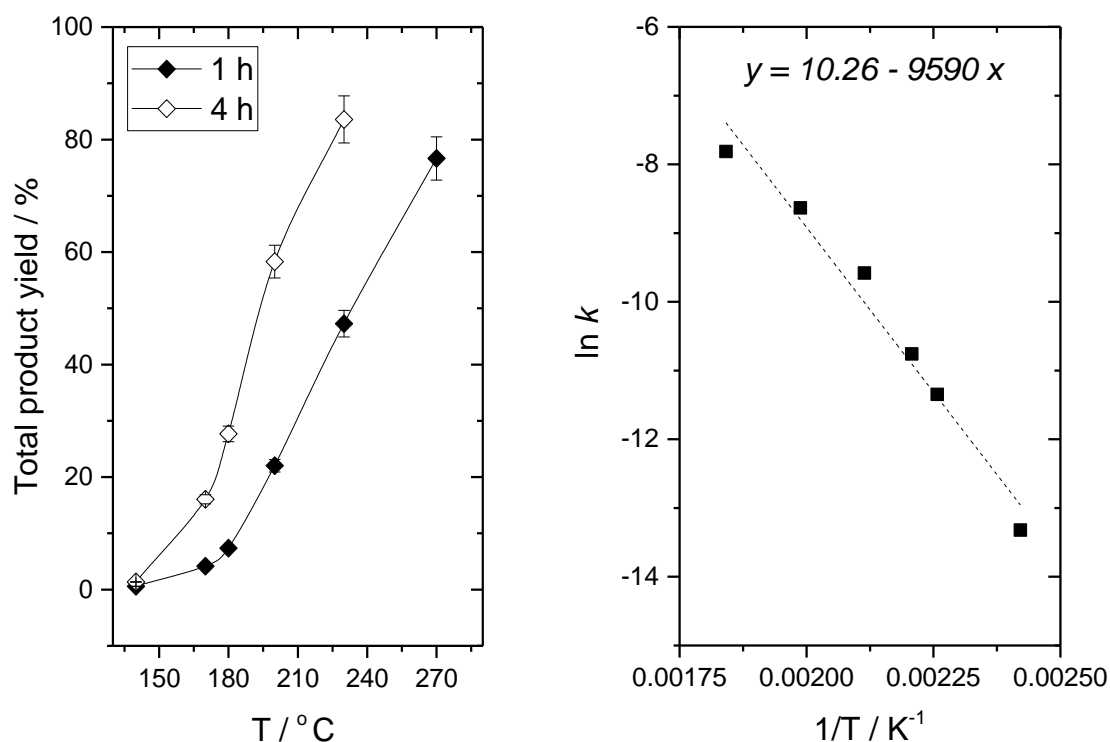


Figure 6.1. (Left) Total product yield obtained from the hydrogenation of SA over $5\text{Ru}/\text{Al}_2\text{O}_3(\text{COM})$ at various reaction temperatures for 1 h and 4 h of reaction time and (Right) Arrhenius plot determined from the effective rate constant at 1 h of reaction at various temperatures. Reaction conditions: 15 mL of 0.2 M SA in 1,4-dioxane, 1 mol. % of Ru respect to SA, 15 bar H_2 .

As can be seen in Fig 6.1, increasing the time (4 h vs. 1 h) and the temperature (140 - 270 °C) of the reaction resulted in an increased amount of product yielded from SA. Under the stated reaction conditions, a maximum product yield of approximately 80 % was achieved, at temperatures of 230 and 270 °C for 4 h and 1 h reactions, respectively.

Subsequently, the series of experiments carried out for 1 h of reaction were used to determine the effective rate constant of each reaction (Equation 6.1) based on the total product yield obtained:

$$k_{eff} = \frac{-\ln(1 - \text{Total product yield}/100)}{\text{time}} \quad [\text{Equation 6.1}]$$

Where time is expressed in seconds and k_{eff} units corresponds to a first order rate constant.

Comparison of k_{eff} at different temperatures allowed a preliminary Arrhenius expression for $5\text{Ru}/\text{Al}_2\text{O}_3(\text{COM})$ to be generated according to Equation 3.3 (Figure 6.1, right). This revealed the activation energy of the system to be 79.7 kJ mol^{-1} .

Although different product distributions were observed depending on the temperature employed, it should be mentioned that all reaction yielded to the same major products: GBL and propionic acid (PA), small amounts of butyric acid (BA) and some traces of BDO, whereas no THF was produced, even at the highest temperature tested (270°C). Additionally, traces ($< 1 \text{ mol. \%}$ carbon) of CO_2 , methane (CH_4), ethane (C_2H_6) and propane (C_3H_8) were detected in the gas phase. In total, these products and the remaining unconverted substrate accounted for $> 95 \%$ of the carbon balance calculated in each of these reactions.

To gain a better insight of how the choice of temperature and time influence the overall reaction performance, the product distribution obtained after 4 h of reaction between $170 - 230^\circ\text{C}$ was investigated in greater detail. Consequently, more thorough analysis was performed by repeating reactions at 170 , 200 and 230°C for various periods of times (Fig 6.2).

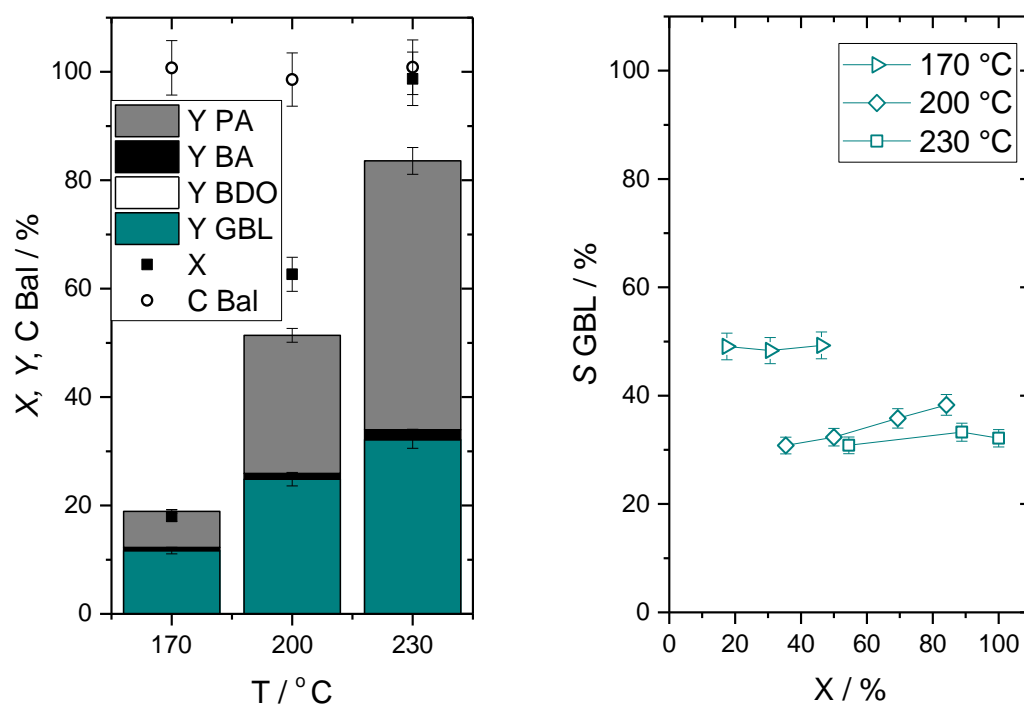


Figure 6.2. (Left) Product distribution obtained following the hydrogenation of SA by $5\text{Ru}/\text{Al}_2\text{O}_3(\text{COM})$ at various reaction temperatures for 4 h and (Right) *iso-conversion* profile obtained between $170 - 230^\circ\text{C}$ for GBL selectivity. Reaction conditions: 15 mL of 0.2 M SA in 1,4-dioxane, 1 mol. % of Ru respect to SA, 15 bar H_2 at the stated working temperature.

As can be seen in Fig 6.2, left, the product distribution was highly dependent on the reaction temperature. By plotting the GBL selectivity observed at several points of SA conversion (Figure 6.2, right),⁴² it can be noticed how, at overlapping levels of conversion, high temperature (230 °C) favoured PA formation with a selectivity ± 50 %, whilst selectivity towards GBL was ± 30 %. However, as the reaction temperature decreased, selectivity towards PA was slowly lowered in benefit to GBL selectivity, resulting in selectivity to PA of 32 % and a selectivity to GBL of 50 % at 170 °C. Interestingly, at each reaction temperature, the GBL selectivity was almost invariant at all levels of product yield, indicating that formation of GBL and PA were not related with $5\text{Ru}/\text{Al}_2\text{O}_3(\text{COM})$, *i.e.* consecutive conversion of these products appears to be unlikely. Therefore, it was clear that the GBL selectivity was always higher at lower reaction temperatures. Given the potential of the SA-GBL process, in addition to the desire of maximising the process selectivity during biomass conversion, all further experiments were conducted at 170 °C, as this provided the best level of selectivity towards GBL.

Further control experiments to evaluate whether the reaction occurred in a catalysed manner, were carried out at the same reactions conditions, but in absence of catalyst or hydrogenating agent (H_2). The results are summarised in Table 6.2.

Table 6.2. Catalytic activity of SA hydrogenation obtained for different control experiments.

Type of reaction	Yield GBL / %	Yield PA / %
Catalyst, H_2	11.6	6.6
H_2 only	0	0
Catalyst only	0	0

Reaction conditions: 15 mL of 0.2 M SA in 1,4-dioxane, at 170 °C for 4 h of reaction with 1 mol. % of Ru respect to SA and 15 bar H_2 where appropriate.

This set of experiments revealed that in the absence of catalyst or H_2 , no conversion of SA was observed, confirming the heterogeneous and hydrogenative nature of the reaction, respectively.

Once the optimal reaction temperature was established (170 °C), the reaction was repeated several times for a period of 4 h to permit determination of the experimental errors (Annex). Based on this, an experimental error of 9 % was applied to the relevant kinetic parameters in all further experiments (conversion (X), yield (Y), selectivity (S) and carbon balance (C Bal)).

Subsequently, the effect of other parameters involved such as pressure and mol. % of catalyst with respect to SA were investigated, in order to ensure maximal GBL productivity.

6.2.1.1 Optimisation of the initial H₂ pressure

Firstly, the initial pressure was varied from 5 to 40 bar of H₂ in a set of experiments carried out for 2 h, using 1 mol. % of Ru at 170 °C. These results are compiled in Fig 6.3.

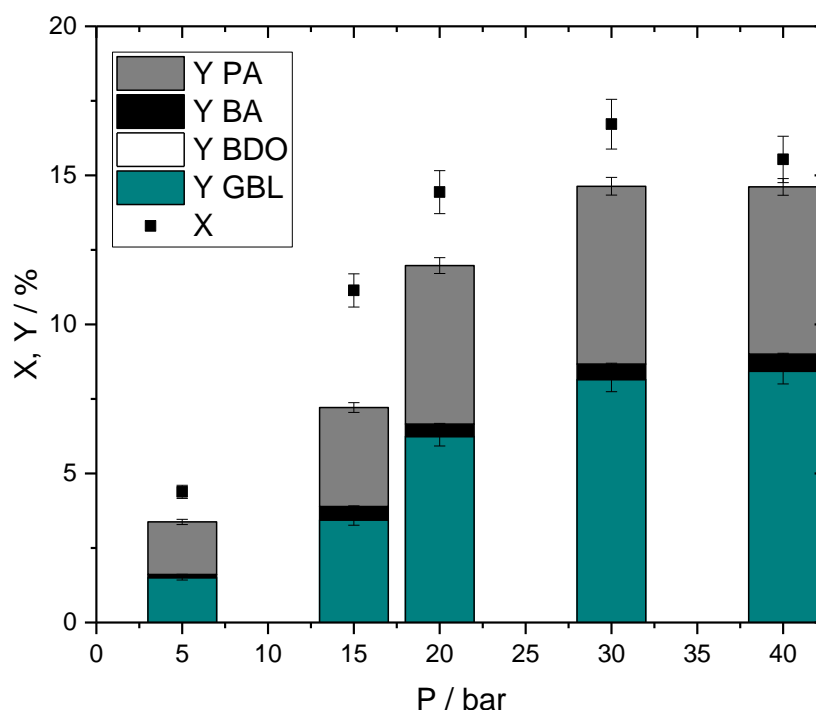


Figure 6.3. Impact of initial H₂ pressure during the hydrogenation of SA by 5Ru/Al₂O₃(COM) at 170 °C. Reaction conditions: 15 mL of 0.2 M SA in 1,4-dioxane, at 170 °C for 4 h of reaction with 1 mol. % of Ru respect to SA and the stated H₂ pressure.

As reported in Fig 6.3, catalytic activity could be improved by increasing the initial H₂ pressure from 5 to 30 bar. However, above this level of initial H₂ pressure, no increase in the reaction rate was observed, indicating the presence of sufficient H₂ in the reaction medium to perform the reaction independently from its initial pressure. Importantly, selectivity towards GBL was not overly affected by modifying the reaction pressure under the influence of 5Ru/Al₂O₃(COM), and comparable selectivity to both GBL and PA were always observed across the entire initial H₂ pressure range tested. Additionally, the carbon balance obtained for this set of experiments was > 98 % across the whole pressure range tested.

It should be mentioned that the reactor used was equipped with a bursting disk with a maximum operational pressure of 65 bar, and that after the heating process, with the additional autogenic pressure generated when using 40 bar of H₂, the pressure was close to 60 bar.

Hence, for safety considerations and given that no further improvement in terms of catalytic activity was observed between 30 and 40 bar of initial H₂ pressure, 30 bar was selected as the optimal initial H₂ pressure for all further experiments.

6.2.1.2 Optimisation of the catalyst loading

Subsequently, a second set of experiments, varying the catalyst loading (catalyst mass) used during the reaction, from 0.5 to 5 mol. % of Ru with respect to SA, was carried out to elucidate the suitable mass of catalyst to be employed in order to ensure catalytic performance in the kinetic regime.

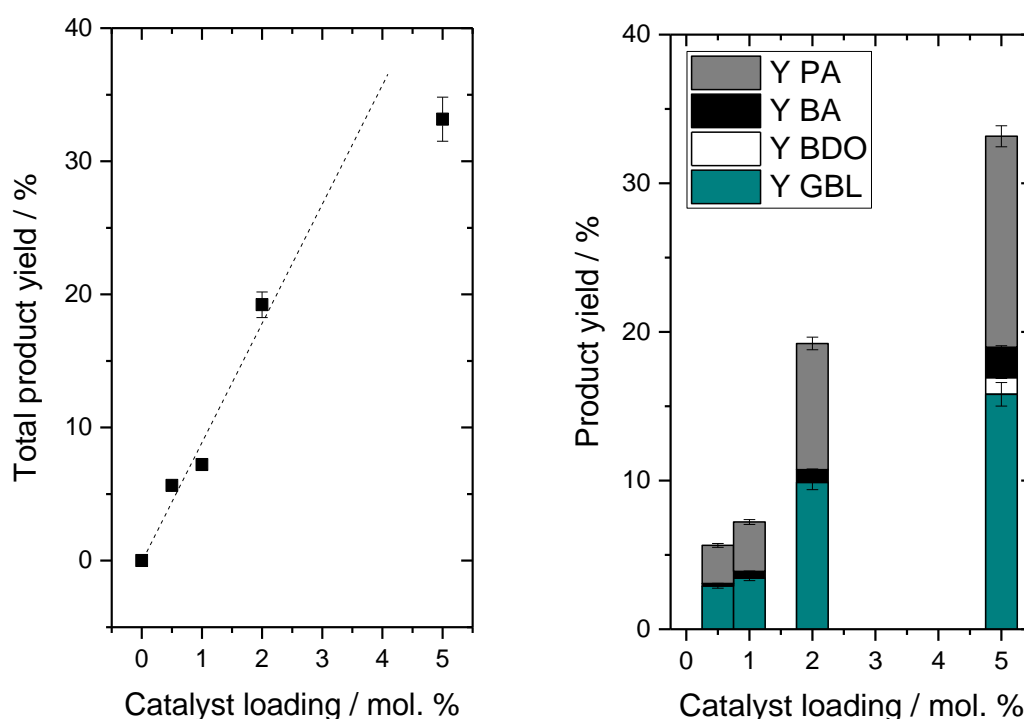


Figure 6.4. Impact of catalyst loading (catalyst mass) during the hydrogenation of SA by 5Ru/Al₂O₃(COM) at 170 °C, 15 bar of H₂ after a period of 2 h of reaction.

As revealed in Fig 6.4, left, a linear relationship between catalyst loading and initial rate of reaction (based on total product yield) could be observed up to catalyst loadings of 2 mol. % Ru. However, at the highest levels of catalyst loading (5 mol. % of Ru, corresponding to 0.3 g of catalyst mass) the reaction rate deviated from linear, reaching lower total product yield than expected. Hence, potential contributions from transport limitations may occur at the highest levels of catalyst loading.

Interestingly, analysis of the products yielded along this set of experiments (Fig 6.4, right) displayed similar product distributions, suggesting that selectivity towards GBL was not overly

affected by modifying the catalyst mass in the reaction and comparable selectivity to both GBL and PA were always observed across the entire catalyst loading range (mol.%) tested. Thus, it is clear that optimal performance in terms of catalytic activity, GBL selectivity and process favourability is achieved at 170 °C, initial H₂ pressures of 30 bar, and catalyst loadings of 2 mol. % or lower.

Accordingly, a time online analysis of SA hydrogenation using 5Ru/Al₂O₃(COM) was carried out by performing individual reaction runs for different periods of time, at 0.5 mol. % of Ru loading. This set of experiments aimed to evaluate the catalytic performance at the chosen optimal conditions, and to identify the evolution of product distribution, especially selectivity towards GBL, across the whole reaction period.

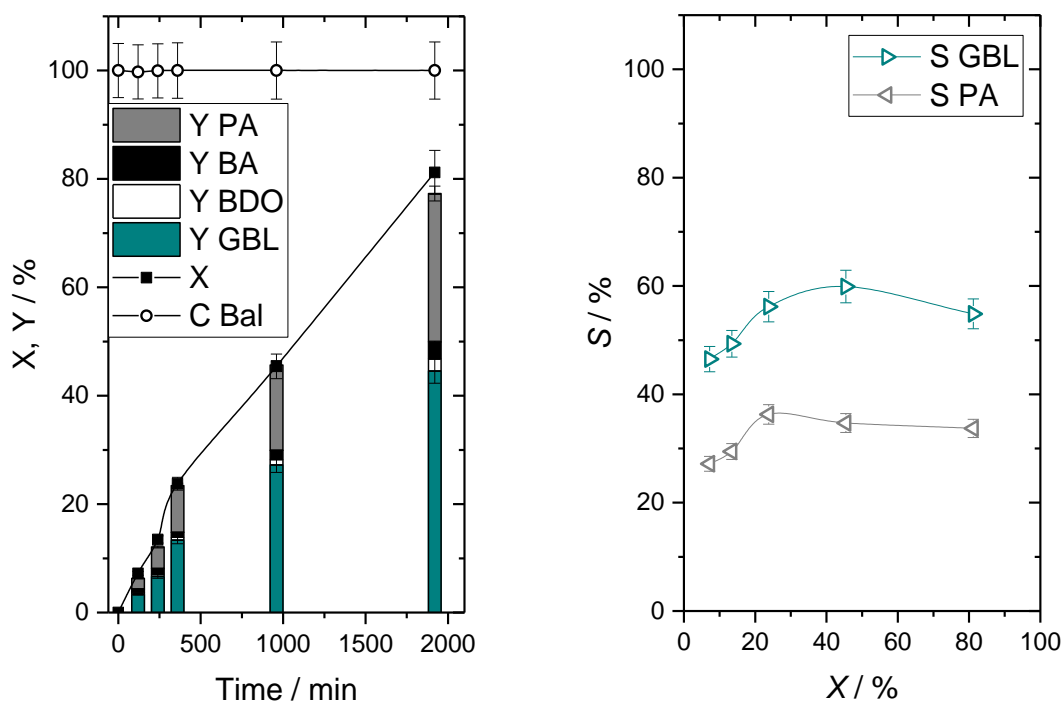


Figure 6.5. (Left) Time online analysis obtained at the optimal reaction conditions and (Right) selectivity to GBL and PA as function of SA conversion. Reaction conditions: 15 mL of 0.2 M SA in 1,4-dioxane, at 170 °C, 0.5 mol. % of Ru respect to SA and 30 bar H₂.

As shown in Fig 6.5, left, conversion gradually increased, reaching levels of 46 and 80 % after 16 and 32 h of reaction, respectively. The carbon balance obtained at the end of each individual reaction was around 100 %, suggesting that no unaccounted products were formed, even at high levels of conversion. It should be highlighted that product distribution remained unchanged across the whole reaction period, and, as observed in Fig 6.5, right, selectivity towards GBL could be maintained between 45 - 60 % along the whole extent of reaction. In

contrast, selectivity towards PA was lower, between 25 - 35 %. This fact strongly suggests, as it was briefly previously mentioned, that the production of GBL and PA are conducted through two different reaction pathways and not by consecutive reactions. Hence, more detail of this aspect is discussed in following sections.

6.2.2 Preliminary identification of the reaction network

From the preliminary studies aimed at elucidating the optimal reaction conditions, it was shown that the main products from the liquid-phase were GBL, PA and some BA and BDO and the gas-phase products detected were traces of CO₂, CH₄, C₂H₆ and C₃H₈.

Accordingly, to gain a greater understanding of the reaction system, product stability studies were performed to investigate the possible interconversion between the products formed during the reaction. This study was performed by substituting the SA substrate from the reaction mixture with other feasible products of the reaction network, including PA, BA, GBL and BDO, and testing their reactivity as substrates under the same reaction conditions.

Table 6.3. Product stability studies performed under typical reaction conditions.

System	Y GBL / %	Y PA / %	Y BA / %	Y BDO / %
GBL, H ₂ , catalyst	-	1.8	3.0	0.9
BDO, H ₂ , catalyst	1.3	-	0	0
PA, H ₂ , catalyst	0.2	0.5	-	0
BA, H ₂ , catalyst	0	0.4	0	-
GBL, H ₂ , no catalyst	-	0	0	0
GBL, N ₂ , catalyst	-	1.0	0	0

Reaction conditions: 15 mL of 0.2 M of substrate in 1,4-dioxane, at 170 °C, 0.5 mol. % of Ru respect to SA and 30 bar H₂ for a period of 6 h.

As reported in Table 6.3, low levels of reactivity were observed for all these substrates under comparable reaction conditions to SA, with only GBL demonstrating more than trace levels of conversion to any other product. The low levels of reactivity observed in each of these cases indicates that there are no major consecutive reactions present, and that the main products observed during SA conversion with 5Ru/Al₂O₃(COM) to GBL and PA, occurred from two separate pathways, as well as SA to BA, at a lower extent. This fact was further supported by the observation that selectivity obtained towards GBL during SA hydrogenation was almost invariant at all levels of product yield (Figure 6.5, right).

It should be noted that other potential products involved in the reaction network, such as THF from further GBL hydrogenation, and propanol and/or butanol, which were reported in previous studies from the extended reaction routes from PA and BA,²⁸ were not detected at the optimal reaction conditions chosen for the hydrogenation of SA over 5Ru/Al₂O₃(COM).

Additionally, the composition of the gas products was further investigated by analysing the gas phase of the experiments above, as described in Section 2.5.1.1.3, and by carrying out a series of control experiments in the absence of the substrate (Table 6.4).

Table 6.4. Gas production obtained for different control experiments.

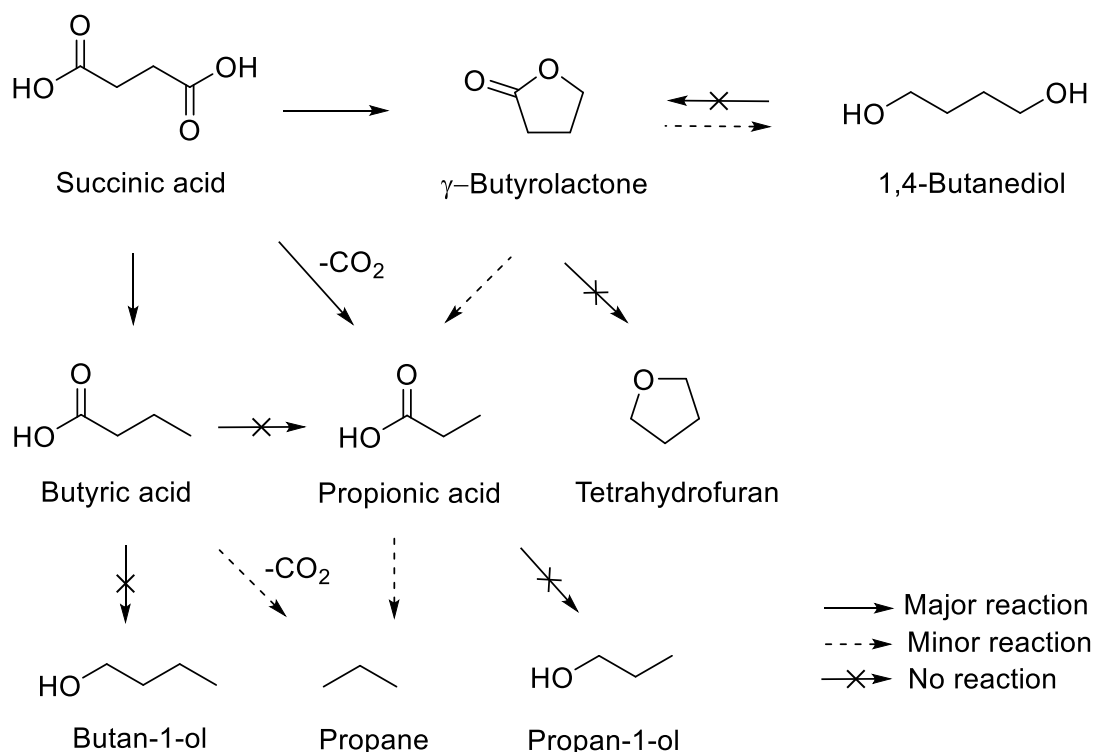
Type of reaction	Y CO ₂ / %	Y CH ₄ / %	Y C ₂ H ₆ / %	Y C ₃ H ₈ / %
Standard reaction	0.002	0.144	0.017	0.001
1,4-dioxane, cat, H₂ (2h)	0	0.303	0.049	0
1,4-dioxane, cat, H₂	0.001	0.830	0.121	0
1,4-dioxane, cat, N₂	0	0	0	0
GBL, cat, H₂	0.001	0.250	0.037	0.003
BDO, cat, H₂	0.003	0.232	0.014	0.003
PA, cat, H₂	0.002	0.967	0.252	0.012
BA, cat, H₂	0.002	0.899	0.173	0.040

Reaction conditions: 15 mL of 0.2M substrate in 1,4-dioxane, at 170 °C, 0.5 mol. % of Ru respect to SA and 30 bar H₂ for a period of 6 h, otherwise stated.

As reported in Table 6.4, at the optimal reaction conditions chosen, the gas products detected were CO₂, CH₄, C₂H₆ and C₃H₈. However, from the control experiments performed in the absence of SA, it could be determined that traces of CH₄ and C₂H₆ originated mainly from the fragmentation of 1,4-dioxane at the hydrogenation conditions used, since their presence was detected in increasing amounts in the 1,4-dioxane / catalyst / H₂ solution (in the absence of substrate) at increasing reaction times, whilst in the absence of hydrogenation agent, 1,4-dioxane did not lead to any gas product formed.

Control experiments starting from the different liquid-phase products (GBL and BDO) showed a gas products distribution similar to the standard reaction, whereas the amount of C₃H₈ increased slightly when starting from PA and BA. This suggests that C₃H₈, observed in the standard reaction gas phase, is likely to mainly be produced from the fragmentation of these two products (PA and BA).

These control experiments demonstrate the high stability of the main products and their low levels of interconversion, allowing to describe the overall reaction network in both, liquid and gas phases, as shown in Scheme 6.3.



Scheme 6.3. Full reaction network of SA hydrogenation at the optimal reaction conditions.

6.2.3 Catalyst design studies

Having optimised the reaction conditions to favour GBL formation and elucidated the complete reaction network, attention was focused on the nature of the catalyst itself, since the choice of a suitable catalyst is crucial to optimise the overall catalytic performance.

In the quest of identifying the most appropriate catalyst for the selective hydrogenation of SA to GBL a series of commercial catalysts available with 5 wt. % metal loading were tested at 170 °C, using 0.5 mol. % of metal with respect to SA, and 30 bar of H₂ over a period of 4 h.

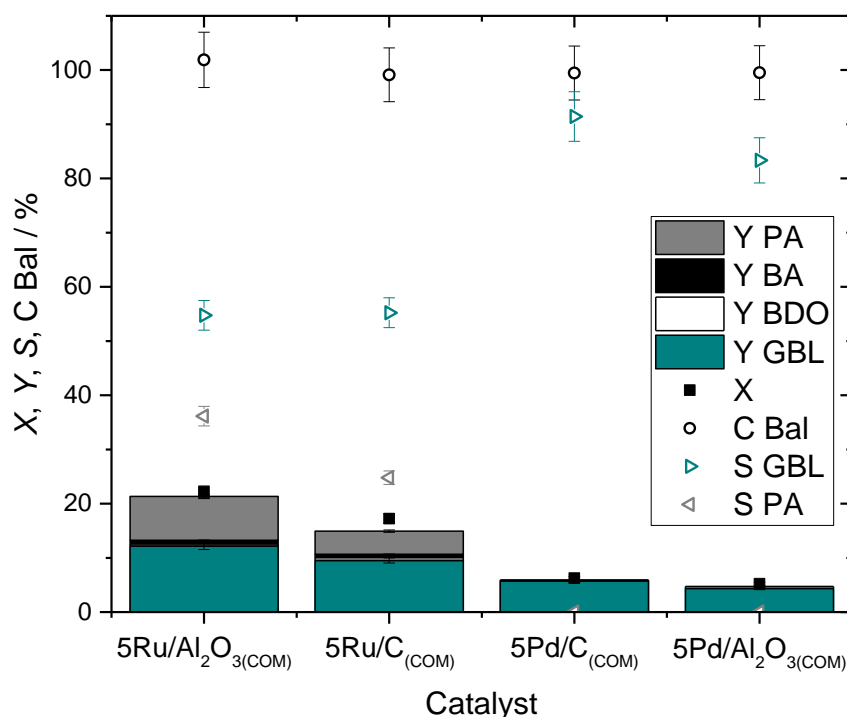


Figure 6.6. Catalytic activity obtained for SA hydrogenation using different commercial catalysts at the optimal reaction conditions after 4 h of reaction. Reaction conditions: 15 mL of SA 0.2 M in 1,4-dioxane, at 170 °C, 0.5 mol. % of Ru respect to SA and 30 bar H₂ for a period of 4 h.

As reported in Fig 6.6, clear differences in terms of product distribution could be observed between Ru and Pd based catalysts. Whilst 5Ru/C_(COM) performed similarly to 5Ru/Al₂O₃(COM), leading to GBL selectivity of approximately 55 %, commercial Pd catalysts presented much higher GBL selectivity, at 92 and 84 % for 5Pd/C_(COM) and 5Pd/Al₂O₃(COM), respectively, with PA selectivity < 5 %. Despite displaying lower SA conversion at the same reaction conditions, the lack of by-products indicate that Pd is a better metal to be used for the selective hydrogenation of SA to GBL.

In view of these results, the properties of a solid, such as the choice of metal, its level of loading on the support, and the method of preparation, manifested to dramatically impact the overall performance of a heterogeneous catalyst. Accordingly, the design of more active and selective heterogeneous catalysts is an essential requirement during the development of optimal chemical processes.

6.2.3.1 Investigating the choice of metal

Given the high activity observed over Al_2O_3 -supported Ru nanoparticles, a variety of analogous Al_2O_3 -supported metal nanoparticles were prepared to be screened for the catalytic hydrogenation of SA. Metals selected for this study were Pd and Ru, which have already positively demonstrated their ability to carry out this reaction when used as commercial catalysts; and Ni, Ir and Cu, also commonly used as hydrogenating catalysts.

Catalysts were prepared by co-precipitation (COP) following the synthetic procedure described in Section 2.3.2.3, as this is known to permit the production of well-dispersed nanoparticles, along with the generation of high surface area (S_{BET}) supports, both critical factors during heterogeneous catalysis.⁴³ Initial metal loadings of 2 wt. % were targeted, henceforth materials were denoted $2\text{M}/\text{Al}_2\text{O}_3(\text{COP})$, where M represents the metal supported. Prior to use, all samples were reduced at 200 °C for 3 h, under a flow of 5 % H_2/Ar . Additionally, the bare support, $\text{Al}_2\text{O}_3(\text{COP})$, was prepared following the same methodology and heat treatment.

All materials were fully characterised by various techniques to ensure a correct preparation of the material prior being tested as catalytic materials for SA hydrogenation. Firstly, catalysts were analysed by X-Ray Diffraction (XRD), to investigate the crystalline structure obtained in the synthetical procedure (Fig 6.7).

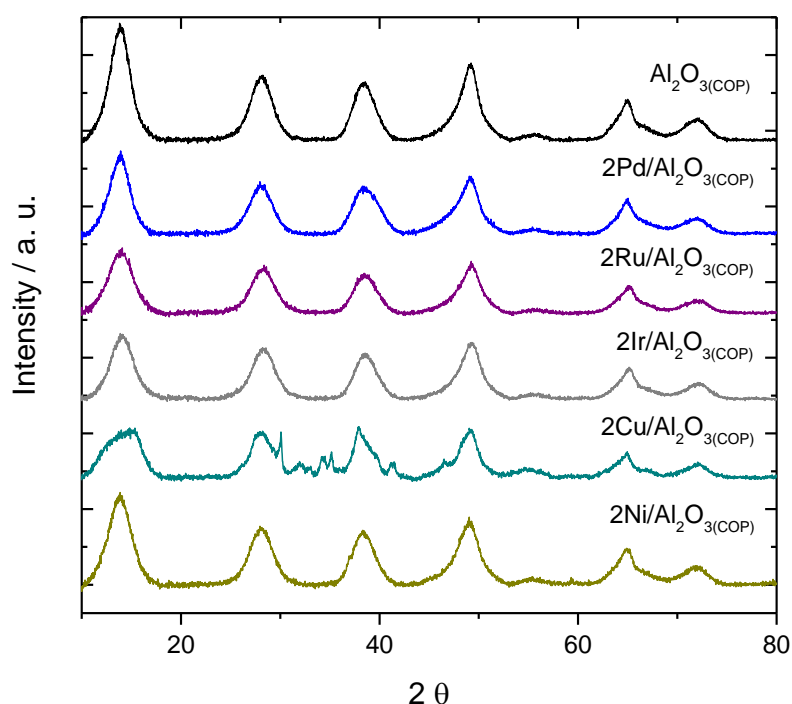


Figure 6.7. XRD patterns obtained for $\text{Al}_2\text{O}_3(\text{COP})$ support and $2\text{M}/\text{Al}_2\text{O}_3$ prepared by COP.

XRD analysis showed that all materials displayed the same diffraction pattern which corresponded to the alumina support, with main diffraction peaks observed at 13.9, 28.5, 38.5, 49.2, 65.0 and 72.0 (2θ). This diffraction pattern can be attributed to the pseudo-boehmite alumina phase.⁴⁴ All samples presented then the same structural pattern and similar crystallinity levels, except for $2\text{Cu}/\text{Al}_2\text{O}_3(\text{COP})$, where some impurities in the XRD pattern were observed, and lower crystallinity could be seen. These impurities are likely to be caused by extra carbonate species from the synthesis not entirely removed during the washing.

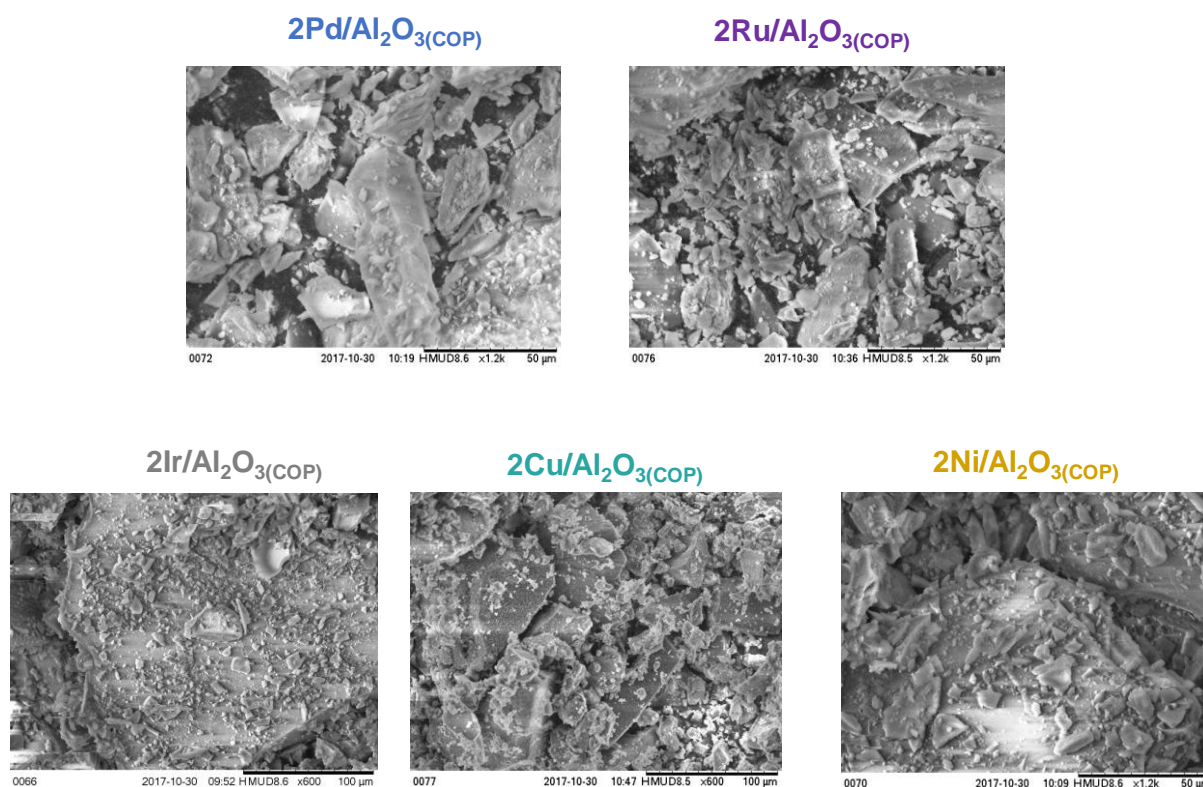


Figure 6.8. SEM images of $2\text{M}/\text{Al}_2\text{O}_3(\text{COP})$.

Additionally, Scanning Electron Microscopy (SEM) was used to investigate the crystal morphology of the catalysts (Fig 6.8). Images obtained by SEM presented a common appearance along the whole set of materials, indicating that all of them possess the same common support material. Subsequently, Energy-Dispersive X-ray (EDX) spectroscopy was employed to verify the metal loading deposited onto the alumina support during the different preparations. The results obtained are summarised in Table 6.5.

Table 6.5. Characterisation of different M/Al₂O₃ prepared by COP method.

Material prepared by COP method	Loading ^a / %	S _{BET} ^b / m ² g ⁻¹
Al ₂ O ₃	-	245
2Pd/Al ₂ O ₃	1.7	256
2Ru/Al ₂ O ₃	2.0	263
2Ir/Al ₂ O ₃	n.d.	218
2Cu/Al ₂ O ₃	1.4	107
2Ni/Al ₂ O ₃	1.8	240

^a Metal loading obtained by EDX measurements and ^b S_{BET} calculated by BET method from the N₂ adsorption isotherm data.

As compiled in Table 6.5, the theoretical loading of 2 wt. % M was only achieved in the case of 2Ru/Al₂O₃(COP), although fairly high loadings could be obtained for the rest of the materials analysed, with all > 1.4 wt. %.

Porosimetry analysis by N₂ adsorption allowed the textural properties of the materials to be characterised, showing all materials to have high S_{BET}. S_{BET} values obtained were in the range of 200 - 270 m² g⁻¹, except for the Cu sample, which presented significantly lower S_{BET}, about the half of the rest of the materials within the series, with only 107 m² g⁻¹.

In view of all the characterisation results described above, generally, all catalytic materials prepared by COP method do not manifest significant differences in terms of structural pattern, morphology and textural properties, except for 2Cu/Al₂O₃, whose characterisation indicates a poor success in its preparation. Despite repeating the preparation several times, to exclude an isolated human error during its first synthesis, all Cu samples presented the same characterisation, suggesting that this synthetical method, is not appropriated to prepare Cu/Al₂O₃ catalyst, at least under the working conditions chosen.

Once fully characterised, 2M/Al₂O₃(COP) catalysts were tested for the catalytic hydrogenation of SA at the optimal conditions identified for the catalyst screening (170 °C, 30 bar H₂, 2 mol. % metal with respect to SA). Note that in Section 6.2.1, it was demonstrated that a linear relationship between total product yield and catalyst loading up to 2 mol. % can be achieved, and within this range, catalytic reaction can be performed under kinetic regime (Fig 6.4). Accordingly, in order to maximise the productivity and allow a better comparison between the catalysts tested in further studies, all following reaction were performed using 2 mol. % of metal, unless otherwise stated.

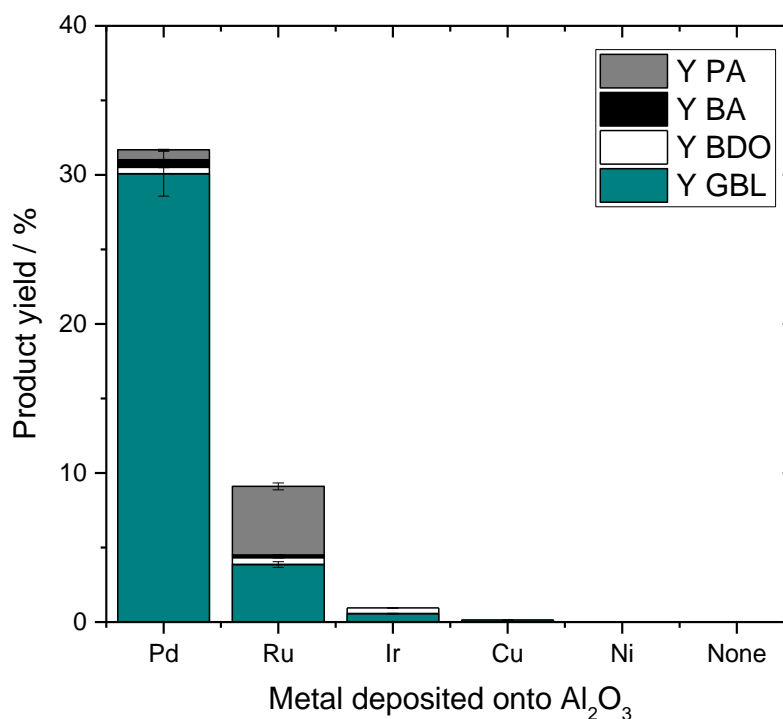


Figure 6.9. Product distribution obtained for SA hydrogenation using various $2\text{M}/\text{Al}_2\text{O}_3(\text{COP})$. Reaction conditions: 15 mL of SA 0.2 M in 1,4-dioxane, at 170 °C, 2 mol. % of metal and 30 bar H_2 , for a period of 4 h.

As can be seen in Fig 6.9, some catalytic activity for SA hydrogenation was observed when Pd or Ru were deposited onto the co-precipitated support Al_2O_3 . In contrast, other established hydrogenation catalysts such as Cu, Ni and Ir were substantially less active, or not active at all. It has been confirmed by the characterisation performed that, except for the Cu samples, which could not be prepared successfully, the rest of the materials possessed very similar characteristics. Hence, the discrepancies in the catalytic activity observed in Fig 6.9 are likely to be due to the nature of the metal itself and its capability to drive the SA hydrogenation reaction. An example of that is given by the observation that although possessing great similarities, Pd and Ru, the only two metals which showed significant activity for SA hydrogenation at the reaction conditions used, manifested considerably different catalytic activity, the activity observed for $2\text{Ru}/\text{Al}_2\text{O}_3(\text{COP})$ being much lower than for $2\text{Pd}/\text{Al}_2\text{O}_3(\text{COP})$. Remarkably, although $2\text{Ru}/\text{Al}_2\text{O}_3(\text{COP})$ was lower in activity than its analogous $5\text{Ru}/\text{Al}_2\text{O}_3(\text{COM})$ (which in 2 h of reaction already achieved ≈ 20 % of total product yield when used at the same catalyst loading of 2 mol. %, Fig 6.4) the product distribution was comparable for both catalysts, with both GBL and PA displaying similar levels of selectivity.

However, $2\text{Pd}/\text{Al}_2\text{O}_3(\text{COP})$, which was over three times more active than the analogous $2\text{Ru}/\text{Al}_2\text{O}_3(\text{COP})$, achieved much greater GBL selectivity. The fact of obtaining dramatically improved GBL selectivity when replacing Ru with Pd onto Al_2O_3 , already indicated by the study on commercial catalysts (Fig 6.6), clearly points to Pd as a better metal to be used for the selective hydrogenation of SA to GBL.

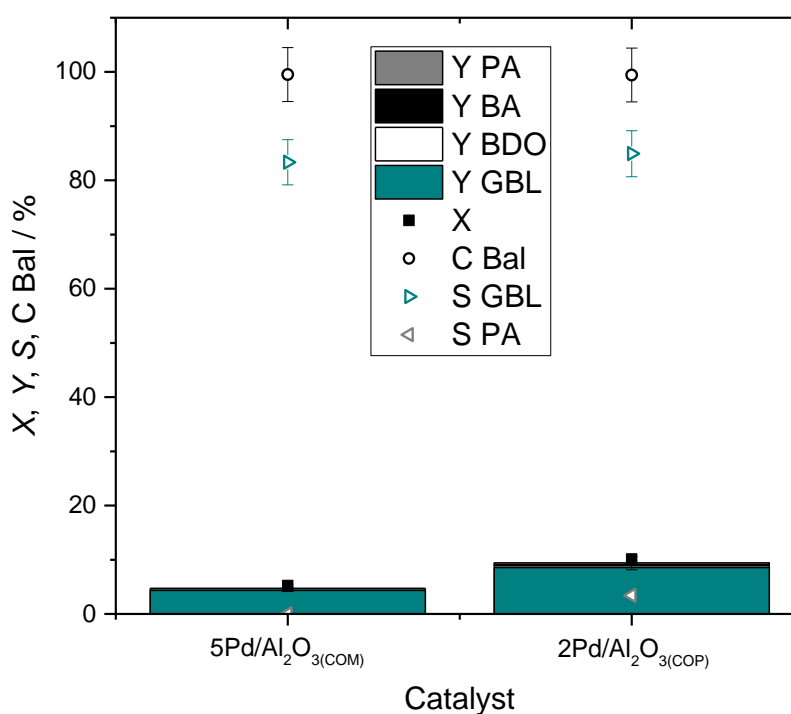


Figure 6.10. Comparison of catalytic activity obtained at identical reaction conditions for $5\text{Pd}/\text{Al}_2\text{O}_3(\text{COM})$ and $2\text{Pd}/\text{Al}_2\text{O}_3(\text{COP})$. Reaction conditions: 15 mL of SA 0.2 M in 1,4-dioxane, at 170 °C, 0.5 mol. % Pd and 30 bar H_2 for a period of 4 h.

It is worth mentioning also that synthesised $2\text{Pd}/\text{Al}_2\text{O}_3(\text{COP})$ tested at identical reaction conditions than $5\text{Pd}/\text{Al}_2\text{O}_3(\text{COM})$, *i.e.* 0.5 mol. % Pd (Fig 6.10), displayed greater levels of catalytic activity, indicating the suitability of the synthesised catalyst. Hence, the catalyst design is moving in the appropriate direction, since equivalent levels of GBL selectivity can be obtained with higher overall catalytic activity observed. Thus, $2\text{Pd}/\text{Al}_2\text{O}_3(\text{COP})$ is a more efficient catalyst for SA valorisation to GBL than the commercial analogue in the context of process intensification.

6.2.3.2 Detailed investigation on $2\text{Pd}/\text{Al}_2\text{O}_3(\text{COP})$

Synthesised $2\text{Pd}/\text{Al}_2\text{O}_3(\text{COP})$ demonstrated an excellent ability to selectively convert SA to GBL at the optimal reaction conditions chosen. However, it was noticed that increasing the catalyst loading from 0.5 to 2 mol. % entailed a drop of carbon balance of around 15 - 20 %, also

observed for all the different metal supported on $\text{Al}_2\text{O}_3(\text{COP})$. This loss of carbon balance may be caused by two factors: i) the formation of other by-products not detectable by HPLC and GC-FID, the two analytical techniques used, or ii) substrate adsorption on the catalyst surface. Accordingly, to get a better insight on the nature of the carbon balance loss observed, whether it was caused by SA adsorption on catalyst surface or not, a series of reactions (Table 6.6) using $2\text{Pd}/\text{Al}_2\text{O}_3(\text{COP})$ were tested at varying mol. % ratios: the bare $\text{Al}_2\text{O}_3(\text{COP})$ (amount equivalent to 2 mol. % Pd), 0.5 mol. % Pd, 0.5 mol. % Pd + $\text{Al}_2\text{O}_3(\text{COP})$, and 2 mol. % Pd. For 0.5 mol % Pd + $\text{Al}_2\text{O}_3(\text{COP})$, extra $\text{Al}_2\text{O}_3(\text{COP})$ was co-added to reach the equivalent total mass of support use for 2 mol. % Pd reaction.

Table 6.6. Experimental details of various SA hydrogenation reactions performed using $\text{Al}_2\text{O}_3(\text{COP})$ and $2\text{Pd}/\text{Al}_2\text{O}_3(\text{COP})$ using different Pd and support quantities.

Entry	Catalyst	mol. % Pd	mg Pd	mg support
A	$\text{Al}_2\text{O}_3(\text{COP})$	0	0	314
B	$2\text{Pd}/\text{Al}_2\text{O}_3(\text{COP})$	0.5	1.6	78
C	$2\text{Pd}/\text{Al}_2\text{O}_3(\text{COP}) + \text{Al}_2\text{O}_3(\text{COP})$	0.5	1.6	314
D	$2\text{Pd}/\text{Al}_2\text{O}_3(\text{COP})$	2	6.4	314

This set of experiments, shown in Fig 6.11, was highly revealing. Firstly, a conversion of 16 % with no products observed was obtained for Entry A, which may indicate that substrate adsorption was occurring, and causing the drop of carbon balance observed due to “fake” conversion. Furthermore, Entries B and C, with the same amount of active species, exhibited similar product distribution and GBL yield, but the co-addition of extra support entailed an increase of SA conversion and higher drop of carbon balance. The same extent of carbon balance loss than at Entry C was also observed for Entry D, suggesting that this loss was proportional to the amount of support and the higher was the amount of support present in the reaction media, the higher was the degree of SA adsorbed. Unfortunately, these experiments also showed how the selectivity towards GBL was affected by the amount of $\text{Al}_2\text{O}_3(\text{COP})$ present, with a decrease from 83 to 61 % for Entries B and D, respectively, and it was even more pronounced for Entry C, where the extra support carried an increase of observed conversion.

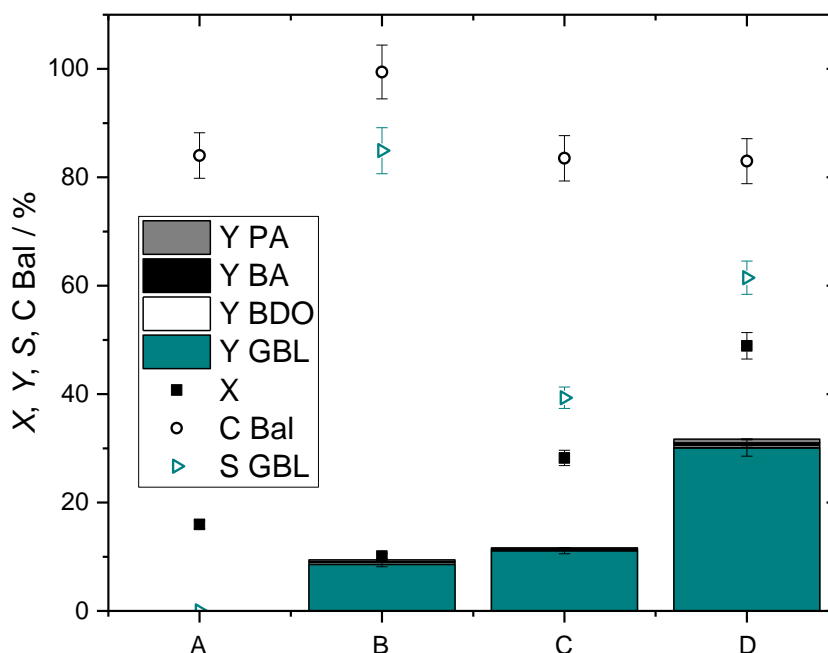


Figure 6.11. Catalytic performances of bare $\text{Al}_2\text{O}_3(\text{COP})$ support and $2\text{Pd}/\text{Al}_2\text{O}_3(\text{COP})$ for SA hydrogenation using different Pd and support quantities (Table 6.6). Reaction conditions: 15 mL of SA 0.2 M in 1,4-dioxane, at 170 °C, 30 bar of H_2 , for 4 h of reaction.

To fully confirm the nature of this conversion observed, *i.e.* to ensure that this level of conversion did not actually occur but was caused by adsorption of SA onto the support surface, some samples of $\text{Al}_2\text{O}_3(\text{COP})$ were investigated by thermogravimetric analysis (TGA) before and after the reaction. This technique was already used with success in Chapter 3 to quantify the amount of product retained onto the Sn- β surface after BVO reaction, which helped to close the final carbon balance. Therefore, following an identical analytical procedure (Section 2.5.5), samples of $\text{Al}_2\text{O}_3(\text{COP})$; fresh, treated with SA in H_2O , with 1,4-dioxane, with SA in 1,4-dioxane; and used, were analysed by TGA (Fig 6.12, left). Considering the observed conversion for the bare support (Table 6.6, Entry A), if the amount of SA adsorbed is confirmed to be around 15 - 20 % and discounted from the observed SA conversion for Entry D, the carbon balance may be maintained closer to 100% and the real kinetic selectivity to GBL should be accounted as > 85 %.

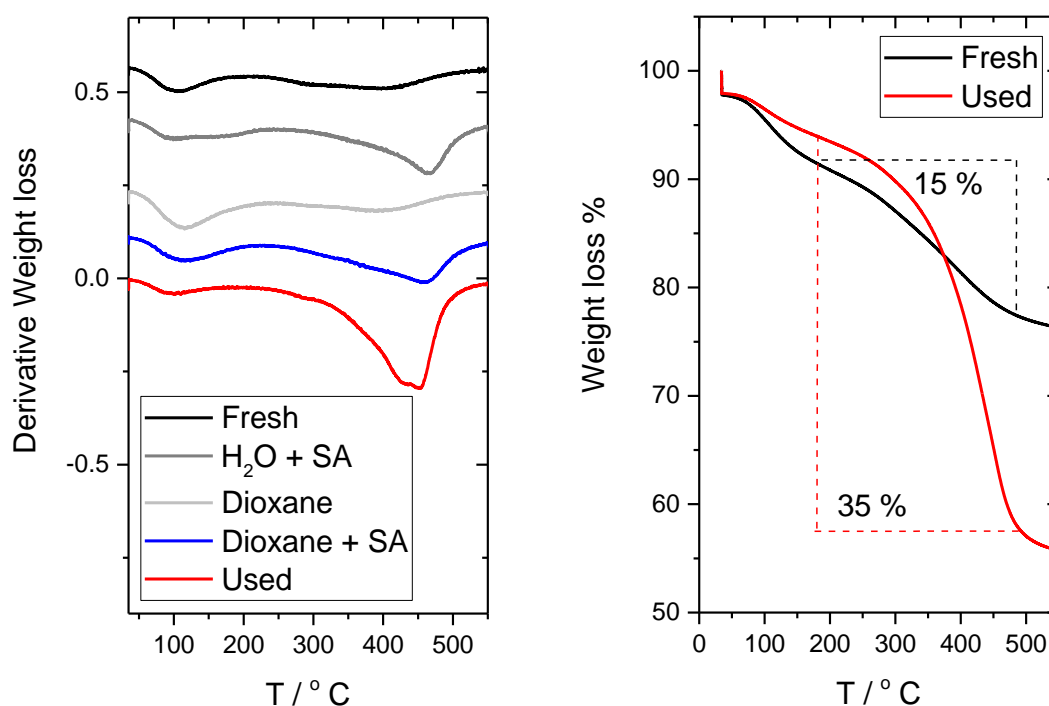


Figure 6.12. (Left) First derivative of TGA of $\text{Al}_2\text{O}_3(\text{COP})$ after the treatments stated in the legend and (Right) the corresponding TGA obtained for $\text{Al}_2\text{O}_3(\text{COP})$ fresh and used.

From the TGA, reported in Fig 6.12, left, it could be clearly stated that the fresh support (heat treated in the same way as the catalyst, at 200 °C for 3 h in 5% H_2/Ar) suffered some structural change at high temperature. Apart from this structural change, the support treated with SA in different solvents manifested a more pronounced weight loss in the same region, suggesting that SA was chemically adsorbed onto the support, and its desorption occurred at temperature higher than its boiling point (235 °C). Analysis on the used support manifested two significant weight losses: the first one, less pronounced, corresponded to some H_2O adsorbed from the environment, desorbed at low temperature (around 100 °C) and the second one could be attributed to the combination of SA adsorbed and the intrinsic structural change on the material at high temperature.

Through study of the TGA data (Fig 6.12, right), it can be noted that the great weight loss at high temperature accounted as 15 % for the fresh support, while it significantly increased to 35 % for the used support. According to the control studies performed, this increment is caused by SA desorption at the same range of temperature. Hence, if the % of weight loss attributed to the intrinsic material change is discounted from the total weight loss observed at this same range of temperature for the used support, a loss of 20 % can be solely ascribed to SA desorbed. Extrapolating this % to the total amount of $\text{Al}_2\text{O}_3(\text{COP})$ used for the reaction, the

total amount of SA adsorbed onto the material can be calculated, and its contribution to the total SA in the reaction accounted as approximately 15 - 20 %.

The % of SA adsorbed is in good agreement with the ± 15 % of SA conversion observed at Entry A (bare $\text{Al}_2\text{O}_3(\text{COP})$) and the results obtained for Entry C (0.5 mol.% Pd + $\text{Al}_2\text{O}_3(\text{COP})$), whose modified conversion, by discounting the % of SA adsorbed ($- 15$ %) from the original conversion, resembled the level of conversion reached for Entry B (0.5 mol. % Pd). Furthermore, considering the modified conversion of Entry D (2 mol. % Pd) (49 % (observed conversion) - 15 % (SA adsorbed) = 34 %), which perfectly matched the total product yield accounted, GBL selectivity purely based on SA converted could be recalculated, obtaining a value of 88 %, very similar to the selectivity obtained at Entry B (0.5 mol. % Pd, 83 %), where no SA adsorption was appreciated.

The detailed investigation carried out on $2\text{Pd}/\text{Al}_2\text{O}_3(\text{COP})$ through the experiments reported in Fig 6.11 and the TGA, confirms that some unconverted SA is retained on the catalyst surface at the reaction conditions chosen (2 mol. % of Pd). Therefore, the observed conversion always is a contribution of the SA converted and the SA adsorbed (± 15 %). As stated above, real kinetic selectivity to GBL, based on total product yield instead of observed conversion, is > 85 % for all reactions, reassuring $2\text{Pd}/\text{Al}_2\text{O}_3(\text{COP})$ as a very good catalyst for SA selective valorisation to GBL.

Subsequently, to get a deeper understanding of the reason behind the substrate adsorption onto the catalyst surface, attention was focused on the nature of the alumina support prepared by COP. The support obtained, $\text{Al}_2\text{O}_3(\text{COP})$, presented a moderate basicity, even after the corresponding washing to ensure the removal of carbonate species in excess coming from the preparation itself (pH in aqueous solution of 9 - 9.5). Accordingly, the nature of the SA adsorption is thought to be caused by an acid-base chemical interaction.

In order to prove this statement, a series of Pd nanoparticles supported in preformed materials with different acid-base properties was prepared by wet impregnation method (IMP). This method appears to be simple, economic and able to give a reproducible metal loading, as it only consists in the drying of the metal precursor onto the support surface by heat treatment and represents a classical catalyst preparation method for many hydrogenation heterogeneous catalysts. Following the synthetical procedure described in Section 2.3.2.2, a series of 2 wt. % Pd catalysts supported on MgO, hydrotalcite, MCM-41 and H- β was prepared and treated at 200 °C for 3 h in 5% H_2/Ar . Additionally, in the interest of obtaining a better comparison, instead of using the original $2\text{Pd}/\text{Al}_2\text{O}_3(\text{COP})$ catalyst, a 2 wt. % Pd on $\text{Al}_2\text{O}_3(\text{COP})$ was prepared following the exact methodology used for the rest of the series, *i.e.* impregnation of Pd onto $\text{Al}_2\text{O}_3(\text{COP})$. This sample is denoted $2\text{Pd}/\text{Al}_2\text{O}_3(\text{IMP@COP})$.

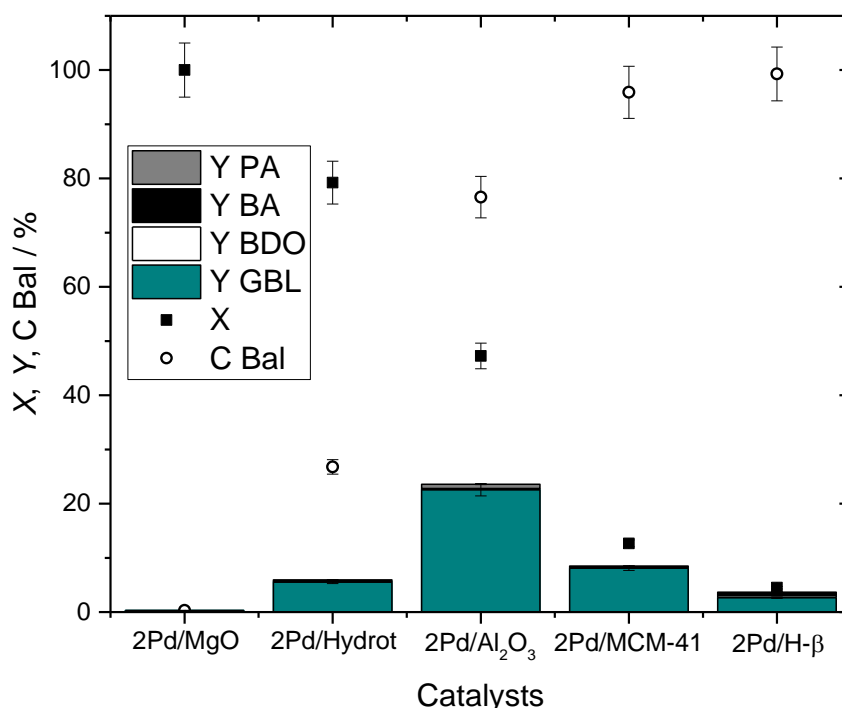


Figure 6.13. Catalytic performance for SA hydrogenation of different 2 wt. % Pd supported materials prepared by IMP method. Reaction conditions: 15 mL of SA 0.2 M in 1,4-dioxane, at 170 °C, 30 bar of H₂, 2 mol. % Pd respect to SA, for 4 h of reaction.

As reported in Fig 6.13, there was a clear correlation in terms of carbon balance drop observed with the basicity of the support involved. The carbon balance loss gradually decrease from the most basic support (MgO) to the most acidic one tested (H-β). For a better understanding of this effect, the most basic and the most acidic bare supports were also tested, and their obtained catalytic activities were compared with their analogous Pd-catalysts (Table 6.7). As displayed in Fig 6.13 and Table 6.7, SA conversion observed for 2Pd/MgO_(IMP), with the most basic support tested, was 100 % although the products yielded were practically null, giving a carbon balance close to 0 %. The observed conversion was proved to be caused by a strong SA adsorption onto the MgO support, since a control experiment carried out using the bare MgO support also led to 100 % of observed conversion with 0 % of products yielded. Hydrotalcite and Al₂O_{3(COP)} supported materials, both with a moderate basicity, presented an adsorption phenomenon somewhere in the middle, adsorbing also certain amount of SA onto their surface which was reflected in their carbon balance loss. SA observed conversion for Pd/Al₂O_{3(IMP@COP)} was in agreement with the conversion shown above for bare Al₂O_{3(COP)} (Fig 6.11), which displayed ± 15 % of SA conversion entirely attributable to the substrate adsorption. On the contrary, MCM-41 and H-β, both acidic materials, manifested a carbon

balance close to 100 %. These results were in agreement with the catalytic performance of H- β bare support, which gave rise to < 1 % of SA conversion with no products detected, confirming that the use of acidic support do not lead to substrate adsorption.

Table 6.6. Comparison of Pd/support catalytic performances for SA hydrogenation with some of the bare supports.

Material	Conversion SA / %	Total Product Yield / %	Carbon Balance / %
MgO	100	0	0
2Pd/MgO _(IMP)	100	0.3	0.3
Al ₂ O ₃ (COP)	16	0	84
2Pd/Al ₂ O ₃ (IMP@COP)	47	23	77
H- β	1	0	99
2Pd/H- β _(IMP)	4.5	4	99

This set of experiments backs up very well the initial hypothesis of the adsorption of SA to be an effect of the acid-base interaction between the substrate and the surface of the support involved. Given that the adsorption of SA onto the Al₂O₃(COP) showed to not affect the catalytic performance of the material in terms of product distribution, *i.e.* high selectivity towards GBL is always obtained, all further experiments overlooked the observed conversion (hence the adsorbed/unconverted SA) and all product selectivity shown from this point on were expressed based on total product yield, which reflects more accurately the pure kinetic selectivity towards each product.

6.2.3.3 Investigation of the preparation method

Another key point to be addressed during the development of the catalyst design was the method of preparation employed, as this can massively influence the physico-chemical properties of the material, such as the particle size, distribution on the support or determine the oxidation state of the metal. Moreover, a thorough study of different preparation methods to produce active Pd catalysts may help to further probe the role of the support.

In order to determine the effects of different preparation methods and gain a better understanding of structure-function relationships of 2Pd/Al₂O₃(COP), analogous samples with different methods of preparation, were investigated. A series of catalysts was prepared with a 2 wt. % Pd loading by COP (2Pd/Al₂O₃(COP)), deposition-precipitation (DP, 2Pd/Al₂O₃(DP)), IMP

(2Pd/Al₂O₃(IMP)), the latter two using commercial γ -Al₂O₃ (Sigma Aldrich), and combination of IMP@COP (2Pd/Al₂O₃(IMP@COP)) and DP@COP (2Pd/Al₂O₃(DP@COP)), both prepared with Al₂O₃(COP). Notably, all catalysts were reduced at 200 °C for 3 h in 5 % H₂/Ar.

Catalysts were fully characterised by various techniques including XRD, porosimetry, X-Ray Photoelectron spectroscopy (XPS), Transmission Electron Microscopy (TEM), and SEM (where needed), to gain a deeper understanding on the structure, textural properties and Pd nanoparticle distribution of the five materials. Firstly, characterisation of both Al₂O₃ supports (commercial and COP) was carried out. XRD and porosimetry analysis, shown in Fig 6.14 revealed the very different nature of Al₂O₃(COP) with respect to commercial γ -Al₂O₃.

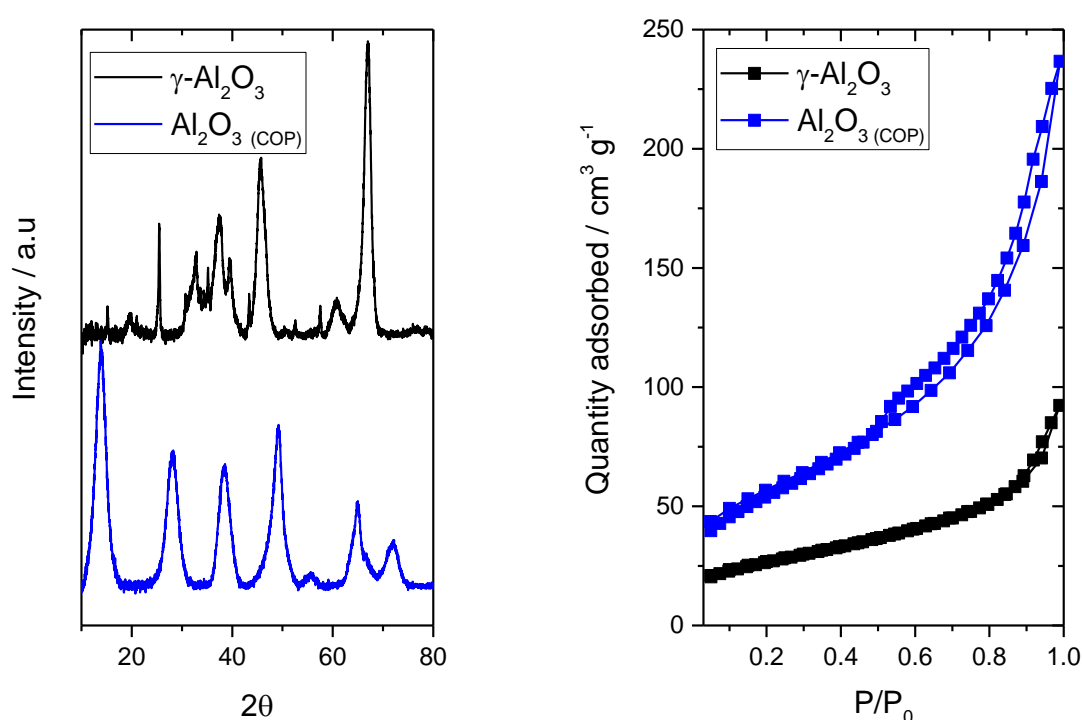


Figure 6.14. (Left) XRD patterns and (Right) N₂ adsorption isotherms obtained for commercial γ -Al₂O₃ and Al₂O₃(COP).

Indeed, the XRD patterns of both supports (Fig 6.14, left) revealed two completely different structural phases. The alumina prepared by COP method was consistent with a pseudo-boehmite phase,⁴⁴ whilst the diffraction peaks of a typical γ -Al₂O₃ phase could be attributed to the XRD pattern of the commercial alumina support. Furthermore, porosimetry analysis (Fig 6.15, right) showed that Al₂O₃(COP) possessed a much larger S_{BET} than that of commercial γ -Al₂O₃, at 245 and 93 m² g⁻¹, respectively.

Another very important aspect to consider when choosing the support is the acid-base properties of its surface, since the support may interact with the substrate in some way,

assisting to drive the reaction. The effect of the acid-base properties of the support surface has already been shown in the previous section, where highly basic support strongly adsorbed SA onto its surface, inhibiting the catalytic reaction to occur, whilst highly acidic support seems to repel the substrate, hence, inhibiting the reaction as well.

Accordingly, the acidity of $\gamma\text{-Al}_2\text{O}_3$ and $\text{Al}_2\text{O}_3(\text{COP})$ was studied by Diffuse Reflectance Infrared Fourier Transform Spectroscopy (DRIFTS) using pyridine as probe molecule (Section 2.6.4.1). Pyridine can be a very useful probe molecule to evaluate both the Lewis and Brønsted acidity of materials. It can bond with both kinds of acid sites, generating characteristic vibrations that allow to determine the kind of acidity. As assigned in the DRIFT spectrum obtained (Fig 6.15), vibrations at 1593 and 1443 cm^{-1} , could be attributed to weak Lewis acid interactions, whereas vibrations at 1615 and 1449 cm^{-1} were assigned to medium-strong Lewis acid interactions. Similarly, the peak at 1540 cm^{-1} , observed only in the $\text{Al}_2\text{O}_3(\text{COP})$ sample, was assigned to Brønsted acid interactions, corresponding to the protonated pyridine. Additionally, the feature at 1490 cm^{-1} could be attributed to protonated pyridine and Lewis acid adduct, hence, this peak can be a contribution of the two kinds of acidities, Lewis and Brønsted acid sites.⁴⁵

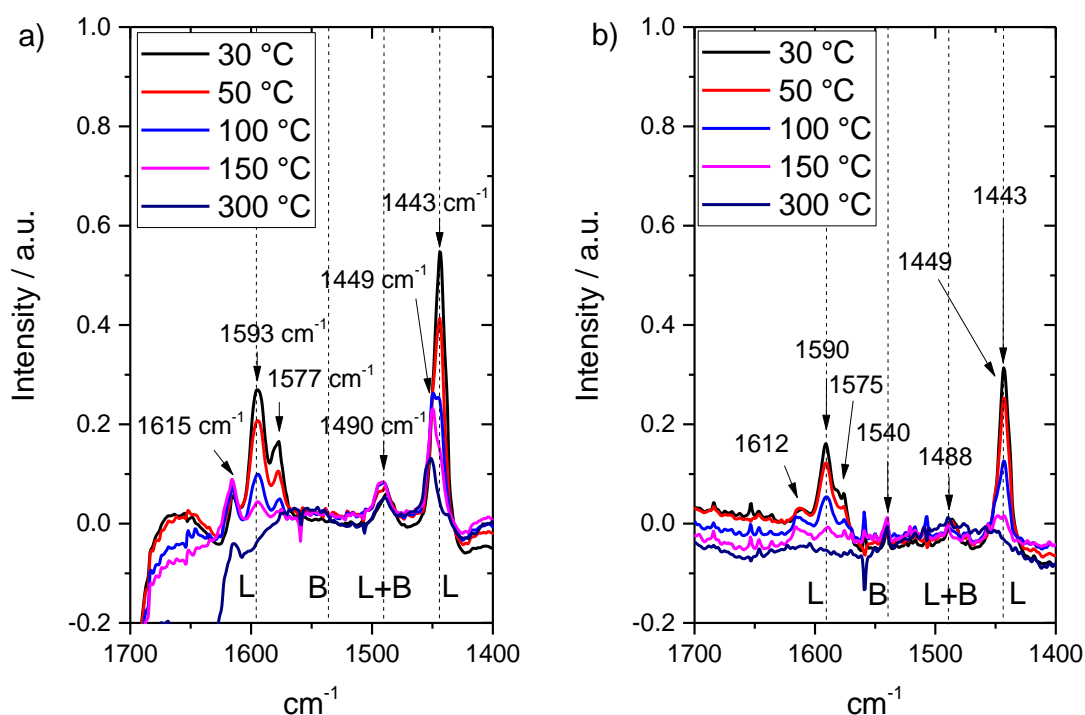


Figure 6.15. DRIFTS experiments on a) $\gamma\text{-Al}_2\text{O}_3$ and b) $\text{Al}_2\text{O}_3(\text{COP})$ using pyridine as probe molecule at increasing desorbing temperatures, where L refers to Lewis Acid assigned modes and B refers to Brønsted Acid assigned modes.

As shown in Fig 6.15, γ -Al₂O₃ presented higher general acidity than Al₂O₃(COP), since the intensity of the peaks corresponding to the pyridine adsorbed onto γ -Al₂O₃ were considerably higher, almost double that for Al₂O₃(COP). Furthermore, pyridine desorption occurred faster (at lower temperature) in the latter, suggesting a weaker interaction between the probe molecule and the surface of the material prepared by COP. For instance, at 300 °C some remaining pyridine was still observed in the γ -Al₂O₃ DRIFT spectra, whilst practically all the pyridine was already desorbed at 150 °C during the Al₂O₃(COP) DRIFT experiment.

Accordingly, although quantification of Lewis and Brønsted acidity could not be properly carried out, semi-quantitatively, it can be said that γ -Al₂O₃ possessed higher Lewis acid strength than Al₂O₃(COP), and the latter possessed also some Brønsted acidity.

These observations clearly indicate that the choice of the alumina support may impact the performance of the Pd active sites during SA valorisation, since structurally and texturally alumina supports showed important differences as well as significant differences in the strength and kind of acid sites present on their surface.

Further characterisation analysis on all the Pd/Al₂O₃ materials are summarised in Table 6.8 in order to compare the major similarities and discrepancies in terms of structure and textural surface with the corresponding alumina supports employed. Further analysis of the Pd supported catalysts were carried out by TEM to investigate the Pd particle size and distribution on the support obtained with the different synthetical methodologies.

Table 6.8. Characterisation of the alumina supports and the 2Pd/Al₂O₃ materials prepared by various methods.

Material	S _{BET} ^a / m ² g ⁻¹	Particle size ^b / nm
Al ₂ O ₃ (COP)	245.2	-
γ -Al ₂ O ₃ (COM)	92.6	-
2Pd/Al ₂ O ₃ (COP)	256.4	2.85 (± 0.76)
2Pd/Al ₂ O ₃ (DP)	68.0	n. d (agglomerations)
2Pd/Al ₂ O ₃ (IMP)	82.5	n. d. (agglomerations)
2Pd/Al ₂ O ₃ (DP@COP)	222.6	3.64 (± 1.61) + agglomerations
2Pd/Al ₂ O ₃ (IMP@COP)	223.9	4.51 (± 2.80)

^a S_{BET} calculated by BET method from the N₂ adsorption analysis data; ^b Particle size mean calculated from a statistical analysis of TEM images.

As reported in Table 6.8, the S_{BET} obtained for the five catalysts were in agreement with the values obtained for the two alumina supports. Samples which involved COP presented high S_{BET} , in the same range than the bare support ($> 220 \text{ m}^2 \text{ g}^{-1}$), while samples supported on commercial $\gamma\text{-Al}_2\text{O}_3$ presented significantly lower S_{BET} ($< 100 \text{ m}^2 \text{ g}^{-1}$).

In regard to the Pd particle size and distribution, important differences could be observed by TEM analysis. For instance, TEM analysis of $2\text{Pd}/\text{Al}_2\text{O}_3(\text{DP@COP})$ (Fig 6.16) showed a non-uniform particle size distribution throughout the whole material surface, with certain zones presenting big agglomerates of Pd nanoparticles, which diffculted their measurement and could not be included in the particle size analysis distribution. Hence, the mean particle size of $3.64 \pm 1.61 \text{ nm}$ given in Table 6.8 was calculated only from the non-agglomerated nanoparticles (< 100 particles) and this value cannot be considered representative of the whole material.

$2\text{Pd}/\text{Al}_2\text{O}_3(\text{DP@COP})$

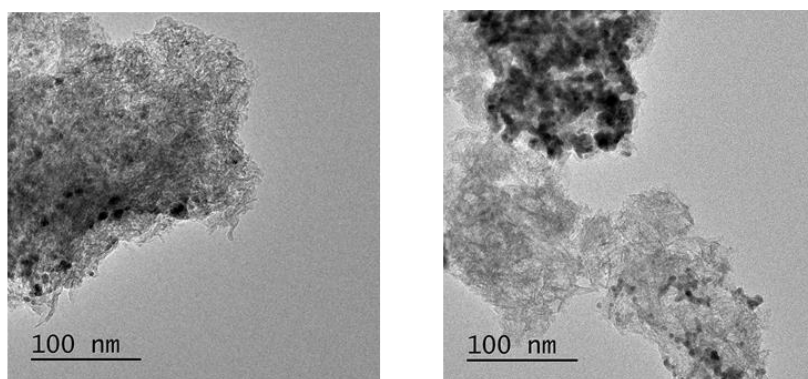


Figure 6.16. TEM images of $2\text{Pd}/\text{Al}_2\text{O}_3(\text{DP@COP})$.

TEM analysis of $2\text{Pd}/\text{Al}_2\text{O}_3(\text{COP})$ and $2\text{Pd}/\text{Al}_2\text{O}_3(\text{IMP@COP})$ (Fig 6.17) revealed that the COP sample, possessed both a smaller mean particle size and a narrower particle size distribution than the IMP analogue, with a mean of $2.85 \pm 0.76 \text{ nm}$ and $4.51 \pm 2.8 \text{ nm}$, respectively.

Unfortunately, samples supported on commercial $\gamma\text{-Al}_2\text{O}_3$, $2\text{Pd}/\text{Al}_2\text{O}_3(\text{DP})$ and $2\text{Pd}/\text{Al}_2\text{O}_3(\text{IMP})$, presented very poor contrast on the $\gamma\text{-Al}_2\text{O}_3$ support and their particle size distribution could not be analysed by TEM. Instead, both samples were analysed by SEM (Fig 6.18), revealing a very unsuccessful distribution of Pd nanoparticles throughout the whole material, with big agglomerates in certain zones.

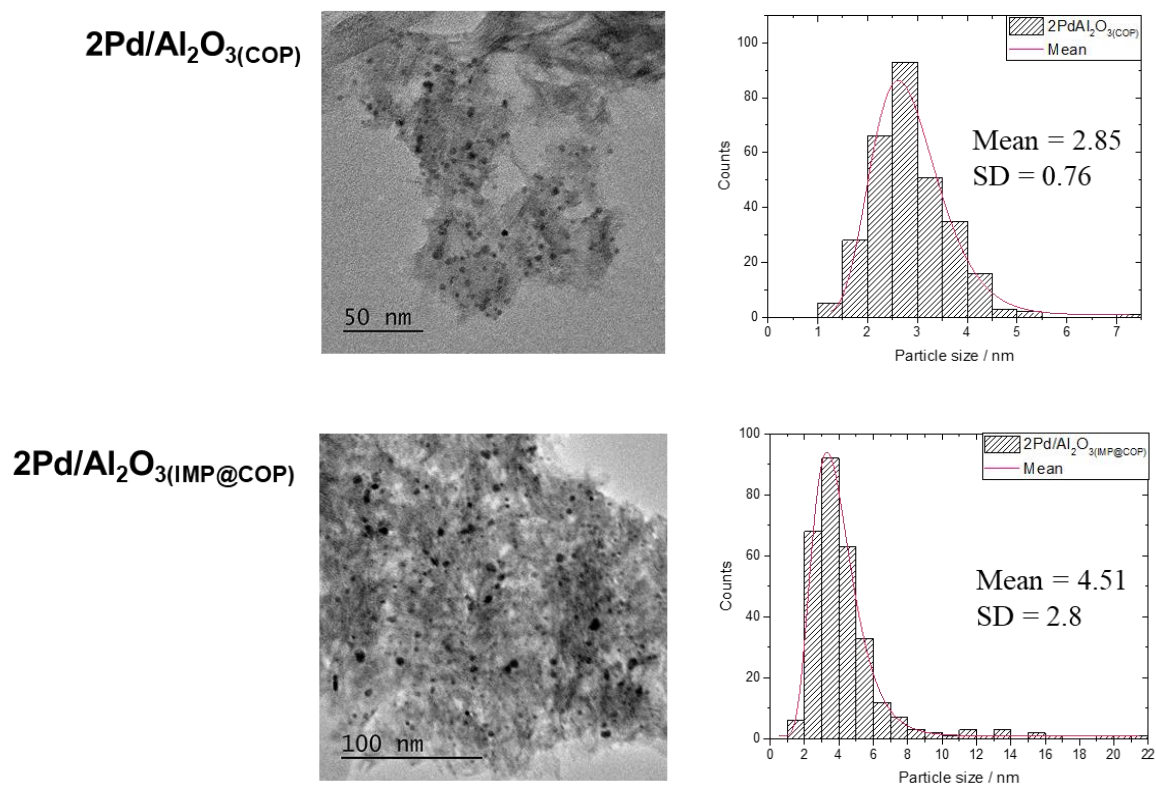


Figure 6.17. TEM images and accompanying particle size distributions for 2Pd/Al₂O₃(COP) and 2Pd/Al₂O₃(IMP@COP).

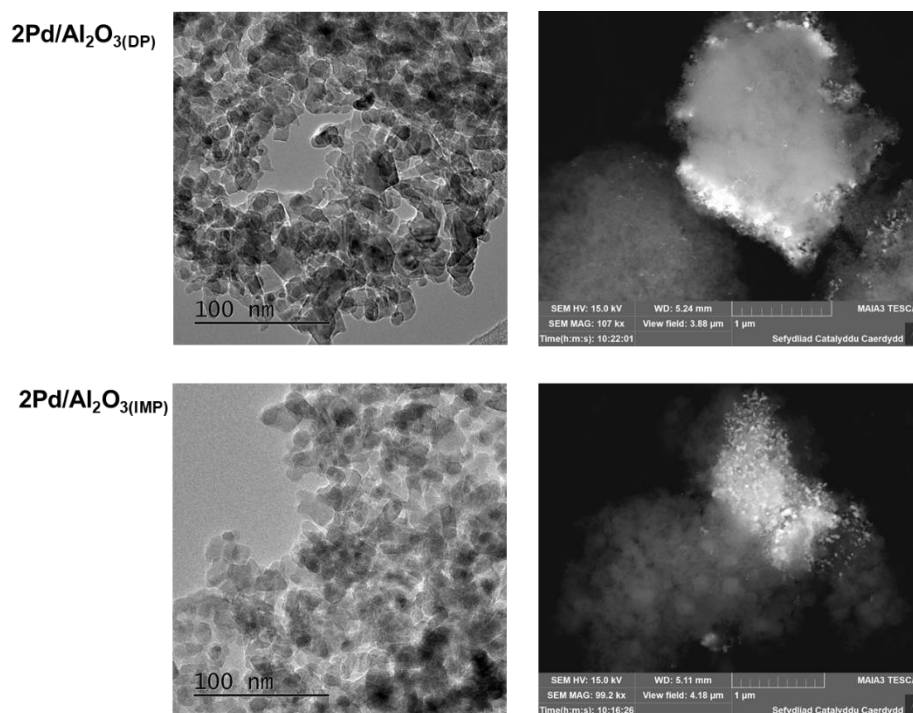


Figure 6.18. TEM and SEM images obtained for 2Pd/Al₂O₃(DP) and 2Pd/Al₂O₃(IMP).

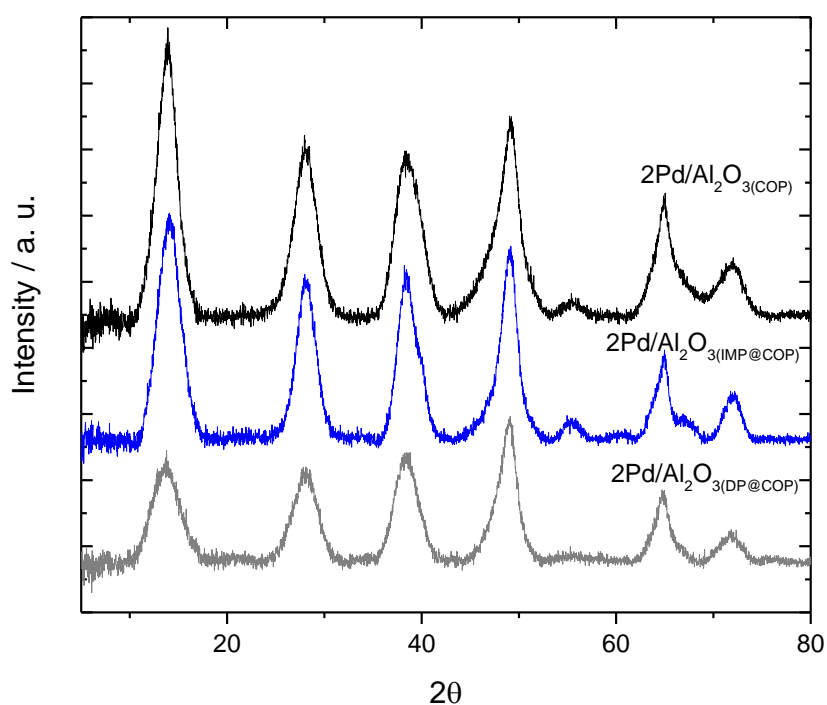


Figure 6.19. XRD patterns obtained for the three 2 wt. % Pd catalysts supported on $\text{Al}_2\text{O}_3(\text{COP})$ prepared by COP, IMP@COP and DP@COP.

XRD analysis represented in Fig 6.19 showed very similar crystallinity levels between the COP and IMP@COP samples. However, significantly lower crystallinity grade was observed for the DP@COP sample, although the IMP@COP and DP@COP samples were prepared using analogous batches of $\text{Al}_2\text{O}_3(\text{COP})$ as support. To exclude a human error during its preparation, $2\text{Pd}/\text{Al}_2\text{O}_3(\text{DP@COP})$ was repeated, however, poor particle distribution and lower intensity in the XRD pattern were regardless observed.

Subsequently samples were analysed by XPS revealing a predominance of metallic Pd in all of them (Fig 6.20). Several batches of $2\text{Pd}/\text{Al}_2\text{O}_3(\text{COP})$ showed some low amounts of Pd oxide and Pd chloride species still present even after the usual reduction treatment (200 °C, 3h in 5 % H_2/Ar). However, additional XPS analysis of used samples confirmed the full *in situ* reduction of all Pd nanoparticles after SA hydrogenation, as can be seen in Fig 6.21.

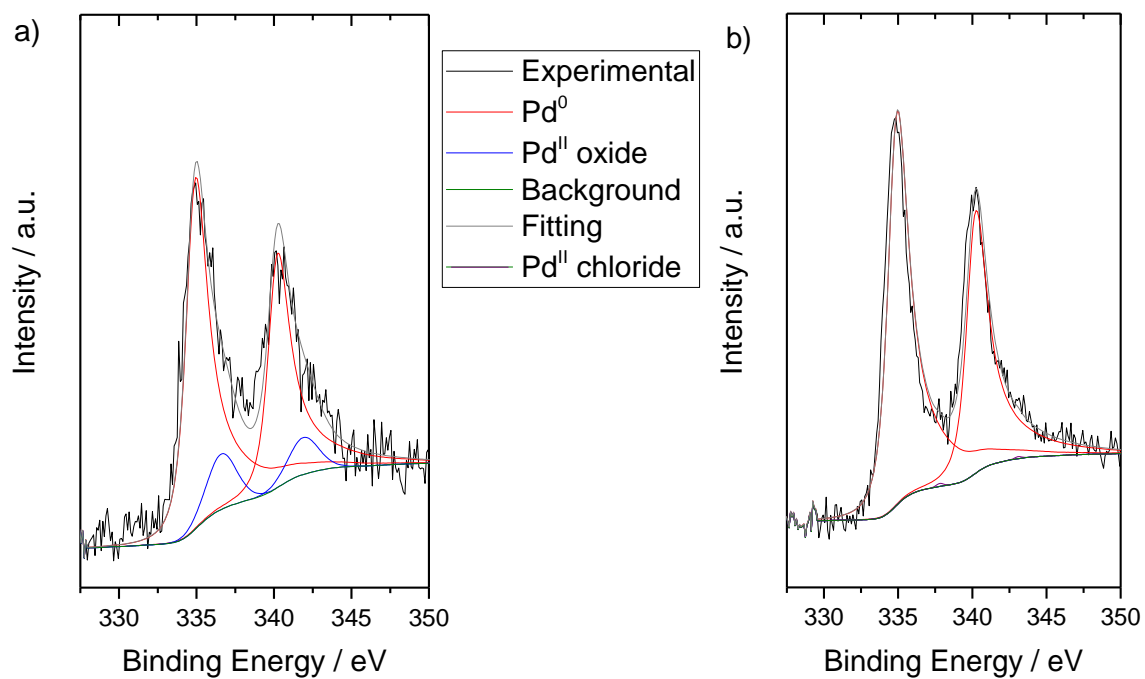


Figure 6.20. XPS analysis of a) 2/Pd/Al₂O₃(COP) and b) 2/Pd/Al₂O₃(IMP@COP).

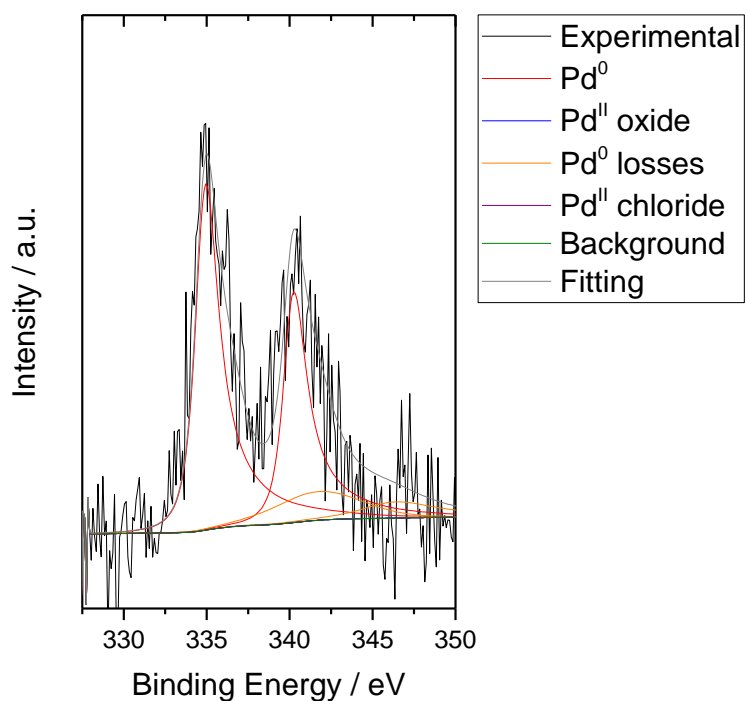


Figure 6.21. XPS analysis of used 2Pd/Al₂O₃(COP).

Once fully characterised, catalysts were tested at the usual reaction conditions for 4 h and their catalytic performances. Compilation of this experiments in Fig 6.22 shows that the catalytic activity obtained for SA hydrogenation using the five materials clearly varied depending on the alumina support involved. While performances of γ - Al_2O_3 -supported materials were quite poor, with a total product yield < 5 % after 4 h of reaction, the performances of $\text{Al}_2\text{O}_3(\text{COP})$ -supported materials were significantly higher, with total product yield comprised between 14 and 24 % after the same reaction period. Regarding the materials supported on $\text{Al}_2\text{O}_3(\text{COP})$ by different techniques, the highest total product yield was obtained with $2\text{Pd}/\text{Al}_2\text{O}_3(\text{COP})$ (32 %), followed by $2\text{Pd}/\text{Al}_2\text{O}_3(\text{IMP@COP})$ (24 %) and $2\text{Pd}/\text{Al}_2\text{O}_3(\text{DP@COP})$ (14 %). Despite the differences in terms of total amount of product yielded, it should be noted that the three catalysts showed comparable product distribution and GBL selectivity (based on total product yielded) > 85 %.

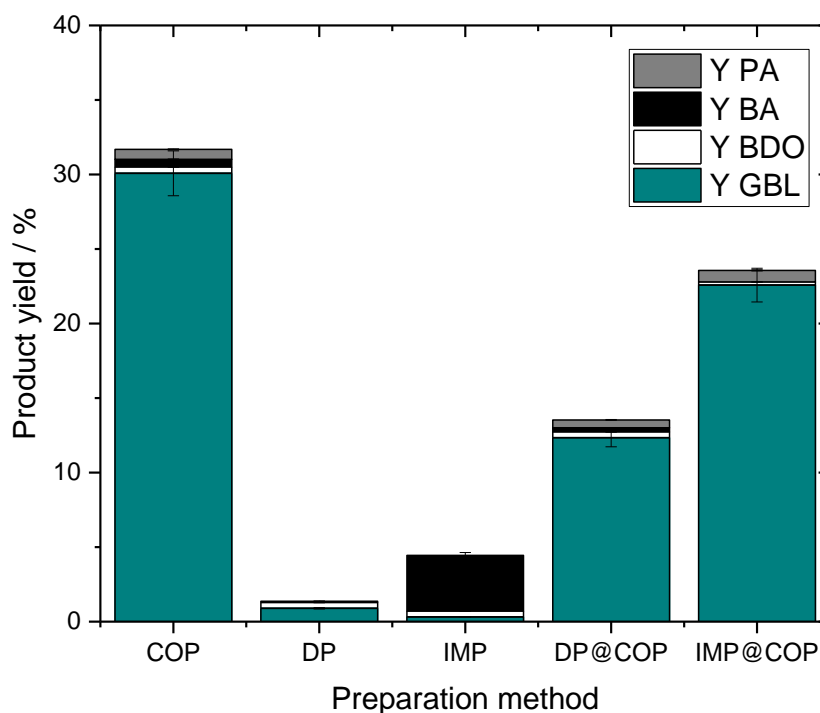


Figure 6.22. Product distribution obtained for various $2\text{Pd}/\text{Al}_2\text{O}_3$ catalysts synthesised by various preparation methods. Reaction conditions: 15 mL of 0.2 M SA in 1,4-dioxane, 2 mol. % of Pd respect to SA, 170 °C, 30 bar H_2 , 4 h.

Given the manifested differences in catalytic behaviour observed between the five materials, correlation with the characterisation analysis described above was enlightening. Firstly, clear differences in terms of structural phase and textural properties were observed between the materials prepared on commercial γ - Al_2O_3 and $\text{Al}_2\text{O}_3(\text{COP})$, with the second one possessing

more than the double of S_{BET} (245 vs. 93 $\text{m}^2 \text{g}^{-1}$). In this regard, analysis of the textural properties of both materials following deposition of Pd by IMP method ($2\text{Pd}/\text{Al}_2\text{O}_3(\text{IMP}@\text{COP})$ and $2\text{Pd}/\text{Al}_2\text{O}_3(\text{IMP})$), collected in Table 6.8, indeed revealed that high porosity for the boehmite phase was retained even after deposition of the metal (224 vs. 85 $\text{m}^2 \text{g}^{-1}$). However, this 2.5-fold decrease in S_{BET} cannot fully account for the 6-fold decrease in activity of $2\text{Pd}/\text{Al}_2\text{O}_3(\text{IMP})$, strongly indicating that other factors, such as support acidity or metal particle size, may influence performance. Secondly, DRIFT experiments has demonstrated that $\text{Al}_2\text{O}_3(\text{COP})$ possesses lower acidity than $\gamma\text{-Al}_2\text{O}_3$. Thirdly, Pd particle distribution throughout the support was poorly successful in $2\text{Pd}/\text{Al}_2\text{O}_3(\text{DP})$ and $2\text{Pd}/\text{Al}_2\text{O}_3(\text{IMP})$ catalysts, obtaining regions with large Pd agglomerates (Fig 6.18). The poorer levels of performance obtained for $\gamma\text{-Al}_2\text{O}_3$ -supported materials compared with $\text{Al}_2\text{O}_3(\text{COP})$ -supported materials is in good agreement with the trend obtained in Fig 6.13, where it was demonstrated that acidic supports significantly lowered the catalytic activity obtained for SA hydrogenation over Pd catalysts.

Therefore, higher catalytic activity observed for $\text{Al}_2\text{O}_3(\text{COP})$ -supported materials compared to $\gamma\text{-Al}_2\text{O}_3$ -supported materials are due to a combination of higher S_{BET} , lower acidity and better Pd nanoparticle dispersion onto the support. All these factor contribute to make $\text{Al}_2\text{O}_3(\text{COP})$ a more suitable support than $\gamma\text{-Al}_2\text{O}_3$ for the preparation of catalytic materials for the system of study, either by hindering interaction of the catalyst with the acidic substrate, and/or by resulting in the deposition of lower activity Pd nanoparticles.

Focusing only on the materials involving $\text{Al}_2\text{O}_3(\text{COP})$, the same structural phase and similar textural properties were obtained, corresponding to the same kind of support employed during the preparation. However, lower crystallinity was observed for $2\text{Pd}/\text{Al}_2\text{O}_3(\text{DP}@\text{COP})$ compared to the other two materials (Fig 6.19), which could explain the lower catalytic activity observed for $2\text{Pd}/\text{Al}_2\text{O}_3(\text{DP}@\text{COP})$ (Fig 6.22), giving about the half of the total product yield obtained with $2\text{Pd}/\text{Al}_2\text{O}_3(\text{COP})$. Regarding $2\text{Pd}/\text{Al}_2\text{O}_3(\text{COP})$ and $2\text{Pd}/\text{Al}_2\text{O}_3(\text{IMP}@\text{COP})$, given their otherwise very similar properties in S_{BET} , crystallinity and dominance of metallic Pd, the higher levels of activity exhibited by $2\text{Pd}/\text{Al}_2\text{O}_3(\text{COP})$ could be attributed to its more uniform distribution of smaller Pd nanoparticles, since smaller particles represent higher metallic surface area available to drive the reaction.

Considering all the facts exposed in this section, IMP proved to be a good method to prepare Pd catalysts, although with broader particle size distribution, when using the appropriate choice of support. This methodology gave the second most active material for hydrogenation of SA, only surpassed by the material prepared entirely by COP. Notably, $2\text{Pd}/\text{Al}_2\text{O}_3(\text{COP})$ displayed the highest catalytic activity in this study for the selective hydrogenation of SA to GBL. Therefore, these remarkable results proved COP to be a valid method for the preparation of Pd catalysts with a narrow, uniform particle size distribution and high catalytic activity.

6.2.3.4 Effect of the Pd loading

From an intensification perspective, the activity of a material per mass charge is one of the most critical factors, given that it determines the choice, design and size of the eventual catalytic reactor. Having this in mind, another key factor to consider during the catalyst design was the metal loading, as utilisation of high Pd loadings could be beneficial to obtain high Space Time Yield (STY) values, and enhance process profitability. Therefore, if the same catalytic performance could be observed even at high Pd loading, the mass of catalyst used for the same catalyst productivity may be reduced significantly.

Additionally, going back to the SA adsorption onto $\text{Al}_2\text{O}_3(\text{COP})$, confirmed in Section 6.2.3.2, the use of catalyst with higher Pd loading implies less support present in the reaction medium when using the same mol. %, which may lead to a beneficial decrease of adsorption and consequently, higher overall carbon balance.

With the aim to investigate the catalyst loading effect, a catalyst with 5 wt. % Pd loading was prepared by COP method ($5\text{Pd}/\text{Al}_2\text{O}_3(\text{COP})$) following the same procedure previously employed. A minor disadvantage was found during the preparation $5\text{Pd}/\text{Al}_2\text{O}_3(\text{COP})$ in the limitation of Pd precipitated on the support, as a coloured solution was obtained after the filtration of the catalyst during the washing step. Analysis by Microwave Plasma-Atomic Emission Spectrometer (MP-AES) determined the coloration to be related to unprecipitated Pd, consistent with the determined loading being 4.75 wt. % of Pd on the catalyst obtained.

Table 6.9. Parameters varied during preparation of $5\text{Pd}/\text{Al}_2\text{O}_3(\text{COP})$.

Entry	pH	Time / h	Real loading ^a / wt. %
1	9	1	4.75
2	9	16	4.75
3	10	1	4.70
4	11	1	4.70

^a Real loading was calculated by discounting the remaining Pd in the filtrate solution measured by MP-AES to the initial Pd used for the preparation of 5 wt. % Pd samples.

Unfortunately, as reported in Table 6.9, variation of parameters such as preparation time or pH did not lead to a full precipitation of Pd, considering that this limitation was intrinsic in the preparation method at such high loading. Despite this, a reaction with this catalyst was carried out at the typical reaction conditions, using the real loading despite denoting the catalyst $5\text{Pd}/\text{Al}_2\text{O}_3(\text{COP})$, and its catalytic activity was compared with $2\text{Pd}/\text{Al}_2\text{O}_3(\text{COP})$ in Fig 6.23.

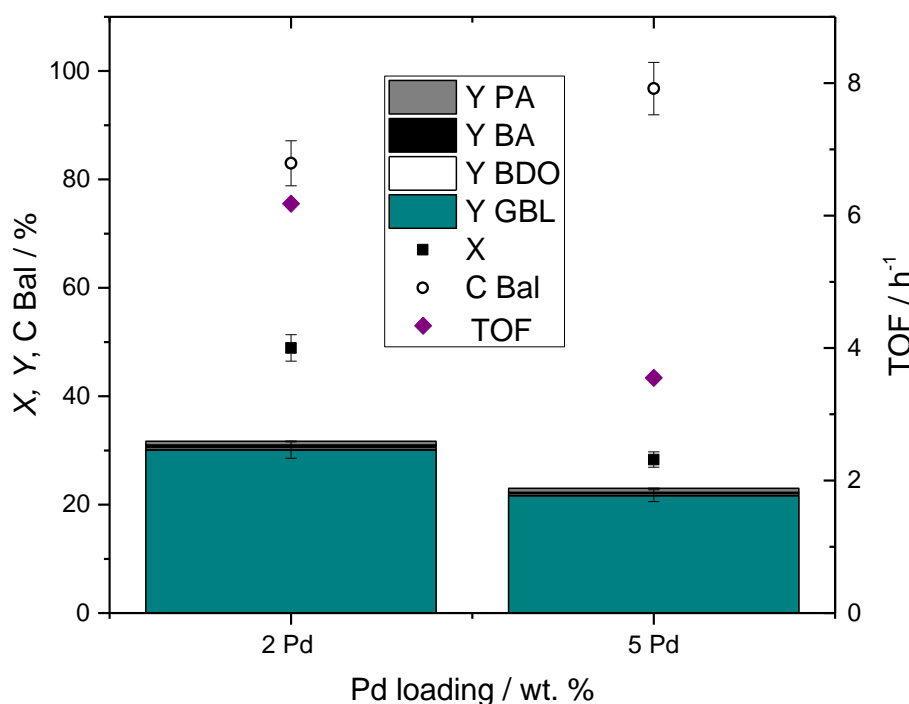


Figure 6.23. Catalytic activity achieved for 2Pd/Al₂O₃(COP) and 5Pd/Al₂O₃(COP). Reaction conditions: 15 mL of 0.2 M SA in 1,4-dioxane, 2 mol. % of Pd respect to SA, 170 °C, 30 bar H₂, 4 h.

As shown in Fig 6.23, the catalytic activity obtained for 5Pd/Al₂O₃(COP) was slightly lower in terms of conversion and product yields. Even though equal amounts of Pd species should lead to the same catalytic activity, 5Pd/Al₂O₃(COP) showed a conversion 20 % lower than its analogue with 2 wt. % Pd loading, and a GBL yield 10 % lower. As consequence of this decrease in activity, higher loading catalyst manifested a lower TOF of 3.6 h⁻¹, 60 % of the value obtained for the 2 % Pd loading of 6.1 h⁻¹. Despite displaying less activity, carbon balance achieved with 5Pd/Al₂O₃(COP) was indeed higher than 2Pd/Al₂O₃(COP), with values of 96 vs. 82 %, respectively. This confirms that at the same reaction conditions, the use of a catalyst with higher Pd loading could palliate the adsorption of the substrate, leading also to higher selectivity towards GBL.

Although the intrinsic activity *i.e.* GBL productivity, calculated as mol of GBL produced per mol of metal per unit of time, of 5Pd/Al₂O₃(COP) was 27 % lower than that of 2Pd/Al₂O₃(COP) (2.9 vs. 3.8 h⁻¹, respectively), the 2.5-fold increase in metal loading did substantially boost the productivity of the catalyst, measured on an activity per gram basis (g(GBL) g(cat)⁻¹ h⁻¹), by a factor of two (0.12 g(GBL) g(cat)⁻¹ h⁻¹ vs. 0.06 g(GBL) g(cat)⁻¹ h⁻¹).

To investigate the cause of this decrease in activity at higher Pd loading, the catalyst was characterised by various techniques and compared to the original 2 wt. % Pd loading.

Table 6.10. Comparison of 2 and 5 wt. % Pd/Al₂O₃(COP) by various techniques.

Material	$S_{\text{BET}} / \text{m}^2 \text{g}^{-1}$	Particle size ^b / nm
2Pd/Al ₂ O ₃ (COP)	256.4	2.85 (\pm 0.76)
5Pd/Al ₂ O ₃ (COP)	242.7	4.83 (\pm 1.27)

^a S_{BET} calculated by BET method from the N₂ adsorption analysis data; ^b Particle size mean calculated from a statistical analysis of TEM images.

As summarised in Table 6.9, the S_{BET} of 5Pd/Al₂O₃(COP) was in the same range of 2Pd/Al₂O₃(COP), both possessed S_{BET} around 250 m² g⁻¹. TEM analysis showed an increment of particle size of approximately 75 % from 2.85 to 4.83 nm from 2 to 5 wt. % Pd loading, respectively. This fact is in accordance with the fact of having more Pd to precipitate on the support, increasing the sintering and growth of the particles. The higher particle size of the 5 wt. % catalyst carried a smaller metallic surface area on the support, which likely leads to reduce the catalytic performance, since implies less surface of active sites available for the reaction. As can be seen in Fig 6.24, as well as occurred for 2Pd/Al₂O₃(COP), 5Pd/Al₂O₃(COP) presented a nice uniform distribution of Pd particles throughout the whole material, manifesting the major advantage of this preparation method.

5Pd/Al₂O₃(COP)

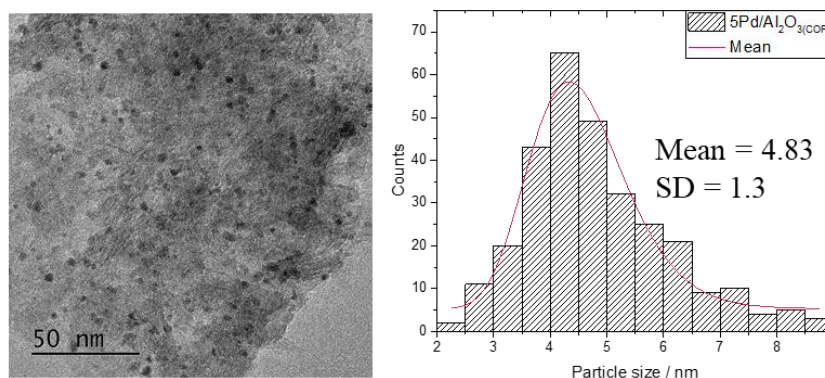


Figure 6.24. TEM images and corresponding particle size distribution for 5Pd/Al₂O₃(COP).

Additionally, analogous XRD pattern to 2Pd/Al₂O₃(COP) and predominance of metallic Pd species were obtained for 5Pd/Al₂O₃(COP) (Fig 6.25), corroborating the reproducibility of COP methodology to prepare similar materials in terms of crystalline phase, porosity and formation of the same active metal species.

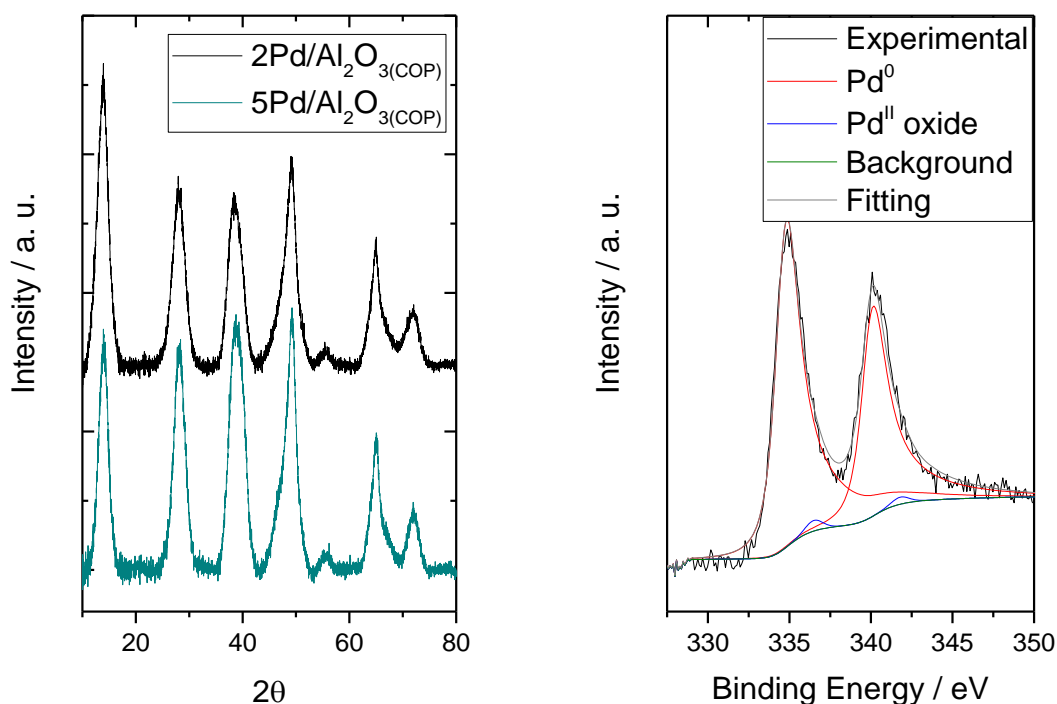


Figure 6.25. (Left) Comparison of XRD pattern of $2\text{Pd}/\text{Al}_2\text{O}_3(\text{COP})$ and $5\text{Pd}/\text{Al}_2\text{O}_3(\text{COP})$ and (Right) XPS analysis obtained for $5\text{Pd}/\text{Al}_2\text{O}_3(\text{COP})$.

Hence, the only determining factor between the two catalyst loadings was the mean of particle size. This fact was a further indication, already observed between $2\text{Pd}/\text{Al}_2\text{O}_3(\text{COP})$ and $2\text{Pd}/\text{Al}_2\text{O}_3(\text{IMP@COP})$, of the impact of the particle size in the catalytic activity. Indeed $5\text{Pd}/\text{Al}_2\text{O}_3(\text{COP})$, exhibited a comparable particle size distribution (4.83 nm) to $2\text{Pd}/\text{Al}_2\text{O}_3(\text{IMP@COP})$ (4.81 nm), and almost identical catalytic activity when tested at the same substrate-to-metal molar ratio.

In regard to the catalyst selectivity towards GBL, kinetic selectivity based on total product yield obtained for both COP catalysts was $\pm 95\%$. However, an increment of carbon balance (from 82 to 96 %) when using $5\text{Pd}/\text{Al}_2\text{O}_3(\text{COP})$, caused by lower proportion of SA adsorbed and the corresponding improvement of GBL selectivity based on SA conversion (from 61 to 75 %), could be observed. Thus overall, $5\text{Pd}/\text{Al}_2\text{O}_3$ resulted in a more convenient catalyst for SA hydrogenation to GBL, with less interferences caused by substrate adsorption.

To further prove the excellent performance of $5\text{Pd}/\text{Al}_2\text{O}_3(\text{COP})$, the SA hydrogenation reaction was carried out for extended times and the time online reaction was represented in Fig 6.26.

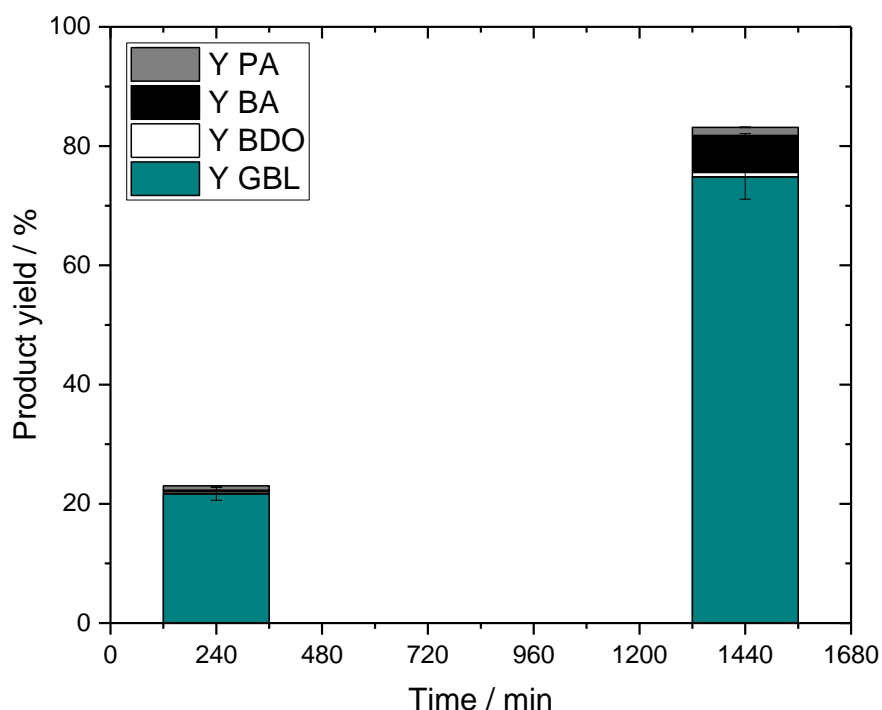


Figure 6.26. Time online analysis of SA hydrogenation over $5\text{Pd}/\text{Al}_2\text{O}_3(\text{COP})$. Reaction conditions: 15 mL of 0.2 M SA in 1,4-dioxane, 2 mol. % of Pd respect to SA, 170 °C, 30 bar H_2 .

As shown in Fig 6.27, similar product distribution was obtained after 24 h of reaction, reaching a total product yield of 83 %. Hence, high GBL yield was achieved (75 %) maintaining the high selectivity towards GBL (> 90 %) even after 24 h of conversion.

Accordingly, for future intensification studies, the higher loaded catalyst ($5\text{Pd}/\text{Al}_2\text{O}_3(\text{COP})$) likely presents the optimal compromise between intrinsic activity and catalyst productivity. To further probe this, an additional reaction with $5\text{Pd}/\text{Al}_2\text{O}_3(\text{COP})$ was also performed at higher temperature (Fig 6.27). As can be observed in Fig 6.27, in only 4 h at 200 °C, the GBL yield was boosted up to 64 %, corresponding to a GBL selectivity of 92 %. This increase in GBL yield represents a productivity of $0.32 \text{ g GBL g}(\text{cat})^{-1} \text{ h}^{-1}$, manifesting the great capability of this kind of Pd catalyst prepared by COP to be used for selective hydrogenation of SA to GBL. Moreover, this GBL productivity value is in the same range of the highest values reported in literature (Table 6.1, Entries 1, 3, 6, 10 and 11), achieving significantly higher GBL selectivity values than Entries 3, 10 and 11 and equivalent GBL selectivity to Entries 1 and 6. However, all of them were obtained at considerably harsher reaction conditions. The catalytic results reported herein, are obtained at the mildest set of operational conditions with high levels of GBL productivity and excellent GBL selectivity reported up to date.

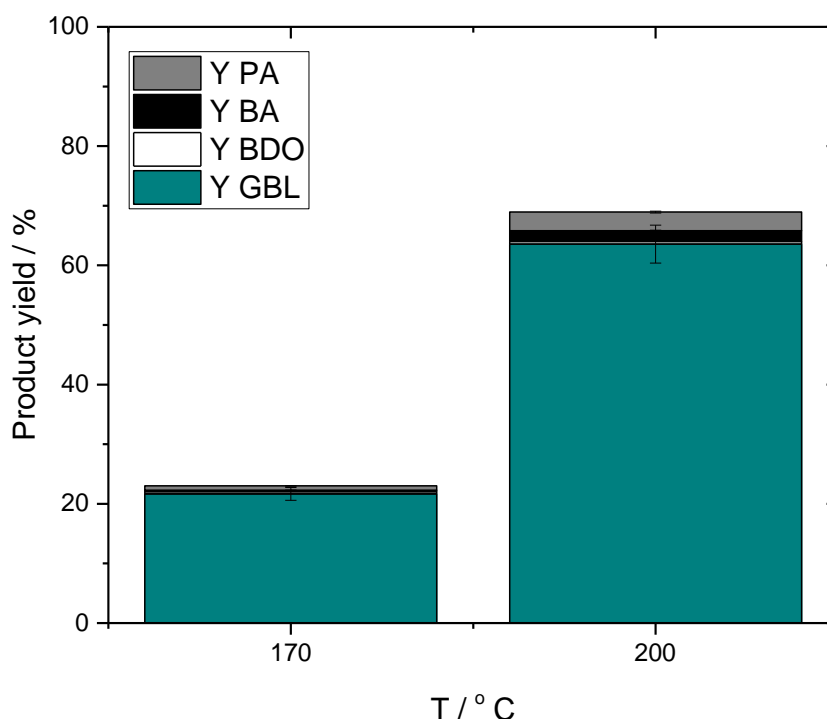


Figure 6.27. Performance of 5Pd/Al₂O₃(COP) at 170 and 200 °C. Reaction conditions: 15 mL of 0.2 M SA in 1,4-dioxane, 2 mol. % of Pd respect to SA, 30 bar H₂, 4 h of reaction.

6.2.3.5 Reusability of 2Pd/Al₂O₃(COP)

Alongside high levels of catalytic activity and selectivity, heterogeneous catalysts must also possess high levels of stability, and an ability to operate for more than one reaction period.⁴⁶ Unfortunately, several factors make the design of reusable catalysts for biomass conversion a major challenge, including the harsh reaction conditions typically required (presence of solvent at high temperature and pressure), and the chelating nature of the oxygenated substrates, such as sugars and acids, which are known to cause leaching and agglomeration of various metallic nanoparticles.^{47,48}

Thus, to gain a preliminary understanding of the reusability properties of 2Pd/Al₂O₃(COP), reusability experiments were performed. To do so, the catalyst was filtered out of the reactor following one kinetic experiment, and subsequently reused in a second and subsequent catalytic experiments. To achieve the most accurate level of insight, and to probe the intrinsic reusability of the catalyst, no intermediate treatments were performed on the material *i.e.* the catalyst was simply filtered from solution, dried at room temperature, and then placed back in the reactor. Following this same procedure, up to 4 cycles were performed. Note that Fresh was considered the first cycle of the reusability runs.

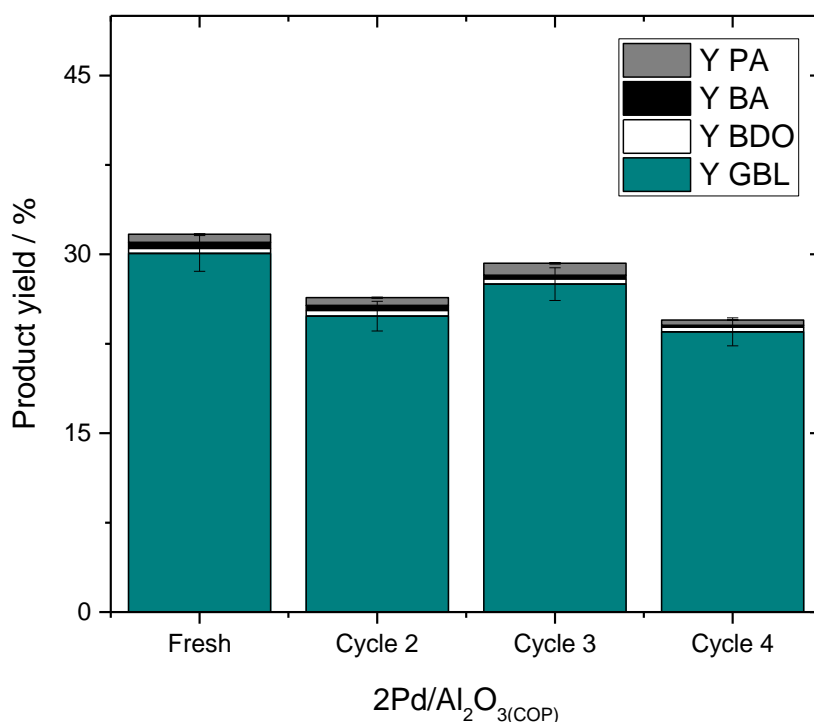


Figure 6.28. Reusability studies of $2\text{Pd}/\text{Al}_2\text{O}_3(\text{COP})$ for SA hydrogenation. No intermediate regeneration treatments were performed between cycles. Reaction conditions: 15 mL of SA 0.2 M in 1,4-dioxane at 170 °C, 30 bar H_2 , 2 mol. % Pd respect to SA, 4 h of reaction.

As reported in Fig 6.28, good reusability was observed for $2\text{Pd}/\text{Al}_2\text{O}_3(\text{COP})$, with no major loss of activity being observed over three kinetic cycles. The high levels of stability exhibited by the catalyst is a promising discovery for future intensification studies.

6.3 Conclusions

Along with the other chapters in this work, the optimisation of a sustainable catalytic route towards valuable lactone monomers from a bio-derived source has been investigated in depth. This chapter shows that SA, a C4 compound increasingly being produced on a several kiloton-scale by the microbial fermentation of sugar, can be converted into a variety of important chemicals, including GBL. Optimisation of the working conditions using $5\text{Ru}/\text{Al}_2\text{O}_3(\text{COM})$ demonstrates how selectivity can be switched in favour of GBL formation against PA by lowering the reaction temperature to 170 °C with only 30 bar of H_2 , obtaining 50 - 60 % of selectivity towards GBL.

Through an extensive catalyst design investigation focus on the choice of metal, support and preparation method used, selectivity towards GBL has been found to be maximised when using Pd catalysts (> 85 %). Best performance in terms of activity and selectivity is observed

for 2 wt. % Pd supported on Al_2O_3 prepared by co-precipitation method. By this preparation method, a pseudo-boehmite Al_2O_3 is precipitated *in situ*, with high S_{BET} , a uniform distribution of Pd nanoparticles throughout the whole material, and a lowly acidic surface. Combination of these three characteristics is what makes $2\text{Pd}/\text{Al}_2\text{O}_{3(\text{COP})}$ a successful catalyst for the chemo-selective lactonization of SA to GBL.

Although this kind of support showed to be chemically adsorbing some of the unconverted SA on its surface affecting the carbon balance, this loss of carbon balance has been confirmed to be only caused by adsorption phenomena. Herein, selectivity can be adequately calculated based on total product yield, displaying excellent results of GBL selectivity > 90 %.

The use of $5\text{Pd}/\text{Al}_2\text{O}_{3(\text{COP})}$ instead of $2\text{Pd}/\text{Al}_2\text{O}_{3(\text{COP})}$, and hence, less support material added in the reaction medium (at the same mol. % Pd employed) effectively palliates this adsorption, as well as benefits the obtainment of higher STY. The $5\text{Pd}/\text{Al}_2\text{O}_{3(\text{COP})}$ catalyst achieved a GBL yield of 23 % with a kinetic selectivity of 93 % after 4 h of reaction at 170 °C. Moreover, its utilisation at 200 °C notably boosted the GBL productivity, obtaining 0.32 g GBL $\text{g}(\text{cat})^{-1} \text{h}^{-1}$, in the range of the most productive systems reported but representing the mildest set of operational conditions to date, with high GBL productivity and selectivity also observed. These promising results point to $5\text{Pd}/\text{Al}_2\text{O}_{3(\text{COP})}$ as being a suitable catalyst for SA hydrogenation to GBL. Furthermore, $\text{Pd}/\text{Al}_2\text{O}_{3(\text{COP})}$ showed good reusability, demonstrating the high stability of the material and its promising employment as catalyst for selective SA valorisation to GBL.

This chapter contributed to the following paper:

K. Yakabi, A. Jones, A. Buchard, A. Roldan, C. Hammond, *ACS Sustainable Chem. Eng.*, 2018, **6**, 16341 – 16351

References

- (1) J. Zhu, X. Zhang, X. Pan, *ACS Symposium Series*. 2011, vol 1067
- (2) C. F. Vilela, A. F. Sousa, A. C. Fonseca, A. C. Serra, J. F. J. Coelho, C. S. R. Freire, A. J. D. Silvestre, *Polym. Chem.*, 2014, **5**, 3119 - 3141
- (3) J. Van Haveren, E. L. Scott, J. Sanders, *Biofuels Bioprod. Bioref.*, 2008, **2**, 41 – 57
- (4) E. De Jong, A. Higson, P. Walsh, M. Wellisch, “*Bio-based Chemicals Value Added Products from Biorefineries*”, IEA Bioenergy, 2012
- (5) J. S. Luterbacher, D. Martin Alonso, J. A. Dumesic, *Green Chem.*, 2014, **16**, 4816 – 4838
- (6) A. Corma, S. Iborra, A. Velty, *Chem. Rev.*, 2007, **107**, 2411 – 2502
- (7) M. J. Climent, A. Corma, S. Iborra, *Green Chem.*, 2014, **16**, 516 – 547
- (8) J. Hill, E. Nelson, D. Tilman, S. Polasky, D. Tiffany, *Proc. Natl. Acad. Sci. U. S. A.*, 2006, **103**, 11206 – 11210
- (9) S. Shylesh, A. A. Gokhale, C. R. Ho, A. T. Bell, *Acc. Chem. Res.*, 2017, **50**, 2589 – 2597
- (10) I. Delidovich, K. Leonhard, R. Palkovits, *Energy Environ. Sci.*, 2014, **7**, 2803 – 2830
- (11) A. J. Ragauskas, C. K. Williams B. H. Davison, G. Britovsek, J. Cairney, C. A. Eckert, W. J. Frederick Jr, J. P. Hallett, D. J. Leak, C. L. Liotta, J. R. Mielenz, R. Murphy, R. Templer, T. Tschaplinski, *Science*, 2006, **311**, 484 – 489
- (12) G. T. Tsao, N. J. Cao, J. Du, C. S. Gong, *Adv Biochem. Eng. Biotechnol.*, 1999, **65**, 243 - 80

- (13) Nexant ChemSystems, "Biochemical Opportunities in the United Kingdom NNFCC project 08-008, A study funded by Defra, project managed by The National Non-Food Crops Centre (NNFCC)", 2008
- (14) C. Delhomme, D. Weuster-Botz, F. E. Kühn, *Green Chem.*, 2009, **11**, 13 – 26
- (15) B. Cok, I. Tsiropoulos, A. L. Roes, M. K. Patel, *Biofuel Bioprod. Bior.*, 2014, **8** (1), 16 - 29
- (16) S. J. Lee, H. Song, S. Y. Lee, *Appl. Environ. Microbiol.*, 2006, **72**, 1939 – 1948
- (17) S. Vaswani, "A private report by the Process Economic Program, Bio-Based Succinic Acid", 2010
- (18) Y. Cao, R. Zhang, C. Sun, T. Cheng, Y. Liu, M. Xian, *Biomed Res Int.*, 2013, Article ID 723412
- (19) J. M. Pinazo, M. E. Domine, V. Parvulescu, F. Petru, *Catal Today*, 2015, **239**, 17 – 24
- (20) T. Werpy, G. Petersen, "Top Value-Added Chemicals from Biomass Volume I — Results of Screening for Potential Candidates from Sugars and Synthesis Gas", 2004
- (21) I. Bechthold, K. Bretz, S. Kabasci, R. Kopitzky, A. Springer, *Chem. Eng. Technol.* 2008, **31** (5), 647 – 654
- (22) J. Xu, B. H. Guo, *Biotechnol. J.*, 2010, **5** (11), 1149 - 1163
- (23) F. Aeschelmann, M. Carus, "Biobased Building Blocks and Polymers in the World – Capacities, Production and Applications: Status Quo and Trends towards 2020", 2015
- (24) M. Hong Y. E. Y. X. Chen, *Nature Chemistry*, 2016, **8**, 42 – 49
- (25) M. Hong, X. Tang, B. S. Newell, E. Y. X. Chen, *Macromolecules*, 2017, **50**, 8469 - 8479
- (26) I. Bechthold, K. Bretz, S. Kabasci, R. Kopitzky, A. Springer, *Chem. Eng. Technol.*, 2008, **31**, 647 – 654
- (27) G. Budroni, A. Corma, *J. Catal*, 2008, **257**, 403 – 408
- (28) R. M. Deshpande, V. V. Buwa, C. V. Rode, R. V. Chaudhari, P.L. Mills, *Catal. Commun.*, 2002, **3**, 269 – 274
- (29) C. Zhang, L. Chen, H. Cheng, X. Zhu, Z. Qi, *Catal Today*, 2016, **276**, 55 – 61
- (30) D. Pham Minh, M. Besson, C. Pinel, P. Fuertes, C. Petitjean, *Top Catal.*, 2010, **53**, 1270 - 1273
- (31) B. Tapin, F. Epron, C. Especel, B. K. Ly, C. Pinel, M. Besson, *Catal Today*, 2014, **235**, 127 - 133
- (32) X. Di, Z. Shao, C. Li, W. Li, C. Liang, *Catal. Sci. Technol.*, 2015, **5**, 2441 - 2448
- (33) X. Di, C. Li, G. Lafaye, C. Especel, F. Epron, C. Liang, *Catal. Sci. Technol.*, 2017, **7**, 5212 – 5223
- (34) U. G. Hong, S. Hwang, J. G. Seo, J. Yi, I. K. Song, *Catal Lett.*, 2010, **138**, 28 - 33
- (35) U. G. Hong, J. Lee, J. S. Hwang, I. K. Song, *Catal Lett*, 2011, **141**, 332 – 338
- (36) C. You, C. Zhang, L. Chen, Z. Qi, *Appl. Organometal. Chem.*, 2015, **29**, 653 – 660,
- (37) K. H. Kang, U. Gi Hong, Y. Bang, J. H. Choi, J. K. Kim, J. K. Lee, S. J. Han, I. K. Song, *Appl. Catal., A*, 2015, **490**, 153 – 162
- (38) U. G. Hong, S. Hwang, J. G. Seo, J. Lee, I. K. Song, *J. Ind. Eng. Chem.*, 2011, **17**, 316 – 320
- (39) B. Tapin, F. Epron, C. Especel, B. K. Ly, C. Pinel, M. Besson, *ACS Catal.* 2013, **3**, 2327 – 2335
- (40) X. Di, C. Li, B. Zhang, J. Qi, W. Li, D. Su, C. Liang, *Ind. Eng. Chem. Res.* 2017, **56**, 4672 – 4683
- (41) Z. Shao, C. Li, X. Di, A. Xiao, C. Liang, *Ind. Eng. Chem. Res.*, 2014, **53**, 9638 – 9645
- (42) F. Schüth, *Chem. Mater.*, 2018, **30**, 11, 3599 – 3600
- (43) A. P. Kumar, B. P. Kumar, A. B. V. K. Kumar, B. T. Huy, Y. I. Lee, *App. Surf. Sci.*, 2013, **265**, 500 - 509
- (44) D. Kuang, Y. Fang, H. Liu, C. Frommen, D. Fenske, *J. Mater. Chem.*, 2003, **13**, 660 – 662
- (45) D. Padovan, A. Al-Nayili, C. Hammond, *Green Chem.*, 2017, **19**, 2846 - 2854
- (46) C. Hammond, *Green Chem.*, 2017, **19**, 2711 - 2728
- (47) I. Sábada, M. López Granados, A. Riisager, E. Taarning, *Green Chem.*, 2015, **17**, 4133 - 4145
- (48) F. Hérogel, B. Rozmysłowicz, J. S. Luterbacher, *Chimia (Aarau)*, 2015, **69** (10), 582 - 91

7. Final conclusions and pertaining challenges

7.1. Final conclusions

Considering the globally increasing concerns on fossil fuel feedstocks, and particularly their negative environmental impact and their prompt depletion, investigation of renewable monomers for the synthesis of polymeric materials with comparable or superior properties than their petroleum-based analogues has become of high importance.

Within all the different kinds of renewable monomers that can be obtained from biomass, the family of the lactones is highly versatile, as they can suitably undergo ROP and give rise to a varied range of polymeric material. Amongst several catalytic routes available to produce lactones, this work focused its attention on two approaches: the BVO of R-CyO and the selective hydrogenation of SA to produce the desired corresponding lactones.

In Chapter 3, the main challenges faced for the performance of BVO of CyO using Sn- β as catalyst and H₂O₂ as oxidant are investigated, as this represents a greener alternative to the industrially employed process with peroxyacid-based oxidants. This chapter shows that this reaction is highly active and selective only up to 60 % CyO conversion. Above this level of conversion, a significant drop in lactone selectivity is observed, caused by the consecutive hydrolysis of the desired lactone to 6-HHA, which is confirmed to be also Sn- β catalysed.

Therefore, the consecutive ring opening reaction occurs simultaneously to BVO at the standard conditions used, substantially decreasing the efficiency (selectivity) and activity (rate) of the process, deactivating the catalyst by poisoning. It should be noted that at the time of this work, this was the first time that the by-product identification and quantification was analysed in such detail. Additionally, optimisation of the reaction conditions in order to minimise 6-HHA formation shows the potential scalability of this system in the continuous regime, obtaining good activity and stability over 180 h and yielding turnover numbers > 5000, thus demonstrating the major advantages of the continuous system, and representing the first time that Sn- β is employed for BVO in continuous flow operation.

The successful results presented in Chapter 3 using BVO of CyO as model reaction set the basis to evaluate the general applicability of the system beyond this typical substrate. To do so, Chapter 4 is focused on the exploration of more complex ketones as substrates for BVO as part of a sustainable route for the synthesis of renewable monomers. Through the study of different 2-R-CyO and 4-R-CyO, from a kinetic and a thermodynamic point of view, this chapter reveals a crucial impact of the substituent position and size. Whilst increasing the size of the R group limits the activity for the bulkiest substrates substituted in position 2 due to steric hindrance, excellent catalytic performance is obtained for the whole 4-R-CyO series, achieving > 90 % of conversion after 6 h of reaction. Additionally, selectivity towards 4-Capr is higher than the one observed with CyO over the whole reaction period. By complementary computational studies, 4-R-CyO are confirmed to be thermodynamically favourable to undergo BVO, whilst the consecutive hydrolysis reactions arising from them are thermodynamically less favoured in the presence of bulkier R-groups in position 4. Furthermore, 4-*i*-Pr-CyO, readily available from terpenes or lignin derivatives, are demonstrated to be an excellent substrate for the potential scalability of BVO in continuous flow obtaining very good stability, productivity and high selectivity to the lactone (up to 85 %) over 1000 substrate turnovers and 56 h of reaction. Additionally, the lactone produced by BVO using Sn- β / H₂O₂ gives rise to good quality polyester *via* ROP mechanism, showing the practical applicability of this catalytic route. These outstanding results demonstrate the successful broadening of the substrate scope of the Sn- β / H₂O₂ BVO system. Moreover, it opens a route towards the sustainable production of renewable monomers through the BVO of sustainably derived ketones.

In Chapter 5, the viability of coupling *in situ* H₂O₂ production with the BVO system is explored. *In situ* generation of H₂O₂ appears to be an attractive solution to reduce the H₂O present in the system, and to upgrade the sustainability of the BVO chemistry, as well as potentially increase the lactone selectivity by limiting the hydrolysis step upon reduction of the amount of H₂O in the system. Nonetheless, coupling of *in situ* H₂O₂ synthesis and BVO reaction represents a great challenge since optimal conditions of both systems present important incompatibilities (reaction temperatures and reaction media). Remarkably, the employment of

a solvent mixture MeOH/1,4-dioxane, in a ratio 1:9, results in benefits to both systems. Unfortunately, coupling the two systems in one pot is unsuccessful, emphasising the very different needs of each system. Nevertheless, a preliminary test in two stages, by first producing *in situ* H₂O₂ in MeOH at 10 °C, and then diluting this reaction mixture to be 1:9 in 1,4-dioxane for the BVO reaction at 50 °C, successfully proves the feasibility of the overall system to work in two stages.

Following this, the other catalytic system investigated along this work, the selective hydrogenation on SA, considered in of the “Top list” of bio-derived platform molecules, to GBL is explored in Chapter 6. The optimisation of the selective hydrogenation in batch mode is first carried out over various commercial catalysts and then GBL selectivity is subsequently maximised by catalyst design. Through the investigation of the structure - activity relationship observed for the metal supported nanoparticles employed, the features of a suitable material required to obtain high productivity of GBL are exposed. Selectivity towards GBL is maximised (> 85 %) when using Pd catalysts, especially Pd/Al₂O₃ prepared by the COP method, at 170 °C with 30 bar of H₂. By this preparation method, a pseudo-boehmite Al₂O₃ is precipitated *in situ*, with high S_{BET}, a uniform distribution of Pd nanoparticles throughout the whole material, and possessing a low acidity surface. The combination of these three characteristics is what makes Pd/Al₂O₃(COP) a successful catalyst for the chemo-selective lactonization of SA to GBL, which also shows great reusability. The levels of GBL productivity reached in this work are in the same range of the most productive systems previously reported, and represents the mildest set of operational conditions employed able to show such high productivity and selectivity towards GBL reported up to date. These promising results point towards Pd/Al₂O₃(COP) as being a suitable catalyst for SA hydrogenation to GBL and its intensification studies.

7.2. Pertaining challenges

Even though many challenges have been tackled and solved during this work, many new questions and future research lines have also been generated.

7.2.1. BVO of R-CyO using Sn-β and H₂O₂

The BVO / Sn-β / H₂O₂ system has proved its viability to operate in continuous flow, the first step towards scalability of the process and potential industrialisation. However, many key points require deeper attention including the catalyst preparation and its lifetime, and the targeted levels of conversion to operate in continuous mode.

Sn-β has been extensively studied for almost 20 years, during which period many different aspects of its chemistry have been covered, from its reactivity for a variety of reactions to the

methods of its synthesis, pointing to Sn- β as of the most promising materials for biomass valorisation processes.¹⁻³ For example, Sn- β , was conclusively reported by Corma *et al.*⁴ to be the most active, selective, and suitable catalyst for this BVO transformation, and its outstanding performance in the academic research level has been also proved through this work.

However, one of the weak points during the development of Sn- β as commercial catalyst is its difficult synthesis. The classical hydrothermal synthesis requires long times, highly hazardous reactants (HF) and can only proceed at low metal contents (< 2 wt. % of Sn), discouraging its production at larger scales.⁵ For this reason, many years of research of Sn- β have been devoted to the search of alternative synthetic methods.⁶ One of the most promising approaches is the post-synthetic synthesis method of SSI, employed for the preparation of the Sn-catalysts used in this work, since it has been shown to be fast and scalable.⁷ Nonetheless, by this methodology the efficiency of Sn incorporation becomes poorer as the metal loading increases (> 5 wt. % of Sn), leading to the formation of inactive SnO₂, and higher metal loadings are always desirable to increase considerably the STY of the process.⁸ Therefore, further studies are needed in regards of the process of incorporation of the metal in the framework, including i) mechanistic studies, to follow the metal incorporation and understand how and when SnO₂ formation starts to become relevant by *in situ* techniques, such as DRIFT, DRUV-Vis, Raman and XRD, ii) the use of different solid sources of Sn, such as Sn (IV) chloride pentahydrate, since the precursor organic ligand may affect the incorporation of the metal in the zeolite framework, allowing to obtain higher Sn loadings and iii) the use of different post-synthetic procedures to form the silanol groups and modify the hydrophilicity of the material prior the Sn incorporation, as this may also affect the formation of inactive SnO₂.

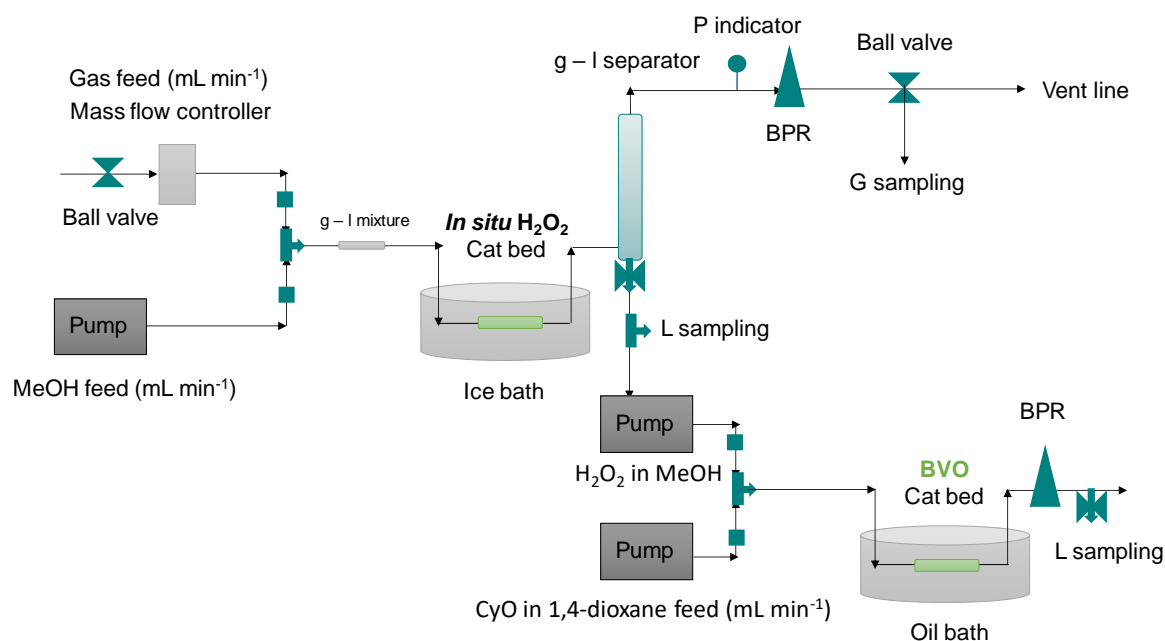
Alternatively, other types of zeolite structures can be explored to introduce higher Sn loadings in their framework and their pertaining performance for this reaction can be investigated.

Additionally, although it has been shown that Sn- β possesses good stability during continuous flow operation of BVO of CyO and 4-*i*-Pr-CyO for the periods tested, reactions performed for longer times should be carried out to study the catalyst stability in this system in more detail. Furthermore, in this work, only deactivation by poisoning has been covered, and by minimising the 6-HHA formation targeting 60 % of CyO conversion, this effect has been significantly palliated. However, Sn- β may suffer some deactivation by fouling due to coking and product absorption causing blockage of the micropores at extended reaction times. In this regard, the use of Sn- β -H, which has demonstrated to be also a highly active material for this reaction, may mitigate the potential deactivation by fouling, by its improved diffusional properties. This fact was demonstrated when studying the MPV reaction of CyO using the same two materials.⁹ In said study, Sn- β -H showed remarkably improved stability, losing only 20 % of its activity over 700 h on stream, whilst in contrast, microporous Sn- β lost \pm 70 % of activity in only 200

h on stream. Therefore, it could be very interesting to investigate if the use of Sn- β -H can decrease the 15.4 % of activity loss observed in Chapter 3 for the continuous operation of BVO of CyO over Sn- β , and as extension, also BVO of the rest of the substrates tested.

The other key point to make this process more industrially appealing is the level of activity targeted for the continuous flow experiments. In Chapter 3, it has been shown that in order to minimise 6-HHA formation during BVO of CyO, to limit deactivation of the catalyst by poisoning, the reaction should be carried out targeting approximately 60 % of CyO conversion with selectivity ± 75 %. However, from an industrial perspective, higher levels of conversion and selectivity are always more desirable, since the separation of the unreacted ketone and by-products and recycling of the substrate can increase considerably the total operational cost. On this subject, it has been demonstrated that the main impediment to target higher levels of activity whilst maintaining high levels of selectivity is the unavoidable ring opening reaction of the lactone, also Sn- β catalysed in the presence of H₂O. Considering that H₂O is formed as by-product and added intrinsically with the oxidant at the start of the reaction, this is where the coupling with *in situ* H₂O₂ can play an important role.

Given the positive result obtained in batch mode for the coupling in two stages, this part of the project can be continued by coupling the two systems in two pots under continuous operation, allowing to perform each individual system at its optimal reaction conditions (Scheme 7.1).



Scheme 7.1. Proposed scheme for the coupling of direct H₂O₂ formation and BVO in two stages in continuous flow.

In this way, *in situ* H₂O₂ production can be carried out in continuous mode in pure MeOH at 10 °C (or even lower, e.g. 2 °C), maximising the amount of oxidant formed, prior to being separated from the gas phase and pumped into the BVO system. This approach allows to further optimisation of *in situ* H₂O₂ production by implementing some of the improvements reported in literature, such as the use of promoters to enhance productivity, and the addition of stabilisers to increase thermal and chemical stability of the oxidant.

Since it was previously shown that a mixture 1:9 of MeOH/1,4-dioxane displayed promising results, the H₂O₂ produced *in situ* can be diluted into the BVO reactant feed in the appropriate ratio and then used as oxidant. The BVO reaction can then also be carried out at optimised temperatures. This part of the system should also be further optimised. For instance, how the acetalisation of CyO proceeds in continuous mode should be studied.

The use of a trickle bed reactor to produce continuously H₂O₂ adds multiple benefits to the overall process. Besides the intrinsic advantages of production *in situ* H₂O₂ from H₂ and O₂ in a more sustainable process, with reduced costs and transportation issues, the trickle bed allows to operate in lower pressure ranges (\pm 10 bar) and the operating conditions can be easily varied during the optimisation of the process. In fact, the use of a trickle bed reactor for direct synthesis of H₂O₂ has been successfully reported in the last decade.¹⁰

Additional studies on appropriate gas - liquid mixtures are required to maximise H₂O₂ productivity, as well as stability studies of the *in situ* H₂O₂ formed, to evaluate its thermal and chemical decomposition until it reaches the catalyst bed for the BVO reaction.

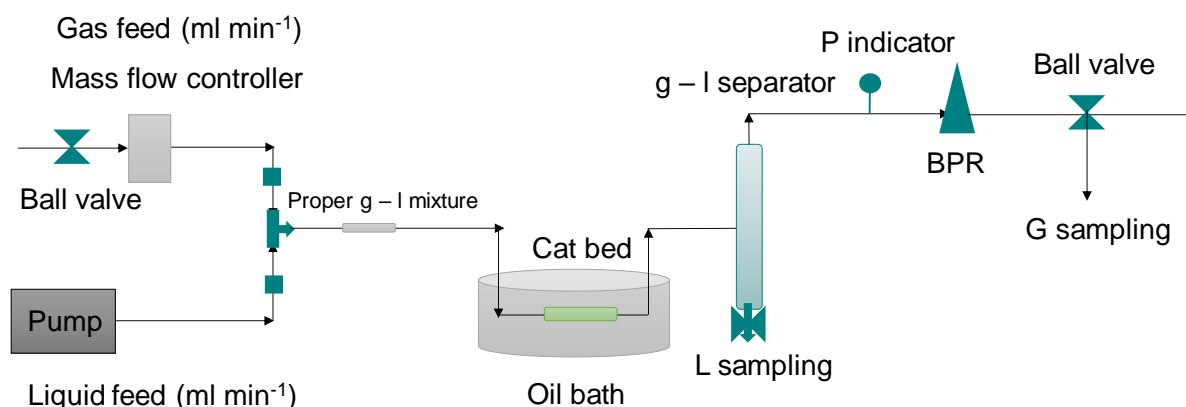
Even so, the challenge may likely still remain in ensuring the production of enough oxidant, whilst preventing its decomposition after the dilution in the BVO feed, in order to obtain good reaction rates for BVO of CyO to Capr. However, this approach may allow a greater optimisation of the overall reaction system and once achieved, imply an upgrade of the sustainability of the BVO chemistry.

Finally, regarding the general sustainability of the production of lactone monomers *via* BVO / Sn- β / H₂O₂, there is still further work to do in order to optimise the reported catalytic routes from bio-derived platform molecules to CyO and R-CyO (Chapter 1) and fulfil the needs of these processes to become scalable and commercially suitable. Moreover, optimisation of the ROP of the corresponding lactones produced by BVO / Sn- β / H₂O₂ along this work and their applicability can be further investigated.

7.2.2 Selective hydrogenation of SA to GBL

Pd/Al₂O₃ prepared by COP method has been shown to be a promising catalyst to selectively hydrogenate SA to GBL at mild conditions, obtaining very high levels of selectivity and

productivity, and demonstrating excellent reusability. Herein, the future work should be focused on the investigation of the viability of this system to operate in continuous mode. Analogously to the direct production of H_2O_2 described above, and upon the successful results obtained in batch, selective hydrogenation of SA to GBL at mild conditions could be carried out in a trickle bed reactor (Scheme 7.2) by optimising the gas - liquid mixture and the general operational conditions.



Scheme 7.2. Proposed scheme for the SA hydrogenation in continuous flow.

Although some recent reports can be found regarding SA hydrogenation to BDO in continuous flow,¹¹ hydrogenation to GBL in flow mode has not yet been reported, hence, the continuation of this work could lead to a very interesting piece of work.

Finally, another revealing point from this work was the obtainment of completely different product distribution using Pd and Ru catalysts, suggesting that they promote different reaction pathways. To gain further insight as to the more selective nature of $\text{Pd}/\text{Al}_2\text{O}_3$ vs. $\text{Ru}/\text{Al}_2\text{O}_3$, preliminary computer simulations focused on the adsorption of SA onto metal surfaces were performed by Dr. Alberto Roldan, using the most stable surfaces for Ru and Pd, *i.e.* (0001) and (111) respectively (Fig 7.1). These calculations suggest that SA binds to both surfaces through the carboxylic groups (left). However, after deprotonation (right), the geometry of this coordination and the type of binding on both metals appears to be different. Whilst the coordination of SA over Ru appears to be bidentate (top), SA coordination over Pd is more unidentate (bottom). Although detailed reaction coordinate analysis is required before definitive mechanistic hypotheses can be made, the choice of metal impacts the coordination and hence, the geometry of SA at the active site, and may therefore account for the improved selectivity towards GBL observed for Pd-catalyst vs. Ru-catalyst during SA hydrogenation.

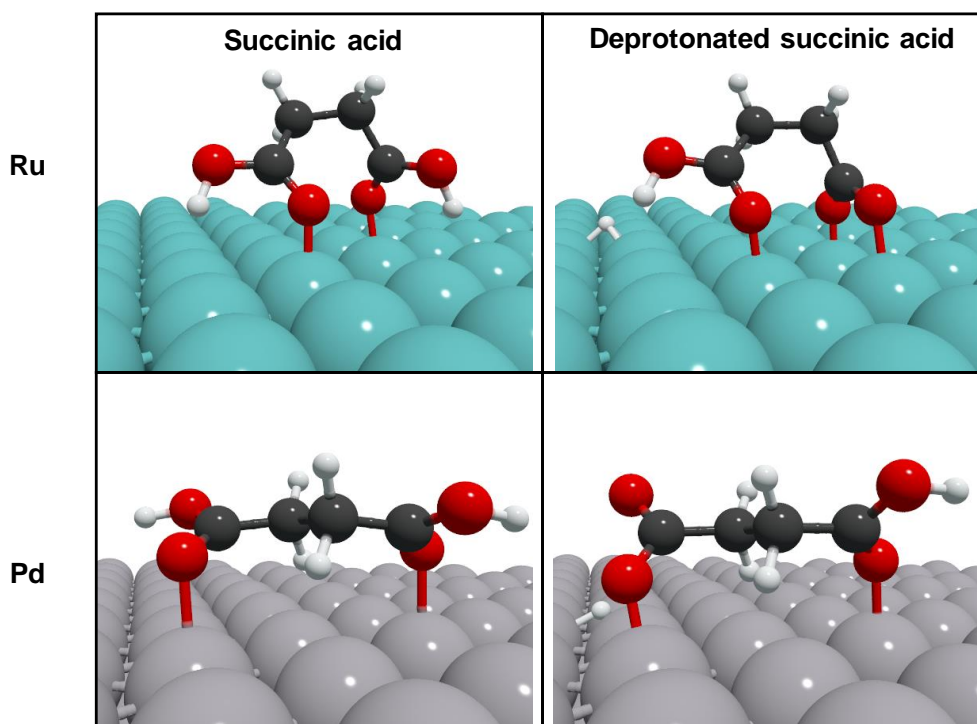


Figure 7.1. Schematic representation of SA (Left) adsorbed on Ru(0001) and Pd(111) and deprotonated molecule (Right) adsorbed onto Ru(0001) and Pd(111).

Herein, these preliminary results open an interesting line of research based on computational studies on a detailed molecular level mechanism and experimental studies by DRIFT spectroscopy using a carboxylic probe molecule to investigate the potential different binding modes through Pd and Ru, to prove how the choice of metal impacts the coordination of SA and hence, determines the reactions pathways followed.

References

- (1) A. Corma, M. E. Domine, S. Valencia, *J Catal*, 2003, **215**, 294 - 304
- (2) Y. R. Leshkov, M. Moliner, J. A. Labinger, M. E. Davis, *Angew. Chem. Int. Ed.*, 2010, **49**, 8954 – 8957
- (3) J. Dijkmans, D. Gabriels, M. Dusselier, F. de Clippel, P. Vanelenderen, K. Houthoofd, A. Malfliet, Y. Pontikes, B. F. Sels, *Green Chem.*, 2013, **15**, 2777 - 2785
- (4) A. Corma, L. T. Nemeth, M. Renz, S. Valencia, *Nature*, 2001, **412**, 423 - 425
- (5) R. van Grieken, C. Martos, M. Sánchez-Sánchez, D. P. Serrano, J. A. Melero, J. Iglesias, A. G. Cubero, *Micr. Mesop. Matter*, 2009, **119**, 176 - 185
- (6) P. Li, G. Liu, H. Wu, Y. Liu, J. Jiang, P. Wu, *J. Phys. Chem.*, 2011, **115**, 3663 - 3670
- (7) C. Hammond, S. Conrad, I. Hermans, *Angew. Chem. Int. Ed.*, 2012, **51**, 11736 - 11739
- (8) C. Hammond, D. Padovan, A. Al-Nayili, P. P. Wells, E. K. Gibson, N. Dimitratos, *ChemCatChem*, 2015, **7**, 3322 – 3331
- (9) A. Al-Nayili, K. Yakabi, C. Hammond, *J. Mater. Chem. A*, 2016, **4**, 1373 - 1382
- (10) P. Biasi, J. García-Serna, A. Bittante, T. Salmi, *Green Chem.*, 2013, **15**, 2502 - 2513
- (11) D. R. Vardon, A. E. Settle, V. Vorotnikov, M. J. Menart, T. R. Eaton, K. A. Unocic, K. X. Steirer, K. N. Wood, N. S. Cleveland, K. E. Moyer, W. E. Michener, G. T. Beckham, *ACS Catal.*, 2017, **7**, 6207 - 6219

Annex

Table A.1. Calculation of the experimental error of BVO of CyO.

Time / min	XR1 / %	XR2 / %	XR3 / %	XR4 / %	XR5 / %	Average	SD	Error / %
10	38.39	33.46	41.12	32.86	31.56	35.48	4.08	11.50
30	61.95	54.15	60.07	55.97	48.24	56.08	5.38	9.59
60	71.12	68.27	73.45	69.32	61.33	68.70	4.56	6.64
120	81.83	77.75	83.88	80.78	73.72	79.59	3.96	4.97
240	88.27	89.11	90.98	90.32	84.20	88.58	2.66	3.01
360	90.59	93.13	93.76	93.27	86.38	91.43	3.08	3.37
								6.51

Reaction conditions: 10 mL of 0.33 M CyO in 1,4-dioxane, 1 mol. % Sn respect to CyO (2Sn- β), 1.5 H₂O₂:CyO, at 100 °C, 6 h of reaction.

Table A.2. Calculation of the experimental error of BVO of 2-Me-CyO.

Time / min	XR1 / %	XR2 / %	Average	SD	Error / %
10	24.59	23.31	23.95	0.90	3.77
30	43.69	42.18	42.94	1.06	2.48
60	54.83	56.39	55.61	1.11	1.99
120	68.51	68.02	68.26	0.34	0.50
240	80.53	81.25	80.89	0.50	0.62
360	86.23	86.61	86.42	0.26	0.31
					1.61

Reaction conditions: 10 mL of 0.33 M CyO in 1,4-dioxane, 1 mol. % Sn respect to CyO (2Sn- β), 1.5 H₂O₂:CyO, at 100 °C, 6 h of reaction.

Table A.3. Calculation of experimental error of BVO of 4-Me-CyO.

Time / min	X R1 / %	X R2 / %	Average	SD	Error / %
10	38.67	35.72	37.20	2.09	5.62
30	57.38	56.20	56.79	0.84	1.47
60	68.99	67.06	68.02	1.36	2.00
120	82.05	80.61	81.33	1.02	1.25
240	87.06	86.37	86.72	0.49	0.56
360	90.51	90.48	90.49	0.02	0.02
					1.82

Reaction conditions: 10 mL of 0.33 M CyO in 1,4-dioxane, 1 mol. % Sn respect to CyO (2Sn- β), 1.5 H₂O₂:CyO, at 100 °C, 6 h of reaction.

Table A.4. Calculation of experimental error of BVO of 4-ⁱPr-CyO.

Time / min	X R1 / %	X R2 / %	X R3 / %	Average	SD	Error / %
10	43.80	36.55	43.80	41.38	4.19	10.11
30	65.85	56.62	65.85	62.77	5.33	8.49
60	78.01	74.80	78.01	76.94	1.85	2.41
120	87.75	85.41	87.75	86.97	1.35	1.55
240	94.22	92.35	94.22	93.60	1.08	1.16
360	96.59	94.51	96.59	95.90	1.20	1.25
						4.16

Reaction conditions: 10 mL of 0.33 M CyO in 1,4-dioxane, 1 mol. % Sn respect to CyO (2Sn- β), 1.5 H₂O₂:CyO, at 100 °C, 6 h of reaction.

Table A.5. Calculation of experimental error of BVO of 4-*t*-Bu-CyO.

Time / min	X R1 / %	X R2 / %	Average	SD	Error / %
10	45.79	49.77	47.78	2.81	5.88
30	70.89	72.21	71.55	0.94	1.31
60	84.52	83.96	84.24	0.40	0.47
120	93.37	91.76	92.56	1.14	1.23
240	96.51	96.16	96.34	0.25	0.26
360	98.88	98.06	98.47	0.58	0.59
					1.63

Reaction conditions: 10 mL of 0.33 M CyO in 1,4-dioxane, 1 mol. % Sn respect to CyO (2Sn- β), 1.5 H₂O₂:CyO, at 100 °C, 6 h of reaction.

Table A.6. Calculation of experimental error of BVO of AcetoPhO.

Time / min	X R1 / %	X R2 / %	Average	SD	Error / %
10	0.57	0.56	0.57	0.00	0.75
30	2.31	2.01	2.16	0.21	9.91
60	3.91	3.06	3.48	0.61	17.37
120	4.75	4.89	4.82	0.09	1.96
240	5.69	6.38	6.03	0.49	8.07
360	7.42	8.26	7.84	0.59	7.55
					7.60

Reaction conditions: 10 mL of 0.33 M CyO in 1,4-dioxane, 1 mol. % Sn respect to CyO (2Sn- β), 1.5 H₂O₂:CyO, at 100 °C, 6 h of reaction.

Table A.7. Compilation of experimental error obtained for BVO of R-CyO.

Substrate	Number of repetitions	Error / %
CyO	5	6.51
2-Me-CyO	2	1.61
4-Me-CyO	2	1.82
4- ⁱ Pr-CyO	3	4.16
4- ^t Bu-CyO	2	1.60
AcetoPhO	2	7.60

As shown in Table A.1 to A.6, experimental error of BVO reactions of various substrates was calculated. However, given that the experimental error was not calculated for all the substrates employed, and the biggest value obtained was 8 % (Table A.7), this is the value of the global experimental error applied to the BVO / Sn-β / H₂O₂ system throughout all the experiments shown in Chapter 3 to 5.

Table A.8. Calculation of experimental error of SA hydrogenation.

Reaction	X / %	Average
1	19.61	18.47
2	21.15	SD
3	18.65	1.69
4	17.61	Error / %
5	17.37	9.12

Reaction conditions: 15 mL of 0.2 M SA in 1,4-dioxane, 0.5 mol. % Ru respect to SA (5Ru/Al₂O₃(COM)), 30 bar of H₂, at 170 °C, 4 h of reaction.

Acknowledgements

Firstly, I would like to sincerely thank Ceri for his constant guidance and support along my stay within his research group, and for encouraging me to be a better researcher.

I am grateful to the EPSRC Centre for Doctoral training in Catalysis (EP/L016443/01) for giving me the opportunity to be part of this programme, providing excellent training and funding this research project.

I also would like to extend my gratitude to Antoine and his team for their participation on the polymerisation and computational studies, to Alberto for his assistance with the succinic acid simulations, and to the students who made their contribution to my work: Kirstie, Thibault and Alex. I would like to acknowledge also the EPSRC UK National Solid-State NMR Service at Durham University for performing the MAS NMR experiments.

A special thanks to Davide for his help with the XPS analysis and to the rest of the people in the group for the nice atmosphere, both inside and outside the lab.

Finally, I would like to thank Guillermo for his unconditional support, his enormous patience and all his kind words.